2014-06-11

Energy and Quality of Service Aware Communication Schemes for Body Area Networks

Egbogah, Emeka

UNIVERSITY OF CALGARY

Energy and Quality of Service Aware Communication Schemes for Body Area Networks

by

Emeka Emmanuel Egbogah

A THESIS

SUBMITTED TO THE FACULTY OF GRADUATE STUDIES

IN PARTIAL FULFILMENT OF THE REQUIREMENTS FOR THE

DEGREE OF DOCTOR OF PHILOSOPHY

DEPARTMENT OF ELECTRICAL AND COMPUTER ENGINEERING

CALGARY, ALBERTA

MAY, 2014

Abstract

The emergence of body area networks (BANs) has garnered interest from the military where body-to-body networks (BBNs) can be employed to facilitate the remote monitoring of soldiers' physiological state, thus preventing unnecessary fatalities. The wireless transmission of physiological data from soldiers to combat medic presents a challenging problem not fully addressed in the literature. The challenge arises from the need to not only manage the limited energy supply of battery-powered devices comprising the BAN, but to overcome deleterious path loss and fading induced on-body and body-to-body wireless channel conditions while also supporting stringent quality of service (QoS) requirements.

In this thesis, energy and QoS aware communication schemes were designed to solve the aforementioned problem. The combination of a BAN-centric adaptive transmission scheme (ATS) and multi-constrained power allocation (MPA) strategy was shown to enhance intra-BAN and inter-BAN transmission link performance. Incorporating ATS and MPA into the BANs of a platoon sized multi-hop BBN, the optimal solution for the minimum energy required to transmit physiological data under reliability and delay constraints was derived. The solution, however, was found to be highly complex and computationally inefficient. Therefore, an energy and QoS aware cross-layer (EQX) communication scheme integrating a constrained routing algorithm at the network layer, interference aware scheduling at the medium access control layer, and multi-constrained power allocation at the physical layer, was designed. EQX was shown to achieve near-optimal performance with polynomial complexity. To support the fully distributed operation of BANs in the multi-hop BBN, an energy and QoS aware distributed (EQD) communication scheme integrating analog network coded cooperative communication at the

BAN level and a multi-receive policy at the BBN level was designed and shown to improve performance.

The EQX and EQD communication schemes developed in this thesis offer valid and useful solutions towards the problem of supporting remote monitoring of soldiers' physiological state in military environments. They provide, as this thesis demonstrates, clear performance benefits in terms of network coverage, energy consumption, reliability, and delay and are thus recommended for implementation in future BANs.

Acknowledgements

I would like to express my sincere gratitude to Dr. Abraham O. Fapojuwo for his dedicated supervision, academic guidance, and motivation throughout this research period. His expertise, professionalism, rigorousness, and compassion have shaped me both as a student and as a person.

The members of my supervisory and examining committee, Dr. Geoffery Messier, Dr. Henry Leung, and Dr. Zongpeng Li have all provided invaluable feedback to enhance the quality of my research and for that, I extend my appreciation and thanks.

My esteemed colleagues Jaya B. Rao, Dr. Liqi Shi, and Xiaobin Li have been the source of great inspiration, mentorship, endless debate, and most importantly friendship. Their presence in the Wireless Networking Research Laboratory has improved my learning experience. They are truly appreciated.

I acknowledge the Faculty of Graduate Studies and the Electrical and Computer Engineering Department of the University of Calgary for affording me consistent academic support allowing me to publish my work, attend conferences, and purchase the equipment and software needed to perform my research activities.

Finally, I would like to convey my deepest of thanks to my wife, Nancy, without whose forbearance and understanding this work would not have been feasible, my parents Emmanuel and Chirota whose unconditional love and belief in me brought me strength through endless hours of work, my sisters Liza and Shirley for their support, and my extended family and friends for their encouragement.

Dedication

To my wife Nancy and

parents Emmanuel and Chirota.

Table of Contents

List of Tables

List of Figures and Illustrations

List of Abbreviations

Abbreviation	Definition
9DoF	Nine degrees of freedom
ACK	Acknowledgement
AIA	ANC-CC ignoring ANC noise
AMA	ANC-CC mitigating ANC noise
ANC	Analog network coding
ANC-CC	Analog network coded cooperative communication
AWGN	Additive white Gaussian noise
BAN	Body area network
BBN	Body-to-body network
BER	Bit error rate
BNC	Body network coordinator
BPM	Blood pressure monitor
BPSK	Binary phase shift keying
BPA	BBN multi-constrained power allocation
BRA	BBN routing algorithm
BS	Base station
BSA	BBN slot assignment
CC	Cooperative communication
CR	Conventional relay
CSMA-CA	Carrier sense multiple access collision avoidance
DRP	Distributed routing protocol
ECG	Electrocardiogram
EEG	Electroencephalogram
EMG	Electromyogram
EOG	Electrooculogram
EQD	Energy and QoS aware distributed communication scheme
EQS	Energy and QoS aware single-hop communication scheme
EQX	Energy and QoS aware cross-layer communication scheme
INA	Interference neglecting assumption
ISM	Industrial, scientific, and medical
JPR	Joint transmit power and retransmission limit
JPRS	Joint transmission power, retransmission limit, and packet size
LOS	Line-of-sight
MAC	Medium access control
MANET	Mobile ad hoc network
MINLP	Mixed integer non-linear problem

MRC	Maximal ratio combiner
MRP	Multi-receive policy
NDR	Neighbor discovery range
NLOS	Non-line-of-sight
NTW	Network layer
OPT	Optimal solution
OQPSK	Offset quadrature phase shift keying
OPA	Optimal multi-constrained power allocation
PDR	Packet delivery ratio
PER	Packet error rate
PHY	Physical layer
PTV	Success probability target values
QoS	Quality of service
RCFM	Route confirm message
RDIS	Route discovery message
REC	Relative energy cost
RF	Radio frequency
RN	Relay node
RREP	Route reply message
RSM	Route selection metric
SINR	Signal-to-interference plus noise ratio
SN	Sensor node
SNR	Signal-to-noise-ratio
S_PO_2	Pulse oximeter
SRA	Slot reuse with reliability awareness
TDMA	Time division multiple access
UWB	Ultra wideband
WSN	Wireless sensor network

List of Symbols

Symbol	Definition
${}_2F_1(a,b;c;z)$	Gauss hypergeometric function
$\mathcal{E}_{th}$	Relative energy cost threshold for slot reuse
$\mathbb{N}_i$	Number of neighboring BNCs of BNC *i*
$\mathbb{N}_{ndr}$	Desired number of soldiers in single hop neighborhood
E_b	Energy per bit, in joules per bit
$E_{init}^s/E_{init}^b/E_{init}^c$	Maximum battery capacity for SN, BNC, and BS, respectively, in joules
$E_{res}^s/E_{res}^b/E_{res}^c$	Residual energy of SNs, BNCs, and BS, respectively, in joules
I_{th}	Threshold for interference neglecting assumption
K_1	Constant for Nakagami BER calculation
K_2	Constant for maximal ratio combiner BER calculation
L_h	Data packet header size, in bits
$L_{p,max}$	Maximum payload size, in bits
$L_{p,min}$	Minimum payload size, in bits
$L_{p,step}$	Payload step size, in bits
L_p	Data packet payload size, in bits
$L_{s,k}$	Sample size extracted from SN *k*, in bits
N_b	Number of BANs/BNCs
N_s	Number of SNs in a BAN
N_{sam}	Number of sampled channels
P_I	Interference power, in decibel milliwatt
P_{max}	Maximum transmit power
P_{min}	Minimum transmit power
P_n	Noise power
$P_{rx,cir}$	Receiver circuit power
$P_{tx,cir}$	Transmitter circuit power
P_{tx}	Transmit power
T_{du}	Data update period, in seconds
T_{rs}	Route update period, in seconds
d_0	Reference distance, in meters
d_{ndr}	Neighbor discovery range, in meters
p_b	Bit error rate
p_e	Packet error rate
p_γ	Probability density function
r_k	Source data rate for SN *k,* in bits per second
t_{slot}	Time slot duration, in seconds

$\mathcal{D}_{agg}$	Average aggregation time, in seconds
$\mathcal{D}_{req}$	Delay objective, in seconds
$\mathcal{D}_{rs}$	Delay to setup a route, in seconds
$\mathcal{D}_{tdma}$	TDMA frame duration, in seconds
$\mathcal{D}_{tx}$	Transmission delay, in seconds
$\mathcal{P}_{req}$	Reliability objective
Ω_i	Number of routing table entries in BNC i
β_{rsm}	Relay selection metric
$\bar{\gamma}$	Average SNR
σ^2	Variance for noise, in decibel milliwatt
ϑ_k	Sample rate for SN k, in bits per second
Δ	Slot schedule
$\mathcal{B}$	Number of diversity branches
$\mathcal{E}$	Relative energy cost
h	Hop number
$\mathcal{R}$	Maximum link data rate, in bits per second
Γ	Gamma function
H	Total number of hops
L	Total data packet size, in bits
N	Total number of BNCs and BS
$PL(d_0)$	Path loss at reference distance, in decibels
$PL(d)$	Total path loss, in decibels
X	Retransmission limit
Y	Number of end-to-end success probability target values
d	Distance separating a transmitter and receiver
f	Total data traffic load, in bits
$g(d)$	Channel gain at distance d
m	Nakagami fading factor
n	Number of packets transmitted per second to sustain source data rate
s	Slot ID
$\mathcal{A}$	Node set for specific network scenario
$\mathcal{D}$	Delay, in seconds
$\mathcal{G}$	Network graph
$\mathcal{P}$	Average success probability
$\mathcal{S}$	Number of required time slots along a link
$\mathcal{V}$	Set of all SNs and BNCs in $\mathcal{G}$
$\mathcal{W}$	Set of all links in $\mathcal{G}$
$\mathcal{Z}$	Number of discrete transmit power levels

α	Path loss exponent
γ	Instantaneous SNR
δ	Incremental gain ratio
η	Power amplifier efficiency
μ	Binary decision variable for route path selection
ξ	Amplification factor for amplify-and-forward operation
ρ	Array of defined end-to-end success probability target values
φ	Number of aggregated samples in a data packet
ψ	Soldier density, in soldiers per square meter
ω	Weighting factor for incremental gain ratio
ϕ	Average number of total transmissions along a link

CHAPTER 1 INTRODUCTION

1.1 Background

Research over the past decade has revealed that 25% of soldiers killed in battle die between 5 minutes and 6 hours of the initial injury infliction [1]. Of all the casualties that combat medics attempt to rescue, 25% of them are already dead before the combat medic arrives [1]. Furthermore, 10% of casualties in the battlefield are injured while attempting to rescue a previously injured soldier, and if a combat medic is part of that 10%, the physiological status of the soldiers he or she is responsible for and the success of their imminent mission are likely to be severely jeopardized [1]. Consequently, the old military systems used to perform triage and monitor injured soldiers have been largely cast as inefficient and inept at providing relevant physiological status information to the combat medic in a reliable and timely manner [2].

With recent advances in sensor technology, soldiers can be fitted with specialized devices that can continuously monitor physiological signals around the body such as oxygen level, blood pressure, electrical activity of the heart, electrical stimulation of the brain, and muscle activity using integrated sensors such as pulse oximeters (S_PO_2) [3], blood pressure monitors (BPM) [4], electrocardiogram (ECG) [5], electromyogram (EMG) [6], and electroencephalogram (EEG) [7], respectively. When affixed to different parts of the soldier body, these specialized radio capable devices, referred to as sensor nodes (SNs), combine with a body network coordinator (BNC) device to form a wireless body area network (BAN). Within the BAN, SNs use an on-body wireless channel to transmit their physiological data to the BNC. Upon receiving the physiological data from the SNs, the BNC uses a body-to-body wireless channel to relay the data to a base station (BS) device held by the combat medic. The combination of multiple BANs and BS forms a body-to-body network (BBN). The BBN is defined as a specialized form of ad hoc

network that supports the sensing, sampling, and wireless transmission of physiological data from one body to another using single-hop or multi-hop communication.

The BBN provides a means to minimize the number of casualties, improve health outcomes of injured soldiers, and enhance mission success by facilitating the ability to remotely monitor the physiological status of soldiers and effectively disseminate physiological status information on the battlefield. However, the deployment of BBNs on the battlefield for the remote monitoring of soldiers is a challenging problem that requires further research. The problem is made challenging due to the energy constrained nature of the battery powered SNs and BNCs, the deleterious path loss and fading conditions inherent of the on-body and body-to-body wireless channels [8]-[15], and the need to support stringent quality of service (QoS) requirements in order to guarantee the reliable and timely delivery of soldiers' critical physiological status information.

Research in the literature have addressed the aforementioned challenges individually or as a combination of different challenges using a number of various approaches. In [16] –[34], the challenge of sustaining energy efficient communication is achieved by either optimizing performance at the network layer, medium access control (MAC) layer, or physical layer or by jointly optimizing performance amongst the three protocol layers. From the perspective of the physical layer, transmission power control is performed at the SNs and BNC to satisfy power and packet error rate[1] (PER) constraints while attempting to achieve the minimum energy consumption. At the MAC layer, retransmissions and packet size configuration are permitted to

[1] Packet error rate is defined as the probability that at least one transmitted bit in a packet is in error.

improve packet success probability[2] whereas link bandwidth and medium access constraints are enforced to attain minimum delay and provide stability. Furthermore, the MAC layer is also responsible for the collision-free scheduling of both intra-BAN and inter-BAN transmissions. At the network layer, routing is performed via single-hop or multi-hop. In both routing scenarios, flow conservation must be maintained between the SNs and BNC to eliminate routing loops and wasteful consumption of energy. Although the individual protocol layer and cross-layer communication schemes adopted in [16] – [34] provide energy efficiency, their solutions are limited to the BAN and do not extend to offer energy efficiency through the BBN. Furthermore, whereas some of the challenges are separately addressed, a comprehensive and holistic consideration of all the collective challenges is lacking and thus requires further research.

Several proposals discussed in [35] have extended the BAN to facilitate the communication of physiological data between BANs via the BBN by using a single-tier approach where the relaying function of the BNC is eliminated such that the SNs perform direct transmission to the destination [36] – [39] or by invoking a two-tier approach where the SNs transmit directly to the BNC in the first tier followed by the BNC transmitting directly to the destination in the second tier [40] – [52]. Both approaches typically retain cross-layer optimization to provide accurate minimum energy solutions but fail to address all the challenges. When measures are explicitly taken to overcome the challenges, the consideration of multiple BANs connected through a BBN introduces additional complexity to the network, MAC, and physical layers. As a result, the overall problem of obtaining minimum energy consumption for the transmission of data from all SNs to the BS under high reliability and low delay constraints

[2] Packet success probability is the probability that all transmitted bits in a packet are received without error.

in fading environments becomes very difficult. For example, at the network layer, multi-hop routing becomes a necessity given that SNs and BNCs could be out of the direct transmission range of the BS because aside from having limited resources, the effective transmission range of the SNs and BNCs is also limited due to the combined impact of fading over the wireless body-to-body channel, body-centric shadowing introduced by soldiers who impinge upon a BAN's line-of-sight (LOS) path to the destination, and soldiers who have their backs to each other thus creating a non-line-of-sight (NLOS) path with severe path loss [11]. Another problem faced in BBNs arises due to interference amongst co-located BANs, which is typically handled at both the MAC and physical layers since the scheduling of transmissions in non-interfering slots and the management of transmission power contributing to interference power are both integral to mitigating interference. The management of interference amongst co-located BANs to avoid collisions, energy increase, increase in delay, and decrease in packet success probability is not a straightforward problem and further complicates the analysis required to obtain minimum energy in BBN without violating the reliability and/or delay constraints. At the physical layer, calculating the end-to-end success probability for transmissions over routing paths spanning multiple hops and two different wireless channels (i.e., on-body and body-to-body) amidst varying fading conditions while maintaining minimum energy consumption is also a difficult task. The works in [45] and [46] have proposed energy efficient solutions for BBNs by neglecting the impact of on-body fading thus simplifying the calculation of the end-to-end success probability. However, Cotton *et al.* have shown that small-scale fading over the on-body channel has a profound impact on intra-BAN transmission performance due to body-centric shadowing and the occurrence of obstructions due to the contour and shape of the human body and different body parts [10].

In this thesis, we design a comprehensive cross-layer optimization framework that jointly integrates the discussed aspects of the network, MAC, and physical layers based on a two-tier architecture unifying the BAN, BBN, and BS. Different from the two-tier architectures in the literature, our proposed architecture reveals a natural synergistic relationship between the SNs and BNC thus motivating an adaptive transmission design for the SNs. Specifically, the adaptive transmission design allows the SNs to either transmit over the on-body or body-to-body channels or simultaneously transmit over the on-body and body-to-body channels. The integration of the adaptive transmission behavior of the SNs adds significant complexity to the cross-layer optimization framework. However, the design of this cross-layer framework for the BBN is fundamental to the work reported in this thesis and highlights a unique treatment and novel contribution not offered in the literature. The main objective of designing the cross-layer optimization framework described in this chapter is to determine the minimum *relative energy cost* (REC) required to guarantee the reliable and timely delivery of physiological data to the BS by accounting for the residual energy of the SNs and BNCs, the additive path loss and multiplicative fading conditions inherent of the on-body and body-to-body wireless channels, end-to-end success probability, and total delay. We define *relative energy cost* as the ratio of energy consumption to residual energy. Since the SNs and BNCs in the BAN and BBN are heterogeneous, it is important to consider residual energy when making routing decisions because consistently transmitting over minimum energy routes without considering the residual energy of the nodes may quickly exhaust energy resources and subsequently limit the duration for which the remote monitoring of soldiers is performed.

1.2 Problem Statement

The research in this thesis addresses the central problem of achieving minimum energy communication in BBNs to facilitate the reliable and timely transmission of physiological data from BANs to a BS device under the conditions of on-body and body-to-body fading. The central problem is addressed as three problems defined as follows:

- *Problem #1 (Chapter 3): Minimum relative energy cost in a single-hop BBN under the constraints of high reliability and low delay*. The problem is that of jointly optimizing the relative energy cost within the BAN and along the BBN link connecting the BAN to the BS while also meeting specified end-to-end reliability and delay objectives. The major issues to be investigated are three fold. The first is how to design the adaptive transmission scheme of the SNs. The second is how to attain energy savings by exploiting synergistic communication between the SNs, BNC, and BS. The third is how to efficiently solve the problem of jointly optimizing transmission power, retransmission limit, and packet size along a transmitting link for achieving enhanced transmission link performance.
- *Problem #2 (Chapter 4): Minimum relative energy cost in a centrally administered multi-hop BBN under the constraints of high reliability and low delay*. The problem is that of optimizing transmission parameters (i.e., transmission power, retransmission limit, packet size) for each link in the multi-hop BBN in order to achieve minimum relative energy cost routing paths from the BANs to the BS without violating the end-to-end reliability and delay constraints. The major issue to be investigated is how to obtain a near-optimal and polynomial complexity solution to the NP-hard (non-polynomial hard) problem using an energy and QoS aware communication scheme that employs accurate and efficient heuristics integrating features from the network, MAC, and physical layers.

- *Problem #3 (Chapter 5): Minimum relative energy cost in a multi-hop BBN operating in a fully distributed fashion under the constraints of high reliability and low delay*. The problem is that of determining how to calculate, acquire, and maintain a reliability and delay constrained minimum relative energy cost routing path between each BAN and BS given the lack of available network-wide information and the requirement for fully distributed operation of the multi-hop BBN. The major issue to investigate is how to incorporate the joint combination of analog network coding and cooperative communication into SNs and their BNC to achieve minimum relative energy cost data transmission to a next hop node and how to take advantage of the wireless propagation characteristics of body-to-body relay paths comprised of multiple BNCs in order to attain energy and delay savings and increased reliability.

The joint optimization of relative energy cost and the guarantee of high end-to-end reliability and low delay for energy and QoS aware communication at the BAN and BBN levels is a topical subject of research in military, industry, and academia because several outstanding issues, challenges, and problems remain to be solved. Amongst them are the issues of minimizing the relative energy cost required to facilitate the transmission of physiological data from BANs to the BS via single-hop or multi-hop BBNs in fading induced military operating environments. The formulation of the cross-layer optimization models described in Chapters 3 and 4 and the performance characterization of proposed communication schemes in Chapters 3, 4, and 5 are very complicated due to the integration of features spanning multiple protocol layers from the BAN and BBN networks, the adaptive transmission behavior of the SNs, and the synergistic communication features shared between the SNs and BNCs, respectively. The

computational complexity of the formulated problems can be prohibitive due to the problem's scale, the connection between system parameters such as the transmission power, retransmission limit, and packet size through the network, MAC, and physical layers, and non-linear relationships between system performance metrics such as energy consumption, bit error rate (BER), PER, link success probability, signal-to-noise-ratio (SNR), and signal-to-interference plus noise ratio (SINR), amongst others. The main novelty of the work presented in this thesis is the derivation of analytical expressions to comprehensively characterize the performance of the proposed energy and QoS aware communication schemes integrating the adaptive transmission behavior of the SNs and exploiting synergistic communications between the SNs and BNCs.

1.3 Thesis Motivation and Objectives

1.3.1 Thesis Motivation

The main motivation of the problem addressed in this thesis is to facilitate fast, accurate, and reliable remote monitoring of soldiers' physiological state on the battlefield in order to prolong their lives and enhance tactical mission success. The careful design of communication schemes to extend the connectivity of BANs to the BS via a BBN and to continuously transmit soldiers' physiological data to a combat medic on the battlefield in an energy efficient, reliable, and timely manner is necessary to support this motivation.

1.3.2 Thesis Objectives

The following research objectives are defined to solve the three research problems described in this thesis.

- *Thesis objective #1 (Chapter 3): Design an extensive cross-layer optimization framework that incorporates the adaptive transmission behavior of the SNs, the synergistic communication feature of the SNs and BNC, and enables the joint consideration of*

transmission power, retransmission limit, and packet size for energy and QoS aware communication in a single-hop BBN. This objective is realized via three tasks. The first task is to design a BAN network model that allows synergistic communication between the SNs and BS through multiple paths consisting of direct transmission between the SNs and BS and indirect transmission between the SNs and BS via the BNC. Cooperative communication schemes are employed in the literature for energy efficiency *within the BAN*, however they rely on the presence of designated on-body relay nodes aside from the BNC, which is not always practical for soldiers who are already laden with other military equipment. The second task is to analyze the performance benefits realized by the joint optimization of transmission power, retransmission limit, and packet size (also referred to as JPRS strategy) for transmission along intra-BAN and inter-BAN links. Typically, works in the literature have sought to minimize energy consumption by optimizing either transmission power [53], packet size [54], or transmission power and retransmission limit [17]. The complexity associated with optimizing two variables is notable but solving a multi-variable optimization problem that jointly considers the three aforementioned parameters introduces even more complexity further exacerbated by the involvement of non-linear BER, PER, and success probability expressions at the MAC and physical layers. The third task is to formulate and solve the cross-layer optimization model using an accurate but inefficient optimal solution and near-optimal but efficient heuristic-based algorithms.

- *Thesis objective #2 (Chapter 4)*: *Design an energy and QoS aware cross-layer communication scheme for a multi-hop BBN*. The extension of a single-hop BBN to a multi-hop BBN injects substantial complexity into the formulation of the cross-layer optimization model employed to determine the minimum relative energy cost required to transmit

physiological data from BANs to the BS while adhering to constraints at the network, MAC, and physical layers and meeting end-to-end reliability and delay objectives over successive on-body and body-to-body wireless channels plagued by varying fading conditions. The multi-hop BBN cross-layer optimization problem is combinatorial in nature and requires significant processing and memory resources to obtain the optimal minimum energy solution due to its exorbitant exponential complexity. Therefore, to reduce the complexity associated with the optimal solution, the main task to perform is the design of a reduced complexity but near optimal energy and QoS aware cross-layer communication scheme comprised of accurate and efficient algorithms to support energy efficient and reliable multi-hop routing at the network layer, energy efficient and reliable multi-constrained power allocation at the combined MAC and physical layers, and energy efficient and minimum delay slot scheduling at the MAC layer employing slot reuse and interference mitigation techniques.

- *Thesis objective #3 (Chapter 5)*: *Design an energy and QoS aware distributed communication scheme for a multi-hop BBN*. The distributed operation of the multi-hop BBN provides autonomous decision making to each BAN (in terms of obtaining minimum relative energy cost routing paths and scheduling transmissions) and alleviates the single point-of-failure issue sometimes experienced in a network fully administered by a central entity such as the BS device. However, given the resource constrained nature of the SNs and BNCs and the control (activities performed aside from data transmission such as route setup, discovery, etc.) overhead and incurred delay associated with building minimum relative energy cost routing paths in a distributed manner, three tasks are performed to meet the objective of designing a fully distributed energy and QoS aware communication scheme for a multi-hop BBN. The first task is to integrate analog network coding and cooperative communication

into the SNs, their BNC, and a desired next hop node. The challenge is to minimize relative energy cost and delay while maximizing reliability and overcoming the presence of noise due to analog network coding. The second task is to exploit the transmission behavior and wireless propagation of BNCs transmitting along routing paths consisting of multiple hops over body-to-body wireless channels in order to reduce relative energy cost, delay, and increase reliability. The consideration of the impact of maximum routing table size of memory constrained nodes on the ability to perform QoS constrained end-to-end minimum relative energy cost routing is noticeably absent from the literature. Therefore, the third task is to develop a memory-friendly route storing strategy and route storing policies incorporating tasks one and two to facilitate minimum relative energy cost distributed routing in a multi-hop BBN.

1.4 Summary of Thesis Contributions

The major contribution of this thesis is the design of energy efficient communication schemes with QoS provision for a joint two-tier BAN and BBN network operating under fading conditions. The specific contributions are further described in the following paragraphs as they relate to each chapter.

In Chapter 3, we design an adaptive transmission scheme for the SNs and subsequently formulate a cross-layer optimization problem that integrates synergistic communication between the SNs and BNC and incorporates joint optimization of transmission power, retransmission limit, and packet size along intra-BAN and inter-BAN transmission links. The optimization problem is decomposed into two easier to solve sub-problems for which two algorithms assigning transmission power, retransmission limit, and packet size to desired links in the single-

hop BBN are proposed to obtain minimum relative energy cost under reliability and delay constraints. Through analysis and simulation, we show that designing an energy and QoS aware single-hop (EQS) communication scheme that foundationally exploits synergistic communication and jointly optimizes the combination of transmission power, retransmission limit, and packet size significantly improves performance along inter-BAN and intra-BAN transmission links. This finding serves as a useful foundation towards the design of energy and QoS aware communication schemes for BBNs.

In Chapter 4, a cross-layer optimization model is formulated to determine the minimum relative energy cost required to support the transmission of physiological data from a soldier platoon sized number of BANs to the BS over a multi-hop BBN comprised of on-body and body-to-body wireless channels laden with different fading conditions. The optimization problem is solved at a centralized entity (i.e., the BS residing on a combat medic) using a global non-linear problem solver employing a heuristic multi-start method and a branch-and-bound algorithm. However, the exponential complexity required to obtain an optimal solution is undesirable due to the time-sensitive nature of the considered remote monitoring application. As a result, an energy and QoS aware cross-layer (EQX) communication scheme is developed comprising of proposed algorithms of polynomial order complexity at the network, MAC, and physical protocol layers. The results obtained through analysis and simulation demonstrates the efficacy of the proposed algorithms. Furthermore, the results show that the EQX communication scheme achieves near-optimal performance in terms of relative energy cost and effectively reduces delay through slot reuse and interference mitigation techniques.

In Chapter 5, an energy and QoS aware distributed (EQD) communication scheme, comprised of energy saving, delay reducing, and reliability enhancing components at the BNC,

BAN, and BBN levels is developed for multi-hop BBNs. At the BNC level, the EQD scheme accounts for the finite maximum routing table size of memory constrained BNCs to support minimum relative energy cost distributed routing. At the BAN level of the EQD scheme, analytical expressions are derived to obtain the relative energy cost, packet success probability, and delay performance for a combined analog network coding (ANC) and cooperative communication (ANC-CC) relay scheme with and without the consideration of ANC noise (the characterization of ANC-CC relay scheme performance in terms of relative energy cost, packet success probability, and delay is noticeably limited in the literature). A reliability constrained minimum joint delay and relative energy cost algorithm is designed to overcome the presence of ANC noise while concurrently minimizing the relative energy cost and delay along each link involved in the ANC-CC relay scheme. The literature mostly attributes the increase in ANC noise to the increase in number of source nodes using the ANC-CC relay scheme. However, our analysis and numerical results show that ANC noise increases when the distance between a BAN and destination decreases and that the performance benefits offered by the ANC-CC relay scheme are more apparent at longer distances separating the BAN and destination. At the BBN level of the EQD scheme, a proposed multi-receive policy, invoked along routing paths consisting of successive BNCs, is shown to reduce relative energy cost, delay, and increase packet success probability. Through the combination of the three previously described components, the EQD scheme is shown to operate in an energy efficient manner while supporting fully distributed operation.

Table 1.1 lists the main contributions of the thesis and their corresponding chapters/sections.

TABLE 1.1 MAIN CONTRIBUTIONS OF THE THESIS

Contribution	Chapter/Section
1. Joint optimization of transmission power, retransmission limit, and packet size for enhanced intra-BAN and inter-BAN link performance	3.3
2. Minimum relative energy cost solution for EQS communication scheme incorporating synergistic communication and JPRS strategy	3.4
3. BBN reliability-constrained routing algorithm	4.4.3
4. BBN multi-constrained power allocation strategy for minimum relative energy cost in EQX communication scheme	4.4.4
5. BBN interference aware slot scheduling strategy for minimum delay in EQX communication scheme	4.4.5
6. Route storing strategy for achieving minimum relative energy cost distributed routing operation	5.3.3
7. BAN ANC-CC relay scheme integrated into EQD communication scheme	5.3.4
8. Multi-receive policy for BBN relay scheme integrated into EQD communication scheme	5.3.5

1.5 Outline of the Thesis

This thesis is organized into six chapters. Chapter 1 provides an introduction to the thesis, which includes the problem statement, motivation and objectives of the thesis, and the main contributions that have been made. In Chapter 2, an overview and background for the work performed in the area of BANs and BBNs is provided. The similarities and differences between the work presented in this thesis and those in the literature are also elaborated. In Chapter 3, the

model for the adaptive transmission scheme, synergistic communication, and the JPRS strategy are incorporated into the EQS communication scheme. Chapter 4 proposes the EQX communication scheme for multi-hop BBNs, which consists of three polynomial complexity heuristic algorithms at the network, MAC, and physical layers. The EQD communication scheme is proposed in Chapter 5. It integrates a route storing strategy, ANC-CC relay scheme for the BAN, and multi-receive policy for transmissions over the routing paths presiding over the BBN to facilitate minimum relative energy cost routing in a multi-hop BBN. The major conclusions of the thesis, engineering significance of thesis findings, and recommendations for future work are presented in Chapter 6.

CHAPTER 2 A REVIEW OF BODY AREA NETWORKS

2.1 Introduction

This chapter presents background knowledge and a literature survey towards energy efficiency and QoS support in BANs. In Section 2.2, we provide a brief background of the military applications that use BANs. Section 2.3 provides an overview of the key physiological parameters that must be monitored to gain a comprehensive picture of a soldier's physiological state and the wireless technology suitable for transmitting the physiological data over the on-body and body-to-body wireless channels. The similarities and differences between the work presented in this thesis and the work in the literature are presented in Section 2.4 and a summary of the chapter is provided in Section 2.5.

2.2 Military Applications for BANs

In this section, we briefly discuss the military applications that have integrated BANs into the soldier platform. The military applications are described in two categories: on-body communications for monitoring physical phenomena in and around a soldier's body and body-to-body communications for transmitting collected information from a soldier to another soldier and/or combat medic.

2.2.1 On-body Communication

Body area networks for sensing and monitoring the physiological state of soldiers was first introduced and experimentally evaluated by the United States Army Research Institute of Environmental Medicine (USARIEM) in 1997 as part of the Dismounted Battlespace Battle Lab's Concept Experimentation Program [56]. In this program, a body worn ambulatory monitoring system (AMS) equipped with an array of wired physiological sensors was developed to measure core body temperature, energy expenditure, and heart rate. However, the portability

and practicality of using the AMS during an actual combat mission was hampered by the fact that the device itself was very large [56], relied on a large power supply, restricted body movement due to a plethora of cumbersome wires, and also did not provide the ability to analyze the results until the data was off-loaded onto an on-site computer. The initial work of the USARIEM led to further research where wireless, lightweight, minimally invasive, and autonomously powered alternatives to the AMS could be realized. The Defense Advanced Research Projects Agency's (DARPA) Augmented Cognition program [57] and the United States Army's Warfighter Physiological Status Monitor (WPSM) program [58] developed wireless sensing systems to measure physiological variables. However, the programs were limited in the number of physiological variables that could be measured simultaneously. These limitations were effectively addressed in [59] by interfacing ECG, EMG, electrooculogram (EOG), and EEG biosensors with low power wireless transceivers to transmit the collected data to a body worn data logger. The data logger uses the IEEE 802.11 protocol to relay the processed and logged data to an external system. A low-power sleep mode and a data burst mode were employed to conserve power for the sensor nodes and data logger. Improving on their previous projects and efforts, DARPA created the Soldier Assist System (SAS) as part of the Advanced Soldier Sensor Information System and Technology (ASSIST) program [60]. The goal of the SAS was to perform on-body data capture for the purpose of automatically recognizing a soldier's activity. In [61], the research and development of advanced monitoring and decision support systems for use on the battlefield and civilian trauma environments was discussed. It was determined that indeed, automation and decision support systems are vital for improving the livelihood of soldiers and for improving the critical care of those soldiers injured in the battlefield environment. A soldier health monitoring system is designed in [39] with a focus towards characterizing the effect that

bomb blasts have on the physiological parameters that are being monitored. A battlefield soldier monitoring system is proposed in [62] to provide up-to-the-minute medical information comprised of the physical and physiological fitness measurements of each soldier so that commanders can generate tactical plans and make better informed decisions on the battlefield.

The early implementations of the BANs designed specifically for remotely monitoring the physiological state of soldiers have collectively neglected to place a high priority on energy efficiency and QoS guarantees. The absence of these considerations is likely due to the designers' initial emphasis on providing the necessary functionality (i.e., remote monitoring) with future ambition to improve its performance.

2.2.2 Body-to-body Communication

The ability to perform on-body communications to collect information from and around the body is as important as the ability to perform body-to-body communications because of the need to share the collected information with other interested parties. Novel transmission techniques have been proposed in the literature to facilitate body-to-body communications in military environments. In [63], a Reliability Map Routing (RMR) protocol for tactical mobile ad hoc networks (MANETs) suited for vast terrain outdoor environments (e.g., mountains, valleys, plains, lakes, etc.) is proposed where a spatial approach adopting QoS metrics, spatial reliability, and trust are used to create long duration reliable routes between mobile soldiers. The RMR protocol reactively discovers routes over special cells or regions whose local reliabilities are distributed throughout the network via a fast dissemination algorithm. This protocol has been shown to perform well in high mobility and high density scenarios because of its controlled overhead and spatial approach to routing. In [64], Lee *et al.* suggest organizing soldiers into a cluster-tree based multi-hop network with optimized cluster head election. By also using link

quality prediction and lost packet recovery mechanisms for maintenance of the network, routing paths between soldiers can be designed to meet QoS requirements while maintaining energy efficiency. The framework for cross layer design is also provided, however the reader is left to make the design decisions which best suits the desired application. Whereas rural outdoor environments are more open, urban outdoor environments feature more obstructions that are densely located and thus require different solutions for body-to-body communications. The United Kingdom Ministry of Defense has funded a project to investigate the feasibility of using 60 GHz millimeter-wave smart antenna technology for soldier-to-soldier communication in urban warfare covert battlefield operations [65]. Transmission in the 60 GHz ultra wideband (UWB) frequency for ad hoc networking between soldiers has several benefits including covertness (i.e., inability for the enemy to intercept signals), high frequency reuse, reduced risk of interference, and high data rates up to several gigabytes per second for short range applications [65]. However, to realize the objective of millimeter-wave communications, several hurdles must be overcome at the physical and MAC layers, requiring future research efforts and heavy investment into new technologically advanced hardware. The research will also require a significant effort to ensure the energy efficient design of the protocol layers resulting in extended battery life for the sensors and communicating devices.

Body-to-body communications are also particularly relevant for the scenario where soldiers have been injured during their mission and require triage and treatment. In [66], Cho *et al.* propose opportunistic delay tolerant medical monitoring where both nurses and patients are equipped with Bluetooth devices to form a peer-to-peer (P2P) network. Device-equipped nurses in a field hospital opportunistically collect, share, and upload patient medical records in a P2P fashion during bedside visits and later download the medical records to a BS where the results

can be later analyzed. Results were shown to demonstrate the ability of the extended inquiring response function of the Bluetooth v2.1 protocol to mitigate the traditionally high latency caused by Bluetooth's slow connection time. While the work in [66] presents a viable solution for monitoring and storing patient data in a wireless manner, its approach is limited by the fact that Bluetooth transmissions are short range thus only supporting intra-BAN communication and inter-BAN communication with an external network (i.e., the Bluetooth enabled device carried by the nurse) when it is in close range. The CodeBlue [36], Medical Emergency Detection in Sensor Networks (MEDiSN) [37], and robust Medical Ad hoc Sensor Network (MASN) projects have all been highlighted in [67] as employing body-to-body communications and having tremendous use for soldiers requiring triage. A single-tier BBN architecture is adopted in CodeBlue where SNs deployed on a body use ad hoc routing to either transmit collected physiological data directly to a medical professional or employ multi-hop routing through other SNs to relay the data to the medical professional. The SNs and BNCs in MEDiSN are organized in a two-tier architecture. However, the number of BNCs employed to perform relay functions in the BBN is minimized due to the presence of a dedicated wireless backbone network comprised of strategically placed static relay nodes (RNs) that also provide extended connectivity to the BS. In MASN, the SNs and BNCs are also organized in a two-tier architecture. Different from MEDiSN, there are no dedicated RNs and thus the physiological data transmitted from the SNs directly to the BNC is only relayed amongst other BNCs in the BBN.

Although this thesis focuses on the deployment of BANs and BBNs to facilitate remote monitoring of a soldier's physiological status on the battlefield, BANs and BBNs can also have other useful applications. For example, in [60], on-body sensors are used to process, digitize, and report key observational and experimental data captured by soldiers during a mission on the

battlefield. These sensors are integrated with a multi-media interface to enhance their post-mission recall and reporting capability. The post-mission reports are essential for communicating information to commanders and for preparing future missions. Aside from the on-body sensors used to measure physiological signals, other sensors such as a microphone, high resolution still camera, a video camera, GPS device, and altimeter are utilized to provide content for the multi-media interface. By considering these other sensors, the operational requirements (in terms of energy and QoS) will also be different when compared against physiological sensors. Therefore, more extensive research would be required for a fully integrated network that considers both physiological measurements and multimedia information.

2.3 Monitoring the Physiological State of Soldiers

In this section, we first list and discuss the key physiological parameters required to attain the physiological state of soldiers. Next, we discuss the wireless technologies most suitable for usage within the BAN and throughout the BBN.

2.3.1 Key Physiological Parameters to Monitor

An extensive number of studies have been performed to determine the set of physiological parameters necessary to gain a comprehensive profile of a soldier's physiological state. The technical report compiled by the North Atlantic Treaty Organization (NATO) and Research and Technology Organization in [68] summarizes these studies and identifies the following physiological parameters measured from their respective physiological signals (indicated in parenthesis): i) EEG (Cognitive state), ii) ECG (heart activity), iii) BP (body core temperature, blood pressure), iv) S_PO_2 (oxygen saturation level), and v) 9DoF (nine degrees of freedom for physical awareness and activity). These physiological parameters, which can be further processed through probabilistic inference algorithms based on Bayesian statistical

methods [69], can provide a combat medic, commander, or headquarters with information regarding whether or not a soldier has experienced severe physical fatigue, endured a significant body injury, or suffered deteriorated cognitive ability. The aforementioned symptoms alert the combat medic as to whether immediate triage and medical attention is needed, provides an indication to a commander of whether the soldier is fit to perform his or her duties, or allows the headquarters to accurately determine which mobile military field hospital the soldier should be transported to based on his or her injuries. The SN devices which monitor the physiological signals and measure the physiological parameters are each different and can be characterized in terms of their sampling frequency, bits per sample, and required data rate. These characteristics are of importance because they have a strong bearing on the communication scheme required to maintain energy efficiency and QoS within a BAN. In the following paragraphs, a brief description of the physiological parameters, their sensor characteristics, and relevant literature work related to BAN research is described.

The cognitive state of a soldier can be measured using an EEG sensor emplaced on the inside of a helmet. An EEG records the electrical signals generated by brain activity which can be analyzed by a combat medic to determine if soldiers need a recovery break to ensure mental fatigue does not lead to poor decisions compromising the mission or safety of personnel. A typical EEG signal comprises one or multiple waveforms measured over one or multiple channels. With knowledge of the frequency at which the channel is sampled ϑ_k, the sample size $L_{sam,k}$, and number of channels N_{sam}, the total data rate r_k for a SN k is calculated as:

$$r_k = \vartheta_k \times L_{sam,k} \times N_{sam,k} \tag{2.1}$$

In the case of the EEG sensor $\vartheta_k = 200$ Hz, $L_{sam,k} = 16$ bits, $N_{sam,k} = 2$, and (2.1) gives $r_k = 6400$ bits per second (bps) [70]. In recent years, dual channel EEG sensors have been

prominently featured in BAN research [7], [62], [70] thereby providing assurance the measured physiological signals are reliably processed and interpreted. For example, [62] details the design of a sensor enabled soldier helmet embedded with EEG sensors to detect the effect of bomb blasts on the human brain.

The cardiovascular signals generated by a soldier's heart can be easily measured by ECG sensors with the objective of providing information about the human state while the soldier is at rest or engaged in a variety of physical activities. ECG sensors sample as few as $N_{sam,k} = 2$ channels, each utilizing a sampling frequency of $\vartheta_k = 200$ Hz with approximately $L_{sam,k} = 16$ bits per sample [71]. The overall data rate is therefore $r_k = 6400$ bps. Research on ECG sensors has been performed at the network [72], MAC [73], and physical [74] layers of the BAN. The wealth of research has produced a number of techniques that improve the accuracy of ECG raw data processing, reduce transmission data rate without negatively affecting signal quality, and lower energy consumption.

The measurement of blood pressure can be performed in a non-invasive manner by using the pulse transmit time (PTT) method where the systolic and diastolic blood pressure is computed by concurrently analyzing the photoplethysmogram (PPG) and ECG signals [75]. The PPG sensor (herein referred to as the BP sensor) is typically connected to a subject's earlobe or finger. The PTT method for acquiring blood pressure measurements has been investigated through theoretical analysis [76] and BAN experimentation [77] and has shown to be a highly energy efficient alternative to the conventional bulky and high power yielding blood pressure sensor monitoring cuffs. Blood pressure measurements are calculated based on a PPG sampling rate of $\vartheta_k = 120$ Hz and digitized with $L_{sam,k} = 16$ bits per sample over a single channel $N_{sam,k} = 1$, resulting in a data stream of $r_k = 1920$ bps [71].

Pulse oximeter sensors have been regularly used for a wide array of health monitoring applications in BANs [3], [77]. In military health monitoring applications, the measurement of oxygen delivery using S_PO_2 sensors provides the true extent of metabolic derangement suffered by a soldier during hemorrhagic shock [68]. Studies have shown that knowing the precise time of the hemorrhagic shock and being able to act on it can reduce the number of soldier deaths by up to 25% [68]. Therefore, the use of S_PO_2 sensors is necessary for the monitoring of a soldier's physiological status. Since oxygen saturation levels are related to the heart rate, both red and infrared light absorption are sampled at $\vartheta_k = 60$ Hz and digitized with $L_{sam,k} = 16$ bits per sample over two channels $N_{sam,k} = 2$ giving a total data rate of $r_k = 2 \times 960 = 1920$ bps [71].

Nine degrees of freedom sensors are commonly used to measure a subject's movement. This sensor combines a tri-axial accelerometer, tri-axial magnetometer, and gyroscope to determine the results of physical activity such as how much energy has been expended during a soldier's mission or whether the soldier has fallen or collapsed. The multiple sensors combining to form a single 9DoF sensor device requires a sampling rate of $\vartheta_k = 100$ Hz with a resolution of $L_{sam,k} = 32$ bits per sample over a single channel $N_{sam,k} = 1$ resulting in a subsequent total data rate of $r_k = 3200$ bps [78].

The main parameters for the transmission of the described physiological parameters are summarized in Table 2.1. It should be noted that all mentioned sensors perform continuous monitoring and thus produce a constant bit rate traffic pattern.

TABLE 2.1 PHYSIOLOGICAL PARAMETERS REQUIRED FOR CONTINUOUS SN DATA TRANSMISSION

Sensor Type	Sensor ID	Sample Rate ϑ_k (Hz)	Sample Size $L_{sam,k}$ (bits)	Number of Channels $N_{sam,k}$	Data Rate r_k (bps)
S_PO_2	1	60	16	2	1920
BP	2	120	16	1	1920
$9DoF_1$	3	100	32	1	3200
$9DoF_2$	4	100	32	1	3200
ECG	5	200	16	2	6400
EEG	6	200	16	2	6400

2.3.2 Wireless Technologies to Communicate Physiological Data

In this section, we motivate the design for a single radio interface at the SN device based on the IEEE 802.15.4 standard to facilitate intra-BAN communication and a dual radio interface at the BNC device also based on the IEEE 802.15.4 standard to facilitate inter-BAN communication over the BBN.

Over the past several years, IEEE 802.15.4, primarily designed for low power and low voltage wireless applications in the 2.4 GHz industrial, scientific, and medical (ISM) frequency band, has gained wide acceptance in the wireless networking community. Its use has particularly been resonant in short-range applications considering health monitoring through BANs (e.g., [73], [79], [80]) and longer-range applications considering athletic performance monitoring (e.g., [43]), disaster recovery (e.g., [37]), and remote patient tracking (e.g., [38]) through BAN range extensions. The IEEE 802.15.4 standard is appealing across a wide number of applications due to its supported data rate of 250 kbps, nominal transmission range of 1 to 100 m, effective security mechanisms, low power consumption, and low protocol complexity [81].

As previously mentioned, the main constraints faced by the SN and BNC devices are limited battery power and processing capability. Therefore, the use of the IEEE 802.15.4 standard as the radio interface technology must ameliorate these resource constraints.

Furthermore, the IEEE 802.15.4 standard must demonstrate superior performance to other existing and relevant wireless technologies in terms of energy consumption and protocol complexity. We thus perform a performance comparison between the IEEE 802.15.4 standard and the IEEE 802.15.1 standard (employed in Bluetooth) for suitability as the radio interface for devices in the BAN and a performance comparison between the IEEE 802.15.4 standard and the IEEE 802.11a/b/g standard (employed in Wi-Fi) for suitability as the radio interface for devices in the BBN.

2.3.2.1 Comparison between IEEE 802.15.4 and IEEE 802.15.1

The Bluetooth protocol supported through the IEEE 802.15.1 standard has been long employed for short-range applications involving the wireless connectivity between computer peripherals and the computer, music player and headphone, mobile cellular device and vehicle, etc. Recently, Bluetooth has also found relevance in BAN applications dealing with health monitoring [66], [82] and thus it is a suitable comparison to IEEE 802.15.4. The complexity of the protocols is evaluated in Fig. 2.1 where the number of primitives and host controller interface events are shown for Bluetooth and the number of MAC and physical layer primitives are shown for IEEE 802.15.4. As evidenced by the results, IEEE 802.15.4 has far less complexity than Bluetooth because it employs almost one quarter the number of primitives and events. The results in Fig. 2.1b shows the energy consumption for IEEE 802.15.4 and Bluetooth calculated based on their operating voltages of 3.0 V and 1.8 V, transmitting current consumptions of 8.8 mA and 57 mA, receiving current consumptions of 19.7 mA and 47.7 mA, and maximum data rates of 250 kbps and 720 kbps achieved with the CC2420 and BlueCore2 radio chipsets, respectively [83]-[85]. From Fig. 2.1a, it is seen that IEEE 802.15.4 has a lower complexity than Bluetooth due to the fact that Bluetooth utilizes primitives for client service access point (SAP),

synchronous connection-oriented SAP, and logical link control and adaptation protocol [85]. In Fig. 2.1b, the normalized energy consumption for transmitting in IEEE 802.15.4 is shown to be 26% less than Bluetooth but almost twice as high for receiving. We deem the transmitting activities to be of higher importance for energy consideration in the BBN and BAN because all SNs and BNCs transmit data. On the other hand, SNs do not receive data and the BS device has significantly higher energy capacity than the SNs and BNCs. Based on the results shown in Fig. 2.1, it is justifiable to select the IEEE 802.15.4 standard as a suitable radio interface for devices within the BAN because of its demonstrated simplicity and lower energy transmission consumption.

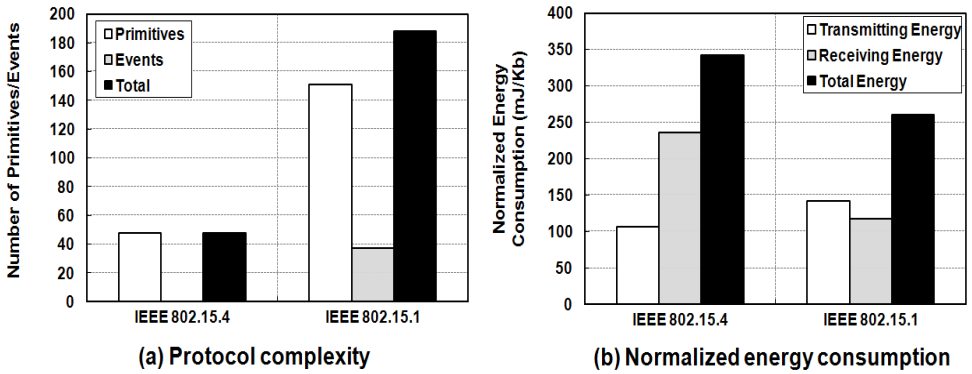

Fig. 2.1. Protocol complexity and energy consumption comparison between IEEE 802.15.4 and IEEE 802.15.1 (Bluetooth).

2.3.2.2 Comparison between IEEE 802.15.4 and IEEE 802.11a/b/g

The IEEE 802.11a/b/g standard, also referred to as Wi-Fi, is commonly employed in mobile ad hoc networks supporting high data rate applications such as video streaming, image processing, and real-time audio. The main benefits offered by Wi-Fi are its maximum data rate of 54 Mbps (802.11a/g), nominal transmission range greater than 100 m (802.11b/g), and strong transmission power between 15 and 20 dBm [85]. The main deterrents to its implementation in

BBNs are high complexity, high idle energy consumption, and severe weaknesses in its offered security mechanisms as discussed in [86]. As a result, we integrate IEEE 802.15.4 into the radio interface of the BBN devices (i.e., the BNC), which also provides for a single radio technology that reduces the complexity of designing energy and QoS aware communications schemes for the BBNs.

2.4 Approaches for Energy and QoS Analysis in BANs

Most of previous research on energy and QoS analysis in BANs have concentrated on the development of communication schemes based on the single protocol layer following the open system interconnection (OSI) reference model set by the International Organization for Standardization (ISO). Decomposing the OSI model into more manageable smaller modules for which the layers can be managed independently, reduces the complexity of the communication scheme development. This decomposition approach, or layered approach, has been often utilized in the literature to achieve energy efficiency and provide QoS for communication schemes serving the BAN and BBN. For example, achieving energy efficiency has been explored through routing in the network layer [16]-[20], scheduling in the MAC layer [21]-[24], and power control in the physical layer [25]-[30]. The integration of QoS into energy efficiency is also seen at the network layer [87]-[90], MAC layer [29], [91] and physical layer [92].

The layered approach offers reduced complexity for communication scheme development. However, experience derived from wireless networking suggests that the performance obtained at a single layer may lead to wrong conclusions for the communication scheme's overall performance [93]. As such, recent research have suggested that the communication scheme's overall performance and its operating efficiency can be improved with the integration of more layers from the OSI model, an approach referred to as cross-layer design.

In the context of networks with energy, resource, and memory constrained devices requiring stringent QoS and energy efficient transmissions such as the SNs and BNCs considered in this thesis, there are two main reasons to incorporate cross-layer design. First, the layered approach suffers from inefficiency due to excessive overhead. Second, the quality of the wireless channel needs to be taken into account in designing higher layer protocols. Consequently, the two reasons serve as motivation to employ a cross-layer approach towards obtaining energy efficiency and QoS. The cross-layer approach is not new per se and work already exists in the literature for BANs and BBNs, where different combinations of the network, MAC, and physical layers have been explored [33], [34], [17]. In this section, we review the works in the literature that use a layered approach and those using a cross-layered approach for communication scheme design.

2.4.1 Layer-Centric Design

2.4.1.1 Network Layer

The network layer is responsible for routing data packets from the source node to the destination node, node addressing, and congestion control. In this thesis, we solely focus on routing because this is the functionality relevant to the problem addressed in the thesis. Specifically, the network layer considers routing at the BAN and BBN levels with an emphasis on achieving minimum energy consumption within certain end-to-end packet success probability and end-to-end delay objectives. Therefore, the network layer is described in terms of routing strategies specified under three categories: single-hop versus multi-hop, energy aware, and QoS aware.

2.4.1.1.1 Intra-BAN Routing: Single-hop versus Multi-hop

Research has shown that the SNs' capability, placement location, movement due to body posture, and functionality have an effect on energy consumption and also factors into whether

single-hop or multi-hop routing is most appropriate within the BAN. In [94], star and multi-hop network topologies are investigated for energy efficiency in BANs. The star topology is a single hop configuration where all SNs transmit to a single sink node such as the BNC. Results suggest that while a star architecture with SNs operating at low power levels might suffice in a cluttered indoor environment, SNs in an outdoor setting will have to operate at higher power levels or revert to a multi-hop architecture to provide for acceptable success probability. An energy efficient topology design considering single-hop and multi-hop routing for SNs placed on the legs, back, torso, arms, and head of a person is evaluated in [34]. Although single-hop routing can minimize energy consumption depending on the distance and body part location of a SN relative to BNC, the authors have shown that the ability to perform multi-hop routing must also be incorporated into the routing scheme when path loss and fading conditions are severe. Furthermore, the designation of RNs along with provisioning chosen nodes the ability to perform cooperative routing may also lead to significant gains in minimizing energy consumption within a BAN. Experimental evaluations are performed in [95] to compare the energy consumption and success probability performance of a single-hop versus multi-hop architecture. Similar to [94], it is found that a singular configuration is not universally acceptable - the configuration is largely dependent on the particular BAN application. However, [95] has determined that multi-hop routing combined with retransmissions has several advantages over single-hop which includes having better network lifetime as well as lower delay and energy consumption.

2.4.1.1.2 Energy Aware Routing Schemes

Energy aware routing schemes implement mechanisms at the network layer to minimize energy consumption for transmissions in the BAN and BBN. In [96], energy efficient transmission strategies invoking energy harvesting is investigated for BANs. A Markov decision

process problem is formulated to determine the transmission that best provides the trade-off between energy consumption and success probability to support objectives such as balanced energy and maximum quality of coverage. The Energy Balanced Rate Assignment and Routing (EBPAR) protocol described in [97] selects routes within the BAN based on the residual energy of SNs and therefore spreads the burden of forwarding data more equally across the other SNs. In [18], a min-max multi-commodity flow model for intra-BAN routing is proposed for minimizing the maximum energy consumption of SNs in the network. Moungla *et al.* deduce that simultaneous criteria for minimum total energy consumption and min-max energy consumption are conflicting criteria for which a good compromise can be achieved by implementing weighting methods. An energy efficient routing protocol referred to as M-ATTEMPT is proposed in [98] to support routing in heterogeneous BANs. The routing scheme implemented in M-ATTEMPT relies on direct communication between the SNs and BNC to support on-demand real-time critical data traffic and multi-hop communication amongst multiple SNs for normal data delivery. M-ATTEMPT is shown to achieve better performance in terms of energy consumption and success probability when compared against routing schemes that only utilize multi-hop communication.

The literature pertaining to minimum energy routing mechanisms has been mostly focused on BANs but seen a steady increase for BBNs over the past 5 years. In [50], an inter-BAN routing strategy incorporating a geographic routing algorithm that leverages the physical layer ranging capability available for UWB communications is proposed for a three-tiered BBN in a hospital environment. The geographic routing algorithm optimizes traffic load and energy consumption at all tiers of the BBN while also intelligently building routing paths based on the class and priority of the data traffic flow. Similar to [50], a Geographic and Energy Aware

Routing (GEAR) protocol is defined in [49] to facilitate routing amongst the multiple tiers organized in the BBN. The energy for each hop is modeled in terms of distance and available residual energy and thus it is purported that minimum energy routes can be achieved by simply selecting routing paths with the lowest distance and highest aggregate residual energy. In [51], an energy minimizing technique for global healthcare monitoring applications is proposed in which three characteristics are analyzed to provide minimum energy routing: distance between BNCs, velocity of the signal transmitted by the BNCs, and the received signal strength.

2.4.1.1.3 QoS Aware Routing Schemes

A heuristic adaptive routing algorithm for energy efficient configuration management is proposed in [99] to reduce energy consumption while guaranteeing QoS for the transmission of emergency data in a BAN. The adaptive algorithm adjusts to the topology changes that occur when the human body is in motion, leading to disconnections between SNs placed on different body parts and the BNC. In [100], the energy efficiency of cooperative communication routing techniques in BANs is investigated under the constraint of a targeted outage probability. Power allocation is combined with postural information to form minimum energy routing paths between SNs and BNC. The data-centric multi-objective QoS-aware routing protocol (DMQoS) proposed in [89] uses a distributed flexible mechanism to optimize QoS and energy in multi-hop BANs based on a modular design architecture which follows several different traffic classes. The different traffic classes represent the different types of SNs used for monitoring health. A lexicographic optimization based approach is employed to tune residual energy levels of the SNs and BNC and provide for energy optimality for intra-BAN routing. Energy efficiency under QoS constraints is achieved for transmissions in the BBN using a number of different techniques. The authors in [101] propose an Energy Efficient and QoS aware multi-path routing (EQSR) protocol

that maximizes network lifetime by balancing energy consumption across multiple BNCs, reduces end-to-end delay by distributing data traffic across multiple paths, and increases network throughput by invoking redundant transmissions. In [102] a multi-objective genetic algorithm based approach for energy efficient routing with QoS support is proposed for two-tiered wireless networks. Optimizations are performed using an elitist non-dominated sorting genetic algorithm to achieve reduced power consumption while also satisfying QoS constraints such as reliability and end-to-end delay.

2.4.1.2 MAC Layer

In recent years, the number of MAC protocols dedicated to operation in BANs has steadily increased, particularly in applications relating to healthcare and remote physiological monitoring. The scheduling of transmissions using schemes such as Time Division Multiple Access (TDMA) and the slotted mode of IEEE 802.15.4 are particularly appealing in BANs because low delay transmissions can be guaranteed through unique slot assignment. To this end, we provide a brief review on the TDMA and IEEE 802.15.4 schemes employed in BANs for healthcare and remote monitoring of physiological state applications.

2.4.1.2.1 IEEE 802.15.4 Protocol based Schemes

A large number of MAC protocols employed in BANs are based on the IEEE 802.15.4 standard for communication in the 2.4 GHz frequency spectrum. The IEEE 802.15.4 MAC protocol can operate in a beacon enabled or beaconless mode and has support for scheduling guaranteed time slots in the contention free period window. In the beaconless mode, IEEE 802.15.4 employ slotted Carrier Sense Multiple Access Collision Avoidance (CSMA-CA) where back-off mechanisms and a contention window are used for medium access. In the beacon enabled mode, a designated network coordinator periodically transmits synchronization and

network association beacons at regular time intervals. Guaranteed time slots are of high interest because it has been shown to provide low end-to-end packet delay [79]. In [73], Liang *et al.* investigate the suitability of IEEE 802.15.4 for scheduling in an ECG based BAN. It is found that transmissions should be performed with small payload sizes between 40 and 60 bytes in order to obtain low end-to-end latency and high success probability using IEEE 802.15.4. Results in [103] demonstrate the ability of IEEE 802.15.4 to guarantee data delivery within defined time constraints with 100% compliance in both contention-based and contention-free scenarios when accommodating in excess of 10 BAN data traffic streams from heterogeneous SNs. The different access schemes of IEEE 802.15.4 are evaluated in [80] and it is shown that the contention based beaconless mode offers better performance than the contention free slotted mode in terms of throughput and latency, but at the cost of higher energy consumption.

2.4.1.2.2 TDMA MAC Schemes

A unique approach towards TDMA scheme design is proposed in [33] for BAN monitoring in wireless healthcare applications. A battery-aware TDMA MAC protocol jointly takes into account the effect of electrochemical properties of the battery, time-varying wireless channels, and packet queuing characteristics to prolong the battery lifespan of SNs while guaranteeing reliable and timely message delivery. Performance analysis based on a case study of ECG monitoring applications shows the proposed scheme outperforms IEEE 802.15.4 in terms of battery lifespan while also meeting specified delay requirements. The BodyMAC protocol proposed in [23] is an energy efficient TDMA-based MAC protocol for BANs. BodyMAC defines an adaptive and flexible TDMA frame structure to provide a more efficient sleep mode. BodyMAC also introduces three bandwidth management schemes tasked with dealing with different types of data communications such as periodic data sensing and important

event reporting. The flexibility of utilizing these three schemes improves the efficiency of the MAC control packet transmission. Performance comparisons against the IEEE 802.15.4 MAC shows it offers superior performance in terms of end-to-end packet delay and energy savings. Reference [22] offers another energy efficient TDMA protocol which implements a TDMA scheme with very little communication overhead, long sleep times for SN transceivers, and robustness to communication errors. Robustness to communication errors is achieved by introducing redundancy in the form of unused time slots that can be used for retransmission. Minimized communication overhead is achieved by using a predetermined slot assignment strategy predicated on knowing the capabilities and functionality of the heterogeneous SNs.

2.4.1.3 Physical Layer

A realistic physical layer model for the BAN and BBN considers the path loss and fading characteristics in addition to the modulation schemes used for transmission. The wireless channel model considered for the BAN must account for the wireless communication which occurs around and along the human body whereas the wireless channel model considered for the BBN must account for the radio frequency (RF) communication between bodies in outdoor environments. In this section, we place our focus on the physical layer of the BAN. Channel characterization of outdoor environments can be found in references [9] – [11].

Research in [34] verifies the oft-cited log-distance path loss model can be used to determine the path loss for transmissions occurring between nodes residing on the body. However, the path loss parameters used in the log-distance path loss model are heavily influenced by the positions and locations of the transmitters and receivers. For example, the path loss exponent for RF propagation emanating from a body's posterior (i.e., the back) and terminating at the frontal position of the body (e.g., torso) is almost double what the path loss

exponent would be for RF propagation along the torso of a body [34]. The difference in path loss exponent is mainly attributable to transmissions travelling along NLOS paths versus transmissions traveling along LOS paths. The propagation of electromagnetic waves through the human body has also been investigated [34]. The human body acts as a communication channel where transmission losses are attributable to the absorption of power in human tissue later dissipated as heat. The human tissue mostly consists of water and is also lossy resulting in a significantly attenuated transmitted signal by the time it is received at the destination. The movement of the body also plays an important role in the strength of the received signal. Experiments performed in [8], [10] have shown that bodily movements such as arm movement can reduce the received signal strength and cause obstructions along otherwise LOS paths. Another feature of the body that influences the fading characteristics of the wireless channel is body curvature. Small-scale fading is experienced for transmissions in the on-body wireless channel because bodily movements transform paths which were previously LOS to NLOS paths due to shadowing from different body parts.

Radio transmissions in BANs predominantly take place in the licensed 2.4 GHz ISM band. Chipcon's CC2420 radio is the most commonly adopted transceiver in the literature [83]. It uses offset quadrature phase shift keying (OQPSK) for the modulation of transmitted data. Performance metrics such as BER are calculated with knowledge of the modulation scheme and fading distribution. The BER calculations determine whether power control mechanisms are required to increase or decrease power transmission levels in an effort to minimize energy consumption while also adhering to QoS requirements. Several power control schemes have been proposed in the literature for BANs. Empirical evidence is presented in [30] to justify the need for adaptive transmission power control due to the rapidly changing wireless link quality in

BANs. Transmission with fixed transmit power either results in wasted energy when the link quality is good or low reliability when the link quality is poor. A set of power control schemes feasible for practical implementation is also presented in [30]. These schemes adaptively change the transmit power based on feedback from a receiver. Depending on the operating environment and chosen application, the parameters fed into the power control schemes are tuned to achieve a desired trade-off between energy savings and reliability. A robust protocol stack for multi-hop BANs with transmit power adaptation is proposed in [53]. The protocol is especially robust against frequent changes in network topology due to postural movements and wireless link quality variability. A novel technique for adapting the transmit power of SNs is implemented at run-time to optimize energy consumption while ensuring a reliable outgoing link in the BAN and minimize the prevalence of network disconnections.

2.4.2 Cross-Layer-Centric Design

The implementation of cross-layer design has yielded improved performance in energy constrained networks such as wireless sensor networks (WSNs) and MANETs in terms of achieving energy efficient routing [105], minimum delay scheduling [106], and QoS-aware power control [107]. Cross-layer design is not yet as prevalent in BANs but its use is growing. In [34], a cross-layer design combining topology information from the network layer and on-body wireless propagation characteristics from the physical layer of a BAN are obtained to determine an energy optimal network topology. Cross-layer optimization is employed in [17] to guarantee energy efficient data streaming in BANs by jointly considering routing information at the network layer and bandwidth allocation at the MAC layer. In [33], the battery lifespan of SNs is prolonged by employing a unique cross-layer design that jointly accounts for the electrochemical properties of a battery, wireless physical channels, and packet queuing characteristics. This

design lends focus to the MAC and physical layers while also satisfying QoS requirements such as reliability and delay. In [108], a cross-layer judgment scheme is proposed to solve the retransmission problem in IEEE 802.15.4 based BANs. The reasons for failed transmissions are rendered by analyzing the MAC layer for collisions and the physical layer for deleterious fading conditions.

2.5 Thesis Work in the Context of Existing Work

In this section, we briefly review and compare the related work in the literature to the work performed in this thesis. Specifically, we are interested in works towards energy and QoS aware communication schemes for BBN connected BANs.

2.5.1 Energy Efficiency and QoS Support for Communication Schemes in BANs

2.5.1.1 Review of Related Work

In [53], an adaptive transmission power control scheme is coupled with multi-hop routing with the motivation of achieving minimum energy in BANs while meeting a specified PER requirement. A mobility model based on postural movements is developed in order to accurately model real-life mobility scenarios. The postural movements are specifically modeled using a Markov process with transition probabilities to represent different postures such as walking, running, standing, sitting, and lying. Multi-hop routing for energy savings is also explored in [16]. The authors integrate multi-hop routing with a data aggregation technique that buffers a SN's data and combines incoming transmission data from other SNs until a data packet of maximum packet size can be transmitted. This approach is motivated by the work in [109] where it is shown that larger data packets consume less transmission energy per bit than smaller data packets. However, this observation may not hold for reliability constrained transmissions. Selecting the multi-hop path requiring the least energy consumption is formulated as an NP-hard

(non-polynomial hard) minimum concave cost multi-commodity flow problem and solved using heuristic methods. The proposed approach of maximizing the amount of data sharing amongst routing paths through data aggregation and multi-hop routing is compared against a shortest-path algorithm and shown to provide considerable energy savings. The analysis performed in [16] is mostly concerned with the network layer and thus does not consider how data aggregation techniques would fair when physical layer impairments are present. The effect of optimal packet size and different error control schemes such as automatic repeat request (ARQ), forward error correction (FEC) block codes, and FEC convolutional codes on energy efficiency is addressed in [54]. The analysis incorporates a simplified power consumption model to determine energy consumption, binary phase shift keying (BPSK) modulation to calculate BER, and error codes combined with a mobility-induced Rayleigh fading channel to determine PER. Forward error correcting schemes are exploited to improve energy efficiency, increase optimal payload size, and extend the effective transmission range for SNs communicating along the on-body wireless channel. A Minimum Energy Packet Forwarding Protocol (MEPF) is proposed in [17] based on the energy consumption trade-off analysis between lower transmission power and packet retransmissions. A transmission power control algorithm is employed to calculate the minimum transmission power required to guarantee a desired PER. Different from the existing literature, the transmission power for acknowledgement (ACK) packets is also optimized to obtain energy savings.

Three energy efficient transmission strategies exploiting energy harvesting are designed in [96]. Decision policies are developed to determine which transmission strategy to enact at any given instant in order to maximize quality of coverage (i.e., balance energy consumption). The caveat is that a trade-off exists between energy consumption and PER depending on the chosen

policy. The problem is formulated as a Markov decision process and the chosen decision policy is shown to provide good performance in terms of energy balancing. Maximum lifetime for a BAN is achieved in [97] by minimizing the maximum energy consumption of SNs in the network and maximizing route reliability. The problem is formulated as a min-max multi-commodity flow problem and solved using a branch-and-bound algorithm. A heuristic algorithm called Fast Path Selection Scheme is developed in [19] to reduce and balance energy consumption while also guaranteeing low delay. Successful routing between SNs is tied to the current posture assumed by the body and is simply represented by a Boolean variable. Network coding is implemented in a BAN for reliable and energy efficient transmission in [20]. Assuming the different channel conditions experienced by the SNs can be accurately predicted, the BNC can request each SN to send the optimal number of coded packets which lowers energy expenditure. Network coding is determined to be beneficial in the scenario where the energy associated with receiving is higher than that of transmitting, such as is the case in SN and BNC devices employing the CC2420 radio.

The energy efficiency of single relay and multiple relay cooperative communication is investigated in [100] under the QoS constraint of outage probability. The analysis incorporates postural inference to determine the small-scale fading between two points in the BAN. The authors jointly consider power allocation with posture state information to achieve energy efficiency for a given outage probability. For the single and multiple relay cooperative transmissions, two orthogonal timeslots are assigned to the source node and a pre-defined single relay or an optimal relay chosen amongst multiple possible relays. The transmitter and circuit energy components are included in the energy consumption model to provide for an accurate energy consumption analysis of the cooperative communication schemes and direct

communication scheme. The results show single relay and multiple relay cooperative communication is more energy efficient than direct communication, only under certain circumstances when the path loss between a transmission pair is higher than a defined threshold.

The placement of dedicated RNs around the body has found benefits for BANs in terms of increasing network lifetime. The implementation of a dedicated relay network in conjunction with a BAN is shown to considerably reduce energy consumption in [110] when compared against a single-hop and multi-hop communication scheme. The number of deployed RNs is continually increased until energy benefits are no longer attained. In [111], the optimal number and location of RNs required to minimize the installation cost and the energy consumed by SNs and RNs in a BAN is determined by solving a minimum energy multi-commodity flow optimization problem constrained by network flow requirements. A weighting parameter biasing the optimization problem towards installation cost minimization or energy minimization is new and novel.

2.5.1.2 Similarities between Related Work and Thesis Research

The key concern for designing communication schemes for intra-BAN transmission is minimum energy under the constraint of high success probability and low delay. Energy efficiency with consideration for the QoS constraints is attained by employing techniques similar to that in the literature.

- *Similarity #1*: To guarantee high success probability where the minimum transmission power is chosen to support the required reliability constraint, we adopt a transmission power scheme similar to [53] and [55].
- *Similarity #2*: The proposed EQS and EQX communication schemes employ data aggregation techniques at the SNs and BNC similar to [16].

- *Similarity #3*: In addition to transmit power, our communication schemes optimize the number of retransmissions and the packet size per transmission similar to the work in [17] and [54], respectively.
- *Similarity #4*: The analysis of network flow within the BAN is typically performed assuming a TDMA based MAC layer because of its analytical tractability. Similar to [16], [17], [18], [53] and [97], we also assume TDMA and the use of slotted transmissions in order to minimize energy consumption and ensure stable network flow.

2.5.1.3 Differences between Related Work and Thesis Research

The work performed in this thesis for energy efficient BAN communication can be distinguished from the literature in six main aspects:

- *Difference #1*: Our analysis for energy consumption in BANs makes use of a detailed power consumption model that incorporates the power attributable to transmitter and receiver circuitry in addition to the power attributed to the non-linear power amplifier expressed as a function of transmission power. The literature typically either assumes the power consumption from the amplifier to be absent [16], [17], [96] a fixed value [20], [54] [100], or a function of the transmitted data bits [18], [110], [111]. As a result, the power consumption models commonly used in the literature do not accurately model energy consumption which negatively impacts the composition of routing paths and transmission schedules.
- *Difference #2:* Our work jointly optimizes transmission power, retransmission limit, and packet size to achieve minimum energy consumption. To the best of the author's knowledge, this approach towards energy efficiency has not yet been used in the literature. The novelty in this approach is that energy savings can be attained under stringent reliability constraints by balancing the contributions of the aforementioned transmission parameters.

- *Difference #3:* The cross-layer optimization framework defined in Chapters 3 and 4 jointly considers flow control at the network layer, retransmissions and transmission stability at the MAC layer, and BER models at the physical layer to obtain energy efficiency under reliability and delay constraints for multiple SNs with variable data rates. Cross-layer optimization has been used in [31] to achieve energy efficiency but the model only focuses on routing in the network layer and bandwidth allocation in the MAC layer and thus does not lend any concern towards QoS metrics such as reliability and delay which are vital to remote physiological monitoring. The cross-layer optimization model employed in this thesis provides a singular and comprehensive framework for which the minimum energy consumption for a BAN can be determined with feedback from the three considered layers as opposed to just a single or combination of two layers.
- *Difference #4:* We introduce an adaptive transmission scheme that exploits the synergistic cooperation between the SNs and BNC to optimally select the minimum relative energy cost route for a SN. Since the battery capacities and energy consumption rates of the SNs and BNC are different, it is necessary to determine, based on a SN's and its BNC's residual energy level and the path loss and fading characteristics of the on-body and body-to-body channels, whether it is more cost effective for a SN to transmit directly to a neighboring node (i.e., neighboring BAN's BNC or BS) or to its own BNC which has a higher transmission range. This strategy encourages minimized relative energy cost and differs from the restrictive intra-BAN routing approaches used in [96], [97] and [99].
- *Difference #5:* The modeling of fading for energy efficient transmissions in BANs is sparse in the literature. The work in [53] has modeled postural inference to dictate the probability of connection and disconnection between two nodes in BAN, but fails to consider the effects of

small-scale fading. Small-scale fading has a measurable effect on the energy consumption of QoS-constrained transmissions within BANs. The treatment of small-scale fading using the Nakagami-*m* distribution as recommended in [8] and [10] is integral to the energy and QoS (in terms of calculating success probability) analysis in this thesis and also offers an original approach towards analyzing energy consumption in BANs.

- *Difference #6*: Accounting for both success probability and delay as QoS metrics in unison with energy consumption is an important feature that separates the BAN performance analysis performed in this thesis from the literature.

A summary of the related works is provided in Table 2.2 in terms of the research's main objective (e.g., minimize energy, maximize network lifetime, etc.), the design approach taken (layer-centric or cross-layer), the considered QoS metrics, the fading model, and the key approach utilized to achieve the objective. The abbreviations NTW and PHY denote network layer and physical layer, respectively.

TABLE 2.2 SUMMARY OF RELATED WORKS FOR ENERGY EFFICIENCY AND QOS SUPPORT IN BANS

Referenced Research	Objective	Protocol Layers	QoS Metrics	Fading Model	Key Approach
Nabi *et al.* [53]	Minimum Energy	NTW, MAC, PHY	Reliability	None	Adaptive transmit power control (ATPC)
Ghasemzadeh *et al.* [16]	Minimum Energy	NTW	None	None	Data Aggregation
Domingo *et al.* [54]	Minimum Energy	NTW, PHY	Reliability	Rayleigh	Optimal Packet Size
Guo *et al.* [17]	Minimum Energy	NTW	Reliability	None	ATPC with Retransmissions
Seyedi *et al.* [96]	Maximum Lifetime	NTW & PHY	Reliability	None	Energy Harvesting
Moungla *et al.* [18]	Maximum Lifetime	NTW	Reliability	None	Min-Max Multi-Commodity Model
Seo *et al.* [19]	Maximum Lifetime	NTW	Delay	None	Adaptive Routing Algorithm
Shi *et al.* [20]	Minimum Energy	NTW	Reliability	None	Network Coding
Huang *et al.* [100]	Minimum Energy	NTW, PHY	Outage	Lognormal	Cooperative Communication
Braem *et al.* [55]	Minimum Energy & Maximum Reliability	NTW, MAC, PHY	Reliability	Lognormal	Multi-hop Routing and ATPC
Elias *et al.* [111]	Minimum Energy	NTW	None	None	Optimal Relay Deployment
Thesis Sections: 3.3, 3.4	Minimum Relative Energy Cost	NTW, MAC, PHY	Reliability and Delay	Nakagami	Adaptive Transmission Scheme and JPRS Strategy

2.5.2 Energy Efficiency and QoS Support for Communication Schemes in Multi-hop Networks

2.5.2.1 Review of Related Work

An analytical framework is derived in [112] to evaluate the trade-off between energy efficiency and responsiveness during a neighbor discovery process. The neighbor discovery process is initiated by a hunting process where short messages are broadcast to advertise a node's presence and followed by a discovery process where the best relay node is selected for routing. On one hand, the longer the time spent in the hunting process, the shorter the time required for discovering new neighbors. On the other hand, more time in the hunting process leads to increased energy consumption due to higher signaling. Therefore, the design of an energy efficient and minimum responsive neighbor discovery process is necessary. A detailed assessment of passive discovery strategies for IEEE 802.15.4 enabled BANs is performed in [113]. Willig *et al.* propose cost optimal and success probability optimal discovery strategies and determine the success probability optimal discovery strategy incurs far higher cost than the cost optimal strategy whereas the cost optimal strategy achieves lower cost and just as high success probability. As a result, the cost optimal strategy is purported to be more desirable for cost constrained BBNs where multiple BANs coexist. The design of an energy efficient network topology supporting QoS constraints is addressed in [114]. The objective is to build a network topology so that the transmission power of nodes is minimized, traffic load is balanced amongst nodes, and the delay along links is less than a maximum delay bound. The problem is formulated as a mixed integer-programming problem and solved using a heuristic greedy approach called Least Power First (LPF) algorithm. In LPF, the transmission power along links with the shortest distance to the sink is gradually incremented until a complete routing tree with satisfied QoS requirements is constructed. Minimum energy routes are created in [115] using a cross-layer

optimization approach which jointly configures the transmission power for each transmitting node and the retransmission limit over each hop. Different from [112] and [114], [115] considers the reliability and delay constraints, which makes the optimization problem a mixed integer non-linear problem (MINLP). To meet the reliability constraint, the automatic repeat request mechanism is invoked where retransmissions are continuously performed until the desired reliability is met. However, the number of retransmissions is bounded to satisfy a delay constraint. A cross-layer method for the joint design of scheduling and power control in wireless ad hoc networks is presented in [116]. Two problems referred to as "divergence" and "transmit-receive collision" are said to directly affect energy efficiency. The transmit-receive collision problem is inherent of TDMA/code-division multiple access (TDMA/CDMA) systems, occurring when a node simultaneously receives and transmits a packet. This problem is resolved using a distributed scheduling algorithm which supports multiple packet receptions where multiple nodes can simultaneously transmit to one another without collision by making adjustments to the request-to-send (RTS) and clear-to-send (CTS) control packets. An iterative power control algorithm is proposed to resolve the divergence problem that occurs when a power control algorithm assumes a constant SINR target and cannot increment the power level high enough to overcome bad channel conditions. An adaptive SINR target is implemented in the power control algorithm preventing wasteful energy consumption during the adjustment of the transmission power under varying channel conditions. As a result, high energy efficiency under QoS constraints is achieved.

In [117], link reliability, link quality, and energy consumption are studied as three key elements to designing an energy and QoS aware communication scheme. A link availability metric is defined to probabilistically predict the connectivity duration for two nodes in order to

achieve a certain level of link reliability. The ETX (Expected Transmissions) metric is used to measure link quality in [118]. It estimates the number of retransmissions required to successfully transmit packets by measuring the packet loss rate on a link using probe packets. Energy consumption is calculated in terms of the energy for receiving, transmitting, and idling, but no power control scheme is assumed. A weighted link stability metric consisting of energy consumption, link unavailability, and route quality is then used as the cost routing metric for building routing paths. The link stability metric is shown to offer good performance in terms of low delay in highly mobile scenarios. Similar to [118], link stability is the main focus of the work performed in [119]. A multi-objective optimization model is proposed to simultaneously minimize energy consumption and maximize link stability when selecting paths for individual transmissions. Given the exponential complexity associated with solving a bi-objective integer program, a Link-stAbility and Energy aware Routing (LAER) protocol integrating a joint energy-stability metric is proposed. The LAER protocol adopts a greedy forwarding strategy based on local topology knowledge derived from a combined Euclidean distance based forwarding and joint energy-stability metric to select the next hop along a routing path. Performance results show LAER achieves high reliability, lower energy consumption, and longer lasting links, when compared against other similar routing schemes.

Minimum energy neighbor discovery, routing paths, scheduling, and network topology are the focus of [120] – [122]. The authors in [120] address minimum energy routing from the perspective of providing low routing overhead, fast route setup time, and route maintenance through the proposal of the Progressive Energy Efficient Routing (PEER) protocol. The novelty of PEER is minimum energy routing paths are populated in a distributed manner using a new link cost metric which more accurately tracks energy consumption due to factors such as traffic

load and link conditions by incorporating transmission power, RTS and CTS packets, and packet error rates. A timer is implemented for the route discovery process to limit the amount of routing overhead while also discovering the path with the lowest energy consumption. In the route maintenance phase *insert*, *remove*, and *replace* policies are invoked to minimize the number of out-of-date or non-performance improving routes stored in the memory of a resource constrained node. Performance results indicate PEER is highly effective in terms of providing energy efficient transmission in scenarios having different network density and data traffic rates. In [121], the presence of powerful nodes, such as the BS referenced in this thesis, is exploited to provide energy conservation while considering end-to-end delay and success probability using a cross-layer framework called Device-Energy-Load Aware Relaying (DELAR). DELAR is designed utilizing power-aware routing, transmission scheduling and power control. The power-aware routing scheme jointly considers a node's residual energy, traffic load, and proximity to a powerful node to perform routing. The transmission scheduling mechanism uses the concept of asymmetric MAC to support MAC layer acknowledgements and multi-packet transmissions to alleviate high transmission delay. Since the transmission power along a forward routing path can be different than a reverse routing path due to the assumption of asymmetry, the asymmetric MAC uses a reverse routing path created by the power-aware routing algorithm at the physical layer, which then permits reliable relay of acknowledgement packets from the receiver to sender. Multi-packet transmissions are similar to packet aggregation where the data packets for two intended receivers are packed into a single packet reducing the number of transmissions from two to one and, subsequently, reducing the transmission delay. When a low number of powerful nodes are considered, DELAR achieves a measureable performance improvement over similar protocols in terms of energy consumption and reliability under different traffic load conditions.

However, the trade-off is increased delay. In [122], Reliable Minimum Energy Cost Routing (RMECR) and Reliable Minimum Energy Routing (RMER) are proposed for the purpose of prolonging network lifetime and minimizing energy, respectively, in ad hoc networks. The energy analysis performed in [122] is differentiated from other work by considering an energy consumption model that accounts for transmitter circuitry, receiver circuitry, and the power amplifier, which makes the analysis more realistic and closer to practical implementations. Lack of consideration for these power components can lead to the underestimation of energy consumption. As part of RMECR and RMER, hop-by-hop retransmission is supported by the MAC layer to increase packet transmission reliability over wireless links. Similar to [121], the energy attributed to acknowledgements is considered. Specifically, the impact of acknowledgement packets on the energy cost of routes is studied in both hop-by-hop and end-to-end configurations, and shown to factor significantly in the total energy consumption. For RMER, the PER along a link must be known in order to determine the energy cost of that link. The PER is determined using a link quality estimation method where the size of a packet (i.e., either an ACK or data packet) is estimated. The accuracy of the estimate relative to the actual packet size determines how accurate the PER estimate actually is. A number of beacons are exchanged between neighboring nodes to determine the minimum transmission power required for nodes to also obtain reliable packet transmission.

The problem of optimally allocating resources to BANs to enable pervasive health monitoring is addressed via two resource optimization problems in [46]. In the first problem, the source rate at each SN is optimized to minimize rate fluctuations and provide uninterrupted monitoring service. The optimal source rates derived in the first problem are used as inputs to the second problem where the transmission power and transmission rate at each BNC is optimized to

guarantee data delivery under specific QoS requirements. The joint optimization technique improves overall system performance in terms of providing high quality and uninterrupted health monitoring. In [45], a remote patient monitoring service is designed by providing users a multi-tiered e-Health (electronic health) service through the deployment of BANs that collected physiological data and heterogeneous wireless access networks that forward that data to a central server for further analysis. The main problem solved in [45] is the optimal number of wireless connections (to transmit collected physiological data to an access point) required to minimize network access cost while satisfying different QoS requirements. The decision of whether or not to connect to a particular wireless access network, modeled as a constrained Markov decision process, is made in a distributed fashion at each BAN. The multi-tiered system architecture and optimization of connections is said to provide flexible and cost-effective health monitoring for remote patients.

2.5.2.2 Similarities between Related Work and Thesis Research

Seven main similarities can be identified between the related work summarized in Table 2.3 and our work:

- *Similarity #1*: A comprehensive modeling of all components leading to a realistic energy consumption model is only considered in [122], which is the same treatment we provide for the transmissions over the multi-hop BBN in this thesis.
- *Similarity #2*: We consider the optimization of transmit power, retransmission limit, and packet as is also done in [122].
- *Similarity #3*: The minimum relative energy cost solutions derived for the EQS and EQX communication schemes are solved using reduced search algorithms that simultaneously optimize multiple decisions variables. The structure of these algorithms is similar to [123]

where the minimum transmission power required to achieve minimum power consumption under a desired PER constraint is obtained for a cooperative communication scheme.

- *Similarity #4*: The composition of the cross-layer optimization models formulated in Chapters 3 and 4 to achieve minimum energy consumption under QoS constraints jointly integrate features from the network, MAC, and physical layers in the same manner as [105] and [123].
- *Similarity #5*: The incorporation of incremental gain ratios in the BBN multi-constrained power allocation algorithm proposed in Chapter 4 to incrementally adjust the transmit power or retransmission limit along a link follows the same concept employed in [105] where incremental gain ratios are defined specifically for the increase in transmit power and increase in retransmission limit.
- *Similarity #6*: The criteria for slot reuse described in [106] are also enforced in the BBN slot scheduling algorithm proposed in Chapter 4.
- *Similarity #7*: The route storing policies implemented in [120] are similar to those used in the EQD communication scheme.

2.5.2.3 Differences between Related Work and Thesis Research

The work in this thesis towards developing energy and QoS aware communication schemes for multi-hop BBNs has the following differences from the literature:

- *Difference #1*: The work reported in [122] investigates the individual effect of optimizing transmit power, retransmission limit, and packet size on energy performance whereas we jointly optimize the three parameters to amass greater performance benefits.
- *Difference #2*: Reliability is a central metric to the operation of each of the reliability aware routing, multi-constrained power allocation, and scheduling algorithms proposed for the

EQX communication scheme. Algorithms in the literature are usually only designed to support the reliability metric for routing [119], routing and scheduling [115], [120], [122], or scheduling and resource allocation [116]. Therefore, the integration of reliability in all relevant layers considered in this thesis is different from the literature.

- *Difference #3*: Immediate single hop information is usually employed to determine the next hop nodes necessary to provide minimum energy routing paths. In this thesis, we propose a novel route prediction scheme based on the distance between a BNC and a neighboring BNC serving as a potential next hop relay node and the distance from the potential relay node to the BS, to determine the most probable path for attaining a minimum relative energy cost route adhering to a specific end-to-end reliability objective.
- *Difference #4*: In the BBN multi-constrained power allocation algorithm, an incremental gain ratio is individually defined for transmit power, retransmission limit, and packet size. Different from [105], the incremental gain ratio computes the obtained increase in success probability and the required increase in energy consumption when the transmit power and retransmission limit are increased and when the packet size is decreased. The incremental gain ratio providing the highest performance improvement then determines which of transmit power, retransmission limit, or packet size is incremented during each iteration of the BBN multi-constrained power allocation algorithm.
- *Difference #5*: The proposed multi-receive policy invoked along routing paths in the multi-hop BBN consisting of successive relay nodes is different from the typical cooperative communication scheme adopted in [123]. The multi-receive policy achieves reductions in relative energy cost and delay while also increasing success probability without the requirement for a diversity combiner at the receiver.

- *Difference #6*: Taking the limited memory size of SNs and BNCs into account, we analytically determine the maximum number of routing table entries required to maintain a minimum end-to-end relative energy cost route to the BS if a conventional distributed routing protocol with energy and QoS awareness were to be utilized. We define a new route storing policy that significantly limits the number of stored routes in the routing table, reduces the amount of control traffic exchanged between neighboring nodes, and reduces route setup time. The route storing policy permits a certain number of routing table entries based on the value of the reliability objective. A summary of the related works is presented in Table 2.3.

TABLE 2.3 SUMMARY OF RELATED WORKS FOR ENERGY EFFICIENCY AND QOS SUPPORT IN MULTI-HOP NETWORKS

Referenced Research	Objective	Protocol Layers	QoS Metrics	Fading Model	Decision Making	Key Approach
He *et al.* [46]	Sustainable service	MAC, PHY	Reliability and Delay	None	Centralized	Multi-tier Resource Allocation
Vazifehdan *et al.* [122]	Minimum Relative Energy Cost	NTW, MAC, PHY	Reliability	Rayleigh	Centralized	Energy & Battery Aware Routing
Galluccuio *et al.* [112]	Minimum Energy	NTW	Delay	None	Centralized	Neighbor Discovery
Liu *et al.* [114]	Minimum Energy	NTW	Delay	None	Centralized	Topology Control
Yang *et al.* [115]	Minimum Energy	NTW, MAC	Reliability and Delay	Rayleigh	Centralized	Route Configuration
Huang *et al.* [116]	Minimum Energy	MAC, PHY	Reliability	Rayleigh	Distributed	ATPC and Scheduling
Yu *et al.* [117]	Link Stability	NTW	Delay	None	Distributed	Link Stability Metric
Zhu *et al.* [120]	Minimum Energy	NTW, MAC	Reliability	None	Distributed	Route Maintenance
Liu *et al.* [121]	Minimum Energy	NTW, MAC, PHY	Delay	None	Distributed	Scheduling
De Rango *et al.* [119]	Minimum Energy and Link Stability	NTW	Reliability	None	Distributed	Energy-Stability Metric
Thesis Sections: 4.4.3, 4.4.4, 4.4.5	Minimum Relative Energy Cost	NTW, MAC, PHY	Reliability and Delay	Nakagami	Centralized	EQX: Heuristic Energy and QoS Aware Algorithms
Thesis Sections: 5.3.3, 5.3.5	Minimum Relative Energy Cost	NTW, MAC, PHY	Reliability and Delay	Nakagami	Distributed	EQD: Multi-Receive Policy and Route Storing Strategy

2.5.3 Interference amongst Co-located BANs

Closely co-located BANs pose potential interference issues due to its negative impact on guaranteeing the QoS requirements for end-to-end transmissions. In this section, we review work related to inter-BAN interference and mitigation techniques.

2.5.3.1 Review of Related Work

The authors in [29] investigate three classic multiple access schemes, namely code division multiple access (CDMA), frequency division multiple access (FDMA), and TDMA as most suitable for BAN co-existence. Amongst the compared schemes, TDMA requires the simplest implementation and achieves the highest success probability as the number of interfering BANs increase. In [28], a distributed power control strategy based on game theory is devised to determine when to transmit and how much power to use for intra-BAN transmissions while maximizing network utility (i.e., high overall throughput), minimizing energy consumption, and avoiding interference. Quality of service metrics and transmission impairments due to fading are not considered. Therefore, the implication of lowering transmission power on the ability to support QoS requires further investigation. In [27], the interference mitigation problem is formulated in the same manner as [28]. However, the power controller in [27] is modified to use reinforcement learning. Since reinforcement learning based solutions suffer from dimensionality and state space issues due to the presence of continuous variables, radial based function approximators are introduced to reduce the complexity of the learning process. Simulation results show that the reinforcement learning approach provides significant savings in energy consumption when compared against the game theoretic approach. The work performed in [26] investigates the minimum distance between BANs providing for a SINR above a desired threshold so as not to impair transmissions. An analytical framework is proposed in which the

mean and variance of the total interference contributed from co-located BANs is calculated and a Gamma distribution is used to model the approximate distribution of the total interference. In [124], inter-BAN interference mitigation techniques are suggested based on the maximum number of tolerable co-located BANs and the reliability requirement. The three main suggestions for inter-BAN interference mitigation are minimizing transmission probability, optimal scheduling to prevent transmission overlap, and adaptive transmission power control.

2.5.3.2 Similarities between Related Work and Thesis Research

Adaptive power control schemes where the transmission power is lowered to mitigate the adverse effects of interference have been employed in [27], [28], and also in our work.

2.5.3.3 Differences between Related Work and Thesis Research

Our work is different from the literature in two main regards.

- *Difference #1*: We quantify the amount of energy required to overcome interference while concurrently satisfying reliability and delay constraints. Our interference mitigation approach is an original technique that minimizes the transmission power level to minimize interference and then compensates for the decrease in success probability caused by the reduced transmit power level by increasing the number of retransmissions and lowering packet size. Most of the literature does not consider any QoS metrics in regards to inter-BAN interference while [124] only measures the resulting reliability as a function of different transmission power levels.
- *Difference #2*: We design a slot assignment algorithm that jointly considers slot reuse, interference, energy consumption, delay, and reliability. To the best of the author's knowledge, an interference-mitigating algorithm concurrently evaluating the five aforementioned characteristics has not yet been proposed in the literature.

TABLE 2.4 SUMMARY OF RELATED WORKS FOR INTERFERENCE AMONGST CO-LOCATED BANS

Referenced Research	Objective	Protocol Layers	QoS Metrics	Fading Model	Key Approach
Fang *et al.* [28]	Maximum Utility	NTW, PHY	None	None	Game Theory
Kazemi *et al.* [27]	Maximum Utility	NTW, MAC	None	None	Reinforcement Learning
Wang *et al.* [26]	Balanced SINR	PHY	None	None	Geometrical Probability Model and Interference Distribution Model
Sun *et al.* [124]	Interference Mitigation	PHY	Reliability	None	Power, SINR, & BER Analysis
Thesis: Section 4.4.5	Slot Reuse and Interference Mitigation	NTW, MAC, PHY	Reliability and Delay	Nakagami	Energy Efficient Interference Mitigation for Minimum Delay and Reliability Preservation

2.5.4 Analog Network Coded Cooperative Communication for Relay Schemes

Analog network coding is the physical layer alternative to the digital network coding performed at the network layer. The benefits of ANC are discussed in the seminal paper written by Katti *et al.* [125] and further investigated in the literature. Performance improvements in terms of mutual information and network throughput are reported. Cooperative communication is a diversity-based technique adopted in the literature to combat fading and enhance performance in wireless networks. In this section, we perform a review of the work in the literature implementing ANC with and/or without cooperative communication to improve the performance of relay networks.

2.5.4.1 Review of Related Work

In [126], the performance of ANC is evaluated for a simple network configuration consisting of two different source nodes, a relay node, and a receiver. An optimum power

allocation scheme is proposed that simultaneously minimizes outage probability and maximizes the total mutual information. Numerical results demonstrate that the maximum mutual information and minimum outage probability is achieved at a certain distance between the source node and relay node. The energy efficiency of ANC for two-way relay networks with asymmetric traffic is investigated in [127]. Numerical results obtained by solving a non-linear fractional energy efficiency maximization problem indicates that optimal power allocation can be incorporated into ANC to achieve the best performance amidst system imbalance caused by traffic asymmetry. Analog network coding for cooperative communications (ANC-CC) is explored in [128]. It is revealed that ANC may not always benefit cooperative communications because of the prevalence of ANC noise. Analog network coding noise is created during the signal combining and decoding process which occurs between the relay node and receiver, and worsens as the number of nodes using the ANC-CC capable relay node is increased past a certain threshold. The effect of the number of sessions and the resulting ANC noise is investigated for outage behavior, achievable rate, and effective SNR. However, the energy, reliability, and delay performance of ANC-CC with or without ANC noise is not studied. The work in [129] tackles the problem of ANC noise by employing power adaptation with the aim of maximizing the achievable transmission rate. According to Shannon's theorem, increased transmission power results in increased achievable transmission rate, albeit only relevant in scenarios without interfering transmitters. Therefore, in the presence of multiple interfering transmitters, a joint method for finding the optimal transmission power required to maximize the transmission rate is proposed. The performance of ANC with power adaptation is shown to offer superior transmission rate performance than transmission schemes with no relay, conventional network coding (via network layer), or traditional relaying. In [130], the relay operating region where

relay-assisted ANC transmission achieves higher energy efficiency than direct transmission is identified. The work in [130] differs from [126] – [129] because it assumes each transmitting node has a distinct data rate and outage probability requirement. It is found that for any set of data rate or outage probability requirements, the best position for relay node placement is the middle point between two nodes exchanging data.

2.5.4.2 Similarities between Related Work and Thesis Research

- *Similarity #1:* Two aspects of ANC-capable relay nodes which offer similarity between the related work and our research is the consideration of the preferred distance to maintain a relay node relative to the receiver and the investigation of ANC noise.
- *Similarity #2:* Similar to [128] and [129] we consider the adverse effects of ANC noise on system performance.

2.5.4.3 Differences between Related Work and Thesis Research

Our work towards achieving energy efficiency and QoS support with ANC-CC has the following three differences from the literature:

- *Difference #1*: Analytical expressions are derived to evaluate the performance of the BNA ANC-CC relay scheme in terms of relative energy cost, reliability, and delay. Although the evaluation of energy performance has been performed for cooperative network coding in BANs, the performance evaluation in terms of energy, reliability, and delay for ANC-CC has not been investigated.
- *Difference #2*: The energy required to overcome ANC noise to prevent decoding errors at a receiver (i.e., the BNC) to maintain success probability above a desired reliability objective is investigated for the first time in this thesis and offers new insight into the importance of accounting for ANC noise.

TABLE 2.5 SUMMARY OF WORKS RELATED TO ANC-CC RELAY SCHEMES

Referenced Research	Objective	Protocol Layers	Energy Analysis	QoS Metrics	Fading Model	Relay Scheme	ANC Noise
Yi *et al.* [126]	Maximum Mutual Information	PHY	No	Reliability	Rayleigh	ANC	No
Zhang *et al.* [127]	Energy Efficiency	PHY	Yes	None	None	ANC	No
Sharma *et al.* [128]	Maximum Achievable Rate	PHY	No	Outage probability	None	ANC-CC	Yes
Wang *et al.* [129]	Maximum Achievable Rate	PHY	No	None	Rician	ANC	Yes
Li *et al.* [130]	Energy Efficiency	PHY	Yes	Outage probability	Rayleigh	ANC	No
Thesis: Section 5.3.4	Minimum Energy	NTW, PHY	Yes	Reliability and Delay	Rayleigh	ANC-CC	Yes

2.6 Summary

In this chapter, an overview discussing BANs for military application, on-body and body-to-body communications for BANs, and the physiological signals from a soldier that should be monitored was provided. The communication infrastructure necessary to facilitate remote monitoring of soldiers' physiological state is based on a two-tier network architecture where the BAN is connected to a BS through a multi-hop BBN in an outdoor environment. The joint consideration of multiple protocol stack layers such as the network, MAC, and physical layers provide for minimum relative energy cost at the BAN and BBN levels while also supporting stringent QoS requirements. We have also provided justification for the selection of the IEEE 802.15.4 wireless standard as the radio interface at the SN and BNC for intra-BAN and inter-BAN communication. The end of the chapter describes the similarities and differences between the proposed work in this thesis and the related work in the literature regarding energy and QoS

aware communication schemes for the BAN and BBN. The subsequent chapters in this thesis further discuss the design, implementation, and analysis of the proposed work.

CHAPTER 3 ENERGY AND QOS AWARE COMMUNICATION SCHEME FOR SINGLE-HOP BODY-TO-BODY NETWORK

3.1 Introduction

In this chapter, the problem of minimizing the relative energy cost for transmitting physiological data from SNs deployed on a soldier to a BS device deployed on a combat medic in a single-hop BBN is addressed using an energy and QoS aware single-hop (EQS) communication scheme. The foundation of the EQS communication scheme is the proposal of a synergistic BAN network model and a JPRS strategy, both of which serve as major contributions of the thesis. The synergistic BAN network model exploits the heterogeneous nature of SNs and the BNC to overcome deleterious conditions caused by on-body and body-to-body channels. The JPRS strategy jointly optimizes transmission power, retransmission limit, and packet size to facilitate minimum relative energy cost transmission over intra-BAN and inter-BAN links while meeting reliability and delay constraints. Solving the QoS constrained minimum relative energy cost optimization problem is highly complex due to the non-linear structure of the objective function and adjoining constraints and the presence of multiple decision variables. Therefore, we first decompose the optimization problem into less complex sub-problems and then provide highly efficient sub-optimal solutions.

The remainder of this chapter is organized as follows. Section 3.2 provides details of the system model including a description of the synergistic BAN network model. The JPRS strategy is described and analyzed in detail in Section 3.3. In Section 3.4, the minimum relative energy cost problem for transmitting data in a single hop BBN using the EQS communication scheme is formulated and solved using optimal and sub-optimal solutions. The performance of EQS is

evaluated in Section 3.5 using analytical and simulation results. The chapter summary is presented in Section 3.6.

3.2 System Model

This section presents details of the synergistic BAN network model and a dual aggregation concept used to support robust communication over on-body and body-to-body channels. A comprehensive system model describing the lossy on-body and body-to-body wireless channels, physical, MAC, and network layers, and a detailed energy consumption model is provided to accurately account for all components that influence the performance of EQS.

3.2.1 Proposed Synergistic Body Area Network Model

The single-hop body-to-body network considered in this chapter comprises a single BS and one BAN that consists of N_s SNs and one BNC. It is assumed that the BS is reachable from the BAN within a single hop. Such an assumption is justified and often encountered in military training exercises where a team of soldiers monitored by a medic perform running, simulated mission, or conditioning drills in close vicinity of each other [131]. The SNs and BNC in each BAN are distributed at set locations around the soldier's body whereas the BS is positioned at the waist level of the medic. The ID of the BS is set as #1 and the BNC has an ID denoted by i. Each SN in the same BAN as BNC i has an ID denoted by $i.k$, where $1 \leq k \leq N_s$. The battery capacity, processing power, and memory space of the N_s SNs are constrained since they are miniature in size and must fit comfortably on human skin. On the other hand, the BNC can take the form of a radio equipped personal device assistant (PDA) attachable to the waist of a soldier where a larger form factor can be supported. The resources of the BNC are also constrained but we assume it has higher battery capacity, superior processing power, and larger memory space than the SNs. To provide compatibility and to ease deployment, it is assumed the SNs and BNCs

are equipped with the same radio device. Therefore, the maximum transmission range and power is the same for both type of nodes. The BS is assumed to be a radio equipped ruggedized laptop device with a large battery which provides extended lifetime (e.g., 9 volt battery). We assume the BS is not resource constrained in terms of its memory and processing ability. It is responsible for receiving, processing, storing, and displaying all physiological data from the active soldier. The SNs in a BAN continuously sample physiological signals from the human body whereas the BNC does not engage in any sensing activity aside from periodic global positioning system (GPS) signal acquisition. The acquired physiological signals are digitized into samples and aggregated into data packets. The BNC performs activities such as the scheduling of intra-BAN and inter-BAN communications, data aggregation, and data forwarding. Throughout this thesis, the term *aggregation* is defined as the concatenation of smaller data packets into a larger singular *aggregated* data packet.

The synergistic BAN model proposed in this chapter and illustrated in Fig. 3.1 is comprised of two possible transmission paths. In path 1 (shown in Fig. 3.1a), the SNs transmit directly to the BS over an inter-BAN link defined by $link(i.k, 1)$. Direct transmission between the SNs and BS is beneficial when the fading conditions and path loss experienced over the body-to-body channels external to the BAN are less severe than the on-body channel conditions. Through extensive propagation characterization studies, [9] has shown the fading behavior for on-body channels in an outdoor environment follows the Nakagami-*m* distribution and possesses a fading factor that can be as low as $m = 1.37$ due to body-centric shadowing whereas clear LOS paths along outdoor body-to-body channels can have a high fading factor such as $m > 10$ [9]. In Nakagami-*m* fading channels, a low fading factor is indicative of severe fading where a dominant path component is absent ($m = 1$ represents Rayleigh fading) and a high fading factor

represents minimal fading where a dominant path is present ($m \to \infty$ represents additive white Gaussian noise (AWGN)). Further characterization studies have shown that the path loss parameters for NLOS conditions on the body can be as high as $PL(d_0) = 48.8$ dB and $\alpha = 4.8$ [34] whereas open area outdoor environments with LOS paths between bodies can be as low as $PL(d_0) = 29.6$ dB and $\alpha = 2.9$ [11], where $PL(d_0)$ is the path loss at a reference distance of d_0 and α is the path loss exponent. Direct transmission between the SNs and BS is also beneficial when the battery capacity of the BNC is lower than that of the SNs. This scenario arises when the BNC is predominantly utilized by the SNs and thus the energy of the BNC drains at a rate that is at least N_s times faster than the SNs. In path 2 (shown in Fig. 3.1b), the SNs transmit directly to BNC i over an intra-BAN link defined by $link(i.k, i)$. Notice the BS is able to overhear transmissions performed over $link(i.k, i)$ using $link(i.k, 1)$. The ability to overhear intra-BAN transmissions is possible when the fading and path loss body-to-body channel conditions are not severe. The data packets successfully received over $link(i.k, 1)$ are stored in a buffer. The contents of the buffer are soon after used to drive the dual aggregation concept that we later detail later in Section 3.2.2. The BNC i receives all the incoming data packets transmitted from the SNs and aggregates the different physiological data samples into single or multiple aggregated data packets that are then transmitted to the BS over a link defined by $link(i, 1)$. The synergy of the proposed model derives from the ability to achieve successful transmission through multiple paths. In particular, overhearing transmissions at the BS from the SNs provides robustness and higher reliability for the received physiological data samples because the contents of the data packets can be combined from multiple paths. The packet combining strategy over multiple paths is not new and has been investigated for different applications such as underwater acoustic sensor networks [132] and terrestrial sensor networks

[133]. However, the benefits offered by the packet combining strategy have not gained extensive study in body area networks.

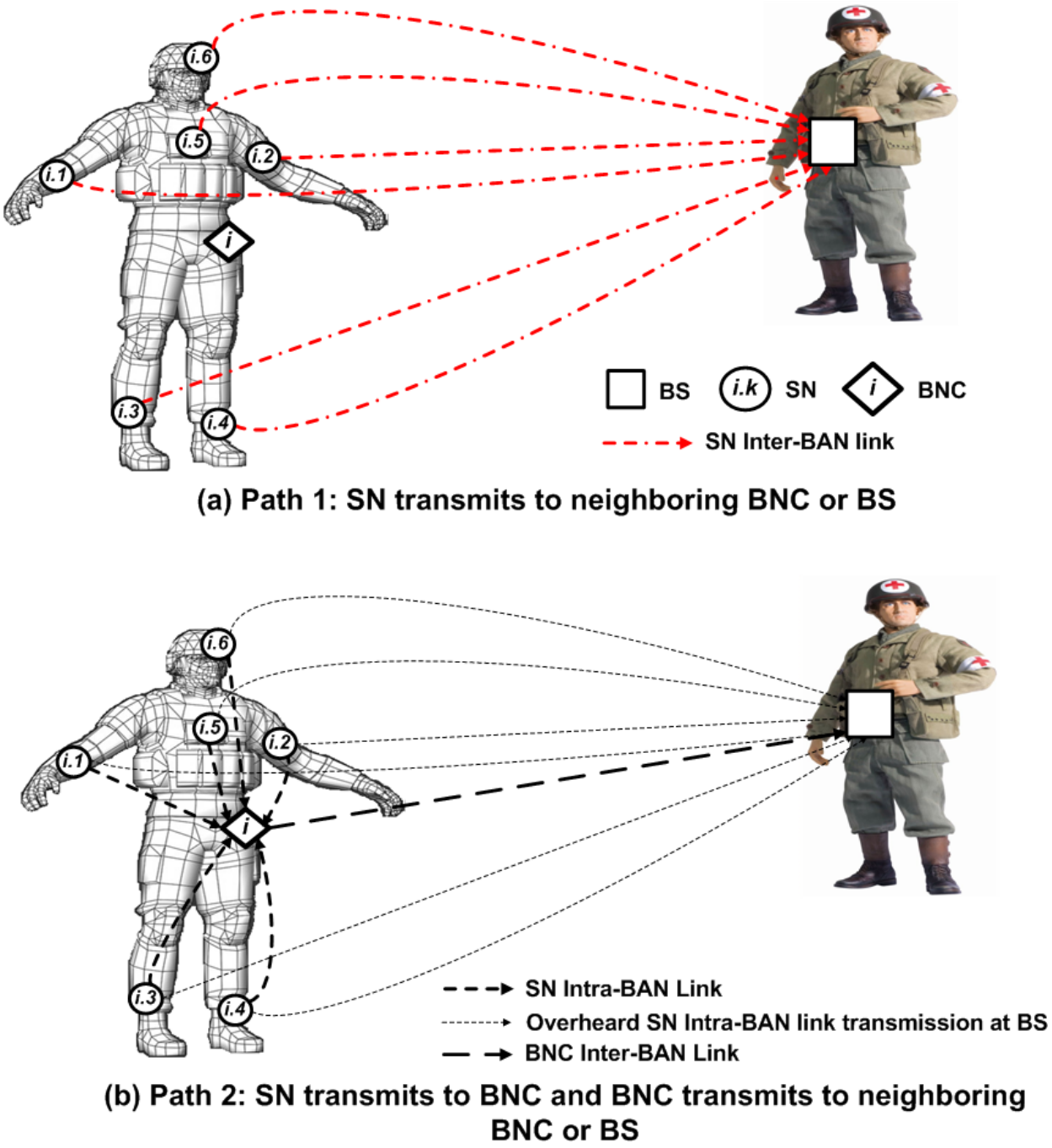

Fig. 3.1. Synergistic BAN model.

3.2.2 Dual Aggregation Concept

The dual aggregation concept leverages the fact that physiological data transmitted from the SNs to the BNC can be overheard by the BS. As a result, the BS can aggregate different physiological data samples (i.e., $\varphi_{i.k}$) into a single stream in the same manner the BNC aggregates incoming physiological data into aggregated packets. When the BNC has completed the aggregation process for the physiological data samples and transmitted them to the BS, the BS is in possession of two sets of aggregated physiological data samples, received over multiple paths. In the following paragraphs, we describe the dual aggregation concept in more detail.

As previously mentioned, sensing tasks are performed at the SN where a physiological signal stream is sampled at a rate of ϑ_k samples per second with each sample having $L_{sam,k}$ bits. The SN aggregates $\varphi_{i.k}$ samples into a data packet and then transmits the data to the BNC. When the BS receives a copy of the data packet from $link(i.k, 1)$ (the data component of the packet may have been corrupted during the transmission process), it first checks whether this copy is erroneous. If there are no errors or the number of errors is acceptable due to an error tolerant reliability constraint, the BS successfully receives the original set of physiological data samples and sends an ACK message to the BNC indicating it does not have to transmit the received data. Otherwise, the BS will keep the corrupted data packet in its buffer. When the BNC has received a certain number of physiological data samples from the SNs, it aggregates them into a single aggregated data packet and transmits it to the BS. After the BS has received the aggregated data packet from the BNC, it will combine its contents with the contents stored in the buffer in order to recover the original data samples. The packet-combining technique employed in this chapter is probabilistic in nature and follows similarly from the packet-combining technique employed in [132] for multi-path routing.

3.2.3 Wireless Channel and Protocol Layers

3.2.3.1 Wireless Channel

Wireless channels are generally impaired by the joint interaction of path loss, small-scale fading, and large-scale fading or shadowing. Shadowing is prominent in both on-body and body-to-body channels when the LOS path between a transmitter and receiver is blocked by a human body part or other obstructions. The effect of shadowing is a substantial attenuation of the received signal. We are aware of the detrimental effects shadowing has on the *instantaneous* performance of intra-BAN and inter-BAN transmissions. However, we neglect shadowing in the analysis for reason of analytical tractability but account for it in our simulation experiments. Therefore, the path loss incurred for transmissions along the on-body and body-to-body wireless channels is calculated in decibel units using a distance dependent path loss model:

$$PL(d)_{dB} = PL(d_0)_{dB} + 10\alpha \log_{10}\left(\frac{d}{d_0}\right) \tag{3.1}$$

where d is the distance separating the transmitter and receiver. The presence of path loss directly influences the signal-to-noise ratio (SNR). The average SNR at a receiver located a distance d from a transmitter is expressed in decibel units as $\bar{\gamma}_{dB}(P_{tx,dBm}, d) = P_{tx,dBm} - PL(d)_{dB} - P_{n,dBm}$, where $P_{tx,dBm}$ and $P_{n,dBm}$ are the transmit power and noise power, respectively, both in decibel milliwatt units. To align with the structure of the analyses performed in this chapter and throughout the thesis, we also express the average SNR in linear units in terms of channel gain $g(d) = 10^{(-PL(d)_{dB}/10)}$ as:

$$\bar{\gamma}(P_{tx}, d) = \frac{P_{tx} g(d)}{P_n} \tag{3.2}$$

Extensive measurements for the received signal characteristics along the on-body channel in an outdoor environment at 2.4 GHz have revealed that the Nakagami distribution [9] may be

used to provide an accurate description of the resulting small-scale fading behavior. Similarly, the small-scale fading experienced along the body-to-body channel in an outdoor environment can also be accurately captured by using the Nakagami distribution. The flexibility of the *m* fading factor of the Nakagami distribution allows the distribution to be representative of Rician or Rayleigh fading. These fading conditions are of great interest for analyzing the performance of BAN communication schemes in different military operating environments. The probability density function for the instantaneous received SNR γ is gamma distributed and given in terms of the Nakagami fading factor *m* as:

$$p_{\gamma}(\gamma|\bar{\gamma}) = \frac{m^m(\gamma)^{m-1}}{(\bar{\gamma})^m\Gamma(m)}\exp\left(-\frac{m\gamma}{\bar{\gamma}}\right) \tag{3.3}$$

where $\Gamma(\cdot)$ is the complete Gamma function.

3.2.3.2 Protocol Layers

L1) *Physical Layer*: In addition to the wireless channel characteristics described in Section 3.2.3.1, another major functionality of the physical layer is to ensure the reliable delivery of data from a transmitter to a receiver. The key function of the physical layer is the channel encoding and modulation of a bit stream to a symbol stream that is then transmitted over the wireless channel. Channel coding is also an element of the physical layer which can provide measureable performance gains. At the receiver, the physical layer is tasked with symbol detection, demodulation, and decoding. The BER expressions are then derived at the input of the channel decoder.

Offset quadrature phase shift keying represents a popular modulation technique often employed for sensor mote devices employed in health care monitoring applications due to its ability to support high data rates with low power [83]. Offset quadrature phase shift keying is

particularly attractive because it can transmit twice the data rate in a given bandwidth when compared to binary phase shift keying (BPSK) while achieving the same BER. The penalty is that the QPSK transmitters and receivers are more complicated than the ones for BPSK. However, the advance in modern electronics has minimized the penalty cost. The exact closed-form BER performance for OQPSK over an AWGN channel is calculated as [81]:

$$p_{b,AWGN}(\gamma) = \frac{8}{15}\frac{1}{16}\sum_{q=2}^{16}(-1)^q \binom{16}{q} \exp\left(20\gamma(q^{-1}-1)\right) \tag{3.4}$$

where q is the number of orthogonal symbols in OQPSK. The expression in (3.4) is involved and undesirable for tractable analysis. To obtain a tractable closed form expression for the BER, we can assume that transmission over the on-body and body-to-body channels use Gray coding and maintains a sufficiently large enough SNR, thus leading one symbol error to cause approximately a single bit error [134]. As a result, the BER for OQPSK over an AWGN channel is approximated by employing a less complicated expression given as [135]:

$$p_{b,AWGN}(\gamma) \approx Q\left(\sqrt{2\gamma}\right) \tag{3.5}$$

where $Q(x)$ is the Q-function. The exact BER for a coherent OQPSK receiver over a non-frequency selective block Nakagami fading channel with average SNR $\bar{\gamma}$ is derived as [136]:

$$p_{b,NAKAGAMI}(\bar{\gamma}, m) = \int_0^{\infty} p_{b,AWGN} \times p_{\gamma}(\gamma|\bar{\gamma}) d_{\gamma} = \frac{(2m)!\, M_{\gamma}(-1)}{2(2^m m!)^2}\ {}_2F_1\left(m, \frac{1}{2}; m+1; \frac{1}{1+\bar{\gamma}/m}\right) \tag{3.6}$$

where ${}_2F_1(a, b; c; z)$ is the Gauss hypergeometric function and $M_{\gamma}(-1) = (1+\bar{\gamma}/m)^{-m}$. The authors in [136] use the Laplace approximation and the steps outlined in [137] to approximate the Gauss hypergeometric function to obtain a very tight approximation for the BER given as:

$$p_{b,NAKAGAMI}(\bar{\gamma}, m) = K_1 \left(\frac{m}{m+\bar{\gamma}}\right)^{m} \sqrt{1 - \left(\frac{m}{m+\bar{\gamma}}\right)\left(\frac{m}{m+1}\right)} \quad (3.7)$$

where $K_1 = \frac{\Gamma(2m+1)}{2\left(2^m \Gamma(m+1)\right)^2}$. The approximation in (3.7) is very tight with an average error less than 0.5% for SNRs in the range defined by $\gamma_{dB} = [0,40]$ dB, which represents a typical range for PER-constrained transmissions. Given a data packet with total packet size of L bits, the average PER over a Nakagami fading channel is calculated as:

$$p_{e,NAKAGAMI}(\bar{\gamma}, m, L) \approx 1 - \left(1 - p_{b,NAKAGAMI}(\bar{\gamma}, m)\right)^{L} \quad (3.8)$$

L2) *MAC Layer*: The MAC layer is primarily designed to manage the contention between transmitting SNs and BNCs potentially interfering with one another. Rather than propose a new MAC layer protocol, we schedule the intra-BAN and inter-BAN transmissions using a version of the slotted mode of IEEE 802.15.4 that can be modeled as a TDMA scheme through the use of guaranteed time slots. TDMA is appealing because nodes only consume energy during their assigned time slots and avoid energy waste incurred by the idle listening, overhearing, and collisions inherent of CSMA [138]. TDMA schemes also offer superior performance to CSMA under medium to high traffic loads and better support low transmission delay guarantees [138]. Although TDMA is plagued by the synchronization issue, this is resolved via periodic beacons that are adequately configured to synchronize time slots and provide robustness to mobility, as demonstrated by mobility-aware TDMA implementations in the literature [139]. Retransmissions are also an integral component of the MAC layer because their implementation ensures successful reception and high reliability.

Let X denote the retransmission limit (including the first transmission and $X-1$ retransmissions) along a link. Assuming the channel gain at each transmission is independent, the

average probability for *successful* packet delivery over the X transmissions is given by:

$$\mathcal{P}_s(\bar{\gamma}, m, L, X) = 1 - \left(p_{e,NAKAGAMI}(\bar{\gamma}, m, L)\right)^X \tag{3.9}$$

Successful delivery is achieved when the average probability of delivery meets or exceeds a reliability objective given by $\mathcal{P}_{req}$. Each successful delivery is acknowledged by the transmission of an ACK packet from the receiver to the transmitter. Since ACK packets are typically significantly smaller than data packets, we assume the ACK packet can be successfully transmitted in one attempt. As a result, we neglect the PER associated with delivering the ACK packet because the PER can be reasonably approximated as zero [140]. It should also be noted that the independence assumption can be made and is reasonable when the transmission time is longer than the channel coherence time, which is often the case for monitoring applications operating at the 2.4 GHz frequency spectrum [105]. The average number of total transmissions to achieve successful delivery is then derived as:

$$\phi(\bar{\gamma}, m, L, X) \approx \frac{1 - \left(p_{e,NAKAGAMI}(\bar{\gamma}, m, L)\right)^X}{1 - p_{e,NAKAGAMI}(\bar{\gamma}, m, L)} \tag{3.10}$$

The transmission delay $\mathcal{D}_{tx}(f, X, \mathcal{R})$ along any link in a TDMA-based network with total traffic load f in bits, unit-less retransmission limit X, time slot duration t_{slot} in seconds, and maximum link data rate $\mathcal{R}$ in bits per second is calculated as:

$$\mathcal{D}_{tx}(f, X, \mathcal{R}) = t_{slot}\mathcal{S} \tag{3.11}$$

where $\mathcal{S}$ is the number of required time slots along a link given by $\mathcal{S} = \lceil (fX)/(t_{slot}\mathcal{R}) \rceil$ and $\lceil x \rceil$ is the smallest integer greater than or equal to x.

L3) *Network Layer*: The network layer is responsible for creating routing paths between a source node and its intended destination. Single-hop intra-BAN routing is performed via the SN-to-

BNC links whereas single-hop inter-BAN routing is performed via SN-to-BS and BNC-to-BS links.

3.2.4 Energy Consumption Model

The energy consumption at the SNs and BNCs is mainly attributed to the transmitter and receiver components of the sensor node device. The sensing energy is a constant value proportional to the sampling rate and bits per sample and highly dependent on the particular sensing hardware. In the thesis, we are mainly interested in the energy consumed during communications and therefore we neglect the analysis of sensing energy. The energy consumed at a SN or BNC operating as a receiver consists of the baseband digital signal processor circuit, front-end circuit, and low noise amplifier. The receiver circuit power $P_{rx,cir}$ is constant and thus the per bit average receiver energy can be calculated as $E_b(P_{rx}) = P_{rx,cir}/\mathcal{R}$. The total per bit energy consumption across a link is determined using a discrete power model and is calculated as:

$$E_b(P_{tx}, \mathcal{R}) = \frac{P_{tx,cir} + (P_{tx}/\eta)}{\mathcal{R}}, P_{tx} \in [P_{min}, P_{max}] \tag{3.12}$$

where $P_{tx,cir}$ is the constant transmitter circuit power, P_{tx} is the output transmit power, η is the power amplifier efficiency calculated as a function of P_{tx}, and P_{min} and P_{max} are the minimum and maximum transmit power, respectively. The transmitter circuit power accounts for the digital to analog converter, frequency synthesizer, mixer, lower noise amplifier, and base digital signal processor and is thus a constant value. The output transmit power can be modeled as continuous or discrete. Using a continuous model where the transmit power can take any value in the range $[P_{min}, P_{max}]$ provides for more tractable power consumption analysis. On the other hand, a discrete model defines a finite number of transmission power levels in the range $[P_{min}, P_{max}]$,

which is representative of practical sensor mote operation and partitioned into $\mathcal{Z}$ discrete power levels (i.e., $P_{tx.ij}(z = 1) = P_{min}, \ldots, P_{tx}(z = \mathcal{Z}) = P_{max}$) for ease of adjusting P_{tx}. For example, by default the MICAz mote is configured with $\mathcal{Z} = 8$ defined transmission power levels [141]. The number of transmission power levels is often configurable and is tailored towards application needs [141]. The power amplifier efficiency is a function of transmission power and has been measured in [142] for each transmission power level for CC2420 devices. We apply a non-linear least squares regression method to the discrete power amplifier efficiency values obtained in [142] to form a continuous power amplifier efficiency function we derive as:

$$\eta(P_{tx}) = 0.356\left(P_{tx}{}^{0.4615}\right) \tag{3.13}$$

The plot provided in Fig. 3.2 demonstrates how well (3.13) is in agreement with the discrete values in [142], achieving a root mean squared error of 0.99.

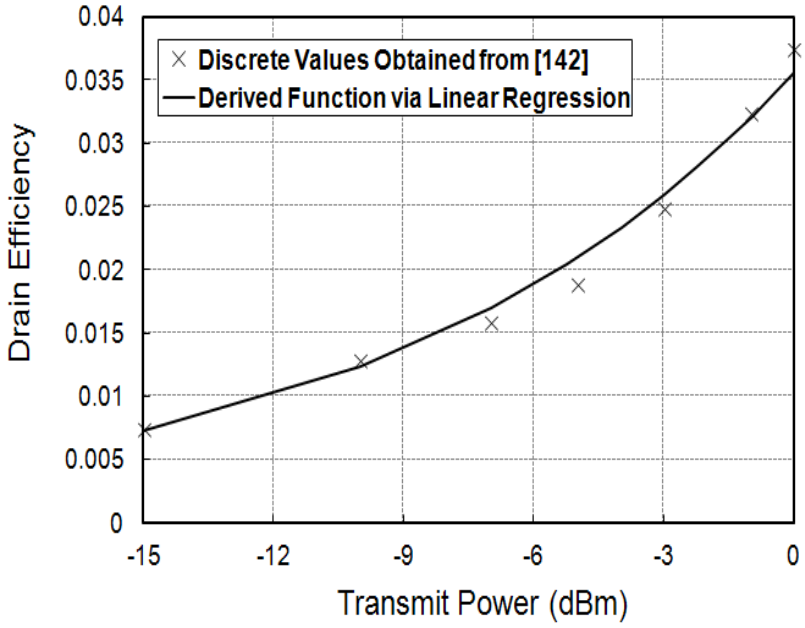

Fig. 3.2. Approximated power amplifier efficiency function for CC2420 radio.

3.3 JPRS Strategy for Enhanced Intra-BAN and Inter-BAN Link Performance

In this section, we design and analyze a strategy to facilitate aggregation and the transmission of aggregated data packets over path 1 and path 2 of the synergistic BAN model. Specifically, the strategy must allow physiological signal samples of different size and number to be transmitted in a single or multiple packets from the SN and/or BNC while achieving minimum relative energy cost under reliability and delay constraints. We thus devise a strategy called **J**oint transmission **P**ower, **R**etransmission limit, and packet **S**ize (JPRS), first introduced in our previous work [143], [144] where the transmission power, retransmission limit, and packet size for transmissions along a link are jointly optimized to achieve minimum relative energy cost under reliability and delay constraints.

The problem of minimizing the relative energy cost using the JPRS strategy to support a data transmission rate of r_{ij} bps over a link (i, j) under reliability and delay constraints is formulated as follows:

$$\text{minimize} \quad n_{ij}L_{ij}\phi\left(P_{tx.ij}, m_{ij}, L_{ij}, X_{ij}\right)\left(\frac{E_b(P_{tx.ij})}{E_{res,i}} + \frac{E_b(P_{rx})}{E_{res,j}}\right) \tag{3.14.0}$$

$$\text{subject to} \quad \mathcal{P}_s\left(P_{tx.ij}, m_{ij}, L_{ij}, X_{ij}\right) \geq \mathcal{P}_{req} \tag{3.14.1}$$

$$\mathcal{D}_{tx}\left(n_{ij}L_{ij}, X_{ij}, \mathcal{R}\right) \leq \mathcal{D}_{req} \tag{3.14.2}$$

$$n_{ij}L_{p,ij} = r_{ij} \tag{3.14.3}$$

$$P_{min} \leq P_{tx,ij} \leq P_{max} \tag{3.14.4}$$

$$L_{p,min} \leq L_{p,ij} \leq L_{p,max} \tag{3.14.5}$$

$$X_{ij} \geq 1 \tag{3.14.6}$$

where n_{ij} is the number of packets transmitted per second to achieve a data transmission rate

requirement of r_{ij} bits per second, L_{ij} is the total packet size calculated as $L_{ij} = L_h + L_{p,ij}$, L_h is the packet header size in bits, $L_{p,ij}$ is the payload size in bits, E_{res} is the residual energy of a node, and $L_{p,min}$ and $L_{p,max}$ are the minimum and maximum payload sizes, respectively, and $\mathcal{D}_{req}$ is the delay objective. The decision variables in (3.14) are X_{ij}, $L_{p,ij}$, and $P_{tx.ij}$ ($P_{tx.ij}$ is expressed in terms of $\bar{\gamma}_{ij}$). They are described as real variables in order to provide average performance over time. The objective function in (3.14.0) consists of three main components accounting for the average relative energy cost along $link(i,j)$. The component $n_{ij}L_{ij}$ is the equivalent number of transmitted bits per second corresponding to a given data payload where the data is partitioned into n_{ij} segments and each segment is transmitted as a separate packet of average size L_{ij} bits. Fig. 3.3 illustrates the preceding concept where an application layer data stream of length L bits is partitioned into n_{ij} smaller segments to minimize relative energy cost and meet the QoS requirements for transmission over a wireless link. It is seen that the total number of transmitted bits resulting from segmentation is higher than the required data stream due to the need to pad each segmented packet with packet header L_h. Under particular scenarios, a trade-off exists where the reduced segment size decreases relative energy cost but may increase delay.

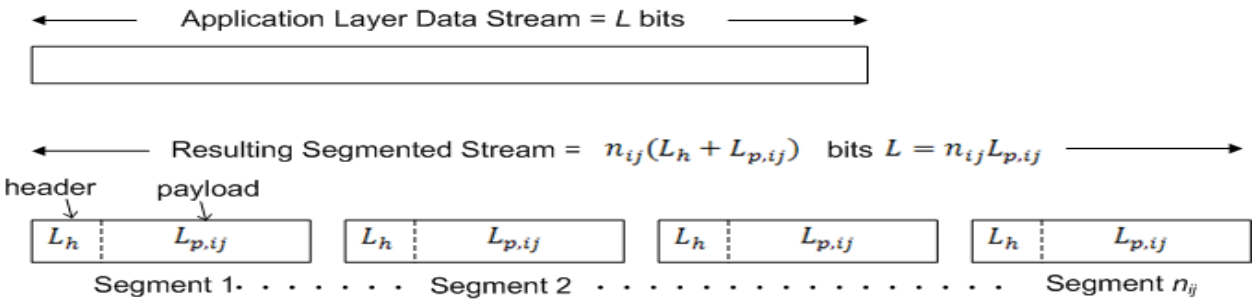

Fig. 3.3. Application layer data stream partitioned into smaller segmented packets for transmission over a generic wireless link.

The next component $\phi(\bar{\gamma}_{ij}, m_{ij}, L_{ij}, X_{ij})$ is the average number of transmissions required to achieve the reliability and delay constraints in (3.14.1) and (3.14.2), respectively, and it scales the average relative energy cost in a non-linear manner. The rightmost component of the objective function determines the average transmission power required to perform transmissions under constraints (3.14.1) and (3.14.4).

We show through an exhaustive search approach and graphical representation, that the objective function is convex by evaluating combinations of $(X_{ij}, P_{tx.ij})$ and $(L_{p.ij}, P_{tx.ij})$ within their defined constraint bounds. In Fig. 3.4a, the relative energy cost for inter-BAN transmission over a link distance of 15 m is evaluated using the path loss and fading parameters from [11] for a Nakagami fading outdoor wireless body-to-body channel ($PL(d_0) = 54.6$ dB, $d_0 = 1$ m, $\alpha = 2.2$, $m_{ij} = 2$) for varying values of $P_{tx.ij} \in [P_{min}, P_{max}]$ and $L_{p,ij} \in [L_{p,min}, L_{p,max}]$, while X_{ij} is kept constant at one. The required variable bounds and constant parameters for determining the relative energy cost are provided in Table 3.1 in Section 3.5.1. We assume $\mathcal{P}_{req} = 99\%$, $\mathcal{D}_{req} = 1$ second, and the residual energy is set as unity (i.e., $E_{res} = 1$ mJ) to provide performance indiscriminant of battery capacity. The convex shape is clearly shown with the minimum relative energy cost occuring within the transmit power range of $P_{tx.ij} \in [-10, -7]$ dBm and packet size range $L_{p,ij} \in [100,700]$ bits. In Fig. 3.4b, the objective function is calculated with $X_{ij} \geq 1$ and $L_{p,ij} = L_{p,max}$ using the same parameters as Fig. 3.4a. Convexity is demonstrated with the minimum occuring in the range $P_{tx.ij} \in [-7,0]$ dBm and $X \in [2,6]$ but the convex shape is not as pronounced mainly due to the limited transmit power ($P_{max} = 0$ dBm) available to overcome the effects of path loss and fading. In Fig. 3.5 the objective function for intra-BAN transmission over a link distance of 50 cm is evaluated using the path loss and fading parameters from [145]

over a Nakagami fading on-body wireless channel ($PL(d_0) = 43$ dB, $d_0 = 10$ cm, $\alpha = 3.8$, $m_{ij} = 1.37$) using varying values of $P_{tx.ij} \in [P_{min}, P_{max}]$. In Fig. 3.5a, the payload size is varied as $L_{p,ij} \in [L_{p,min}, L_{p,max}]$ whereas $X_{ij} = 1$. The convex shape is seen by observing the curvature along each line that separates the different shades of color, particularly the red and deep blue regions. Fig. 3.5b shows the convex shape when the transmit power and retransmission limit are varied while the payload size is held constant at $L_{p,ij} = L_{p,max}$. Convexity is clearly demonstrated with the minimum relative energy cost obtained in the range $P_{tx.ij} \in [-6, -4]$ dBm for various values of the retransmission limit.

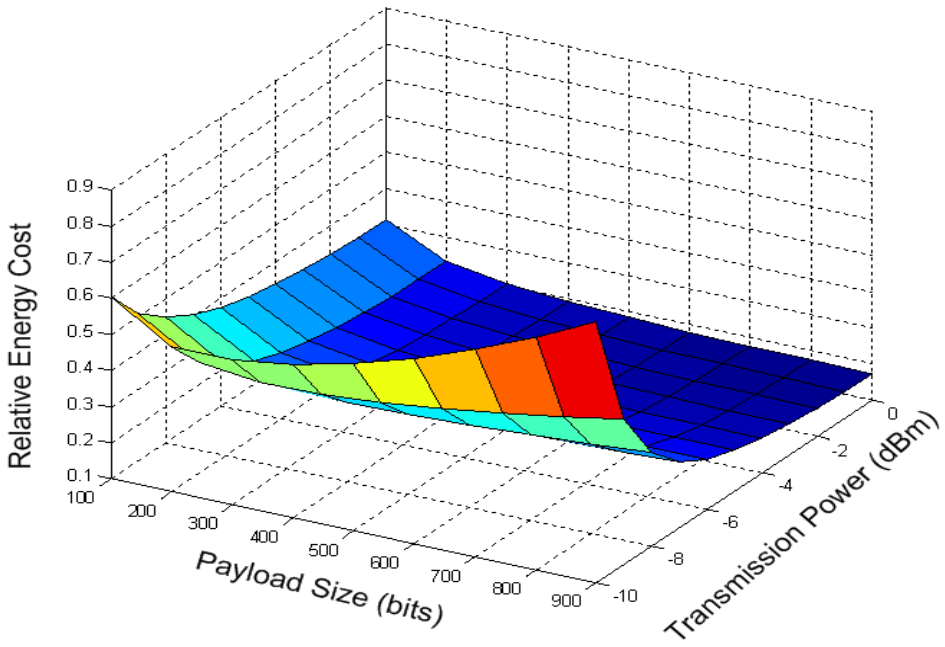

(a) Transmission power and payload size are varied

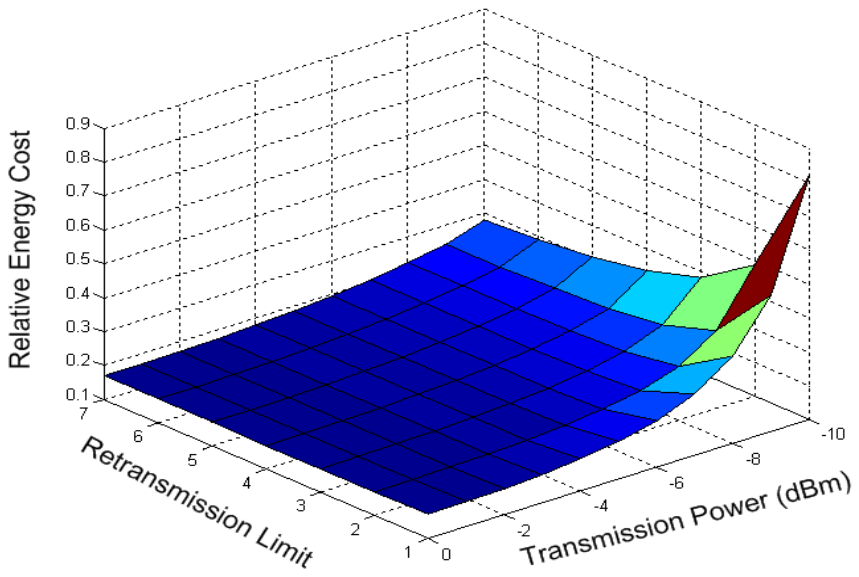

(b) Transmission power and retransmission limit are varied

Fig. 3.4. Convex shape of the objective function in (3.14.0) when transmission power, retransmission limit, and payload size are varied for inter-BAN transmission over a 15m Nakagami fading body-to-body outdoor wireless channel.

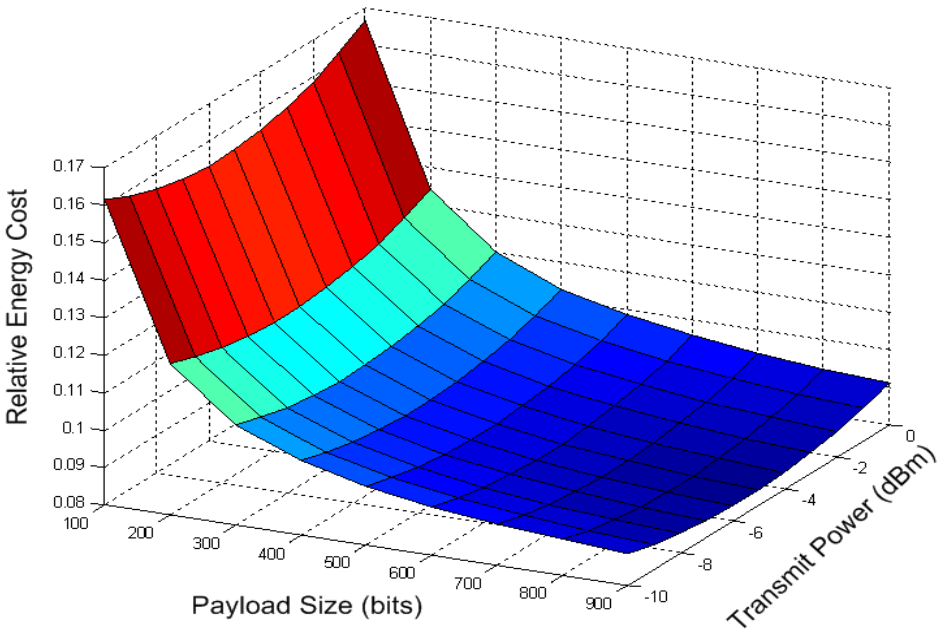

(a) Transmission power and payload size are varied

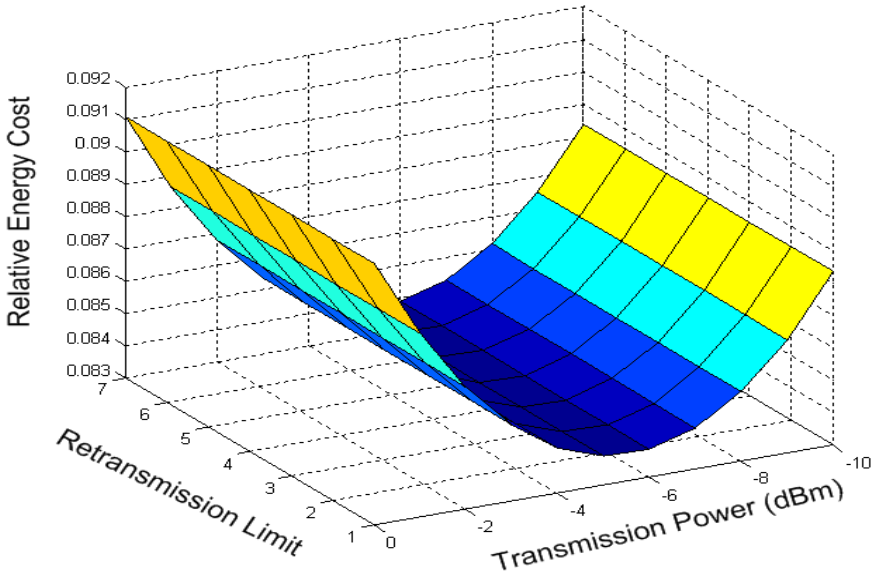

(b) Transmission power and retransmission limit are varied

Fig. 3.5. Convex shape of the objective function in (3.14.0) when transmission power, retransmission limit, and payload size are varied for intra-BAN transmission over a 50cm Nakagami fading on-body wireless channel.

3.4 Minimum Relative Energy Cost for Single-hop BBN

3.4.1 Optimization Problem Formulation

An optimization problem incorporating the JPRS strategy is formulated to determine the minimum relative energy cost path the SNs should utilize in order to transmit data packets to a destination BS. The optimization problem is formulated with the criterion that all SNs either transmit along the links in path 1 or path 2, thus representing adaptive transmission behavior.

minimize

$$\sum_{k=1}^{N_s} n_{i.k}L_{i.k}\left(\mu\phi\left(\bar{\gamma}_{i.k,i}, m_{i.k,i}, L_{i.k}, X_{i.k}\right) + (1-\mu)\phi\left(\bar{\gamma}_{i.k,1}, m_{i.k,1}, L_{i.k}, X_{i.k}\right)\right)\frac{E_b(P_{tx.i.k})}{E_{res,i}} + \cdots$$

$$+n_{i.k}L_{i.k}\left(\mu\phi\left(\bar{\gamma}_{i.k,i}, m_{i.k,i}, L_{i.k}, X_{i.k}\right)\frac{E_b(P_{rx})}{E_{res,i}}\right.$$

$$\left. + \phi\left(\bar{\gamma}_{i.k,1}, m_{i.k,1}, L_{i.k}, X_{i.k}\right)\left(\mu\frac{E_b(P_{rx})}{E_{res,i}} + \frac{E_b(P_{rx})}{E_{res,1}}\right)\right) + \cdots$$

$$+\mu n_{i1}F_{i1}\phi(\bar{\gamma}_{i1}, m_{i1}, L_{i1}, X_{i1})\left(\frac{E_b(P_{tx.i1})}{E_{res,i}} + \frac{E_b(P_{rx})}{E_{res,1}}\right), \forall i \in [2, N_b+1] \quad (3.15.0)$$

subject to

$$1 - \left(1 - \mu\bar{\mathcal{P}}_{i.k,i}\mathcal{P}_s(\bar{\gamma}_{i1}, m_{i1}, L_{i1}, X_{i1})\right)\left(1 - \bar{\mathcal{P}}_{i.k,1}\right) \geq \mathcal{P}_{req}, \forall i \in [2, N_b+1], \forall k \in [1, N_s]$$

(3.15.1)

$$\sum_{k=1}^{N_s}\left(\mathcal{D}_{tx}(n_{i.k}L_{i.k}, X_{i.k}, \mathcal{R})\right) + \mu\mathcal{D}_{tx}(n_{i1}L_{i1}, X_{i1}, \mathcal{R}) + \mathcal{D}_{agg}(\varphi_{i.k}, \vartheta_k) \leq \mathcal{D}_{req},$$

$$\forall i \in [2, N_b+1], \forall k \in [1, N_s] \quad (3.15.2)$$

$$n_{i.k}L_{p,i.k} = r_k, \forall i \in [2, N_b+1], \forall k \in [1, N_s] \quad (3.15.3)$$

$$n_{i1}L_{p,i1} = \mu \sum_{k=1}^{N_s} r_k \, , \forall i \in [2, N_b + 1] \tag{3.15.4}$$

$$\sum_{k=1}^{N_s} n_{i.k} L_{i.k} \left(\frac{\mu \phi\left(\bar{\gamma}_{i.k,i}, m_{i.k,i}, L_{i.k}, X_{i.k}\right)}{\mathcal{R}} + \frac{(1-\mu)\phi\left(\bar{\gamma}_{i.k,1}, m_{i.k,1}, L_{i.k}, X_{i.k}\right)}{\mathcal{R}} \right) + \cdots$$

$$\cdots + \frac{\mu n_{i1} F_{i1} \phi(\bar{\gamma}_{i1}, m_{i1}, L_{i1}, X_{i1})}{\mathcal{R}} \leq \mathcal{D}_{req}, \forall i \in [2, N_b + 1] \tag{3.15.5}$$

$$\mu = [0,1], \varphi_{i.k} \geq 1, L_{p,min} \leq L_{p,i1} \leq L_{p,max}, X_{i.k} \geq 1, X_{i1} \geq 1, \forall i \in [2, N_b + 1], \forall k \in [1, N_s] \tag{3.15.6}$$

where $\bar{\mathcal{P}}_{i.k,i} = \sum_{k=1}^{N_s} \frac{r_k}{r_i} \mathcal{P}_s\left(\bar{\gamma}_{i.k,i}, m_{i.k,i}, L_{i.k}, X_{i.k}\right)$ and $\bar{\mathcal{P}}_{i.k,1} = \sum_{k=1}^{N_s} \frac{r_k}{r_i} \mathcal{P}_s\left(\bar{\gamma}_{i.k,1}, m_{i.k,1}, L_{i.k}, X_{i.k}\right)$. The binary decision variable μ decides whether data packets are routed through the BNC (i.e., $\mu = 1$) or directly to the BS (i.e., $\mu = 0$), $L_{i.k}$ is the size of each packet transmitted by SN $i.k$ and is calculated as $L_{i.k} = L_h + \varphi_{i.k} L_{sam,k}$, where $L_{sam,k}$ is the fixed number of bits for each sample extracted from the physiological signal stream and $\varphi_{i.k}$ is the variable number of samples aggregated into a single data packet. We take advantage of the JPRS strategy and the ability to optimize the packet size in order to vary the number of samples that can be aggregated into a data packet. The variable $X_{i.k}$ is the retransmission limit for any transmission emanating from SN *i.k*. The Nakagami fading factors $m_{i.k,1}$ and m_{i1} are representative of the body-to-body fading in the outdoor environment and $m_{i.k,i}$ is the on-body fading between the particular body part SN *i.k* resides on and BNC *i*. The reliability constraint over path 1 and path 2 is provided as a singular expresssion in (3.15.1). Reliability over the SN-to-BS links is always considered for path 1 and also path 2. When path 2 is employed, the dual aggregation concept is employed to form a set of two data streams at the BS. The first data stream consists of all the physiological

data that was succesfully transmitted directly from the BNC (i.e., $\bar{\mathcal{P}}_{i.k,i}$) and and the second data stream consists of the overheard physiological data that was successfully transmitted by the SNs (i.e., $\bar{\mathcal{P}}_{i.k,1}$). The reliability constraint is then satisfied by combining the reliability of each data stream. The delay constraint is provided in (3.15.2). The average delay experienced for the transmission of each SN data sample consists of the TDMA frame duration $\mathcal{D}_{tx}$ for transmitting one second's worth of physiological data and the average wait time at a SN, denoted by $\mathcal{D}_{wait}$. The average wait time is the time duration from when a data sample is first extracted from a physiological signal stream to when it is subsequently transmitted by a SN. Assume a data packet at SN $i.k$ is transmitted when $\varphi_{i.k}$ ($\varphi_{i.k} \geq 1$) samples have been aggregated and each sample is extracted at a rate of ϑ_k samples per second. The average wait time per sample is calculated as:

$$\mathcal{D}_{wait}(\varphi_{i.k}, \vartheta_k) = \frac{1}{\vartheta_k} \sum_{a=1}^{\varphi_{i.k}} \frac{(\varphi_{i.k} - a)}{\varphi_{i.k}} = \frac{\varphi_{i.k} - 1}{2\vartheta_k} \tag{3.16}$$

Constraints (3.15.3) and (3.15.4) are imposed to maintain the traffic flow in the network. The source data rate at each SN $i.k$ is given by $r_{i.k}$, $L_{p,ik} = \varphi_{i.k} L_{sam,k}$, and $L_{p,i1}$ is the payload at the BNC. Constraint (3.15.5) provides stability for the MAC layer so that the total data traffic rate does not exceed the available maximum data rate. Constraint (3.15.6) describes the bounds for the decision variables. The optimization problem in (3.15) represents a mixed integer non-linear problem (MINLP) due to the non-linear structure of (3.15.0) and (3.15.1) and the integer variable μ. The problem of jointly optimizing multiple variables over several links is combinatorial in nature and thus an optimal solution is difficult to obtain in an efficient manner. We thus decompose (3.15) into two easier to solve sub-problems.

3.4.2 Optimization Problem Decomposition and Solution

In the first sub-problem, the minimum relative energy cost $\mathcal{E}_{path1}$ is obtained for all SN transmissions over path 1. In the second sub-problem, the minimum relative energy cost $\mathcal{E}_{path2}$ is obtained for all SN transmissions over path 2.

3.4.2.1 Sub-Problem #1: Path 1 Minimum Relative Energy Cost Solution

The relative energy cost over $link(i.k,1)$ in path 1 is

$$\mathcal{E}_{i.k,1} = n_{i.k,1}L_{i.k,1}\phi\left(\bar{\gamma}_{i.k,1}, m_{i.k,1}, L_{i.k,1}, X_{i.k,1}\right)\left(E_b(P_{tx.i.k,1})/E_{res,i.k} + E_b(P_{rx})/E_{res,1}\right).$$

The probability of successful delivery is $\mathcal{P}_{i.k,1} = \mathcal{P}_s\left(\bar{\gamma}_{i.k,1}, m_{i.k,1}, L_{i.k,1}, X_{i.k,1}\right)$ and the delay towards the TDMA frame is $\mathcal{D}_{i.k,1} = \mathcal{D}_{tx}\left(n_{i.k,1}L_{i.k,1}, X_{i.k,1}, \mathcal{R}\right)$ and the average wait time is $\mathcal{D}_{wait}(\varphi_{i.k}, \vartheta_k)$. The total minimum relative energy cost for path 1 is then determined using the following optimization problem:

$$\text{minimize} \quad \sum_{k=1}^{N_s} \mathcal{E}_{i.k,1} \tag{3.17.0}$$

$$\text{subject to} \quad \mathcal{P}_{i.k,1} \geq \mathcal{P}_{req}, \forall k \in [1, N_s] \tag{3.17.1}$$

$$\mathcal{D}_{wait}(\varphi_{i.k}, \vartheta_k) + \sum_{k=1}^{N_s} \mathcal{D}_{i.k,1} \leq \mathcal{D}_{req}, \forall k \in [1, N_s] \tag{3.17.2}$$

$$n_{i.k,1}L_{p,i.k,1} = r_k, \forall k \in [1, N_s] \tag{3.17.3}$$

$$\sum_{k=1}^{N_s} n_{i.k,1}L_{i.k,1}\frac{\phi\left(\bar{\gamma}_{i.k,1}, m_{i.k,1}, L_{i.k,1}, X_{i.k,1}\right)}{\mathcal{R}} \leq 1, \forall i \in [2, N_b + 1] \tag{3.17.4}$$

The optimization problem represents a non-linear problem (NLP) whose solution is challenging to obtain due to the non-linearity and complexity of (3.17.0) and (3.17.1). Note that the transmission power $P_{tx.i.k,1}$, retransmission limit $X_{i.k,1}$, and number of samples per packet $\varphi_{i.k,1}$ for each SN $i.k$ ($k \in [1, N_s]$) are the decision variables to (3.17). Solving (3.17) is

equivalent to finding $P_{tx.i.k,1}$, $X_{i.k,1}$, and $\varphi_{i.k,1}$ such that the total relative energy cost is minimized without violating the reliability and delay constraints. The optimal solution to (3.17) can be obtained using an exhaustive search algorithm where all combinations of $P_{tx.i.k,1}$, $X_{i.k,1}$, and $\varphi_{i.k,1}$ are explored. However, assuming each of the N_s SNs has $\mathcal{Z}$ power levels, a maximum retransmission limit of X_{max}, and $\varphi_{max} = \left\lceil L_{p,max}/\min(L_{sam,1}, \ldots, L_{sam,N_s}) \right\rceil$ is the maximum number of samples that can be aggregated into a data packet, the number of combinations that must be explored to obtain an optimal solution using an exhaustive search is $N_s \mathcal{Z} X_{max} \varphi_{max}$. Given the need to deliver physiological data updates in a real-time manner, it is imperative for (3.17) to be solved in a fast and efficient manner. We propose Algorithm 3.1 to obtain the minimum relative energy cost and delay along each $link(i.k, 1)$ by evaluating a maximum of $\mathcal{Z}(X_{max} + \varphi_{max})$ combinations. Algorithm 3.1 is designed to eliminate unnecessary combinations of $P_{tx.i.k,1}$, $X_{i.k,1}$, and $\varphi_{i.k,1}$ that do not meet the QoS constraints. It should be noted that the destination node of the inter-BAN SN link in Algorithm 3.1 is assigned an ID of j. Therefore, $j = 1$ when considering $link(i.k, 1)$.

Algorithm 3.1 Minimum Joint Delay and Relative Energy Cost for Inter-BAN SN Link

Input: $PL(d_0), \alpha, d_0, d, j, m, P_{min}, P_{max}, X_{max}, L_{sam,k}, \varphi_{max,k}, \vartheta_k, r_k, \mathcal{P}_{req}, \mathcal{D}_{req}, E_{res,i.k}, E_{res,j}$.
Output: $FS, \hat{\mathcal{E}}$, and $\widehat{\mathcal{D}}$;
Initialization: $P_{tx}(z) = P_{max}$ (i. e. , $z = \mathcal{Z}$); $\mathcal{E}_{min} = \infty$; $\mathcal{E}''_{min} = \infty$; $FS = \emptyset$;
while $(P_{tx}(z) \geq P_{min})$ **do**
  $\varphi = \varphi_{max,k}$; $X = X_{max}$;
  while $(\varphi \geq 1)\&\&(X \geq 1)$ **do**
    Calculate $\mathcal{P}_{i.k,j} = \mathcal{P}_s\left(\bar{\gamma}_{i.k,j}, m, L_h + \varphi L_{sam,k}, X\right)$ using $P_{tx}(z)$;
    Calculate $n = r_k/(\varphi L_{sam.k})$; $L = L_h + \varphi L_{sam,k}$;
    Calculate $\mathcal{D}_{i.k,j} = \mathcal{D}_{tx}(nL, X, \mathcal{R})$;
    if $(\mathcal{P}_{i.k,j} \geq \mathcal{P}_{req})$ && $\left(\mathcal{D}_{i.k,j} \leq \mathcal{D}_{req}\right)$ **then**
      Calculate $\mathcal{E}_{i.k,j} = nL\phi\left(\bar{\gamma}_{i.k,j}, m, L, X\right)\left(E_b(P_{tx}(z))/E_{res,i.k} + E_b(P_{rx})/E_{res,j}\right)$;
      if $(\mathcal{E}_{i.k,j}\left(\mathcal{D}_{i.k,j} + \mathcal{D}_{wait}(\varphi, \vartheta_k)\right) < \mathcal{E}'_{min})$ **then**
        $\mathcal{E}'_{min} = \mathcal{E}_{i.k,j}\left(\mathcal{D}_{i.k,j} + \mathcal{D}_{wait}(\varphi, \vartheta_k)\right)$; $\hat{\mathcal{E}} = \mathcal{E}_{i.k,j}$; $\widehat{\mathcal{D}} = \mathcal{D}_{i.k,j}$; $FS = (P_{tx}(z), X, \varphi)$;
      end if
      $X = X - 1$; //decrement retransmission limit
    else
      $\varphi = \varphi - 1$; // decrement number of samples per packet
    end if
  end while
  if $(\mathcal{E}'_{min} \geq \mathcal{E}''_{min})$ && $(\mathcal{E}'_{min} \neq \infty)$ **then** //no improvement in joint delay and REC
    terminate while loop
  else
    $z = z - 1$; //decrement power level
  end for
  $\mathcal{E}''_{min} = \mathcal{E}'_{min}$; //store the lowest relative energy cost obtained at $P_{tx}(z)$
end while
return *FS*, $\hat{\mathcal{E}}$, and $\widehat{\mathcal{D}}$;

In Algorithm 3.1, let $(P_{tx}(z), X, \varphi)$ denote the current combination of decision variables required to minimize the relative energy cost, $\mathcal{E}'_{min}$ the minimum joint delay and relative energy cost obtained for $P_{tx}(z)$, and $\mathcal{E}''_{min}$ the minimum joint delay and relative energy cost obtained for $P_{tx}(z-1)$ where $z > 1$. We are interested in minimizing the joint delay and relative energy cost

instead of just the relative energy cost for the following reason. Since we use Algorithm 3.1 to determine the link performance for each SN instead of the BAN performance for all SNs (i.e., (3.17)), there is no guarantee that the delay constraint $\mathcal{D}_{req}$ can be met. By jointly considering delay and relative energy cost as one expression, we can minimize delay and relative energy cost simultaneously which also improves the probability of satisfying the delay constraint.

We describe the operation of Algorithm 3.1 using the following four cases that are captured within the two while loops:

Case 1 $(\mathcal{P}_{i.k,j} \geq \mathcal{P}_{req})$ && $\left(\mathcal{D}_{i.k,j} \leq \mathcal{D}_{req}\right)$: In this case $(P_{tx}(z), X, \varphi)$ provides a feasible solution because the reliability and delay constraints are satisfied. The product of the current relative energy cost $\mathcal{E}_{i.k,j}$ calculated in line 11 and delay $\mathcal{D}_{i.k,j}$ calculated in line 9 is taken and compared against the minimum joint delay and relative energy cost $\mathcal{E}'_{min}$ in line 12. If $(\mathcal{E}_{i.k,j}\mathcal{D}_{i.k,j} < \mathcal{E}'_{min})$, $(P_{tx}(z), X, \varphi)$ becomes the up-to-date solution and $\mathcal{E}'_{min}$ is set to $\mathcal{E}_{i.k,j}\mathcal{D}_{i.k,j}$. Combinations of $(P_{tx}(z), X, \varphi')$, $\varphi' < \varphi$, $\varphi' \in [1, \varphi_{max}]$ can be eliminated because even though they may satisfy the reliability and delay constraint, it may come at the expense of higher joint delay and relative energy cost (i.e., increased overhead from transmitting more packet headers since the total traffic increases as the number of samples per packet decreases). Furthermore, since the combinations with $\varphi'' > \varphi$, $\varphi'' \in [1, \varphi_{max}]$ have been previously evaluated (i.e., line 17), the next search direction for a possible reduction in joint delay and relative energy cost is to decrease the retransmission limit, as shown in line 15. The eliminated combinations may provide the optimal solution, however, we sacrifice algorithmic accuracy for solution efficiency and determine the ramifications of this sacrifice in the numerical results.

Case 2 $(\mathcal{P}_{i.k,j} < \mathcal{P}_{req})$ || $\left(\mathcal{D}_{i.k,j} > \mathcal{D}_{req}\right)$: In this case $(P_{tx}(z), X, \varphi)$ does not provide a feasible solution because at least one of the two QoS requirements has not been satisfied. As a result, the combinations encompassing $(P_{tx}(z), X', \varphi)$, $X' < X$, $X' \in [1, X_{max}]$ can be eliminated because the combination $(P_{tx}(z), X, \varphi)$ violates at least one of the constraints and thus any further combination with a reduced retransmission limit could violate the reliability constraint. It is possible that only the delay constraint was violated which implies that reducing the retranmission limit makes it more likely to satisfy the delay constraint. Again, the reduction in combinations and solution accuracy is sacrificed to improve efficiency. We also note that the combinations containing X'', $X'' > X$, $X'' \in [1, X_{max}]$ have already been evaluated and thus the next search direction would be to decrease the number of samples per packet to attain a feasable solution that satisfies the reliability and delay objectives.

Case 3 $(\mathcal{E}'_{min} \geq \mathcal{E}''_{min})$ && $(\mathcal{E}'_{min} \neq \infty)$: The joint delay and relative energy cost $\mathcal{E}'_{min}$ obtained at $P_{tx}(z)$ is the same or higher than the joint delay and relative energy cost $\mathcal{E}''_{min}$ obtained at $P_{tx}(z-1)$, $z > 1$, meaning the decrementing of power level z does not provide an improved solution and thus the algorithm can be terminated. This terminating loop eliminates unnecessary combinations involving z that do not improve the final solution.

Case 4 $(\mathcal{E}'_{min} < \mathcal{E}''_{min})$: The joint delay and relative energy cost $\mathcal{E}'_{min}$ obtained at $P_{tx}(z)$ is lower than the joint delay and relative energy cost $\mathcal{E}''_{min}$ obtained at $P_{tx}(z-1)$, $z > 1$, which means decreasing the power level z provides an improved solution.

In Algorithm 3.1, the decision variables are initialized as $(P_{tx}(z), X, \varphi) = (P_{tx}(\mathcal{Z}), X_{max}, \varphi_{max})$ to provide an initial worst case solution, if a solution exists, and to encourage fast solution convergence. If the combination $(P_{tx}(z), X, \varphi)$ is a feasible

solution, the search direction for Algorithm 3.1 is along X, decreasing the retransmission limit by one each time and resulting in a maximum of X_{max} steps. On the other hand, if the combination isn't a feasible solution the search direction decreases along φ, decreasing the number of samples per packet one at a time, resulting in a maximum of φ_{max} steps. Furthermore, the third search direction is guided by a decrease in transmit power $P_{tx}(z)$, decrementing the power level z by one if the minimum joint delay and relative energy cost solution hasn't been improved, resulting in a maximum of $\mathcal{Z}$ steps. The described search directions do not overlap since the region given by $(\mathcal{P}_{i.k,j} \geq \mathcal{P}_{req})$ && $\left(\mathcal{D}_{i.k,j} \leq \mathcal{D}_{req}\right)$ is mutually exclusive of the union of regions $(\mathcal{P}_{i.k,j} < \mathcal{P}_{req})$ && $\left(\mathcal{D}_{i.k,j} \leq \mathcal{D}_{req}\right)$ and $(\mathcal{P}_{i.k,j} \geq \mathcal{P}_{req})$ && $\left(\mathcal{D}_{i.k,j} > \mathcal{D}_{req}\right)$. Therefore, it is straightforward to see that the maximum and minimum number of combinations explored by Algorithm 3.1 is $\mathcal{Z}(X_{max} + \varphi_{max})$ and $(X_{max} + \varphi_{max})$, respectively.

The final solution to (3.17) is obtained by executing Algorithm 3.1 for each $link\ (i.k, 1)$. The total relative energy cost and average end-to-end delay for transmissions over path 1 is $\mathcal{E}_{path1} = \sum_{k=1}^{N_s} \mathcal{E}_{i.k,1}$ and $\mathcal{D}_{path1} = \mathcal{D}_{wait}\left(\varphi_{i.k,1}, \vartheta_k\right) + \sum_{k=1}^{N_s} \mathcal{D}_{i.k,1}$.

3.4.2.2 Sub-Problem #2: Path 2 Minimum Relative Energy Cost Solution

The relative energy cost for the links emanating from SN $i.k$ (i.e., $link(i.k, i)$ and overhearing $link(i.k, 1)$) is $\mathcal{E}_{i.k} = n_{i.k,i} L_{i.k,i} \phi\left(\bar{\gamma}_{i.k,i}, m_{i.k,i}, L_{i.k,i}, X_{i.k,i}\right)\left(E_b(P_{tx.i.k,i})/E_{res,i.k} + E_b(P_{rx})/E_{res,i} + E_b(P_{rx})/E_{res,1}\right)$ and the relative energy cost for BNC i over $link(i.k, i)$ is $\mathcal{E}_{i1} = n_{i1} L_{i1} \phi(\bar{\gamma}_{i1}, m_{i1}, L_{i1}, X_{i1})\left(E_b(P_{tx.i1})/E_{res,i} + E_b(P_{rx})/E_{res,1}\right)$. The probability of succesful delivery over $link\ (i.k, i)$ is $\bar{\mathcal{P}}_{i.k,i}$ and overhearing the transmitted packets over $link(i.k, 1)$ is $\bar{\mathcal{P}}_{i.k,1}$. The TDMA frame delay over $link(i.k, i)$ is $\mathcal{D}_{i.k,i} = \mathcal{D}_{tx}\left(n_{i.k,i} L_{i.k,i}, X_{i.k,i}, \mathcal{R}\right)$ and over $link(i.k, 1)$ is $\mathcal{D}_{i1} = \mathcal{D}_{tx}(n_{i1} L_{i1}, X_{i1}, \mathcal{R})$. The total

minimum relative energy cost for path 2 is then determined using the following optimization problem:

$$\text{minimize} \quad \sum_{k=1}^{N_s} \mathcal{E}_{i.k} + \mathcal{E}_{i1} \tag{3.18.0}$$

$$\text{subject to} \quad 1 - \left(1 - \overline{\mathcal{P}}_{i.k,i}\mathcal{P}_{i1}\right)\left(1 - \overline{\mathcal{P}}_{i.k,1}\right) \geq \mathcal{P}_{req}, \forall k \in [1, N_s] \tag{3.18.1}$$

$$\mathcal{D}_{wait}(\varphi_{i.k}, \vartheta_k) + \sum_{k=1}^{N_s} \mathcal{D}_{i.k,i} + \mathcal{D}_{i1} \leq \mathcal{D}_{req}, \forall k \in [1, N_s] \tag{3.18.2}$$

$$n_{i.k,1} L_{p,i.k,1} = r_k, \forall k \in [1, N_s] \tag{3.18.3}$$

$$n_{i1} L_{p,i1} = \mu \sum_{k=1}^{N_s} r_k, \tag{3.18.4}$$

$$\sum_{k=1}^{N_s} \frac{n_{i.k,i} L_{i.k,i} \phi\left(\bar{\gamma}_{i.k,i}, m_{i.k,i}, L_{i.k,i}, X_{i.k,i}\right)}{\mathcal{R}} + \frac{n_{i1} L_{i1} \phi(\bar{\gamma}_{i1}, m_{i1}, L_{i1}, X_{i1})}{\mathcal{R}} \leq 1 \tag{3.18.5}$$

Obtaining the optimal solution to (3.18) remains a nontrivial task due to the complicated expressions in (3.18) and (3.18.1). An exhaustive search algorithm requires the exploration of $N_s(\mathcal{Z} X_{max} \varphi_{max})^2$ combinations in order to obtain the optimal solution, which is exorbitantly high. We propose Algorithm 3.2 to obtain a reduced complexity sub-optimal solution. The inputs to Algorithm 3.2 consider the transmission parameters used at the SNs and BNC and the path loss and fading parameters used for propagation through the on-body and body-to-body channels. The bold inputs represent sets. For example, $\boldsymbol{m} = \{m_{i1}, m_{i.k,i}, m_{i.k,1}\}, \boldsymbol{r} = \{r_k\}, \boldsymbol{L_{sam}} = \{L_{sam,i.k}\}\ \forall k \in [1, N_s]$.

Algorithm 3.2 Minimum Joint Delay and Relative Energy Cost for Intra and Inter BAN Links

Input: $\boldsymbol{PL(d_0)}, \boldsymbol{\alpha}, \boldsymbol{d_0}, \boldsymbol{d}, \boldsymbol{m}, P_{min}, P_{max}, X_{max}, \boldsymbol{L_{sam}}, \boldsymbol{\varphi_{max}}, \boldsymbol{\vartheta}, \boldsymbol{r}, \mathcal{P}_{req}, \mathcal{D}_{req}, \boldsymbol{E_{res,i.k}}, E_{res,i}, E_{res,j}$.
Output: $\boldsymbol{FS}, \widehat{\boldsymbol{\mathcal{E}}}, \widehat{\boldsymbol{\mathcal{D}}}, \hat{\mathcal{E}}_{min}, \widehat{\mathcal{D}}_{min}$;
for each SN *i.k* **do**
  $P_{tx}(z) = P_{max}$ (i.e., $z = \mathcal{Z}$); $\mathcal{E}_{min} = \infty$; $\mathcal{E}''_{min} = \infty$;
  while $(P_{tx}(z) \geq P_{min})$ **do**
    $\varphi = \varphi_{max,k}$; $X = X_{max}$;
    while $(\varphi \geq 1)\&\&(X \geq 1)$ **do**
      Calculate $\mathcal{P}_{i.k,i} = \mathcal{P}_s\left(\bar{\gamma}_{i.k,i}, m_{i.k,i}, L_h + \varphi L_{sam,k}, X\right)$ using $P_{tx}(z)$;
      Calculate $\mathcal{P}_{i.k,j} = \mathcal{P}_s\left(\bar{\gamma}_{i.k,j}, m_{i.k,j}, L_h + \varphi L_{sam,k}, X\right)$ using $P_{tx}(z)$;
      Calculate $n_{i.k,i} = r_k/(\varphi L_{sam.k})$; $L_{i.k,i} = L_h + \varphi L_{sam,k}$;
      Calculate $\mathcal{D}_{i.k,i} = \mathcal{D}_{tx}\left(n_{i.k,i}L_{i.k,i}, X, \min(\mathcal{R}_{i.k,i}, \mathcal{R}_{i.k,j})\right)$
      if $(\mathcal{P}_{i.k,i} = 1)$ && $\left(\mathcal{D}_{i.k,i} \leq \mathcal{D}_{req}\right)$ **then**
        Calculate $\mathcal{E}_{i.k,i} = n_{i.k,i}L_{i.k,i}\phi\left(\bar{\gamma}_{i.k,i}, m_{i.k,i}, L_{i.k,i}, X\right)\left(\frac{E_b(P_{tx}(z))}{E_{res,i.k}} + \frac{E_b(P_{rx})}{E_{res,i}} + \frac{E_b(P_{rx})}{E_{res,j}}\right)$;
        if $\left(\left(\mathcal{E}_{i.k,i}\mathcal{D}_{i.k,i}\right)/\left(\mathcal{P}_{i.k,i}\mathcal{P}_{i.k,j}\right) < \mathcal{E}'_{min}\right)$ **then**
          $\mathcal{E}'_{min} = \left(\mathcal{E}_{i.k,i}\mathcal{D}_{i.k,i}\right)/\left(\mathcal{P}_{i.k,i}\mathcal{P}_{i.k,j}\right)$; $\hat{\mathcal{E}}_{i.k} = \mathcal{E}_{i.k,i}$; $\widehat{\mathcal{D}}_{i.k} = \mathcal{D}_{i.k,i}$; $\widehat{\mathcal{P}}_{i.k} = \mathcal{P}_{i.k,j}$;
          $FS(i.k) = (P_{tx}(z), X, \varphi)$;
        end if
        $X = X - 1$; //decrement retransmission limit
      else
        $\varphi = \varphi - 1$; // decrement number of samples per packet
      end if
    end while
    if $(\mathcal{E}'_{min} \geq \mathcal{E}''_{min})$ && $(\mathcal{E}'_{min} \neq \infty)$ **then** //no improvement in joint delay REC
      terminate while loop
    else
      $z = z - 1$; //decrement power level
    end for
    $\mathcal{E}''_{min} = \mathcal{E}'_{min}$; //store the lowest joint delay REC obtained at $P_{tx}(z)$
  end while
end for
$P_{tx}(z) = P_{max}$ (i.e., $z = \mathcal{Z}$); $\mathcal{E}_{min} = \infty$; $\mathcal{E}''_{min} = \infty$; $\varphi_{max} = L_{p,max}/\min(\boldsymbol{L_{sam}})$;
while $(P_{tx}(z) \geq P_{min})$ **do**
  $\varphi = \varphi_{max,k}$; $k = \text{argmin}(\boldsymbol{L_{sam}})$; $X = X_{max}$;
  while $(\varphi \geq 1)\&\&(X \geq 1)$ **do**
    Calculate $\mathcal{P}_{ij} = \mathcal{P}_s\left(\bar{\gamma}_{ij}, m_{ij}, L_h + \varphi\min(\boldsymbol{L_{sam}}), X\right)$ using $P_{tx}(z)$;

35: Calculate $n_{ij} = \left(\sum_{k=1}^{N_s} r_k\right)/\left(\varphi \min(\boldsymbol{L_{sam}})\right)$; $L_{ij} = L_h + \varphi \min(\boldsymbol{L_{sam}})$;
36: Calculate $\mathcal{D}_{ij} = \mathcal{D}_{tx}\left(n_{ij}L_{ij}, X, \mathcal{R}\right) + \max\left(\mathcal{D}_{wait}(\boldsymbol{\varphi}, \boldsymbol{\vartheta})\right)$;
37: **if** $\left(1 - \left(1 - \mathcal{P}_{ij}\overline{\mathcal{P}}_{i.k,i}\right)\left(1 - \overline{\mathcal{P}}_{i.k,j}\right) \geq \mathcal{P}_{req}\right)$ && $\left(\mathcal{D}_{ij} + \sum_{k=1}^{N_s} \widehat{\mathcal{D}}_{i.k} \leq \mathcal{D}_{req}\right)$ **then**
38: Calculate $\mathcal{E}_{ij} = n_{ij}L_{ij}\phi\left(\bar{\gamma}_{ij}, m_{ij}, L_{ij}, X\right)\left(\frac{E_b(P_{tx}(z))}{E_{res,i}} + \frac{E_b(P_{rx})}{E_{res,j}}\right)$;
39: **if** $(\mathcal{E}_{ij}\mathcal{D}_{ij} < \mathcal{E}'_{min})$ **then**
40: $\mathcal{E}'_{min} = \mathcal{E}_{ij}\mathcal{D}_{ij}$; $\hat{\mathcal{E}}_{ij} = \mathcal{E}_{ij}$; $\widehat{\mathcal{D}}_{ij} = \mathcal{D}_{ij}$; $FS(i) = (P_{tx}(z), X, \varphi)$;
41: **end if**
42: $X = X - 1$; //decrement retransmission limit
43: **else**
44: $\varphi = \varphi - 1$; // decrement number of samples per packet
45: **end if**
46: **end while**
47: **if** $(\mathcal{E}'_{min} \geq \mathcal{E}''_{min})$ && $(\mathcal{E}'_{min} \neq \infty)$ **then** //no improvement in joint delay REC
48: terminate while loop
49: **else**
50: $z = z - 1$; //decrement power level
51: **end for**
52: $\mathcal{E}''_{min} = \mathcal{E}'_{min}$; //store the lowest joint delay REC obtained at $P_{tx}(z)$
53: **end while**
54: Calculate REC and delay $\hat{\mathcal{E}}_{min} = \sum_{k=1}^{N_s} \hat{\mathcal{E}}_{i.k} + \hat{\mathcal{E}}_{ij}$; $\widehat{\mathcal{D}}_{min} = \sum_{k=1}^{N_s} \widehat{\mathcal{D}}_{i.k} + \widehat{\mathcal{D}}_{ij}$;
55: **return** $\boldsymbol{FS}, \widehat{\boldsymbol{\mathcal{E}}}, \widehat{\boldsymbol{\mathcal{D}}}$, $\hat{\mathcal{E}}_{min}$,and $\widehat{\mathcal{D}}_{min}$;

The operation of Algorithm 3.2 is based on the same multi variable search direction concept employed in Algorithm 3.1. We thus focus our description of Algorithm 3.2 on the features that distinguish it from Algorithm 3.1. The for loop entailing lines 3 to 29 determine the minimum relative energy cost and delay for each SN link. In line 9, $\mathcal{P}_{i.k,j}$ is calculated to account for transmissions overheard from the SN-to-BNC links. Line 11 calculates the delay for the transmissions over $link(i.k, i)$. The reliability constraint in line 12 is modified to require error free transmission over $link(i.k, j)$ (i.e., $\mathcal{P}_{i.k,i} = 1$). The stringent reliability constraint increases the probability of successfully overhearing transmissions at the BS while also guaranteeing

successful delivery for all intra-BAN transmissions. The joint delay and relative energy cost $\mathcal{E}'_{min}$ in line 15 also accounts for the probability of success over $link(i.k,i)$ and $link(i.k,j)$. By selecting transmission parameters for $link(i.k,i)$ that increase the probability of success over $link(i.k,j)$, the probability of success requirement for $link(i,j)$ in line 37 becomes less stringent since reliability is enhanced by exploiting the overheard transmissions. The while loop encapsulated by lines 31 to 53 determines the minimum relative energy cost and delay for the BNC link while also incorporating the delay and reliability due to the overheard transmissions calculated from the preceding for loop. In line 30, φ_{max} is recalculated to account for the minimum data sample size received from all the SNs (i.e., $\min(\boldsymbol{L_{sam}})$). Note that the delay calculation for $link(i,j)$ in line 36 accounts for the single highest wait time achieved by the set of SNs as opposed to accounting for the sum of wait times because we are interested in the average end-to-end delay that consists of the TDMA frame delay and average wait time. By accounting for the highest wait time we can guarantee the delay constraint is satisfied for all SN transmissions. Line 37 considers the joint reliability over $link(i,j)$ and $link(i.k,i), \forall k \in (1,N_s)$ in addition to the reliability from the overheard transmissions from $link(i.k,j), \forall k \in (1,N_s)$. The success probability for transmissions over $link(i.k,i)$ is constrained to achieve $\mathcal{P}_{i.k,i} = 1$ so that we can guarantee that the end-to-end reliability between all SNs and the BS is satisfied. The total relative energy cost and delay for path 2 are calculated in line 54 and Algorithm 3.2 is subsequently terminated in line 55. The solution to (3.18) is then obtained by executing Algorithm 3.2 and setting the total relative energy cost and average end-to-end delay for transmissions over path 2 as $\mathcal{E}_{path2} = \hat{\mathcal{E}}_{min}$ and $\mathcal{D}_{path2} = \widehat{\mathcal{D}}_{min}$, respectively.

The final solution to (3.15) is obtained by first comparing $\mathcal{E}_{path1}$ and $\mathcal{E}_{path2}$. If $\mathcal{E}_{path1} < \mathcal{E}_{path2}$ then the SNs route their physiological data along path 1, otherwise if $\mathcal{E}_{path1} > \mathcal{E}_{path2}$ the SNs route their physiological data along path 2. If $\mathcal{E}_{path1} = \mathcal{E}_{path2}$, $\mathcal{D}_{path1}$ and $\mathcal{D}_{path2}$ are compared next. If $\mathcal{D}_{path1} < \mathcal{D}_{path2}$, path 1 is utilized. Otherwise, path 2 is utilized. Both Algorithm 3.1 and Algorithm 3.2 guarantee a solution to (3.15) if a solution exists. However, in the scenario a solution cannot be obtained due to the stringent delay requirement, we set $\mathcal{D}_{req} = \infty$ effectively relaxing the delay constraint.

3.5 Performance Evaluation

This section presents numerical results for the relative energy cost, success probability, and delay of the EQS communication scheme in a single-hop body-to-body network. While analytical techniques provide approximate expressions for relative energy cost, success probability, and delay, a discrete-event simulator is designed to model EQS in detail and to check the accuracy and validity of the approximations and assumptions made in the analysis. Most notably, we have neglected shadowing in both the on-body and body-to-body channels and have also neglected the relative energy costs associated with transmitting and receiving ACK packets.

3.5.1 Input Parameter Values

In order to conduct a realistic analysis we model the Crossbow platform on the MICAz [141] sensor motes which is a popular choice for BAN research [23], [37], [38]. The components contributing to the major energy consumption on the MICAz devices are the ATmega128L low-power microcontroller and the Chipcon CC2420 low-power wireless transceiver. The power consumption of the CC2420 and ATmega128L are characterized by the following parameters

[83]: $P_{tx,cir} = 25.7$ mW, $P_{rx} = 59.1$ mW, $P_{min} = -20$ dBm, $P_{max} = 0$ dBm, and the number of power levels is set at $\mathcal{Z} = 21$. The power amplifier efficiency is provided in (3.13). The maximum data rate for the MICAz is stated as $\mathcal{R} = 250$ kbps [83]. We set the packet header as $L_h = 104$ bits and the maximum payload size as $L_{p,max} = 920$ bits which follows from the IEEE 802.15.4 standard [81]. The maximum battery capacity for each SN is calculated assuming a lithium ion battery with 560 mAh operating at 3 volts providing $E_{init}^{s} = 6048$ joules [146] whereas the BNCs use a larger capacity 2000 mAh battery also operating at 3 volts providing $E_{init}^{b} = 21{,}600$ joules. The BS uses a large 9V battery that provides $E_{init}^{c} = 302{,}400$ joules. The sampling rate, sample size, and data rate characteristics for each SN are summarized in Table 3.1 along with the sensor mote hardware and MAC layer parameters.

TABLE 3.1 SENSOR MOTE AND MAC LAYER PARAMETER VALUES

Description	**Parameters and Values**
SN ID Mapping	$k = \{1,2,3,4,5,6\} \rightarrow \{\mathrm{S_pO_2}, \mathrm{BP}, \mathrm{9DoF_1}, \mathrm{9DoF_2}, \mathrm{ECG}, \mathrm{EEG}\}$
SN Sample Rate	$\theta_k = \{60,120,100,100,200,200\}$ samples per second
SN Sample Size	$L_{sam,k} = \{32,16,32,32,32,32\}$ bits
SN Data Rate	$r_k = \{1920,1920,3200,3200,6400,6400\}$ bps
Power Consumption	$P_{min} = -20$ dBm, $P_{max} = 0$ dBm, $\mathcal{Z} = 21$, $P_{tx,cir} = 25.7$ mW, $P_{rx} = 59.1$ mW
MAC Layer	$\mathcal{R} = 250$ kbps, $X_{max} = 20$, $L_h = 104$ bits, $L_{p,max} = 920$ bits, $t_{slot} = 5$ ms
Initial Battery Capacity	$E_{init}^{s} = 6{,}048$ J, $E_{init}^{b} = 21{,}600$ J, $E_{init}^{c} = 302{,}400$ J

The path loss and fading parameters for the physical layer of the on-body and body-to-body wireless channels are obtained from the outdoor characterization studies conducted in [9], [11]. The path loss parameters for signal propagation around a human body in an outdoor environment are given in [145] as follows: $PL(d_0) = 43$ dB, $\alpha = 3.8$, and $d_0 = 10$ cm. The fading parameters are dependent on the specific area of the body where the transmitting device

resides. In [9], the Nakagami fading factor parameters are obtained for transmission from the head, chest, wrist, ankle, and shoulder areas to a receiver on the waist. Using these results we assign fading factor parameters to characterize the small scale fading experienced between the SNs and the BNC. Each SN $i.k$ represented by the index $k = \{1, 2, 3, 4, 5, 6\}$ is mapped to the array of fading factors $m_{i.k,i} = \{1.37, 5.29, 1.41, 1.41, 5.29, 2.42\}$ characterized from the wireless signal propagation originating at the specific body parts given by {right wrist, shoulder, ankle, ankle, chest, head} and terminating at the waist where the BNC resides. The average distance between a SN $i.k$ and BNC i is $d_{i.k,i} = \{56, 36, 80, 89, 45, 98\}$ cm. The path loss in the body-to-body channel is taken as an average of the LOS and NLOS scenarios characterized in [11], resulting in $PL(d_0) = 54.6$ dB, $\alpha = 2.2$, and $d_0 = 1$ m. We consider two Nakagami fading factors to account for the fading conditions between the SN and BNC ($m_{i.k,1} = 1$ for Rayleigh fading) and between the BNC and the BS ($m_{i1} = 2$ for Rician fading). The fading conditions for the SNs are more severe than the BNC because the SNs are often located on parts of the body where soldier worn equipment act as obstructions (e.g., a soldier's bullet proof vest, composed of signal attenuating material, could completely cover the ECG SN), preventing a clear line of sight scenario. On the other hand, the BNC is located on an external spot of the soldier where equipment or military clothing does not serve as obstructions. The physical layer characteristics for the on-body and body-to-body channels are summarized in Table 3.2. The literature pertaining to QoS for remote monitoring applications is not definitive, especially in the context of the combat medic remotely monitoring the physiological state of a soldier over a BBN in the battlefield. Nevertheless, judging the QoS requirements used for monitoring health in a hospital environment [37] ($\mathcal{P}_{req} > 90\%$ and $\mathcal{D}_{req} < 5$ seconds), transmitting medical information over

an IP-based e-Health system [147] ($\mathcal{P}_{req} \approx 100\%$ and $\mathcal{D}_{req} < 10$ seconds), and supporting the delivery of critical information for network centric applications in tactical networks [148] ($\mathcal{P}_{req} > 90\%$ and $\mathcal{D}_{req} \leq 1$ second), we set the reliability and delay constraint for each numerical study in this section as $\mathcal{P}_{req} = 99\%$ and $\mathcal{D}_{req} = 1$ second, respectively, to support the recommended stringent QoS requirements of remote monitoring in a single-hop BBN.

TABLE 3.2 PHYSICAL LAYER CHARACTERISTICS FOR ON-BODY AND BODY-TO-BODY CHANNELS IN OUTDOOR ENVIRONMENT

Channel	**Description**	**Parameters and Values**
On-body	Path Loss	$PL(d_0) = 43$ dB, $\alpha = 3.8$, and $d_0 = 10$ cm
	Fading Factors	$m_{i.k,i} = \{1.37, 5.29, 1.41, 1.41, 5.29, 2.42\}$
	SN-to-BNC Distance	$d_{i.k,i} = \{56, 36, 80, 89, 45, 98\}$ cm
Body-to-body	Path Loss	$PL(d_0) = 54.6$ dB, $\alpha = 2.2$, and $d_0 = 1$ m
	Fading Factors	SN: $m_{i.k,1} = 1$ (Rayleigh), BNC: $m_{i1} = 2$ (Rician)

3.5.2 Numerical Studies

3.5.2.1 Effect of the JPRS Strategy on Intra-BAN Link Performance

In order to determine the effect of JPRS strategy on the performance of intra-BAN links, the solution to the optimization model in (3.14) is obtained using the MAC layer parameters, power consumption parameters, and initial battery capacity for the SNs and BNC as provided in Table 3.1 and the on-body path loss parameters in Table 3.2. We compare the performance of the JPRS strategy against the **J**oint **P**ower allocation and **R**etransmission Limit (JPR) strategy that has been employed in [105]. Different from JPRS, JPR assumes a constant packet size of $L_p = L_{p,max}$. The transmission of maximum packet sizes due to aggregation is often employed to support energy efficiency in BANs [16]. Fig. 3.6 presents the intra-BAN link performance results using the JPRS and JPR strategies for transmissions over the on-body channel with link distance

in the range $d_{i.k,i} \in [20,100]$ cm, source data rate $r = 1024$ bps, and worst case on-body fading conditions (i.e., Rayleigh fading). We consider transmission link distance in the range $d_{i.k,i} \in [20,100]$ cm to account for the full range of SN-to-BNC distances in Table 3.2. In Fig. 3.6a, the relative energy cost performance of JPRS and JPR is seen to be the same when the intra-BAN distance is less than 50 cm. However, as the intra-BAN distance increases from 50 cm to 100 cm and the negative effect of increased path loss and severe fading on link success probability become more pronounced, the reduced relative energy cost in JPRS compared to JPR increases from 2% to 60%. The reduced relative energy cost in JPRS is mainly attributable to the ability to jointly optimize the retransmission limit and payload size in addition to the transmit power. In Fig. 3.6c, the transmit power in both JPRS and JPR increase at the same rate until the maximum transmit power is reached. When the maximum transmit power is reached at an intra-BAN distance of 50 cm, Fig. 3.6d shows that the retransmission limit in JPR is increased 10 fold when the intra-BAN distance is increased from 50 cm to 100 cm, thus resulting in a 7 fold increase in average number of transmissions (Fig. 3.6e) and relative energy cost (Fig. 3.6a). On the other hand, the retransmission limit in JPRS is only increased 3 fold, resulting in a 2 fold increase in average number of transmissions and relative energy cost. Different from JPR, Fig. 3.6f shows that the payload size in JPRS is decreased in concert with the increase in retransmission limit in order to sustain the success probability required to satisfy the reliability objective. In Fig. 3.6b, the delay incurred in JPRS is shown to increase 4.5 fold as the intra-BAN distance is increased from 50 cm to 100 cm. The increase in delay is more than twice the increase in average number of transmissions for the following reason. Decreasing the payload size for each data packet results in more data packets that must be transmitted in order to meet the source data rate

requirement. Furthermore, each data packet consists of a header component that subsequently contributes to higher transmitted data traffic, thus increasing delay.

The main significance of the results obtained in this study is the improved relative energy cost and delay performance offered by JPRS which subsequently provides a longer duration for remote physiological monitoring and also improves the ability to meet QoS requirements while incurring less relative energy cost than a power allocation strategy that only optimizes transmission power and the retransmission limit such as JPR. It should also be noted that by considering Rayleigh fading, the worst case performance along any transmission link distance on the body is considered. Nevertheless, the performance analysis performed in Fig. 3.6 can also be conducted for each SN to BNC link using the appropriate Nakagami fading factor values. Generally speaking, the JPRS strategy has a stronger impact (in terms of reducing relative energy cost and delay) upon the SN to BNC links that experience a higher path loss and lower fading factor value (e.g., S_PO_2, $9DoF_1$, $9DoF_2$).

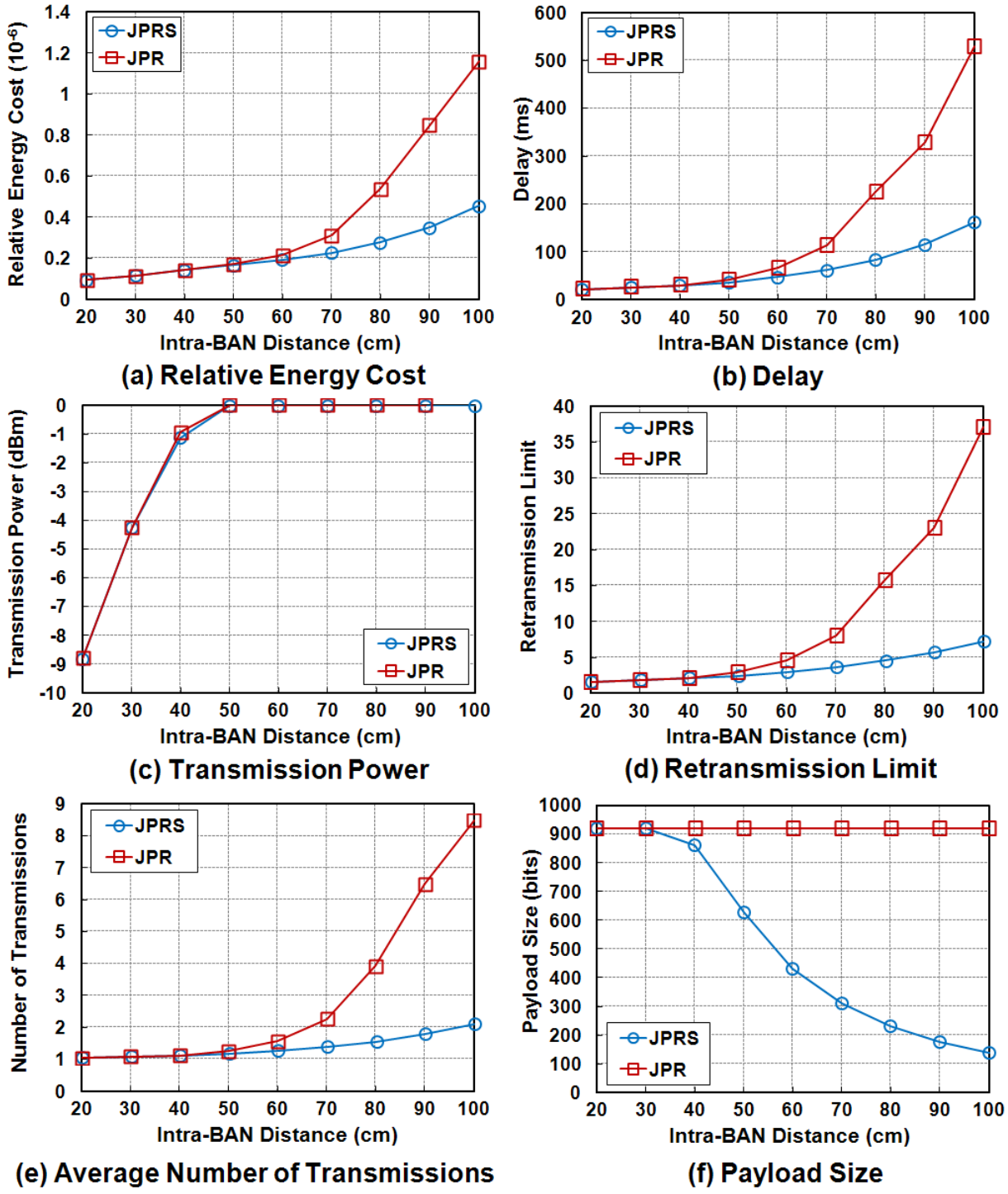

Fig. 3.6. Intra-BAN link performance as a function of intra-BAN distance achieved with JPRS and JPR strategies.

3.5.2.2 Effect of the JPRS Strategy on Inter-BAN Link Performance

To determine the effect of JPRS strategy on the performance of inter-BAN links we obtain the solution to the optimization model in (3.14) using the configuration parameters in Table 3.1 and the body-to-body physical layer parameters presented in Table 3.2 for both Rayleigh and Rician fading. We compare the performance of JPRS against JPR and present the inter-BAN link performance results in Fig. 3.7 from which two main observations are made. The first observation is made based on the results in Fig. 3.7a where it can be seen that JPRS consistently achieves a lower relative energy cost than JPR in the presence of Rayleigh fading. The relative energy cost achieved in JPRS is up to 6 times lower than JPR for the inter-BAN distances between 5 m and 15 m. The reduced relative energy cost realized in JPRS is due to the transmission of packet sizes with smaller payload (Fig. 3.7e). The transmission of smaller payload sizes incurs fewer fading and path loss induced errors and thus fewer retransmissions (Fig. 3.7d) are required to satisfy the reliability constraint. Fig. 3.7b shows that the delay produced in JPRS is significantly lower than JPR because JPR is forced to endure a high retransmission limit to accommodate the maximum payload size. The second observation is that JPRS achieves an inter-BAN transmission distance that is 2.3 and 1.7 times longer than JPR in Rayleigh and Rician fading environments, respectively. The increased transmission distance of JPRS is obtained because JPRS is able to jointly optimize the retransmission limit and payload size to overcome the increased frequency of errors in high path loss scenarios. The two observations made from the results in Fig. 3.7 clearly demonstrate the performance benefits offered when a JPRS strategy is adopted as opposed to a JPR strategy. Therefore, the JPRS strategy is deemed to be viable and also beneficial for inter-BAN transmissions.

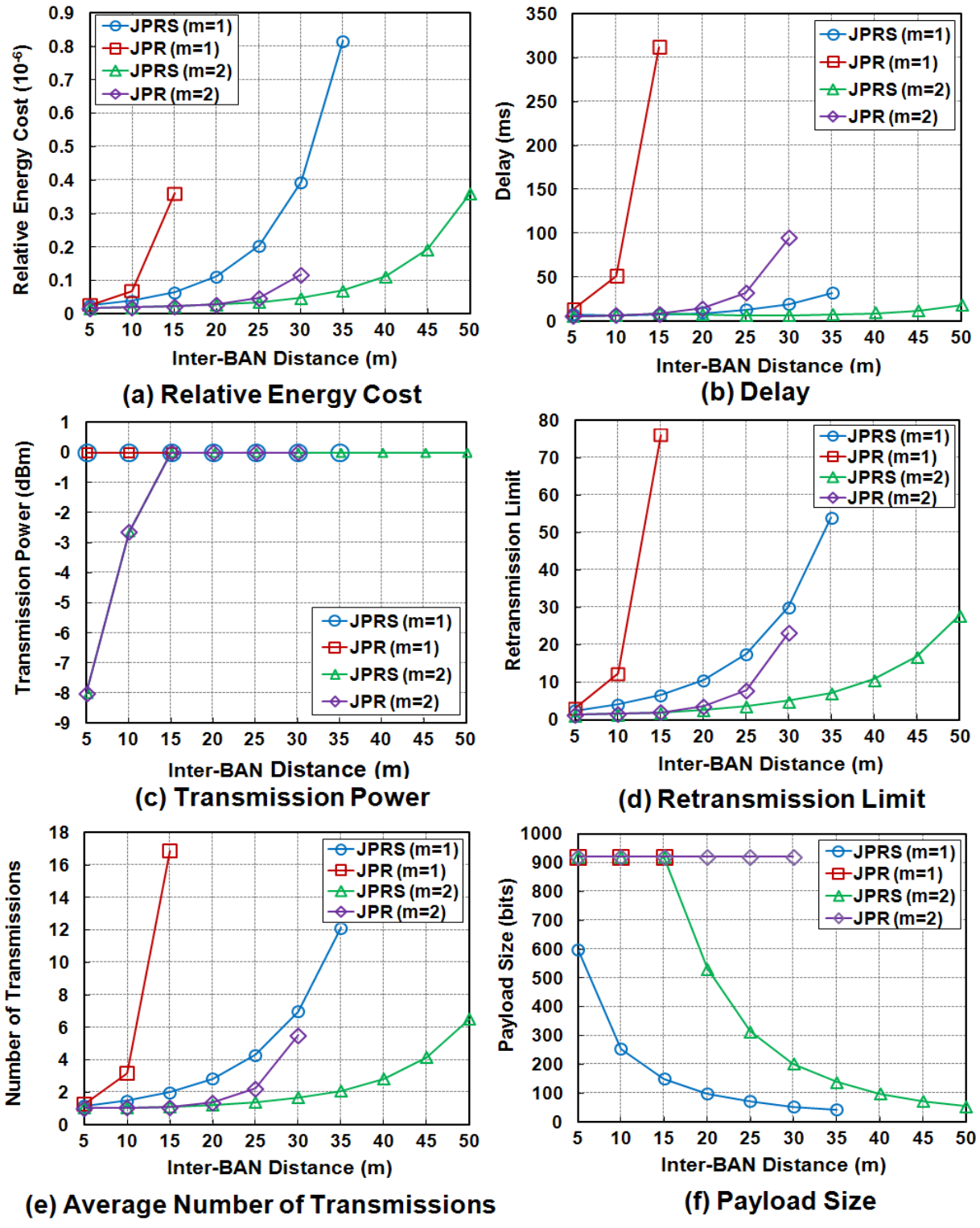

Fig. 3.7. Inter-BAN link performance as a function of inter-BAN distance achieved with JPRS and JPR strategies.

3.5.2.3 Evaluation of Minimum Relative Energy Cost for BBN

In this study we evaluate the performance of the sub-optimal algorithms proposed in Sections 3.4.2.1 and 3.4.2.2 and compare them against the optimal solution obtained from solving (3.14) using an exhaustive search algorithm that considers every combination of transmission power, retransmission limit, and packet size to achieve the minimum relative energy cost while satisfying the desired QoS requirements. The evaluation is performed using the parameters in Table 3.1, Table 3.2, BAN to BS distances in the range $d_i = [5, 25]$ meters, and the following set of residual energy parameters: S1) $E_{res,i.k} = E^s_{init}, E_{res,i} = E^b_{init}, E_{res,1} = E^c_{init}$: These parameters are representative of the scenario where the SNs, BNC, and BS have their maximum energy capacity and are first deployed on the soldier and combat medic. S2) $E_{res,i.k} = 0.25E^s_{init}, E_{res,i} = 0.5E^b_{init}, E_{res,1} = 0.95E^c_{init}$: These parameters depict the remaining residual energy in the SNs, BNC, and BS after the SNs have delivered a large number of physiological data samples using both path 1 and path 2. It is then realistic to assume the SNs consume more energy than the BNC. The goal of evaluating S1 and S2 is to show how well the sub-optimal algorithms adapt to the changing battery state of the SNs, BNC, and BS. The adaptation is demonstrated by accurately determining whether the transmission of data is performed through path 1 or path 2. Accuracy is measured by how close the minimum relative energy cost obtained through the sub-optimal algorithms is to the optimal minimum relative energy cost.

In Fig. 3.8a, the relative energy cost for the sub-optimal algorithms is only 8% higher than the optimal solution when the distance is less than or equal to 20 m and 18% higher when the distance is equal to 25 m. The relative energy cost obtained from the sub-optimal algorithms is seemingly high when the distance is 25 m, for the following reason. The set of feasible solutions at a distance of 25 m is greatly reduced compared to the feasible solutions available at

lower distances because of the stringent delay requirement which becomes increasingly difficult to meet as the path loss increases with distance and an increase in retransmission limit is undergone to satisfy the reliability constraint. Furthermore, because the sub-optimal algorithms operate with a reduced search, the probability of selecting the minimum relative energy cost result is also reduced. The paths taken by the optimal and sub-optimal algorithms are also shown in Fig. 3.8a. A significant penalty in relative energy cost is not observed although the sub-optimal algorithm transitions from path 1 to path 2 at a distance of 20 m as opposed to a distance of 15 m for the optimal solution. Fig. 3.8b shows the sub-optimal relative energy cost results for S2 are between 2% and 15% higher than the optimal relative energy cost. The increased relative energy cost is more pronounced when the sub-optimal solution is obtained for path 2 at a distance greater than or equal to 15 m. Specifically, the increased relative energy cost in the sub-optimal solution can be attributed to the lower success probability of the overheard SN-to-BS transmissions. The optimal solution reveals that the success probability of the overheard SN-to-BS transmissions is 30% higher than the sub-optimal algorithms and thus higher relative energy cost is incurred at the BNC for the sub-optimal algorithms because the BNC-to-BS must employ a higher number of transmissions and lower payload to satisfy the end-to-end reliability constraint over path 2. The average end-to-end delay for S1 and S2 is shown in Fig. 3.8c. The curves of the delay for the optimal solutions are erratic because the minimum delay is not tied to the minimum relative energy cost owing to the wait time that injects delay penalties as the aggregation data packet size approaches the maximum permitted. The sub-optimal algorithms jointly minimize relative energy cost and delay to ensure the delay constraint is satisfied and thus the delay increases with the relative energy cost in a monotonic manner. It is also observed that the delay for the sub-optimal algorithms steadily increases as the distance increases, which is

expected. The number of iterations required to perform an exhaustive search and to converge to a solution using the sub-optimal algorithms is shown in Fig. 3.8d in log10 scale. It is obviously clear that the sub-optimal algorithm is significantly more efficient than the optimal algorithm. However, efficiency comes at the price of increased relative energy cost.

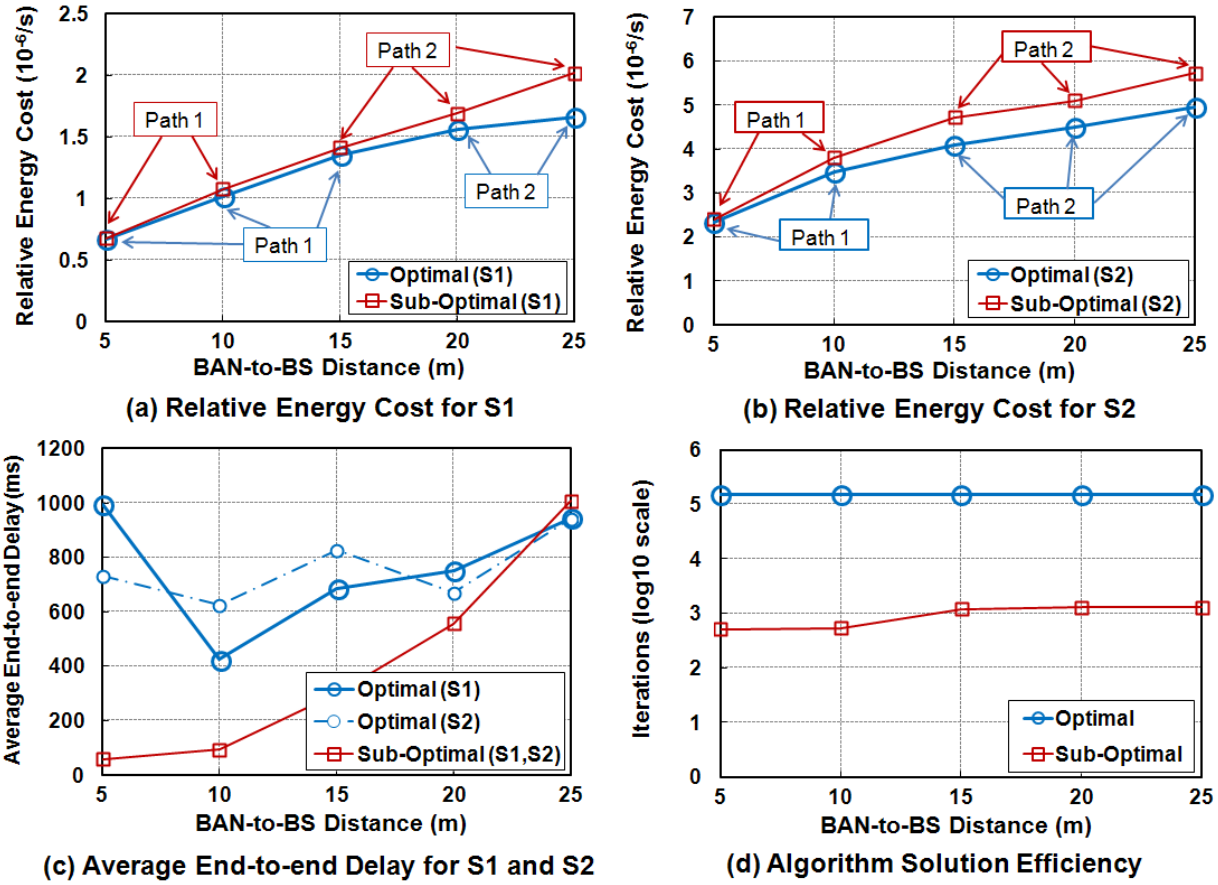

Fig. 3.8. Performance of sub-optimal algorithms against optimal solution for minimum relative energy cost BAN transmissions in EQS.

3.5.3 Simulation Experiments

3.5.3.1 Simulation Settings

The simulation experiments performed in this section are driven by a simulator primarily designed to model the operation and evaluate the performance of EQS in a simulated single-hop body-to-body network environment that accounts for on-body and body-to-body shadowing in

addition to the transmission of ACK packets. The consideration of shadowing in the simulations represents a major difference from the analysis where shadowing was excluded. Each simulation features a single soldier fitted with a BAN comprised of six SNs and one BNC and a combat medic equipped with a BS device. Since we do not consider multi-hop routing in this chapter, it is sufficient to execute the simulation experiments with a single BAN because we can evaluate the performance of EQS in terms of the distance between the BAN and the BS. Unless otherwise specified, the distance between the BAN and BS is varied between 5 m and 25 m. We use a simple TDMA scheme as the MAC layer protocol. The channel state information required to build a minimum relative energy cost route between the SNs and BS is exchanged between the BNC and BS every $T_{rs} = 30$ seconds. The SNs and BNC transmit their data in time slots assigned to them by the BS based on the retransmission limit and packet size that was computed to achieve the minimum relative energy cost route, every $T_{rs} = 30$ seconds. If a SN or BNC successfully delivers the required data in fewer slots than was allocated, the SN or BNC reverts from a transmitting mode to a listening idle mode. The SNs generate data at the same rate specified in Table 3.1. The generated data streams are modulated and demodulated using OQPSK and transmitted along Nakagami-*m* on-body and body-to-body fading channels. The shadowing along the on-body and body-to-body channels are randomly generated using zero mean and standard deviation of $\sigma_{i.k,i} = 6.1$ dB [34] and $\sigma_i = 9$ dB, respectively [11]. The transmit power, retransmission limit, and packet size for each SN and BNC transmission is determined by the BNC every $T_{ru} = 1$ second using Algorithm 3.1 and Algorithm 3.2. For each of the ten independent simulation runs we conduct, 5000 rounds of physiological data updates are performed from which 95% confidence intervals are calculated from the simulation results. For each simulation experiment, we measure three performance metrics: *total relative energy*

cost, *average end-to-end delay*, and *QoS outage*. The average end-to-end delay is the average of the total end-to-end delay incurred by each SN. QoS outage measures the percentage of time the reliability or delay constraint is violated. The reliability and delay requirements are set at 99% and 1 second, respectively.

3.5.3.2 Simulation Results

3.5.3.2.1 Comparison of Analytical and Simulation Results

The total relative energy cost obtained with analytical and simulation techniques is shown in Fig. 3.9a for a Rician fading body-to-body channel with varied BAN-to-BS distance. The analytical results narrowly fall outside the confidence interval of the simulation results, which provides enough confidence in the accuracy of the approximations made in the analysis. Notice that the confidence interval widens as the distance increases. At longer distances, specifically when the distance is equal to or greater than 25 m, body-to-body shadowing increases the experienced path loss to a certain threshold level where a high increase in retransmissions and smaller packet sizes must be employed to meet the reliability requirement and overcome low SNR. The simulation and analytical results for the average end-to-end delay are shown in Fig. 3.9b. A good agreement is observed between the simulation and analytical results. Similar to Fig. 3.9a, the confidence interval widens as the BAN-to-BS distance increases. At a distance of 25 m, it can be seen that the average end-to-end delay is approximately 20% higher than the delay requirement again attributed to the variance in body-to-body shadowing. When shadowing increases the path loss above a certain threshold, the increase in retransmissions allows the reliability constraint to be satisfied but consequently forces the delay constraint to be violated. Fig. 3.9c shows the QoS constraint, specifically the delay constraint, is increasingly violated when the distance is greater than 25 m. From the results shown in Fig. 3.9 we can deduce that

single hop BAN communication is only practical in Rician fading channels when the BAN-to-BS distance is equal to or less than 15 m where the QoS requirements are consistently satisfied while achieving the minimum relative energy cost. Furthermore, the relative energy cost and delay performance for the simulation results do not vary much as demonstrated by the small confidence interval bounds.

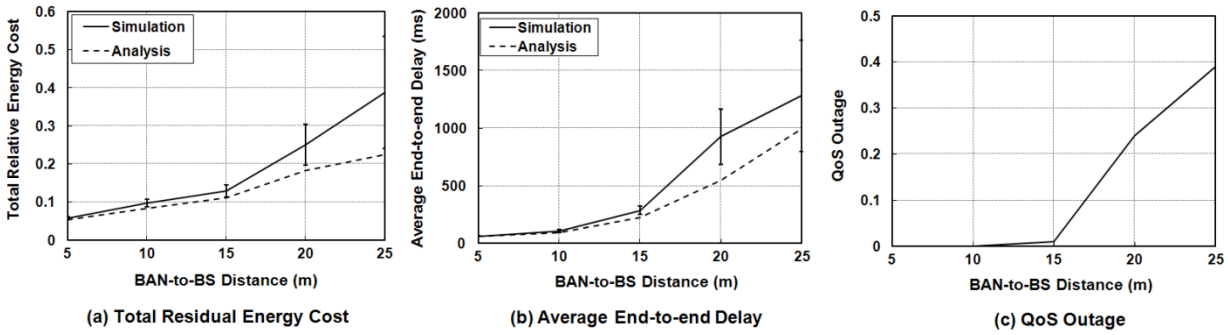

Fig. 3.9. Comparison of analysis and simulation performance of EQS for Rician fading single hop body-to-body channel.

The performance results yielded from the analytical and simulation techniques for a Rayleigh fading body-to-body channel are shown in Fig. 3.10. It is clear to see that the relative energy cost (Fig. 3.10a) and average end-to-end delay (Fig. 3.10b) analytical results are in good agreement with the simulation results since they consistently reside within the confidence interval. Notice the relative energy cost attained from the analysis is consistently higher than the simulation, which is in contrast to the results shown in Fig. 3.9a. We hypothesize that the impact of Rayleigh fading on relative energy cost and reliability is greater than that of body-to-body shadowing at $\sigma_{i1} = 9$ dB. Therefore, the analytical results provide the upper bound relative energy cost performance for single hop BAN transmissions. From Fig. 3.10c, we also observe that the effective BAN transmission distance is only up to 10 m because the QoS outage only occurs 7% of the time as opposed to 65% at 15 m.

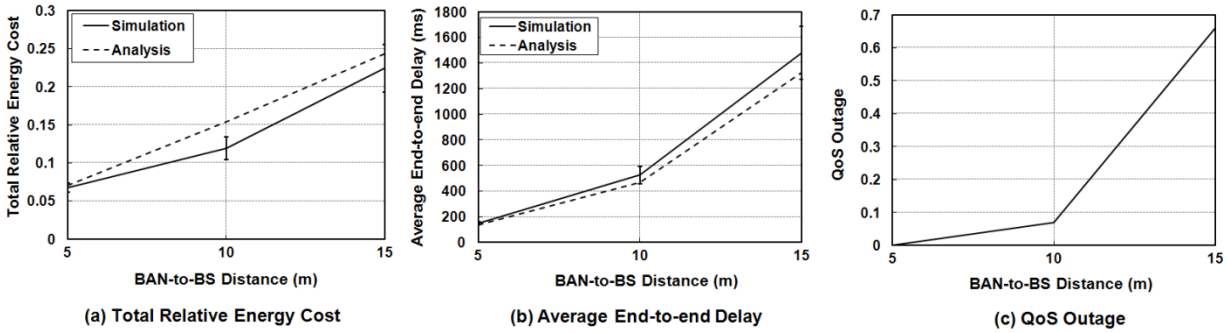

Fig. 3.10. Comparison of analysis and simulation performance of EQS for Rayleigh fading single hop body-to-body channel.

3.5.3.2.2 EQS Performance Comparison against Other Schemes

We implement two other schemes to compare the performance of EQS. The first scheme only performs routing using path 1 and thus we name the scheme as EQP1. In this scheme all SNs transmit directly to the BS and the resident BNC uses Algorithm 3.1 to determine the transmission power, retransmission limit, and packet size required to attain minimum cost routes. The EQP1 scheme is employed for the transmission of SN data in several BAN projects in the literature such as CodeBlue [36], AID-N [38], and MEDiSN [37]. The second scheme performs routing using path 2 but without the benefit of overhearing the intra-BAN transmissions. We name the scheme as EQP2. In EQP2 all SNs transmit directly to the BNC and the BNC then transmits the aggregated data to the BS. We consider this scheme because it represents the typical two-tier communication scheme employed in the literature for energy efficient BAN transmissions [40]-[52]. The minimum relative energy cost routes for the SNs and BNC in EQP2 are determined by executing Algorithm 3.2. However, the following changes are made to the algorithm: line 11 becomes, $\mathcal{D}_{i.k,i} = \mathcal{D}_{tx}\left(n_{i.k,i}L_{i.k,i}, X, \mathcal{R}_{i.k,i}\right)$, line 13 becomes $\mathcal{E}_{i.k,i} = n_{i.k,i}L_{i.k,i}\phi\left(\bar{\gamma}_{i.k,i}, m_{i.k,i}, L_{i.k,i}, X\right)\left(\frac{E_b(P_{tx}(z))}{E_{res,i.k}} + \frac{E_b(P_{rx})}{E_{res,i}}\right)$, line 14 becomes $\mathcal{E}_{i.k,j}\mathcal{D}_{i.k,i}/\mathcal{P}_{s,i.k,i}$, and

the reliability expression in line 37 becomes $\mathcal{P}_{ij} \geq \mathcal{P}_{req}$ since there is no overhearing and we require $\mathcal{P}_{i.k,i}$ to be one. In addition to the three performance metrics previously discussed, we also evaluate the average end-to-end packet delivery ratio (PDR) defined as the percentage of data packets that have been successfully delivered in the network. The minimum requirement for PDR in the simulation experiments is set as $\mathcal{P}_{req} \geq 99\%$ and the delay requirement remains $\mathcal{D}_{req} \leq 1$ s. Based on the delay requirement and aggregate data transmitted from the BAN, the maximum retransmission limit is set as $X_{max} = \left\lceil \mathcal{D}_{req} / \left(1\text{second} \times \sum_{k=1}^{N_s} r_k / \mathcal{R}\right) \right\rceil$. The maximum number of samples per packet permitted at each SN is calculated as $\varphi_{max,k} = F_{p,max} / \vartheta_k$.

The performance results in Fig. 3.11 are presented for Rician fading where the BAN-to-BS distance of interest is defined by the range $d_{i1} = [5, 20]$ meters. The QoS outage for all the considered schemes exceeds 50% when the distance is greater than 20 m and therefore the results in that range do not provide any meaningful insight towards real-time physiological status monitoring.

Fig. 3.11a shows the total relative energy cost for the various schemes. From this figure, we can see that EQS benefits from its ability to adaptively switch its routing between path 1 and path 2. The overlapping confidence intervals between EQS and EQP1 in the distance range [5m, 15m] shows that the relative energy cost for path 1 is significantly lower than for path 2 (employed in EQP2). At a distance of 20 m, we see that the confidence interval for EQS and EQP1 no longer overlap and the relative energy cost for EQS is 17% lower than EQP1. This indicates that EQS predominantly uses path 2 for transmission as opposed to path 1. EQP2 always uses path 2 for transmission but the relative energy cost achieved by EQS at a distance of 20 m is 24% lower than EQP2 for the following two reasons. First, the BNC benefits from the

PDR gained from the overheard SN transmissions. When the overheard transmissions achieve a PDR greater than 0% the BNC performs its transmissions with lower power and fewer retransmissions because it can deliver the aggregated packets with a PDR less than the required PDR of 99%. Second, the data transmitted through the routing paths available in EQP2 endure both on-body and body-to-body shadowing. When the shadowing has largely deleterious effects along both channels, the energy required to overcome the high path loss while meeting the reliability constraint, is significant. On the other hand, when EQS is exposed to the same severe shadowing conditions, the overheard transmissions provide a means to compensate for the high on-body or body-to-body (via BNC to BS link) path loss by possibly having a less harmful shadowing condition available over the SN-to-BNC on-body link. Observing the results in Fig. 3.11a and Fig. 3.11b, we can see that a trade-off exists between lower relative energy cost and higher delay. Specifically, when the distance is 20 m, the delay resulting from EQS is 50% higher than EQP1. The delay is higher because the link delay for the transmissions emanating from the SNs is bounded by the link delay of the overheard SN-to-BS links. The average end-to-end PDR for the three schemes is shown in Fig. 3.11c and only EQP2 violates the reliability requirement because it is exposed to multiple degrees of shadowing that can be so severe that unrecoverable packet loss occurs. The severity of the shadowing is most evident when the BAN-to-BS distance is greater than 10 m. In Fig. 3.11d, the QoS outage endured by EQS is primarily attributed to the violation of the delay constraint. Fig. 3.11c shows that EQS consistently maintains a PDR above the 99% threshold whereas Fig. 3.11b shows that the confidence interval for EQS exceeds the delay threshold. We do not provide performance results for the schemes in a Rayleigh fading environment due to the limited transmission distance that can be supported for real-time transmission.

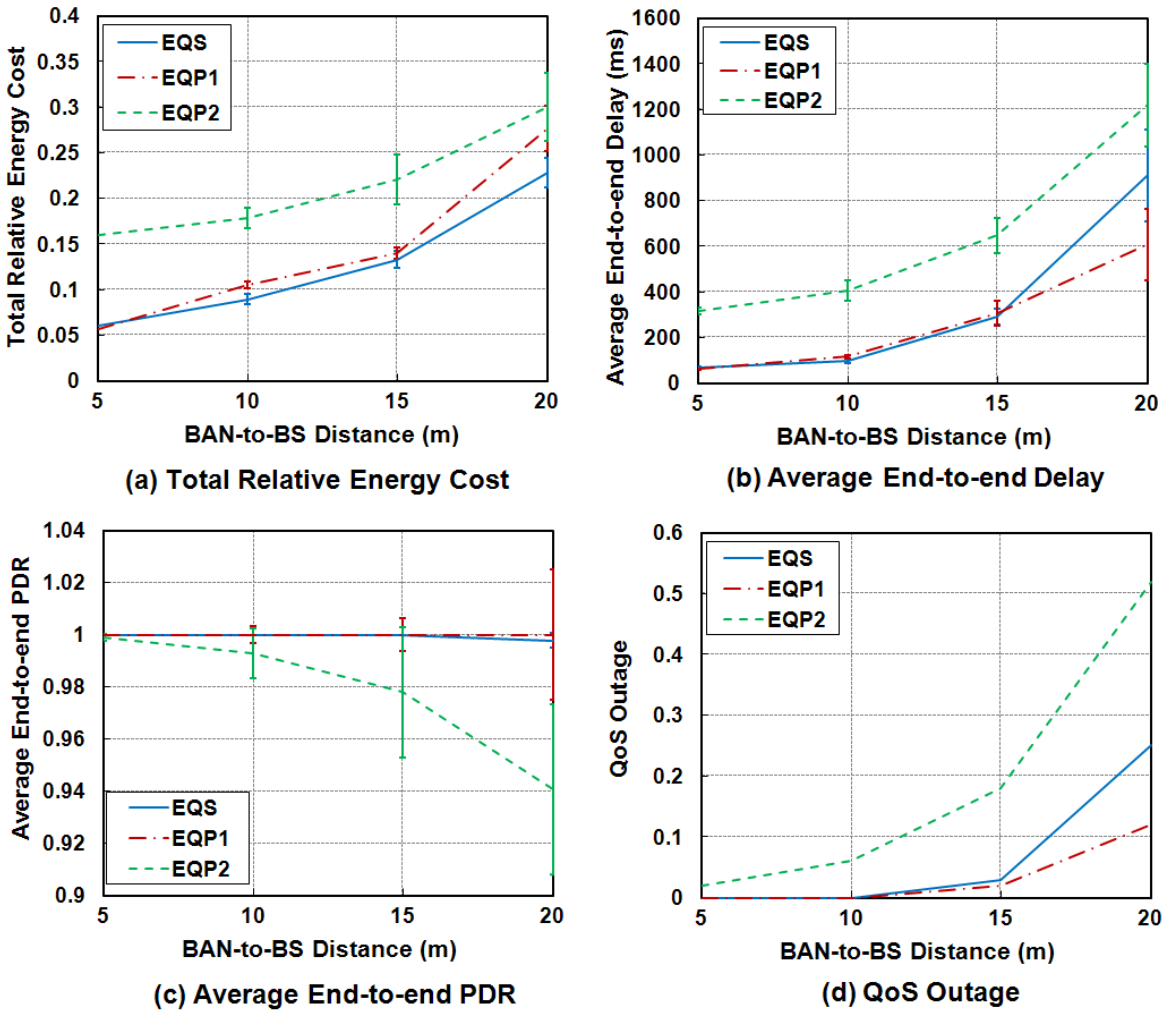

Fig. 3.11. Performance with varying BAN-to-BS distance for EQS, EQP1, and EQP2.

3.6 Summary

In this chapter we proposed a synergistic BAN model to exploit the resource heterogeneity of the SNs and BNC in a BAN and their ability to conduct synergistic cooperative communication. The synergistic BAN model is based on a dual aggregation strategy that combines aggregated data samples received over multiple paths to enhance overall reliability and provide robustness to path loss and fading induced errors. We designed an EQS communication scheme for single-hop body-to-body networks based on the synergistic BAN model and the dual

aggregation concept. The EQS scheme uses the JPRS strategy to jointly optimize transmission power, retransmission limit, and payload size while minimizing relative energy cost under the constraint of reliability and delay requirements. The JPRS strategy is particularly conducive to the aggregation process because the optimal number of samples per aggregated data packet leading to minimum relative energy cost can be determined. Our analytical results show significant reductions in relative energy cost and delay are achieved for transmissions over inter-BAN and intra-BAN links, when compared against a power allocation strategy that only optimizes power and retransmissions such as the JPR strategy. Using the JPRS strategy to determine the minimum relative energy cost for transmitting physiological data from SNs to a BS is a non-linear optimization problem with NP-hard complexity which we solved using sub-optimal algorithms that sacrifice solution accuracy for efficiency. Our analytical results show that the sub-optimal algorithms predominantly achieve relative energy cost between 2% and 15% higher than the optimal relative energy cost while requiring 100 times fewer iterations to converge to a solution. The performance of EQS was evaluated through analytical and simulation techniques and the results showed that EQS offered up to a 62% improvement over EQP2 and 17% improvement over EQP1 for BAN-to-BS distances between 5 m and 20 m.

CHAPTER 4 ENERGY AND QOS AWARE CROSS-LAYER COMMUNICATION SCHEME FOR MULTI-HOP BODY-TO-BODY NETWORK

4.1 Introduction

In this chapter, the problem of minimizing the relative energy cost for transmitting physiological data from SNs deployed on a soldier to a BS device deployed on a combat medic in a multi-hop BBN is addressed using an energy and QoS aware cross-layer (EQX) communication scheme. Extending the synergistic BAN model to a multi-hop BBN while employing the JPRS strategy to form reliability and delay constrained minimum relative energy cost routes between the SNs and BS introduces considerable complexity to the aforementioned problem. The problem is solved by deriving an accurate but inefficient optimal solution based on cross-layer optimization and a sub-optimal but efficient solution using heuristic algorithms.

The remainder of this chapter is organized as follows. Section 4.2 provides details of the multi-hop BBN model and the system model consisting of the wireless channel and protocol layers. The problem formulation and optimal solution for the multi-hop BBN minimum relative energy cost problem is provided in Section 4.3. In Section 4.4, the operational and design details and heuristic algorithms comprising the EQX scheme are presented. Section 4.5 provides the performance metrics used to evaluate the optimal solution and the EQX scheme. The performance of EQX is evaluated in Section 4.6 using numerical and simulation results. The summary provided in Section 4.7 concludes the chapter.

4.2 System Model

4.2.1 Multi-hop BBN Network Model

The multi-hop BBN model considered in this chapter is an extension of the single-hop BBN introduced in Section 3.2.1. Different from Section 3.2.1, it is assumed that the BS is *not reachable* from every BAN within a single hop. Such a scenario is often encountered in an urban battlefield where the soldiers and combat medic no longer maintain close proximity to one another. However, soldiers are typically located within a single hop of each other and thus communication with the BS is feasible through multi-hop routing.

The multi-hop BBN is comprised of N_b BANs, each consisting of N_s SNs and one BNC, and is represented in graph form by $\mathcal{G} = (\mathcal{V}, \mathcal{W})$, where $\mathcal{V}$ is the set of all SNs and BNCs and $\mathcal{W}$ is the set of all links. The set of links includes all the feasible SN based links that either terminate at its own BNC i forming $link(i.k, i)$, a neighboring BNC denoted by j forming $link(i.k, j)$, or BS denoted by #1 forming $link(i.k, 1)$. Additionally, the set of links includes all feasible BNC i ($i \in [2, N_b + 1]$) based links that either terminate at a neighboring BNC denoted by j ($j \in [2, N_b + 1], j \neq i$) forming $link(i, j)$ or BS denoted by #1 forming $link(i, 1)$. The SNs are only responsible for generating and transmitting their own traffic whereas the BNCs can either forward traffic from its own BAN or relay traffic from other BANs.

Fig. 4.1 illustrates the multi-hop BBN model employed for monitoring the physiological status of soldiers in an open battlefield. The alignment of soldiers shown in the model depicts that of a platoon column formation [149]. The platoon column formation has been shown to provide the most effective organization for soldiers engaged in battle. Each soldier is equipped with a BAN within which the SNs collecting physiological data serve as source nodes. Transmission between SNs and a relay BNC or BS is performed over path 1 or path 2. For

example, the SNs in BAN17 use path 1 to transmit their data to the BNC in BAN18. The path 1 equivalent link shown to the left of the BAN17 to BAN18 link shows the direct connection between the SNs in BAN17 and BNC in BAN18. An example of the path 2 link is shown between BAN11 and BAN12. The path 2 equivalent link shown to the left of the BAN11 to BAN12 link shows the three connections comprising communication over path 2 which includes the intra-BAN link between SN and BNC, overheard intra BAN link between SN and neighboring BNC, and inter-BAN link between the BNC and neighboring BNC. After the source data transmitted from BAN11 has been received by BAN12, it is relayed through the BNC to BNC link connecting BAN12 to BAN13 and the BNC to BS link connecting BAN13 to BS1.

In the network model, we assume the relative distance between soldiers and the distance between soldiers and combat medic remain the same. This assumption stems from the fact that soldiers must maintain their relative position in the platoon formation in order to maintain a balanced attack. Studies have shown that mission success decreases and fatality rates amongst soldiers increase when platoon formations become disorganized [149]. While the consideration of mobility provides useful insight into the performance of a multi-hop BBN communication scheme in tactical scenarios, it is outside the scope of this thesis. As a result, the analysis performed in this thesis does not consider mobility and is identified as future work in Chapter 6.

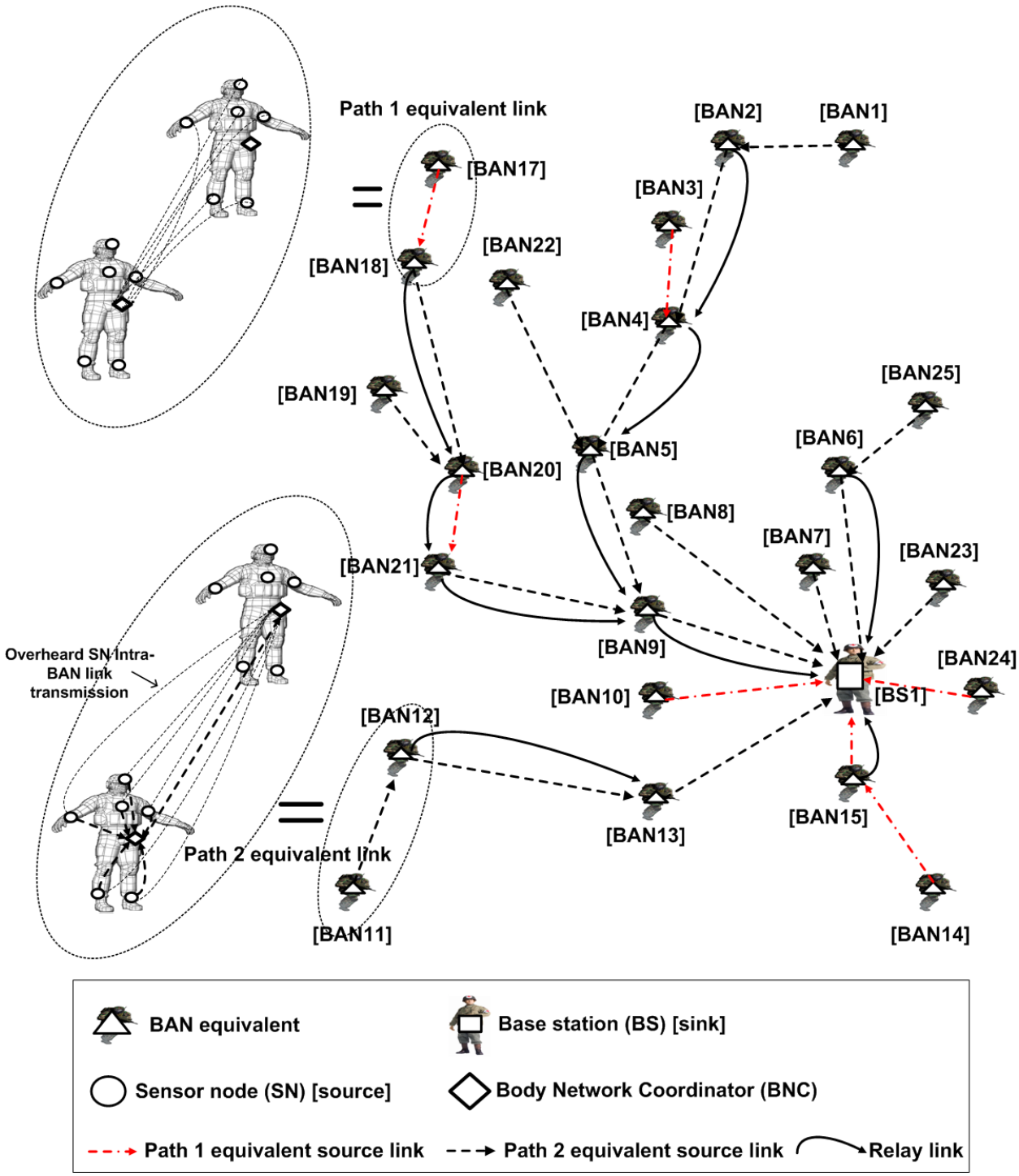

Fig. 4.1. Multi-hop BBN network model for EQX communication scheme.

4.2.2 Wireless Channel and Protocol Layers

The description of the wireless channel, physical layer, and MAC layer are the same as those provided in Section 3.2.2. Multi-hop routing is permitted in the network layer of the BBN to support transmission for the BNCs that reside outside the direct communication range of the BS. Furthermore, existing research [118]-[122] have shown significant energy savings are realized by employing multi-hop routing, especially when stringent reliability constraints are concerned.

4.3 Minimum Relative Energy Cost for Multi-hop BBN

In this section, we determine the minimum relative energy cost required to transmit physiological data from SNs to a BS in a multi-hop BBN under the constraints of stringent reliability and delay requirements. We formulate an optimization problem that is an extension of the single-hop BBN problem formulated in (3.14). The optimal solution to the problem is also discussed.

4.3.1 Optimization Problem Formulation

Given the QoS constraints $\mathcal{P}_{req}$ and $\mathcal{D}_{req}$ representing the end-to-end reliability objective and end-to-end delay objective, respectively, the residual energy $E_{res,i.k}$ $(\forall i \in [2, N], \forall k \in [1, N_s], N = N_b + 1)$ for all SNs, $E_{res,i}$ $(\forall i \in [2, N])$ for all BNCs, and $E_{res,1}$ for the BS, and the graph input $\mathcal{G}$, the following optimization problem is formulated to minimize the network relative energy cost using information from the network, physical, and MAC layers:

minimize

$$\sum_{i=2}^{N}\sum_{j=2,j\neq i}^{N}\sum_{k=1}^{N_s}(1-\mu_i)\mu_{i.k,j}\left(\mathcal{E}_{tx,i.k,j}+\mathcal{E}_{rx,i.k,j}\right)+\cdots$$

$$\cdots+\sum_{i=2}^{N}\sum_{k=1}^{N_s}\mu_i\left(\mathcal{E}_{tx,i.k,i}+\mathcal{E}_{rx,i.k,i}\right)+\mu_i\sum_{j=2}^{N}\mu_{i.k,j}\mathcal{E}'_{rx,i.k,j}+\cdots$$

$$\cdots+\sum_{i=2}^{N}\sum_{j=2,j\neq i}^{N}\mu_{ij}\left(\mathcal{E}_{tx,ij}+\mathcal{E}_{rx,ij}\right)+\sum_{i=2}^{N}\sum_{j=2,j\neq i}^{N}\mu_{ji}\mathcal{E}_{rx,ji}+\cdots$$

$$\cdots+\sum_{i=2}^{N}\sum_{k=1}^{N_s}\mu_i\mu_{i.k,1}\mathcal{E}'_{rx,i.k,1}+\sum_{i=2}^{N}\sum_{k=1}^{N_s}(1-\mu_i)\mu_{i.k,1}\mathcal{E}_{rx,i.k,1}+\sum_{i=2}^{N}\mu_{i1}\mathcal{E}_{rx,i1} \quad (4.1.0)$$

subject to

$$\mu_i\mathcal{P}_{ete,p2,i}+(1-\mu_i)\mathcal{P}_{ete,p1,i}\geq\mathcal{P}_{req},\forall i\in[2,N],\forall j\in[1,N],\forall k\in[1,N_s],j\neq i, \quad (4.1.1)$$

$$\mathcal{D}_{wait}(\varphi_{i.k},\vartheta_k)+\sum_{i=2}^{N}\sum_{j=2,j\neq i}^{N}\sum_{k=1}^{N_s}\mu_i\mathcal{D}_{tx,i.k,i}+(1-\mu_i)\mu_{i.k,j}\mathcal{D}_{tx,i.k,j}+\cdots$$

$$\cdots+\sum_{i=2}^{N}\sum_{j=2,j\neq i}^{N}\mu_{ij}\mathcal{D}_{tx,ij}\leq\mathcal{D}_{req}\forall i\in[2,N],\forall k\in[1,N_s] \quad (4.1.2)$$

$$\mu_i n_{i.k,i}L_{p,i.k,i}+(1-\mu_i)n_{i.k,j}L_{p,i.k,j}=r_k,\forall i\in[2,N],\forall j\in[1,N],\forall k\in[1,N_s] \quad (4.1.3)$$

$$\left(\sum_{i=2}^{N}\sum_{j=2,j\neq i}^{N}\sum_{k=1}^{N_s}(1-\mu_i)\mu_{i.k,j}n_{i.k,j}L_{p,i.k,j}+\sum_{i=2}^{N}\sum_{j=2,j\neq i}^{N}\mu_{ij}\,n_{ij}L_{p,ij}\right)=\sum_{i=1}^{N}\sum_{j=2,j\neq i}^{N}\mu_{ji}n_{ji}L_{p,ji}$$

(4.1.4)

$$\sum_{i=2}^{N}\sum_{j=2,j\neq i}^{N}\sum_{k=1}^{N_s}\frac{\mu_i n_{i.k,i}L_{p,i.k,i}\phi_{i.k,i}}{\mathcal{R}}+\frac{(1-\mu_i)\mu_{i.k,j}n_{i.k,j}L_{p,i.k,j}\phi_{i.k,j}}{\mathcal{R}}+\cdots$$

$$\cdots + \sum_{i=2}^{N} \sum_{j=2, j\neq i}^{N} \frac{\mu_{ij} n_{ij} L_{p,ij} \phi_{ij}}{\mathcal{R}} \leq 1 \quad (4.1.5)$$

$$\mu_i n_{i.k,i} L_{i.k,i} \phi_{i.k,i} E_b\left(P_{tx.i.k,i}\right) + \sum_{j=1, i\neq j}^{N} (1-\mu_i) \mu_{i.k,j} n_{i.k,j} L_{i.k,j} \phi_{i.k,j} E_b\left(P_{tx.i.k,j}\right) \leq E_{res,i.k},$$

$$\forall i \in [2, N], \forall k \in [1, N_s] (4.1.6)$$

$$\sum_{k=1}^{N_s} \mu_i n_{i.k,i} L_{i.k,i} \phi_{i.k,i} E_b(P_{rx}) + \sum_{j=1, i\neq j}^{N} \mu_{ij}\, n_{ij} L_{ij} \phi_{ij} E_b\left(P_{tx.ij}\right) + \cdots$$

$$\cdots + \sum_{j=1, i\neq j}^{N} \mu_{ji}\, n_{ji} L_{ji} \phi_{ji} E_b(P_{rx}) \leq E_{res,i} \forall i \in [2, N], (4.1.7)$$

$$\sum_{i=2}^{N} \sum_{k=1}^{N_s} \mu_i \mu_{i.k,1} n_{i.k,i} L_{i.k,i} \phi_{i.k,1} E_b(P_{rx.1}) + \sum_{i=2}^{N} \sum_{k=1}^{N_s} (1-\mu_i) \mu_{i.k,1} n_{i.k,1} L_{i.k,1} \phi_{i.k,1} E_b(P_{rx.1}) + \cdots$$

$$\cdots + \sum_{i=2}^{N} \mu_{i1} n_{i1} L_{i1} \phi_{i1} E_b(P_{rx.1}) \leq E_{res,1}, (4.1.8)$$

$$\sum_{j=1}^{N} \mu_{ij} \geq \mu_i, \forall i \in [2, N] \quad (4.1.9)$$

$$\mu_i = [0,1], \mu_{ij} = [0,1], \mu_{i.k,j} = [0,1], \forall i \in [2, N], \forall j \in [1, N], \forall k \in [1, N_s] \quad (4.1.10)$$

where $\mathcal{E}_{tx,x,y}$ is the relative energy cost for transmitting from a source x to a destination y and is given as $\mathcal{E}_{tx,x,y} = n_{xy} L_{xy} \phi_{xy}\, E_b\left(P_{tx.xy}\right)/E_{res,x}$, $\mathcal{E}_{rx,x,y}$ is the relative energy cost for receiving data at destination y from source x and is given as $\mathcal{E}_{rx,x,y} = n_{xy} L_{xy} \phi_{xy}\, E_b(P_{rx})/E_{res,y}$, and $\mathcal{E}'_{rx,xy}$ is the receiving relative energy cost at node y for overhearing a transmission from source x intended for a destination node different from node y (i.e., path 2). The binary decision variable μ_i specifies whether the SNs belonging to the same BAN as BNC i transmit along path 1 or path

2, $\mu_{i.k,j}$ indicates the neighboring BNC or BS that overhears the transmission of SN $i.k$, and μ_{ij} specifies whether the next hop for BNC i is a BNC j or the BS. The expressions $\mathcal{P}_{ete,p1,i}$ and $\mathcal{P}_{ete,p2,i}$ represent the end-to-end success probability for BAN transmissions using path 1 where the first hop of the path is to BNC j or the BS and path 2 where the first hop of the path is to BNC i, respectively, and the final hop is to the BS.

The objective function in (4.1.0) aims to minimize the total relative energy cost. It has four main components which we describe from top to bottom. The topmost component is the total relative energy cost for all SN transmissions along $link(i.k,j)$ of path 1, given $\mu_{i.k,j} = 1$. The next component is the total relative energy cost for all SN transmissions along $link(i.k,i)$ of path 2, given $\mu_i = 1$. The third component is the relative energy cost for transmitting, receiving, and/or relaying data between BNCs in the BBN. The last component is the total relative energy cost at the BS for receiving data either directly from SNs over path 1, indirectly from SNs over path 2, or from BNCs.

Multiple constraints are imposed at the network, MAC, and physical layers to capture the cross-layer optimization feature of the problem formulation. Constraint (4.1.1) imposes an end-to-end reliability constraint for each transmission originating from a SN. The end-to-end reliability for first hop transmissions using path 1 is calculated as the product of the success probability along each link selected by the binary decision variables μ. On the other hand, the end-to-end success probability for first hop transmissions using path 2 is calculated as the product of the path 2 success probability and the success probability along each $link(i,j)$ connecting BNC i to other BNCs or the BS. The end-to-end delay constraint is imposed in (4.1.2) such that the average wait time for each SN and the TDMA frame duration for scheduling

a unique slot to each link in the BANs and BBN is less than or equal to the delay objective. In (4.1.3) and (4.1.4), network flow conservation must be maintained within the BAN and between each BNC in the BBN, respectively, such that the total traffic generated and the total incoming traffic is equal to the outgoing traffic. The total traffic load is constrained in (4.1.5) to not exceed the maximum data rate $\mathcal{R}$ in order to maintain stability in the TDMA scheme. In (4.1.6), (4.1.7), and (4.1.8), the energy consumed at each SN, BNC, and BS must be less than the residual energy available in their respective batteries. Constraint (4.1.9) indicates the binary decision variable μ_{ij} must at least be the same value as μ_i in order to route the path 2 BAN traffic through the BBN.

Similar to (3.14), obtaining the optimal solution to the optimization problem in (4.1) is highly complex due to the non-linearities introduced by the product of success probabilities over multiple hops in (4.1.1) and the availability of several route combination possibilities in (4.1.0) and (4.1.4). Furthermore, given that each SN and BNC has multiple power levels, multiple possibilities for the retransmission limit, different payload size options, and numerous possible transmission destinations, the minimum total relative energy cost cross-layer optimization problem is clearly a combinatorial MINLP.

4.3.2 Optimization Problem Solution

The following process is used to solve this MINLP. First, the objective function and constraints are programmed in an advanced and highly efficient optimization tool called TOMLAB [150]. The OptQuest/NLP (OQNLP) algorithm [151], which uses multistart heuristic methods to find global optima for MINLP problems with a large number of constraints and variables, is employed as our desired solver. The superior accuracy of OQNLP in obtaining global optima is aided by its use of an exhaustive search branch-and-bound algorithm with constant-space best-first search. The combinatorial nature of the MINLP makes the problem NP-

hard and the combination of OQNLP and branch-and-bound algorithm has been shown to be capable of providing optimal solutions to NP-hard problems [152]. In the worst case, a branch-and-bound algorithm must explore all solution possibilities in the solution state space [152]. Therefore, the computational complexity is determined as follows. At each BNC, the combination of X_{max} transmission attempts, $\mathcal{Z}$ power levels, and φ_{max} different packet sizes is evaluated between all possible N_b neighboring links (i.e., $N_b - 1$ BANs and the BS), where we assume X_{max} is set high enough that the maximum number of retransmissions required to satisfy the reliability objective while also satisying the delay objective, is met. Since there are N_b BNCs in the network, the total number of iterations required to determine a minimum relative energy cost route from each BNC is $X_{max}\mathcal{Z}{N_b}^2$. At each SN, the combination of X_{max} transmission attempts, $\mathcal{Z}$ power levels, and φ_{max} different packet sizes is evaluated for N possible links (i.e., N_b BNCs and one BS). Since there are N_s SNs per BAN and N_b BNCs in the network, the total number of iterations required to determine a minimum relative energy cost for each SN is $X_{max}\mathcal{Z}N_bN_sN$. The optimal solution relies on combining the routing decisions of the SNs and BNCs and therefore, the worst case complexity for the multi-hop BBN minimum relative energy cost problem is $\mathcal{O}({X_{max}}^2\mathcal{Z}^2N_sN{N_b}^3)$. This complexity is computationally taxing and requires intensive processing, both of which are highly undesirable for resource constrained devices. Furthermore, in the dynamic military environment where soldiers' lives are at stake, fast responding and resource efficient algorithms must be employed to transmit critical physiological information. Consequently, the subsequent section in this chapter proposes heuristic routing, constrained power allocation, and slot scheduling algorithms to significantly reduce the complexity of the optimal solution.

4.4 EQX Communication Scheme for Multi-hop BBN

4.4.1 Overview

The optimal solution to the multi-hop BBN minimum relative energy cost problem is shown to have very high complexity unconducive to delivering physiological data in a time-efficient manner. As a result, we design the EQX communication scheme which solves (4.1) by separately addressing the main components required to obtain the minimum relative energy cost for the multi-hop BBN in a manner similar to our previous work [153]. Namely, the network layer flow conservation constraints given in (4.1.3) and (4.1.4) are addressed in a QoS aware routing algorithm. The reliability constraint in (4.1.1) is addressed in a multi-constrained power allocation algorithm that assigns the minimum transmission power, retransmission limit, and payload size to each link from the routing paths formed in the QoS aware routing algorithm, in order to concurrently minimize relative energy cost and satisfy the end-to-end reliability requirements. We further discuss this later in the section. The TDMA related constraints in (4.1.2) and (4.1.5) are addressed through a QoS aware slot scheduling algorithm that calculates the interference level between co-located BANs in order to discover opportunities for slot reuse.

4.4.2 Description and Operation

The operation of EQX is described in terms of the routing, multi-constrained power allocation, and scheduling algorithms and consists of four main phases as is illustrated in Fig. 4.2. The initial phase marks the initial deployment of the SNs, BNCs, and BS, followed by the initiation of the EQX communication scheme. The subsequent four phases are described as follows:

- *Phase #1:* The routing algorithm is enacted periodically every T_{rs} in order to build and maintain end-to-end routing paths between the SNs and BS. At the start of the routing

algorithm phase, the BNC of each BAN calculates its single-hop neighbor discovery range. The BNC broadcasts a "Route Discovery" message (RDIS) to the neighbors that reside within the calculated neighborhood discovery range and the neighbors within the specified range respond to the message with a "Route Reply" message (RREP). The RREP message contains the channel state information between the neighbor and the BNC, the neighbor's residual energy level, and distances from the neighbor to BNC and neighbor to BS. The BNC executes Algorithm 3.1, Algorithm 3.2, and some newly proposed algorithms (described later in the section) using the information received from the neighbors and selects the neighbor achieving the minimum relative energy cost as the relay node. The selected neighbor is set as the next hop of the SNs if path 1 is selected from Algorithm 3.1 and Algorithm 3.2. Otherwise, the selected neighbor is set as the next hop of the BNC if path 2 is selected from Algorithm 3.1 and Algorithm 3.2. The BNC sends the selected neighbor a "Route Confirm" message (RCFM) which has the neighbor's ID stored in it. The process is continued from the BNC to neighboring BNC until the BS receives a RCFM message holding all the IDs for the BNCs combining to form the end-to-end routing path between the source SNs and the BS. When RCFM messages have been received from all BNCs, phase two is enacted.

- *Phase #2:* The BS allocates the minimum transmit power, retransmission limit, and payload size to all the transmitting links in the routing tree (collection of routing paths) using a multi-constrained power allocation algorithm such that the end-to-end success probability along each routing path in the routing tree satisfies the reliability constraint while achieving a minimum relative energy cost.
- *Phase #3:* Following the joint power and retransmission allocation phase, the BS builds a network-wide transmission slot schedule for all the links in the routing tree.

- *Phase #4:* The configured routes, transmit power levels, retransmission limits, payload size, and TDMA frame consisting of the scheduled slots are broadcast by the BS to the BNCs in the multi-hop BBN. The BNCs relay this information to their SNs. If a SN has run out of energy or is unable to successfully deliver its data to the BS, EQX terminates. Otherwise, phase one is re-enacted.

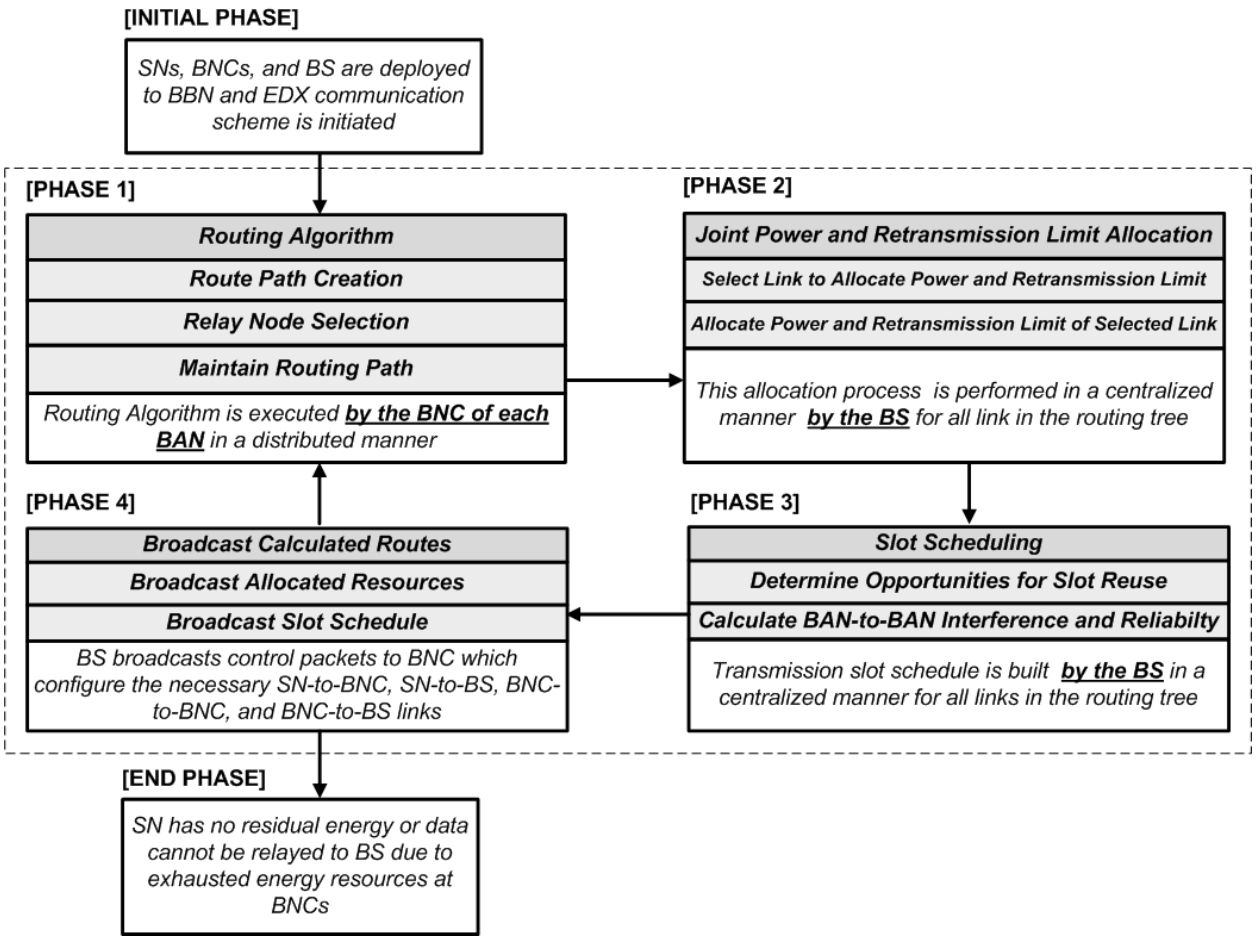

Fig. 4.2. Operational cycle and functional elements of the EQX communication scheme.

4.4.3 BBN Routing Algorithm

The main objective of the BBN routing algorithm, which we refer to as BRA, is to build minimum relative energy cost routes between the source SNs and BS via intermediate BNCs while also maintaining a certain level of reliability under an end-to-end reliability objective.

4.4.3.1 Route Discovery and Creation Process

Different metrics have been defined in the literature for discovering the appropriate relay nodes required to build a routing path between a source node and a sink node. In time critical applications, the neighbor discovery radius is configured using the maximum transmission power and thus relay nodes performing low delay transmissions over a minimum number of hops are preferred. In energy conscious applications, the neighbor discovery radius is configured using the transmission power providing for the highest energy efficiency and thus the relay nodes providing energy efficiency are chosen to build a route. Erasure networks aim to satisfy an end-to-end reliability objective by selecting relay nodes which have high success probability along each link. In this case, the neighbor discovery range is calculated based on the transmission power meeting the specific per link success probability requirement such that the product of all link success probabilities is equal to the end-to-end reliability objective.

The main motivation for computing neighbor discovery range is the desire to build a single hop neighborhood that provides network connectivity to the BS while incurring low route setup time and minimum relative energy cost and control traffic for route creation. Furthermore, since the transmission of data packets over the neighborhood hops must also adhere to QoS requirements, the neighbor discovery range must also specifically support reliability and delay constraints at low relative energy cost.

Assume N_b soldiers are evenly distributed in a battlefield with coverage area A^2 m^2. The

soldier density is then calculated as $\psi = N_b/A^2$. The average number of desired soldiers in a single hop neighborhood is $\mathbb{N}_{ndr}$ and calculated as $\mathbb{N}_{ndr} = \lceil A^2/(\pi d_{ndr}^2) \rceil$, where d_{ndr} is the neighbor discovery range and πd_{ndr}^2 is the circular coverage area provided by d_{ndr}. To obtain d_{ndr} and $\mathbb{N}_{ndr}$ using the minimum relative energy cost while adhering to reliability and delay constraints of $\mathcal{P}_{req}$ and $\mathcal{D}_{req}$, respectively, a reduced search based algorithm is employed where different combinations of transmission power and retransmission limit are explored for various distances given a maximum payload size of $L_{p,max}$. A maximum packet size is employed to guarantee that the full range of possible payload sizes (i.e.,$L_p \in [L_{p,min}, L_{p,max}]$) is supported for SN data transmission within the chosen neighbor discovery range.

In Algorithm 4.1 the transmit power P_{tx} and retransmission limit X are initialized to its maximum P_{max} and minimum level X_{min}, respectively. The distance d is zero and subsequently incremented by d_{step} until either the reliability constraint or delay constraint is violated. The maximum number of neighbors per relative energy cost $\mathcal{C}_{max}$ is stored for the (X, z) combination when the average number of neighbors $\mathbb{N}$ is equal to the average number of desired neighbors in a single hop neighborhood $\mathbb{N}_{ndr}$. When the inside while loop (lines 6 to 15) has been terminated, three conditions are presented in lines 17 to 23 for updating the transmission power or retransmission limit. If a solution has yet to be obtained (i.e.,$\mathcal{C}_{max} == 0$), it is because the reliability constraint has been violated since the retransmission limit is initialized to its lowest value and the transmit power to its highest value. Therefore, the retransmission limit is incremented by one. If the current neighbors per relative energy cost $\mathcal{C}_{max}$ is greater than the previous neighbors per relative energy cost $\mathcal{C}'_{max}$ obtained with combination (X', z') where $X' \geq X$ and $z' < z$, the transmit power level is decremented because the search space possibly

providing a higher value for $\mathcal{C}_{max}$ must be explored since a lower value of z leads to a lower value of $\mathcal{E}$ and higher $\mathcal{C}$. In lines 21 to 23, if $\mathcal{C}_{max}$ is not higher than $\mathcal{C}'_{max}$, the retransmission limit and transmit power are decreased to find a higher value for $\mathcal{C}_{max}$. If Algorithm 4.1 cannot compute a solution for $\mathbb{N}_{ndr}$, the neighbor discovery range is returned as $d_{ndr} = 0$. In this case, the BNC that executes Algorithm 4.1 can provide different values of $\mathbb{N}_{ndr}$ until a non-zero neighbor discovery range is obtained.

Algorithm 4.1 Neighbor Discovery Range Calculation

1: **Input:** $PL(d_0), \alpha, d_0, m, P_{min}, P_{max}, X_{max}, L_{p,max}, \mathcal{P}_{req}, \mathcal{D}_{req}, E_{res,i}, E_{res,j}, d_{step}, \mathbb{N}_{ndr}, A$;
2: **Output:** $d_{ndr}, X_{ndr}, P_{tx}(z_{ndr})$;
3: **Initialization:** $P_{tx}(z) = P_{max}$ (i. e. , $z = \mathcal{Z}$); $X = X_{min}$; $d_{ndr} = 0$; $\mathcal{C}_{max} = 0$; $\mathcal{C}'_{max} = 0$;
4: **while** $(X \leq X_{max})\&\&(P_{tx}(z) \geq P_{min})$ **do**
5: $\mathcal{P}_{ndr} = 1; \mathcal{D} = 0; d = 0$;
6: **while** $(\mathcal{P}_{ndr} \geq \mathcal{P}_{\mathrm{req}})\ \&\&\ (\mathcal{D} \leq \mathcal{D}_{\mathrm{req}})$ **do**
7: $d = d + d_{step}$;
8: Calculate reliability: $\mathcal{P}_{ndr} = \mathcal{P}_s(\bar{\gamma}, m, L_{p,max}, X)$ using $P_{tx}(z), PL(d_0), \alpha, d_0, d$;
9: Calculate delay: $\mathcal{D} = \mathcal{D}_{tx}(L_{p,max}, X, \mathcal{R})$;
10: Calculate REC: $\mathcal{E} = L\phi(\bar{\gamma}, m, L_{p,max}, X)\left(E_b(P_{tx}(z))/E_{res,i} + E_b(P_{rx})/E_{res,j}\right)$;
11: Calculate average number of neighbors: $\mathbb{N} = \lceil A^2/(\pi d^2) \rceil$;
12: Calculate average number of neighbors per REC: $\mathcal{C} = \mathbb{N}/\mathcal{E}$;
13: **if** $(\mathcal{C} > \mathcal{C}_{max})\&\&(\mathbb{N} == \mathbb{N}_{ndr})$ **then**
14: $\mathcal{C}_{max} = \mathcal{C}; d_{ndr} = d; X_{ndr} = X; z_{ndr} = z$;
15: **end if**
16: **end while**
17: **if** $(\mathcal{C}_{max} == 0)$ **then**
18: $X = X + 1$;
19: **else if** $(\mathcal{C}_{max} > \mathcal{C}'_{max})$ **then**
20: $z = z - 1$;
21: **else**
22: $X = X - 1; z = z - 1$;
23: **end if**
24: $\mathcal{C}'_{max} = \mathcal{C}_{max}$;
25: **end while**
26: **return**

The complexity of Algorithm 4.1 is estimated as follows. The worst case number of iterations from the iteration in the first and second loops in Algorithm 4.1 is $X_{max} + \mathcal{Z}$ and d_{max}/d_{step}, respectively, where d_{step} is the maximum distance between two locations in the network coverage area. Thus, the complexity of Algorithm 4.1 is approximated as $\mathcal{O}\left(\frac{d_{max}(X_{max}+\mathcal{Z})}{d_{step}}\right)$.

4.4.3.2 Relay Node Selection

The QoS constrained routing paths connecting the SNs and BNCs to the BS are built in a distributed manner. At each BNC *i,* a RDIS message is broadcast up to X_{ndr} times at a power level of $\mathcal{z}_{ndr}$ to reach all neighbors residing within the neighbor discovery range of d_{ndr}. As previously stated, each neighboring BNC *j* responds to the RDIS message with a RREP message that includes its residual energy level $E_{res,j}$, its distance to the sender d_{ij}, and its distance to the BS d_{j1}. When the RREP message is received by BNC i, Algorithm 3.1 and Algorithm 3.2 are executed to determine the minimum relative energy cost for the SNs. However, in order to set the reliability requirement $\mathcal{P}_{req}$ for Algorithm 3.1 and Algorithm 3.2, we must estimate the number of hops that connect the SNs to the BS. This process is required in multi-hop BBNs because the minimum success probability achieved along each hop of a routing path must at least be equal to or greater than the end-to-end reliability requirement. Since the only knowledge BNC *i* possesses for the path connecting BNC *j* to the BS is d_{j1}, we estimate the minimum number of hops between BNC *j* and the BS based on the maximum neighbor discovery distance d_{ndr} as $h_{j1} = \lceil d_{j1}/d_{ndr} \rceil$ and the average distance per hop as $d = d_{j1}/h_{j1}$. Therefore, assuming the minimum reliability along $link(i.k, i)$ is set as one when the SNs transmit using path 2 (this assumption

was put forth and justified for Algorithm 3.2), the total number of hops between the SNs and BS for transmissions through path 1 or path 2 is estimated as $h_{ij1} = h_{j1} + 1$.

Let d_{ij} and $d_h(\forall h \in [1, h_{j1}])$ represent the distance and $\mathcal{P}_{ij,min}$ and $\mathcal{P}_{h,min}(\forall h \in [1, h_{j1}])$ represent the minimum reliability for the path between the SNs and BNC j and for each hop betweeen BNC j and the BS, respectively. When $d_{ij} = d_h(\forall h \in [1, h_{j1}])$ and the end-to-end reliability requirement between the SNs and BS is $\mathcal{P}_{req}$, it is reasonable to assume $\mathcal{P}_{ij,min} = \left(\mathcal{P}_{req}\right)^{\frac{1}{h_{ij1}}}$ and $\mathcal{P}_{h,min} = \left(\mathcal{P}_{req}\right)^{\frac{1}{h_{ij1}}}$ given that $\mathcal{P}_{ij,min} \times \left(\mathcal{P}_{h,min}\right)^{h_{j1}} = \mathcal{P}_{req}$ because path loss is directly proportional to distance and the transmission power and retransmission limit required to overcome the packet errors stemming from pathloss is directly related to the reliablity requirement. When $d_{ij} > d_h$, $\mathcal{P}_{ij,min}$ and $\mathcal{P}_{h,min}$ should not be equal because a higher amount of resources are required to satisfy $\mathcal{P}_{ij,min}$ given the higher distance leads to higher path loss. Therefore, the disparity between path loss must be accounted for when determining values for $\mathcal{P}_{ij,min}$ and $\mathcal{P}_{h,min}$. We propose a heuristic where the values for $\mathcal{P}_{ij,min}$ and $\mathcal{P}_{h,min}$ are determined based on the following three cases:

$$\text{Case } 1(d_{ij} > d_h): \mathcal{P}_{ij,min} = \left(\mathcal{P}_{req}\right)^{\frac{d_h}{d_{ij}}}, \mathcal{P}_{h,min} = \left(\mathcal{P}_{req}\right)^{\frac{(d_{ij}-d_h)}{d_{ij}h_{j1}}} \tag{4.2.1}$$

$$\text{Case } 2(d_{ij} < d_h): \mathcal{P}_{ij,min} = \left(\mathcal{P}_{req}\right)^{\frac{d_{ij}}{d_h}}, \mathcal{P}_{h,min} = \left(\mathcal{P}_{req}\right)^{\frac{(d_{hop}-d_{ij})}{d_{hop}h_{j1}}} \tag{4.2.2}$$

$$\text{Case } 3(d_{ij} = d_h): \mathcal{P}_{ij,min} = \left(\mathcal{P}_{req}\right)^{\frac{1}{h_{ij1}}}, \mathcal{P}_{h,min} = \left(\mathcal{P}_{req}\right)^{\frac{1}{h_{ij1}}} \tag{4.2.3}$$

We demonstrate the efficacy of the heuristic with the following example. Assume $\mathcal{P}_{req} = 0.95$, $d_h = 10$ m, $d_{ij} = 15$ m, and $h_{j1} = 1$. Using (4.2), $\mathcal{P}_{ij,min} = 0.9664$ and $\mathcal{P}_{h,min} = 0.9915$, which follows from our assertion that a path with longer distance experiencing higher

path loss should have a less stringent reliability constraint. Now, substituting $\mathcal{P}_{ij,min}$ for $\mathcal{P}_{req}$ in Algorithms 3.1 and 3.2, the minimum relative energy cost achieved when the SNs either transmit using path 1 or path 2 is $\mathcal{E}_{rns,ij}$. The minimum relative energy cost $\mathcal{E}_{rns,j1,h}$ for each estimated hop between BNC j and the BS with distance d_h, traffic load r (from the source SNs), and reliability constraint $\mathcal{P}_{h,min}$ substituted for $\mathcal{P}_{req}$ is calculated using Algorithm 4.2.

Algorithm 4.2 Minimum Joint Delay and Relative Energy Cost for Relay Node to BS

Input: $PL(d_0), \alpha, d_0, d, m, P_{min}, P_{max}, X_{max}, r, L_{p,min}, L_{p,step}, \mathcal{P}_{req}, \mathcal{D}_{req}, E_{res}$;
Output: $FS, \hat{\mathcal{E}}$, and $\widehat{\mathcal{D}}$;
Initialization: $P_{tx}(z) = P_{max}$ (i. e. , $z = \mathcal{Z}$); $\mathcal{E}_{min} = \infty$; $\mathcal{E}''_{min} = \infty$; $FS = \emptyset$;
while $(P_{tx}(z) \geq P_{min})$ **do**
  $L_p = L_{p,max}$; $X = X_{max}$;
  while $\left(L_p \geq L_{p,min}\right)\&\&(X \geq 1)$ **do**
    Calculate $\mathcal{P} = \mathcal{P}_s\left(\bar{\gamma}, m, L_h + L_p, X\right)$ using $P_{tx}(z)$;
    Calculate $n = r/L_p$; $L = L_h + L_p$;
    Calculate $\mathcal{D} = \mathcal{D}_{tx}(nL, X, \mathcal{R})$;
    if $(\mathcal{P} \geq \mathcal{P}_{req})$ && $\left(\mathcal{D} \leq \mathcal{D}_{req}\right)$ **then**
      Calculate $\mathcal{E} = nL\phi(\bar{\gamma}, m, L, X)(E_b(P_{tx}(z))/E_{res} + E_b(P_{rx})/E_{res})$;
      if $(\mathcal{E}\mathcal{D} < \mathcal{E}'_{min})$ **then**
        $\mathcal{E}'_{min} = \mathcal{E}\mathcal{D}$; $\hat{\mathcal{E}} = \mathcal{E}$; $\widehat{\mathcal{D}} = \mathcal{D}$; $FS = \left(P_{tx}(z), X, L_p\right)$;
      end if
      $X = X - 1$; //decrement retransmission limit
    else
      $L_p = L_p - L_{p,step}$; // decrement number of samples per packet
    end if
  end while
  if $(\mathcal{E}'_{min} \geq \mathcal{E}''_{min})$ && $(\mathcal{E}'_{min} \neq \infty)$ **then** //no improvement in joint delay and REC
    terminate while loop
  else
    $z = z - 1$; //decrement power level
  end for
  $\mathcal{E}''_{min} = \mathcal{E}'_{min}$; //store the lowest relative energy cost obtained at $P_{tx}(z)$
end while
return *FS*, $\hat{\mathcal{E}}$, and $\widehat{\mathcal{D}}$;

Algorithm 4.2 is based on the same multi variable search direction concept employed in Algorithm 3.2 and provides the minimum relative energy cost $\mathcal{E}_{rns,j1,h}$ for each hop between BNC j and the BS. The maximum number of iterations performed in Algorithm 4.2 is $\mathcal{Z}(X_{max} + L_{p,max}/L_{p,step})$. We can assume that $L_{p,max}/L_{p,step}$ is greater than X_{max} because a small value of X_{max} must be used in order to support delay intolerant applications such as the physiological status monitoring. Therefore, the algorithmic complexity is given as $\mathcal{O}\left(\frac{\mathcal{Z}L_{p,max}}{L_{p,step}}\right)$. The total estimated relative energy cost for transmitting data from the SNs to the BS via relay node BNC j is then calculated as $\mathcal{E}_{rns,ij1} = \mathcal{E}_{rns,ij} + h_{j1}\mathcal{E}_{rns,j1,h}$. Using the relative energy cost $\mathcal{E}_{rns,ij1}$, a relay node selection metric is now provided to determine the neighbor BNC j ($\forall j \in [2, N]$) that should be chosen as a relay node. The relay node selection metric considers the following: 1) The relative energy cost saved when BNC i uses BNC j as a relay node instead of using no relay node. The higher relative energy cost that is saved, the more desirable BNC j is as a relay node. 2) The difference between the relative energy cost at BNC j when it is used as a relay node and the relative energy cost at BNC i when no relay node is used. A negative difference indicates the relative energy cost of BNC j exceeds the relative energy cost when BNC i does not use a relay node, which then deems BNC j as an undesirable relay node. With the two above points in mind, the relay node selection metric is calculated as:

$$\beta_{rsm,ij} = \frac{(\mathcal{E}_{rns,ij1} - \mathcal{E}_{rns,ij})(\mathcal{E}_{rns,ij1} - h_{j1}\mathcal{E}_{rns,j1,h})}{\mathcal{E}_{rns,ij1}} \tag{4.3}$$

The first factor in the numerator in (4.3) describes the relative energy cost difference between $\mathcal{E}_{rns,ij}$ and $\mathcal{E}_{rns,ij1}$ whereas the second factor describes the relative energy cost difference between $h_{j1}\mathcal{E}_{rns,j1,h}$ and $\mathcal{E}_{rns,ij1}$. The neighbor of BNC i yielding the highest positive

value of $\beta_{rsm,ij}$ is selected as the relay node. Otherwise, if $\beta_{rsm,ij} \leq 0$, BNC i transmits directly to the BS. The relay node selection process is executed until routing paths are formed between all BNCs and the BS.

4.4.3.3 Maintaining a Routing Path

New routing paths are created periodically every route update period T_{rs}. The route update period is configured prior to a mission and its value depends on the type of mission. The time required to setup a route $\mathcal{D}_{rs}$ must be less than the route update period, providing $\mathcal{D}_{rs} < T_{rs}$. A mission requiring higher soldier group speeds will have a lower value for T_{rs} (i.e., routes updated more frequently) whereas a mission requiring lower soldier group speeds will have a higher value for T_{rs} (i.e., routes updated less frequently).

4.4.4 BBN Multi-constrained Power Allocation Strategy

The BRA routing algorithm described in Section 4.3.4 builds end-to-end routing paths between all the SNs in the network and the BS. However, the minimum relative energy cost routing paths are determined in a distributed manner based on approximations given in (4.2) and thus it is possible that the end-to-end success probability computed by the BS for each of the routing paths does not satisfy the end-to-end reliability objective when the product of success probability along each link is computed. In this section, we devise a BBN multi-constrained power allocation strategy based on our previous work [154] to iteratively configure the transmit power, retransmission limit, and packet size for each data packet transmitted on each link along the populated routing paths, until the end-to-end reliability objective for each routing path is satisfied. We consider the collection of routing paths as a single connected routing tree represented by the network graph $\mathcal{G}$. That is, each link belonging to each routing path is mapped to $\mathcal{G}$. The BBN multi-constrained power allocation strategy is designed to use the minimum

number of iterations in order to simultaneously achieve minimum relative energy cost for the routing tree while also satisfying a desired end-to-end reliability constraint. The BBN multi-constrained power allocation strategy is described in two parts. First, the incremental gain ratio used to determine the link in $\mathcal{G}$ to update is detailed. Next, a BBN multi-constrained power allocation algorithm is provided in order to update the links in $\mathcal{G}$ until the reliability objective along each routing path is met.

4.4.4.1 Incremental Gain Ratio

The transmit power, retransmission limit, and packet size (in this section, for the sake of brevity, we refer to this combination as transmission parameters) belonging to each link in $\mathcal{G}$ emanating from SN *i.k* ($\forall i \in [2, N], \forall k \in [1, N_s]$) and BNC i ($i \in [2, N]$) is reconfigured to the initial values $P_{tx}(z) = P_{min}, X = X_{min}$, and $L = L_{p,max}$, if the routing path they reside on does not satisfy the end-to-end reliability objective. Throughout this section, we predominantly use the link notation $link(x, y)$ to represent the link between a transmitter x (i.e., SN or BNC) and receiver y (BNC or BS). For each link in $\mathcal{G}$, we define incremental ratios δ_{xy}^{p}, δ_{xy}^{r}, and δ_{xy}^{s} for the link success probability and change in relative energy cost contributed by incrementing the transmit power, incrementing the retransmission limit, and decrementing the packet size, respectively, of $link(x, y)$. The three incremental ratios are given as follows:

$$\delta_{xy}^{p} = \left(\frac{\mathcal{P}_s\left(\bar{\gamma}_{xy}(z+1), m, L_{xy}, X_{xy}\right)}{\mathcal{P}_s\left(\bar{\gamma}_{xy}(z), m, L_{xy}, X_{xy}\right)}\right) \Big/ \left(\frac{\phi\left(\bar{\gamma}_{xy}(z+1), m, L_{xy}, X_{xy}\right) E_b(P_{tx.xy}(z+1))}{\phi\left(\bar{\gamma}_{xy}(z), m, L_{xy}, X_{xy}\right) E_b(P_{tx.xy}(z))}\right) \quad (4.4.1)$$

$$\delta_{xy}^{r} = \left(\frac{\mathcal{P}_s\left(\bar{\gamma}_{xy}(z), m, L_{xy}, X_{xy}+1\right)}{\mathcal{P}_s\left(\bar{\gamma}_{xy}(z), m, L_{xy}, X_{xy}\right)}\right) \Big/ \left(\frac{\phi\left(\bar{\gamma}_{xy}(z), m, L_{xy}, X_{xy}+1\right)}{\phi\left(\bar{\gamma}_{xy}(z), m, L_{xy}, X_{xy}\right)}\right) \quad (4.4.2)$$

$$\delta_{xy}^{s} = \left(\frac{\mathcal{P}_s\left(\bar{\gamma}_{xy}(z), m, \tilde{L}_{xy}, X_{xy}\right)}{\mathcal{P}_s\left(\bar{\gamma}_{xy}(z), m, L_{xy}, X_{xy}\right)}\right) \Big/ \left(\frac{\tilde{n}_{xy}\tilde{L}_{xy}\phi\left(\bar{\gamma}_{xy}, m, \tilde{L}_{xy}, X_{xy}\right)}{n_{xy}L_{xy}\phi\left(\bar{\gamma}_{xy}(z), m, L_{xy}, X_{xy}\right)}\right) \quad (4.4.3)$$

For the ratios provided in (4.4.1) to (4.4.3), the incremental gain in success probability is represented on the left hand side of the equations and the incremental gain in relative energy cost is represented on the right hand side. The energy per bit expressions in (4.4.2) and (4.4.3) are absent because they cancel each other out since the transmit power is the same. In (4.4.3), $\tilde{L}_{xy}$ is the next lowest packet size calculated as $\tilde{L}_{xy} = L_{xy} - L_{step}$ and $\tilde{n}_{xy}$ is the updated number of packets required to support a packet size of $\tilde{L}_{xy}$ for a given data source rate. The incremental gain ratio from (4.4.1) to (4.4.3) with the highest gain in success probability for the lowest gain in relative energy cost is calculated as $\max(\delta_{xy}^{p}, \delta_{xy}^{r}, \delta_{xy}^{s})$.

In addition to determining the highest incremental gain ratio, we also exploit the fact that updating the transmission parameters along a single SN link or SNs' BNC links can simultaneously increase the success probability along multiple links and routing paths. For example, assume a SN link given by $link(i.k, i)$ uses path 2 of the synergistic BAN model for data transmission. The reliability along $link(i.k, i)$ simultaneously impacts the success probability of the $link(i, j)$ where BNC i uses BNC j as a relay node and the success probability of $link(i.k, j)$ where the transmission from SN $i.k$ is overheard by the neighboring BNC j due to the dual aggregation concept between neighboring BANs. Therefore, it is advantageous to preferentially allocate transmission parameters to $link(i.k, i)$ in order to provide fast solution convergence. Similarly, it is also advantageous to preferentially allocate transmission parameters for transmission to a BNC i that aggregates and forwards data from its source SNs to a neighboring BNC j because the reliability along $link(i, j)$ impacts the success probability of at least N_s links. To take advantage of the multiple incoming and outgoing links whose success probability is affected by either a SN or BNC link we define the weighting factor ω_x as the total

number of incoming and outgoing links from transmitter *x* with link success probability less than one. If the incoming and outgoing links belong to a routing path where the end-to-end success probability satisfies the reliability objective, ω_x is set to zero because there is no need to update the transmission parameters of a link belonging to node *x* if the end-to-end reliability objective has already been satisfied.

The final incremental gain ratio δ_{xy} for $link(x, y)$ is calculated by combining (4.4) and ω_x to obtain:

$$\delta_{xy} = \left(\max(\delta_{xy}^{p}, \delta_{xy}^{r}, \delta_{xy}^{s}) \frac{\mathcal{E}_{xy}^{p,r,s}}{\mathcal{E}_{xy}} \right)^{\omega_x} \tag{4.5}$$

where $\mathcal{E}_{xy}$ is the initial relative energy cost for $\left(P_{tx.xy}(z), L_{xy}, X_{xy}\right)$ and $\mathcal{E}_{xy}^{p,r,s}$ the relative energy cost for the incremental ratio given by $\max(\delta_{xy}^{p}, \delta_{xy}^{r}, \delta_{xy}^{s})$. The relative energy cost gain in (4.5) is detached in order to eliminate the scenarios where the relative energy cost gain is far higher than the success probability gain. Furthermore, the goal of the BBN multi-constrained power allocation algorithm is to converge to a minimum relative energy cost solution in a fast manner. The speed of the algorithm is dictated by the reliability constraint and thus the primary design of the BBN multi-constrained power allocation algorithm is to satisfy the reliability constraint, while obtaining the minimum relative energy cost.

4.4.4.2 BBN Multi-constrained Power Allocation Algorithm

The BBN multi-constrained power allocation (BPA) algorithm operates in four cyclic phases and its operation is provided in Algorithm 4.3. In the first phase depicted by lines 4 to 7, the end to end success probability for all routing paths is calculated and compared against the reliability objective given by $\mathcal{P}_{req}$. If all routing paths satisfy the reliability objective, the algorithm returns the configured transmission parameters (line 6). In the second phase depicted

by lines 8 and 9, each $link(x, y)$ in $\mathcal{G}$ calculates its weighting factor ω and incremental gain ratio δ_{xy} along with its current link success probability $\mathcal{P}$. In the third phase, the link with the highest incremental gain ratio is selected, as shown in line 10. In the fourth phase, Algorithm 4.2 is executed to obtain the transmission parameters that minimize the relative energy cost for a reliability objective of $\mathcal{P}_{x'y'}$, which is the current success probability for $link(x'y')$. It should be noted that line 10 of Algorithm 4.2 must be modified from '$(\mathcal{P} \geq \mathcal{P}_{req})$ && $\left(\mathcal{D} \leq \mathcal{D}_{req}\right)$' to '$\mathcal{P} > \mathcal{P}_{req}{}'$. The delay constraint is removed because we are only concerned with meeting the reliability objective. The delay constraint is handled separately in Section 4.4.5 using a slot scheduling algorithm. The success probability is changed to be greater than the reliability objective in order to ensure that $link(x'y')$ always improves its link success probability.

Algorithm 4.3 BBN Multi-constrained Power Allocation

1: **Input:** $\mathcal{G}, P_{min}, X_{min}, L_{max}, \mathcal{P}_{req}, \boldsymbol{E_{res}}$, ;
2: **Output:** *FS;*
3: Allocate $P_{tx}(z) = P_{min}, X = X_{min}$, and $L = L_{max}$ to all links in $\mathcal{G}$;
4: Calculate end-to-end success probability for each routing path in $\mathcal{G}$;
5: **if** (End-to-end success probability for all routing paths are equal to or greater than $\mathcal{P}_{req}$) **then**
6: **return** $FS = (\boldsymbol{P_{tx}(z)}, \boldsymbol{X}, \boldsymbol{L})$;
7: **end if**
8: Calculate weighting factor ω for each node in $\mathcal{G}$;
9: Calculate δ and $\mathcal{P}$ for all links in $\mathcal{G}$ using (4.5);
10: Select link in $\mathcal{G}$ with the highest incremental gain ratio: $(x'y') = \text{argmax}_{\forall(x,y)\in\mathcal{G}}\, \delta_{xy}$;
11: Update $\left(P_{tx.x'y'}(z), X_{x'y'}, L_{x'y'}\right)$ for $link(x', y')$ using Algorithm 4.2 ($\mathcal{P}_{x'y'}$ as input for $\mathcal{P}_{req}$)
12: **goto** Step 4;

The computational complexity of the BPA algorithm is determined as follows: In each iteration, $\mathcal{W}$ comparisons are needed to determine the link with the highest incremental gain ratio. The end-to-end success probability along a path is multiplied by at least $\delta_{min} =$

$\mathcal{P}_s\left(\bar{\gamma}_{\hat{x}\hat{y}}(z^*), m, L^*_{\hat{x}\hat{y}}, X^*_{\hat{x}\hat{y}}\right)/\mathcal{P}_s\left(\bar{\gamma}_{\hat{x}\hat{y}}(z^*-1), m, L^*_{\hat{x}\hat{y}}, X^*_{\hat{x}\hat{y}}\right)$ when incrementing the transmit power provides the maximum incremental gain ratio, $\delta_{min} = \mathcal{P}_s\left(\bar{\gamma}_{\hat{x}\hat{y}}(z^*), m, L^*_{\hat{x}\hat{y}}, X^*_{\hat{x}\hat{y}}\right)/\mathcal{P}_s\left(\bar{\gamma}_{\hat{x}\hat{y}}(z^*), m, L^*_{\hat{x}\hat{y}}, X^*_{\hat{x}\hat{y}}-1\right)$ when incrementing the retransmission limit provides the maximum incremental gain ratio, or $\delta_{min} = \mathcal{P}_s\left(\bar{\gamma}_{\hat{x}\hat{y}}(z^*), m, L^*_{\hat{x}\hat{y}}, X^*_{\hat{x}\hat{y}}\right)/\mathcal{P}_s\left(\bar{\gamma}_{\hat{x}\hat{y}}(z^*), m, L^*_{\hat{x}\hat{y}}-L_{step}, X^*_{\hat{x}\hat{y}}\right)$ when decrementing the packet size provides the maximum incremental ratio, where $(\hat{x},\hat{y}) = \arg\max_{(x,y)} \mathcal{P}_s\left(\bar{\gamma}_{xy}(z), m, L_{xy}, X_{xy}\right)$, $P^*_{tx.\hat{x}\hat{y}}(z)$, $X^*_{\hat{x}\hat{y}}$, and $L^*_{\hat{x}\hat{y}}$ are the smallest integer values satisfying

$\mathcal{P}_s\left(\bar{\gamma}(P_{tx.\hat{x}\hat{y}}(z), d_{\hat{x}\hat{y}}), m, L_{\hat{x}\hat{y}}, X_{\hat{x}\hat{y}}\right)\prod_{\forall(x,y)\in W_x,(x,y)\neq(\hat{x},\hat{y})}\mathcal{P}_s\left(\bar{\gamma}(P_{tx.xy}(z), d_{xy}), m, L_{xy}, X_{xy}\right) \geq \mathcal{P}_{req}$, and $\forall(x,y) \in \mathcal{W}_x$ are the set of links along the routing path that node *x* resides on. The number of iterations is at most $\log_{\delta_{min}} \mathcal{P}_{req}$ and therefore the worst case complexity is $\mathcal{O}\left(\left(L_{p,step}|\mathcal{W}|\, log_{\delta_{min}} \mathcal{P}_{req}\right)/\left(\mathcal{Z}L_{p,max}\right)\right)$ when the complexity of Algorithm 4.2 is also considered.

4.4.5 BBN Interference Aware Slot Scheduling Strategy

In most BAN and BBN oriented TDMA schemes, unique time slots are assigned to each link to avoid the occurrence of collisions and interference during packet transmissions [23], [33]. Slot collisions can occur when two different transmissions take place at the same time within the same transmission radius or when the slot schedule is not properly synchronized. Without the ability to reuse slots, the TDMA frame length grows linearly as the number of links in the network increases thus leading to increased packet delay. To curtail these effects, we design a conflict free slot scheduling algorithm building upon the work performed in [106] where slot reuse is employed to minimize the TDMA frame length. Slot reuse assumes the same time slot is

used by multiple transmitting nodes without negatively affecting the probability of successful data packet transmission. The design of a minimum length TDMA frame is an NP-hard problem [106] that can be solved using heuristics. The heuristic must be designed in a manner guaranteeing the conflict free nature of a TDMA frame. In [106], three criteria are described which must be satisfied concurrently to guarantee the conflict free feature. However, the criteria are based on the governing assumption that interference at a receiving node is negligible only if the interference is less than 10 percent of the noise floor [106]. In reliability-constrained applications, this assumption may negatively affect the resulting success probability of transmitting links sharing the same transmission slot because interference may not be completely negligible. Rather than generalizing the condition for neglecting interference, we analytically determine the exact relationship between the received power over a transmitting link and the combined interference power from all the transmitting links that share the same transmission slot, given a desired reliability objective. Using the knowledge gained from this analysis, we then propose a slot assignment algorithm that is based on SINR and accounts for its effect on end-to-end success probability along routing paths.

4.4.5.1 Maximum Interference Power to avoid Reliability Degradation

In this section, we again use the link notation $link(x, y)$ to represent the link between a transmitter x (i.e., SN or BNC) and receiver y (BNC or BS). Let $link(x, y)$ represent a candidate link for being scheduled in a slot s that has already been scheduled on another $link(x', y')$. The SINR experienced over $link(x, y)$ is calculated as the ratio of received power over $link(x, y)$ to the combined interference power from all the transmitting links that share slot s, in addition to the noise power. The SINR is given by:

$$\bar{\gamma}_{I.xy}(P_{tx.xy}, d_{xy}, P_{tx.x'y'}, d_{x'y}) = \frac{g(d_{xy})P_{tx.xy}}{\sum_{\forall\Delta(x',y',q)=s} g(d_{x'y})P_{tx.x'y'} + P_n} \tag{4.6}$$

where $\Delta(x', y', q) = s$ is the slot schedule indicating the q^{th} time slot of the interfering $link(x', y')$ is assigned slot ID s and $g(d_{x'y})$ is the channel gain for $link(x', y)$ and is required to calculate the interference experienced at node y from node x' since both node x and node x' transmit in slot ID s on $link(x, y)$ and $link(x', y')$, respectively. The number of elements in $\Delta(x', y')$ is equal to $\mathcal{S}_{x'y'}$ and therefore $q \in [1, \mathcal{S}_{x'y'}]$.

Assume a $link(x', y')$ has been scheduled in slot ID $s = 1$ and $link(x, y)$ has been scheduled in slot ID $s = 2$. The success probability over $link(x, y)$ is $\mathcal{P}_{xy}$ and the end-to-end success probability along the path $link(x, y)$ resides on is $\mathcal{P}_{ete,xy}$. If $link(x, y)$ is scheduled in slot ID $s = 1$, the interference power from $link(x', y')$ impacts the success probability over $link(x, y)$ such that the end-to-end success probability with slot reuse is:

$$\mathcal{P}^{sr}_{ete,xy} = \mathcal{P}_{ete,xy} \frac{\mathcal{P}_s\left(\bar{\gamma}_{I.xy}(P_{tx.xy}, d_{xy}, P_{tx.x'y'}, d_{x'y}), m, L_{xy}, X_{xy}\right)}{\mathcal{P}_s\left(\bar{\gamma}(P_{tx.xy}, d_{xy}), m, L_{xy}, X_{xy}\right)} \tag{4.7}$$

The numerator term in (4.7), denoted by $\mathcal{P}_s$, is the link success probability with interference and the denominator is the link success probability without interference. Since interference can cause additional noise to be experienced at the intended receiver, the success probability at the receiver is less with interference than without. Therefore, $\mathcal{P}^{sr}_{ete,xy}$ is at least equal to or less than $\mathcal{P}_{ete,xy}$ when interference is present.

The maximum tolerable interference power that does not negatively impact the success probability of a transmitting link is determined as follows. Assume the success probability over $link(x, y)$ must be equal to or greater than a reliability objective such that $\mathcal{P}_{xy} \geq \mathcal{P}_{req}$.

Rearranging (3.8) and (3.9), the reliability objective can be rewritten in terms of the BER $p_{b,xy}$, retransmission limit, and packet size, as:

$$p_{b,xy} \leq 1 - \sqrt[L_{xy}]{1 - \sqrt[X_{xy}]{1 - \mathcal{P}_{req}}} \tag{4.8}$$

To express $p_{b,xy}$ in terms of SINR $\bar{\gamma}_{I.xy}$, we must make a lower bound approximation of the BER. From [136], the lower bound to $p_{b,xy}$ in (3.7) can be obtained owing to the fact that $\left(\frac{m}{m+\gamma}\right)^m \leq \frac{m}{m+\gamma}$ for $0 < \frac{m}{m+\gamma} \leq 1$, and is given as [136]:

$$p_b(\bar{\gamma}, m) \geq \tilde{p}_b = K_1 \left(\frac{m}{m+\bar{\gamma}}\right)^m \sqrt[-1]{1 - \left(\frac{m}{m+\bar{\gamma}}\right)^m \left(\frac{m}{m+1}\right)} \tag{4.9}$$

The expression in (4.8) is invertible with respect to $\bar{\gamma}$ and is shown to be [136]:

$$\bar{\gamma}(\tilde{p}_b) = m \left(\sqrt[m]{\frac{m}{2(m+1)} + \sqrt{\left(\frac{m}{2(m+1)}\right)^2 + \left(\frac{K_1}{\tilde{p}_b}\right)^2}} - 1 \right) \tag{4.10}$$

Combining (4.6) and (4.10), the maximum interference power $P_{I.x'y'}$ from interfering $link(x', y')$ tolerable by $link(x, y)$ to maintain the success probability along $link(x, y)$ above the reliability objective is expressed as:

$$P_{I.x'y'} \leq g(d_{xy}) P_{tx.xy} \left[m \left(\sqrt[m]{\frac{m}{2(m+1)} + \sqrt{\left(\frac{m}{2(m+1)}\right)^2 + \left(\frac{K_1}{p_{b,max}(X_{xy}, L_{xy}, \mathcal{P}_{req})}\right)^2}} - 1 \right) \right]^{-1} - P_n \tag{4.11}$$

where $p_{b,max}$ is the maximum BER given as the upper bound in (4.8) and $P_{I.x'y'} = \sum_{\forall I(x',y',q)=s} g(d_{x'y}) P_{tx.x'y'}$. In the expression for $p_{b,max}$, increasing X_{xy} and

decreasing L_{xy} decreases the BER. Therefore, increasing X_{xy} and decreasing L_{xy} in (4.11) subsequently increases the maximum interference power that does not reduce the success probability along $link(x,y)$ below the reliability objective. It should be noted that (4.11) must hold simultaneously for both scenarios where $link(x',y')$ acts as an interferer to $link(x,y)$ and $link(x,y)$ acts as an interferer to $link(x',y')$. As a result, increasing $P_{tx.xy}$ in (4.11) does not increase the maximum tolerable interference power because it subsequently increases the interference received at $link(x',y')$ from $link(x,y)$.

Given $P_{I,max.x'y'}$ as the maximum interference power from the right side of (4.11), we can also compute the minimum interference distance required to avoid degradation in success probability as:

$$d_{x'y} = d_0 10^{\frac{P_{tx.x'y'} - PL(d_0) - 10\log_{10}\left(P_{I,max.x'y'}\right)}{10\alpha}} \tag{4.12}$$

The minimum interference distance required to support the interference neglecting assumption from [106], where the total interference power from $link(x',y')$ received at the receiver node of $link(x,y)$ must be less than $I_{th} = 10\%$ is calculated as:

$$d_{x'y} = d_0 10^{\frac{P_{tx.x'y'} - PL(d_0) - 10\log_{10}\left(I_{th} 10^{\frac{P_n}{10}}\right)}{10\alpha}} \tag{4.13}$$

In the numerical results, we compare (4.12) and (4.13) and show how the interference neglecting assumption is inappropriate for reliability-constrained applications.

4.4.5.2 BBN Slot Assignment Algorithm

In this section, we propose a BBN slot assignment (BSA) algorithm to minimize the number of slots that can be assigned to the links emanating from the SNs and BNC. The BSA algorithm is designed with three key features:

1) Conflict free schedule – In order for a slot *s* to be assigned to any link belonging to SN *i.k* or BNC *i* ($i \in [2, N], k \in [1, N_s]$) using slot reuse, we define the following reliability-driven criteria that must be satisfied to provide a conflict free slot schedule.

Criterion 1*:* SN *i.k* or BNC *i* is not the transmitter or receiver of a link that was previously scheduled using slot *s*.

Criterion 2: The link of SN *i.k* or BNC *i* to be scheduled using slot s does not have the same receiver(s) as another previously scheduled link assigned to slot *s*.

Criterion 3: The interference resulting from scheduling slot s to one of SN *i.k*'s or BNC *i*'s links does not decrease the end-to-end success probability along the path of a receiver's link that is also scheduled to slot *s*, below the end-to-end reliability requirement.

Criterion 4: The transmitter of a scheduled link using slot *s* does not decrease the end-to-end success probability along the path of the current receiver if it is using slot *s* on one of SN *i.k*'s or BNC *i*'s links, below the end-to-end reliability requirement.

2) Maximized opportunities for slot reuse - the number of unique slots that can be reused is maximized by configuring the slot assignment order (i.e., the sequence in which slots are assigned to all links) to first assign slots to the links requiring the most slots. The premise for this decision is that links requiring the most slots present the most opportunities for slot reuse.

3) Adaptive slot reuse – in the circumstances where slot reuse cannot be achieved due to the violation of the reliability constraint, we attempt to improve the link success probability along the transmitting and interfering links by increasing the retransmission limit. While increasing the retransmission limit improves the link success probability (3.9) and can subsequently present more opportunities for slot reuse (4.11), it also has the negative impact of increasing the number of required slots along a link since retransmission limit is directly proportional to the number of slots (3.11) and to relative energy cost. Therefore, the decision to use slot reuse is guided by

evaluating whether the total number of overlapping slots that would be assigned to multiple links using slot reuse is lower than the total number of unique slots that would be assigned to multiple links. If the number of slots is lower for slot reuse, we then determine whether the increase in relative energy cost resulting from employing slot reuse exceeds a certain relative energy cost gain threshold in the range [0, 1]. If the relative energy cost gain threshold is not exceeded, slot reuse is implemented. Otherwise, unique slots are assigned.

The operation of the BSA algorithm is described in Algorithm 4.4. The inputs $\boldsymbol{P_{tx}}$, $\boldsymbol{X}$, and $\boldsymbol{L}$ represent the set of transmit powers, retransmission limits, and packet sizes for the links in $\mathcal{W}$, respectively, and are obtained as a result of executing Algorithm 4.3. The input $\boldsymbol{S}$ to Algorithm 4.4 is the set that holds the number of time slots required for each of the SN and BNC links. The input $\mathcal{E}_{th}$ is the threshold for the increase in relative energy cost caused by slot reuse.

We describe the systematic operation of Algorithm 4.4 as follows. The slot schedule is first initialized to null. The main while loop covering lines 4 to 34 is continuously executed until all the required slots specified by $\boldsymbol{S}$ have been assigned to all the links in Δ. After the $link(i,j)$ requiring the most number of slots has been selected in line 5, the opportunities for slot re-use is evaluated for each unassigned link in $\Delta(i,j)$ with all the other links in $\mathcal{W}$ denoted by $link(x,y)$. In lines 9 to 12, the first available slot ID that satisfies interference criteria 1 and 2 is discovered. Only criteria 1 and 2 is explored in this loop because it provides an indication of the slots that have already been used. In lines 13 to 15, the current slot ID is assigned to both links because the reliability constraints stipulated by criteria 3 and 4 have been satisfied. If the criteria have not been satisfied, a while loop covering lines 18 to 21 is executed to determine the retransmission limit X_I and subsequent link success probability with interference $\mathcal{P}'_{I.ij}$ required to sustain $\mathcal{P}_{ij}$, the link success probability without interference. Two conditions that must be satisfied in order

to invoke slot reuse are presented in line 23. First, in line 23, the total number of slots $\mathcal{S}_I$ resulting from slot reuse using X_I is compared against the total number of unique slots $\mathcal{S}_{ij} + \mathcal{S}_{xy}$ that would be assigned without slot reuse. The link success probability calculated with the original retransmission limit X_{ij} and interference is $\mathcal{P}_{I.ij}$. Since the gain in relative energy cost is directly proportional to the gain in link success probability when only the retransmission limit is varied (relative energy cost scales linearly with the average number of transmissions ϕ which is a function of the retransmission limit), the second condition given by $\left(\left(\mathcal{P}'_{I.ij}/\mathcal{P}_{I.ij} - 1\right) < \mathcal{E}_{th}\right)$ checks whether the gain exceeds $\mathcal{E}_{th}$. If the two conditions are true, the retransmission limit for $link(i,j)$ is set as X_I. Subsequently, all slot IDs that have been assigned are deleted and the slot assignment algorithm is recalibrated with the new retransmission limit and restarted in line 3. Therefore, increased opportunities are discovered for slot reuse when the algorithm is rerun. In lines 31 to 33, slot IDs are assigned to the slots belonging to $link(i,j)$ that have not qualified for slot reuse. As a result, each slot is assigned a unique slot ID. Algorithm 4.4 returns the conflict free TDMA slot schedule Δ.

The total delay for the TDMA frame is $\mathcal{D}_{tdma} = t_{slot} \times \max\{\Delta\}$. To ascertain the end-to-end delay objective is satisfied, the following check must take place: $\mathcal{D}_{tdma} \leq \mathcal{D}_{req}$. If the constraint is not satisfied, the number of time slots in $\boldsymbol{\mathcal{S}}$ must be regenerated using a lower value of t_{slot}. The delay constraint is violated if the smallest value of t_{slot} is not sufficient to satisfy the delay objective.

Algorithm 4.4 BBN Slot Assignment

Input: $\mathcal{G}, \mathcal{W}, \boldsymbol{P_{tx}}, \boldsymbol{X}, \boldsymbol{L}, \boldsymbol{\mathcal{S}}, X_{max}, \mathcal{P}_{req}; \mathcal{E}_{th}$;
Output: Δ;
Initialization: $\Delta = \emptyset$;
while $(|\Delta| < |\boldsymbol{\mathcal{S}}|)$ **do**
  Find $link(i,j)$ in $\mathcal{W}$ requiring the most number of slots: $(i,j) = \text{argmax}_{\forall (i,j) \in \mathcal{W}} |\boldsymbol{\mathcal{S}} - \Delta|$;
  for each $link(x,y)$ in $\mathcal{W}$ **do**
    if $(link(i,j) \neq link(x,y))$ and $\left(\mathcal{S}_{xy} - |\Delta(x,y)| > 0\right)$ **then**
      for each unassigned slot q_{ij} in $\Delta(i,j)$ **do**
        Attempt to assign first slot ID: $s = 1$;
        while interference criteria 1 and 2 are not satisfied **do**
          Attempt to assign next slot ID: $s = s + 1$;
        end while
        if interference criteria 3 and 4 are satisfied **then** //all interference criteria satisfied
          Assign current slot ID to $link(i,j)$: $\Delta\left(i,j,q_{ij}\right) = s$;
          Assign current slot ID to $link(x,y)$: $\Delta\left(x,y,q_{xy}\right) = s$; $q_{xy} = \mathcal{S}_{xy} - |\Delta(x,y)| + 1$;
        else
          $X_I = X_{ij}; \mathcal{P}'_{I.ij} = 0$;
          while $\left(\mathcal{P}'_{I.ij} < \mathcal{P}_{ij}\right)$ and $(X_I \leq X_{max})$ **do**
            Increment retransmission limit: $X_I = X_I + 1$;
            Calculate new success probability after interference: $\mathcal{P}_I = \mathcal{P}_s\left(\bar{\gamma}_{I.ij}, m, L_{ij}, X_I\right)$;
          end while
          Calculate total number of slots after slot reuse: $\mathcal{S}_I = \left\lceil \left(f_{ij} X_I\right) / \left(t_{slot} \mathcal{R}\right) \right\rceil$;
          if $\left(\mathcal{S}_I < \mathcal{S}_{ij} + \mathcal{S}_{xy}\right)$ and $\left(\left(\mathcal{P}'_{I.ij} / \mathcal{P}_{I.ij} - 1\right) < \mathcal{E}_{th}\right)$ **then**
            Set new retransmission limit to exploit slot reuse $X_{ij} = X_I$;
            Goto step 3: Restart algorithm and calculate slot schedule using new value of X;
          end if
        end if
      end for
    end if
  end for
  if $\left(\mathcal{S}_{ij} - |\Delta(i,j)| > 0\right)$ **then** //not all the slots belonging to $link(i,j)$ have been assigned
    Assign remaining slot IDs: $\Delta\left(i,j,(|\Delta(i,j)| + 1) : \mathcal{S}_{ij}\right) = [s, \ldots, s + \mathcal{S}_{ij} - |\Delta(i,j)|]$;
  end if
end while

To compute the complexity of Algorithm 4.4, we calculate the worst case number of iterations in each of the four major loops within lines 4 and 34. The worst case number of iterations for the first three loops are $|\mathcal{W}|$, $\max\{\mathcal{S}_{ij}\}, (i,j) \in \mathcal{W}$, and $(|\mathcal{W}|-1)\max\{\mathcal{S}_{ij}\}$ resulting in approximately $\left(|\mathcal{W}|\max\{\mathcal{S}_{ij}\}\right)^2$ iterations. The fourth loop (lines 18 to 21) is executed a maximum of X_{max} times if there are no slot reuse opportunities created by increasing the retransmission limit. On the other hand, Algorithm 4.4 is restarted $(\mathcal{E}_{th}+1)X_{max}$ times if slot reuse opportunities are created during each process of increasing the retransmission limit. Since $\left(|\mathcal{W}|\max\{\mathcal{S}_{ij}\}\right)^2$ is much greater than $(\mathcal{E}_{th}+1)X_{max}$ in delay constrained networks and $\max\{\mathcal{S}_{ij}\}$ is much greater than $|\mathcal{W}|$ in average sized military teams (e.g., platoon size between 10 and 36 soldiers) requiring the continuous transmission of high data rate real-time physiological data, the complexity of Algorithm 4.4 is approximated as $\mathcal{O}\left(\max\{\mathcal{S}_{ij}\}^2\right)$.

4.4.6 Summary of Algorithmic Complexity

In Table 4.1, we provide a summary for the complexity of the all algorithms proposed in this chapter. The complexity of the proposed algorithms is in the polynomial class and thus provides significantly less solution complexity than the optimal solution.

TABLE 4.1 SUMMARY OF ALGORITHM COMPLEXITY

Algorithm	Description	Complexity
OPT: Optimal Solution	Optimal route formation and allocation of transmit power, retransmission limit, and packet size	$\mathcal{O}({X_{max}}^2 \mathcal{Z}^2 N_s N {N_b}^3)$
EQX: Algorithm 4.1	Calculation of neighbor discovery range	$\mathcal{O}\left(\frac{d_{max}(X_{max}+\mathcal{Z})}{d_{step}}\right)$
EQX: Algorithm 4.2	Minimum Joint Delay and Relative Energy Cost for Relay Node to BS	$\mathcal{O}\left(\frac{\mathcal{Z}L_{p,max}}{L_{p,step}}\right)$
EQX: Algorithm 4.3	BBN Multi-constrained Power Allocation	$\mathcal{O}\left(\frac{L_{p,step}\lvert\mathcal{W}\rvert \log_{\delta_{min}} \mathcal{P}_{req}}{\mathcal{Z}L_{p,max}}\right)$
EQX: Algorithm 4.4	BBN Slot Assignment	$\mathcal{O}\left(\max\{\mathcal{S}_{ij}\}^2\right)$

4.5 Network Performance Analysis of EQX and OPT

In this section we derive analytical expressions to determine the network performance of EQX and the optimal solution obtained from solving (4.1). Specifically, we derive the network relative energy cost, energy consumption for route setup, route setup time, average end-to-end success probability, and maximum end-to-end packet delay.

4.5.1.1 Network Relative Energy Cost

The network relative energy cost for the optimal solution (OPT) is derived from solving (4.1) and denoted as $\mathcal{E}_{OPT}$. The network relative energy cost for EQX is calculated based on the traffic load, transmit power, retransmission limit, and packet size values belonging to the set of links $\mathcal{W}$ belonging to the routing tree formed using the BRA algorithm. Let the set of SN links be represented by $\mathcal{W}_{i.k}$ and the BNC links be represented by $\mathcal{W}_i$ such that $\mathcal{W}_{i.k} \cup \mathcal{W}_i = \mathcal{W}, \forall i = [2, N], \forall k = [1, N_s]$. Therefore, the network relative energy cost for EQX is:

$$\mathcal{E}_{EQX} = \sum_{i=2}^{N}\sum_{k=1}^{N_s}\left(\sum_{\forall(i.k,i)\in\mathcal{W}_{i.k}}\left(\mathcal{E}_{tx.i.k,i} + \mathcal{E}_{rx.i.k,i} + \mathcal{E}_{rx.i.k,j}\right) + \sum_{\forall(i.k,j)\in\mathcal{W}_{i.k}}\left(\mathcal{E}_{tx.i.k,j} + \mathcal{E}_{rx.i.k,j}\right)\right) + \cdots + \sum_{i=2}^{N}\sum_{j=1}^{N}\left(\sum_{\forall(i,j)\in\mathcal{W}_i}\mathcal{E}_{tx.ij} + \mathcal{E}_{rx.ij}\right) \quad (4.14)$$

where $\mathcal{E}_{rx.i.k,j}$ in the leftmost summation is the receiving relative energy cost for relay node BNC j overhearing the transmission along $link(i.k,i)$.

4.5.1.2 Energy Consumption for Route Setup

The BS is tasked with obtaining the optimal solution. It requires the node ID, location coordinates, and residual energy for each SN and BNC in the BBN, in addition to the channel state information for each possible link in the network. To obtain the channel state information, each SN and BNC uses the minimum transmit power and retransmission limit required to reach the most number of neighbors while minimizing the required relative energy cost and maintaining a reliability objective high enough to ascertain successful delivery of channel state information and a delay objective low enough to support fast route setup. The end-to-end reliability objective $\mathcal{P}_{req}$ used to perform data delivery is suitable to perform route setup. The problem to find the relative energy cost and transmission range to cover the most number of neighbors is different from the problem solved by Algorithm 4.1. Consequently, Algorithm 4.1 is modified to discover the most number of neighbors by changing line 10 to calculate energy E instead of the relative energy cost $\mathcal{E}$, eliminating line 12, replacing line 13 with $(\mathbb{N} > \mathbb{N}_{rs})$ to store the maximum number of neighbors required for route setup (where $\mathbb{N}_{rs}$ is initialized in line 3 to zero), replacing $(\mathcal{C}_{max} = \mathcal{C})$ with $(\mathbb{N}_{\mathrm{rs}} = \mathbb{N})$ in line 14, and adding $(E_{rs} = E)$ to line 14 to save the energy cost for broadcasting a control packet to the $\mathbb{N}_{rs}$ neighbors. Now, assuming the

control packet holding the necessary information for route setup is L_{rs} bits, the average number of neighbors is $\mathbb{N}_{rs}$, and the energy required to reach each of the neighbors is E_{rs}, the total energy required to obtain all the necessary information required to build the optimal routing paths at the BS is calculated as:

$$E_{OPT,rs} = N_b(N_s + 1)\mathbb{N}_{rs}E_{rs} + N_b E_{rs} \tag{4.15}$$

We explain the formulation of (4.15) as follows. The first component on the right hand side accounts for the energy consumed for all SNs and BNCs to broadcast route setup packets to their neighbors. The second component on the right hand side accounts for the energy required for each BNC to transmit its own and its SNs route setup information to the BS.

We now derive the total energy required to setup routing paths using the BRA algorithm of EQX. For each link (i, j) along a routing path, a RDIS message is transmitted from BNC *i* to all of its neighbors within the computed neighbor discovery range. Upon receiving RDIS, a RREP message is sent from each of the neighbors back to BNC *i*. A RCFM message is then transmitted from BNC *i* to its SNs and from BNC *i* to BNC *j*. Each control message (e.g., RDIS, RREP, RCFM, etc.) has size L_{rs} bits and is transmitted with power $P_{tx.ndr}$ (i.e., transmit power to achieve neighbor discovery range) and retransmission limit of X_{ndr} resulting in a total energy consumption of $E_{rs,bbn} = E_{rs,bbn,tx} + E_{rs,bbn,rx}$, where $E_{rs,bbn,tx} = \phi_{ndr}L_{rs}E_b(P_{tx.ndr})$ for transmitting and $E_{rs,bbn,rx} = \phi_{ndr}L_{rs}E_b(P_{rx})$ for receiving. We assume the SNs can use the minimum transmit power with a single transmission to deliver its route setup information to its BNC because the size of the route setup packet is small compared to a physiological data packet. Therefore, the total energy consumption for transmitting the route setup information from the N_s

SNs to the BNC i is $E_{rs,ban} = N_s L_{rs}\big(E_b(P_{min}) + E_b(P_{rx})\big)$. Given there are N_b routing paths in the BBN, the total energy consumed for route setup in EQX is calculated as:

$$E_{EQX,rs} = N_b E_{rs,ban} + \sum_{i=2}^{N}\sum_{j=1}^{N}\left(\sum_{\forall(i,j)\in\mathcal{W}_i}\left(E_{rs,bbn,tx} + \mathbb{N}_{ndr}E_{rs,bbn,rx}\right) + E_{rs,bbn}\mathbb{N}_{ndr} + E_{rs,bbn}\right) \tag{4.16}$$

where $\mathbb{N}_{ndr}$ is the number of desired neighbors of BNC i during neighbor discovery. The first term on the right hand side of (4.16) accounts for the energy consumed during the exchange of route setup information between the SNs and BNC. The second term of (4.16) consists of three energy consuming components. The first component is the energy consumed for the single broadcast and multiple reception of the RDIS message by the $\mathbb{N}_{ndr}$ neighbors. The next component is the energy consumed for transmitting and receiving the RREP message $\mathbb{N}_{ndr}$ times. The last component is the energy consumed for the transmission and reception of the RCFM message between BNC i and the selected relay node BNC j.

4.5.1.3 Route Setup Time

The route setup time is calculated as the total time required to build routing paths for all the SNs and BNCs. The calculation follows the same methodology as that of the energy consumption for route setup in (4.15) and (4.16). For OPT, the route setup time is $\mathcal{D}_{OPT,rs} = (N_b(N_s+1)\mathbb{N}_{rs}\phi_{ndr}L_{rs} + N_b\phi_{ndr}L_{rs})/\mathcal{R}$ and for EQX it is derived as:

$$\mathcal{D}_{EQX,rs} = \frac{N_b N_s L_{rs}}{\mathcal{R}} + \sum_{i=2}^{N}\sum_{j=1}^{N}\left(\sum_{\forall(i,j)\in\mathcal{W}_i}\frac{\phi_{ndr}L_{rs}(\mathbb{N}_{ndr}+2)}{\mathcal{R}}\right) \tag{4.17}$$

4.5.1.4 Average End-to-end Success Probability

The average end-to-end success probability for each BAN is calculated as the product of

the success probability achieved over path 1 and path 2 throughout the multi-hop BBN. In OPT, the average end to-end success probability is simply calculated as:

$$\mathcal{P}_{OPT} = \frac{1}{N_b}\sum_{i=2}^{N}\mathcal{P}_{ete,i} \tag{4.18}$$

where $\mathcal{P}_{ete,i}$ is derived from satisfying the reliability constraint in (4.1.1). In EQX, the end-to-end success probability from a source BAN to the BS over path 1 is derived as:

$$\mathcal{P}_{ete,p1,i} = 1 - \left(1 - \sum_{k=1}^{N_s}\frac{r_k}{r_i}\mathcal{P}_{s,i.k,x}\right)\left(\prod_{\forall(x,y)\in\mathcal{W}_i}\mathcal{P}_{s,xy}\right), \forall i \in [2,N] \tag{4.19}$$

where $link(x,y) \in \mathcal{W}_i, x \in [2,N], y \in [1,N], x \neq i, y \neq i, x \neq y$, represents each link in the BBN connecting the SNs of BNC *i* to the BS. The end-to-end success probability from a source BAN to the BS over path 2 is calculated as:

$$\mathcal{P}_{ete,p2,i} = 1 - \left(1 - \sum_{k=1}^{N_s}\frac{r_k}{r_i}\mathcal{P}_{s,i.k,x}\right)\left(\sum_{k=1}^{N_s}\frac{r_k}{r_i}\mathcal{P}_{s,i.k,i}\prod_{\forall(x,y)\in\mathcal{W}_i}\mathcal{P}_{s,xy}\right), \forall i \in [2,N] \tag{4.20}$$

The average end-to-end success probability in the network is the average of the end-to-end success probabilities from either (4.13) or (4.14) and is given as:

$$\mathcal{P}_{EQX} = \frac{1}{N_b N_s}\sum_{i=2}^{N}\sum_{k=1}^{N_s}(1-\mu_i)\mathcal{P}_{ete,p1,i} + \mu_i\mathcal{P}_{ete,p2,i} \tag{4.21}$$

where μ_i decides whether path 1 or path 2 is taken by the SNs belonging to BNC *i*.

4.5.1.5 Average End-to-end Packet Delay

The average end-to-end delay for OPT is derived as:

$$\mathcal{D}_{OPT} = \frac{1}{N_s N_b}\sum_{i=2}^{N}\sum_{k=1}^{N_s}\mathcal{D}_{i.k} \tag{4.22}$$

where $\mathcal{D}_{i.k}$ is derived from satisfying the delay constraint in (4.1.2). The maximum duration of the TDMA frame for EQX is calculated as $\mathcal{D}_{tdma}$ from Algorithm 4.4. Therefore, the average end-to-end packet delay required to deliver physiological data from a SN *i.k* to the BS is:

$$\mathcal{D}_{EQX} = \frac{1}{N_b N_s} \sum_{i=2}^{N} \sum_{k=1}^{N_s} \mathcal{D}_{wait}(\varphi_{i.k}, \vartheta_k) + \mathcal{D}_{tdma} \tag{4.23}$$

4.6 Performance Evaluation

In this section, we conduct numerical studies and perform simulations to achieve the following three objectives. The first objective is to compare the performance of the BRA and BPA algorithms against the optimal routing and power allocation solutions obtained from solving the optimization problem in (4.1). The impact of slot reuse is investigated by comparing the performance of the BSA algorithm against a slot scheduling algorithm that assumes interference can be neglected and a slot scheduling algorithm where no slot reuse is performed. The second objective is to compare the performance of the comprehensive EQX scheme against the optimal solution from (4.1), which is referred to as the OPT scheme. The third objective is to compare our analytical results for the EQX scheme with its simulated counterpart and also to compare the simulation performance of EQX against other schemes. Unless otherwise specified, the SNs and BNCs are configured according to the parameters in Table 3.1 and the assumed path loss and fading parameters for the on-body and body-to-body channels are given in Table 3.2.

4.6.1 Numerical Studies

4.6.1.1 Evaluation of Neighbor Discovery Range

To determine the neighbor discovery range suitable for the platoon column formation shown in Fig. 4.1 where 25 soldiers are distributed in a 100 m x 100 m area, we first calculate the average network density as $\psi = \frac{1}{400} \frac{soldiers}{m^2}$. The desired neighbor discovery range is

obtained by executing Algorithm 4.1 using ψ, $d_{step} = 2$ m, $E_{res,i} = E_{init}^{b}$, $\mathcal{P}_{req} = 99\%, \mathcal{D}_{req} = 10$ ms, and the body-to-body path loss and fading parameters as inputs. The input value d_{step} is set as 2 m to represent the minimum spacing between two soldiers, the reliability objective is set to support ensuing data transmissions, and the delay objective is set to enable fast route discovery. The neighbor to relative energy cost ratio shown in Fig. 4.3 maintains a concave relationship with respect to the increasing average number of neighbors. The concave relationship exists for the following reason. An increase in neighbor discovery range is required to support an increase in average number of neighbors. Increased neighbor discovery range is achieved by increasing the transmit power and retransmission limit which subsequently results in higher relative energy cost. Furthermore, as the neighbor discovery range increases, the relative energy cost increases in a non-linear manner due to the structure of the success probability function in (3.9). As evidenced in Fig. 4.3, the higher rate of relative energy cost increase when the average number of neighbors is increased from 4 to 8 as compared to the increase from 1 to 4, results in a steady decline in the neighbors to relative energy cost ratio. Therefore, the maximum neighbors to relative energy cost ratio is obtained when the average number of neighbors is 4. The results provided in Fig. 4.3 are particularly beneficial for route discovery because selecting relay nodes within the neighbor discovery range with the maximum neighbors to relative energy cost ratio can lead to more efficient data transmission than when a neighboring node outside of the neighbor discovery range is selected.

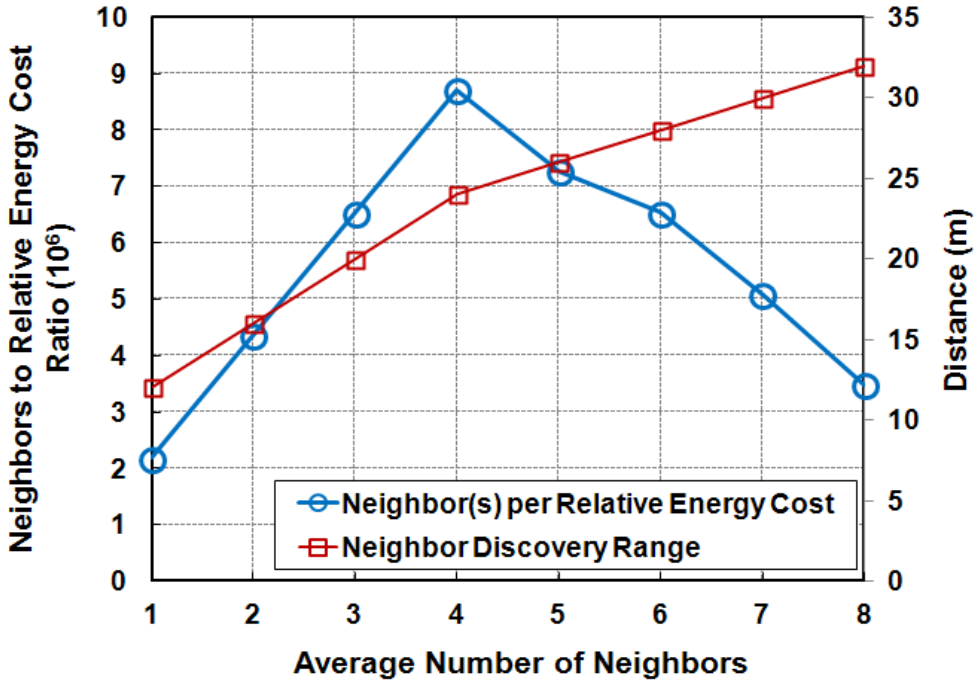

Fig. 4.3. Neighbors to relative energy cost ratio as a function of average number of desired neighbors.

4.6.1.2 Evaluation of Route Discovery Process

The route discovery process of the BRA algorithm is performed in a distributed manner amongst the BNCs after which the BS is responsible for allocating the transmission parameters required to minimize relative energy cost while meeting the end-to-end reliability objective. In order to assess the quality of the created routing paths, we calculate the minimum relative energy cost achievable from the distributed routes by assigning the optimal transmission power, retransmission limit, and packet size to each link along the routing path then comparing it against the relative energy cost achieved with the optimal routing solution obtained from solving (4.1). The performance of the route discovery scheme is evaluated using 50 different random topology networks where 25 BANs are uniformly distributed in a 100 m x 100 m area and a BS is located at (0, 0) m. A single BAN is randomly selected as the source and the BS serves as the sink. We

use different random topologies as opposed to the single network topology in Fig. 4.1 to fully demonstrate the effectiveness of BRA under a myriad of different network topologies. The residual energy level for each SN and BNC is randomly assigned in the range $[1, E_{res}^{s}]$ J and $[1, E_{res}^{b}]$ J, respectively, whereas the BS is set as E_{res}^{c}. Utilizing different values of relative energy cost further demonstrates the ability of the routing algorithm to select a minimum relative energy cost route. The QoS requirements are set as $\mathcal{P}_{req} = 99\%$ and $\mathcal{D}_{req} = 1$ second.

Fig. 4.4 shows the minimum relative energy cost of the routing paths achieved with BRA for $\mathbb{N}_{nbr} = \{4,8\}$ and the optimal solution, or 'OPT' for short, as a function of the average distance to the BS. When the average number of neighbors is $\mathbb{N}_{nbr} = 4$ the relative energy cost for BRA is consistently less than 10% higher than OPT. It is also seen that the difference in relative energy cost between BRA and OPT increases from 5% to 9.6% as the average distance increases from 26 m to 95 m. This increase provides some indication that the success probability approximation made in (4.2) loses accuracy as the average route distance and route length (in hops) increases. Nevertheless, given the substantial complexity saved by employing a distributed route discovery scheme as opposed to a centralized route discovery scheme, the difference in relative energy cost is deemed as acceptable. Another set of observations made from Fig. 4.4 derive from the impact of the average number of neighbors on relative energy cost as the average distance to the BS increases. We see that when the average distance is equal to or less than 72 m, the relative energy cost of the routing paths produced with $\mathbb{N}_{nbr} = 4$ is between 9% and 15% higher than when $\mathbb{N}_{nbr} = 8$ for the following reason. Although the average number of hops to the BS with $\mathbb{N}_{nbr} = 4$ is higher than $\mathbb{N}_{nbr} = 8$, the average distance per hop is shorter such that high relative energy cost transmissions are avoided. On the other hand, when the average distance to the BS is greater than 82 m, the average number of hops to the BS increases such that

the average hop distance for $\mathbb{N}_{nbr} = 8$ is reduced below the threshold where a high increase in relative energy cost is incurred. As well, the average number of hops for $\mathbb{N}_{nbr} = 4$ increases to the point where approximation (4.2) again loses accuracy thus producing routing paths that incurs 6% higher relative energy cost than when $\mathbb{N}_{nbr} = 8$.

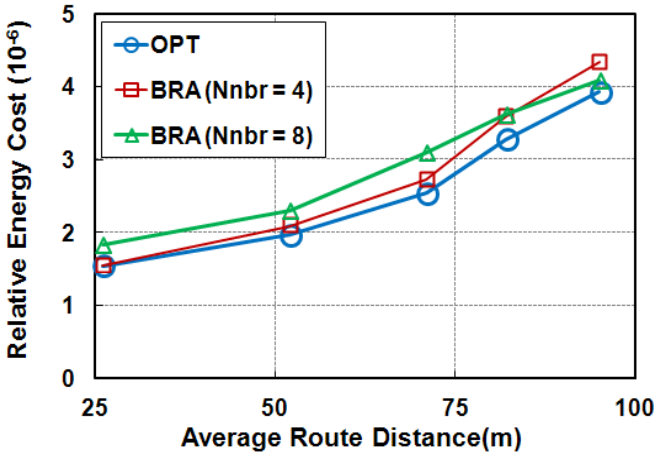

Fig. 4.4. Relative energy cost for route discovery as a function of average route distance.

4.6.1.3 Evaluation of BBN Multi-constrained Allocation Algorithm

The purpose of this numerical study is to evaluate the accuracy with which the BPA algorithm assigns the transmit power level, retransmission limit, and payload size required to minimize the total relative energy cost along the $|\mathcal{W}|$ links in a routing tree while satisfying a desired end-to-end reliability objective. Accuracy is determined in terms of how close the relative energy cost obtained with the BPA algorithm is to the optimal solution. The BRA algorithm is used to create the necessary number of routing paths that combine to form the routing tree. The BPA algorithm is then applied to the routing tree to configure it to satisfy the reliability objective. The performance of the BPA algorithm is compared against the OPA (Optimal Multi-constrained Power Allocation) algorithm that optimally allocates transmission parameters to the routing links in order to minimize relative energy cost for a desired reliability

constraint. The process for obtaining the optimal solution using OPA is described in the following steps. First, the link decision variables μ_{ij}, $\mu_{i.k,j}$, and μ_i $(\forall(i,j),(i.k,j) \in \mathcal{W}, i \in [2,N], j \in [1,N], k \in [1,N_s])$ are configured to determine whether a transmitting node is connected to a receiver node in the routing tree are obtained from the BRA algorithm. Second, the variables are used as inputs to (4.1). Third, the minimum relative energy cost for the routing tree is obtained by computing the transmit power level, retransmission limit, and packet size for the chosen links. The performance of BPA and OPA is evaluated under a number of different network configurations where the number of routing paths in a routing tree is varied between 5 and 25, the route length for each of the routing paths in a routing tree is uniformly distributed in the range $[1, H_{max}]$, where H_{max} is the specified maximum number of hops, and the distance of each hop for each routing path is uniformly distributed in the range $[10,30]$ m. We investigate the relative energy cost performance for end-to-end reliability objective of 99%.

In Fig. 4.5a, the ratio of routes that violate the reliability objective is shown for the routes populated by the BRA algorithm, before the BPA algorithm is employed. From the results, it is clear that the constrained power allocation performed by the BNCs in order to build end-to-end routing paths to the BS using intermediate BNCs as relay nodes is insufficient due to the fact that over 60% of the routes do not satisfy the end-to-end reliability objective. The QoS violation is an artifact of the multi-hop reliability approximation in (4.2). The number of routes that violate the reliability constraint steadily increases as the number of routes increase because the average route length also increases, thus decreasing the accuracy of (4.2). The total relative energy cost resulting from allocating transmit power, retransmission limit, and packet size to each link in the routing paths discovered by the BRA algorithm is shown in Fig. 4.5b for the BPA algorithm and the OPA algorithm. The relative energy cost achieved by BPA is only 15% higher than OPA. As

the number of routes in the routing tree increases and the constrained power allocation problem becomes more complicated, the relative energy cost difference between BPA and OPA remains approximately constant. These two observations are explained as follows. The low relative energy cost difference between OPA and BPA is attributed to the adaptive link selection metric that selects the link in the routing tree providing the highest increase in reliability for the lowest relative energy cost. Therefore, the BPA algorithm obtains fast solution convergence while minimizing the relative energy cost that exceeds the optimal minimum energy. The consistent relative energy cost achieved by BPA as the maximum route length increases is attributable to the weighting factor in (4.4) designed to preferentially allocate transmission parameters to the links along the routing paths with the highest number of hops and links with reliability less than one.

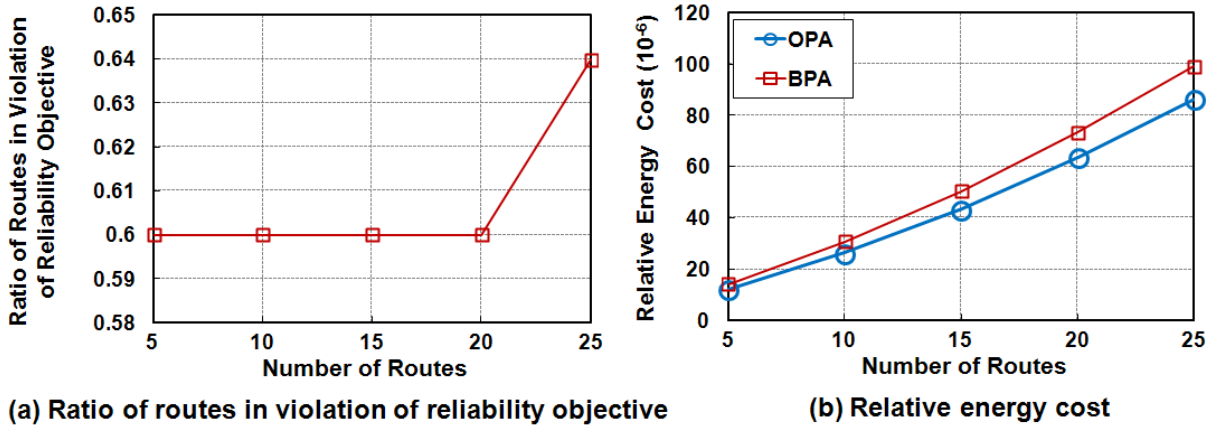

Fig. 4.5. Multi-constrained power allocation performance of BPA and OPA algorithms as a function of number of routes.

4.6.1.4 Effect of Interference Distance and Transmit Power on Link Success Probability

In this numerical study we evaluate (4.12) and (4.13) to determine the minimum interference distance required to maintain the packet success probability without violating a reliability objective and the minimum interference distance required to satisfy the interference neglecting assumption (INA), respectively, when the same slot is utilized for transmission. For

the results shown in Fig. 4.6, the interfering transmitter power is incremented in the range $[P_{min}, P_{max}]$ whereas the transmitting power is configured to the minimum value required to transmit a data rate of 23 kbps (i.e., $\sum_{k=1}^{N_s} r_k$ from Table 3.1) from BNC i to BNC j over a link distance varied in the set $\{20,40,60\}$ m while minimizing relative energy cost and satisfying a reliability objective of 99%. We conduct the numerical study assuming the transmissions performed over the body-to-body channel have path loss parameters $PL(d_0) = 54.6$ dB, $\alpha = 2.2$, and fading parameter $m_{ij} = 2$. The results in Fig. 4.6a show that the minimum interfering distance with INA is consistently lower than slot reuse with reliability awareness (SRA). The explanation of these results derives from further analyzing the results in Fig. 4.6b and Fig. 4.6c. In Fig. 4.6b, we can see that the success probability achieved with INA is always less than the reliability objective. This is because the assumption that interference can be neglected when the interference power is less than 10% is an inaccurate assumption, as further demonstrated in Fig. 4.6c. Fig. 4.6c shows that the reliability objective is satisfied when the ratio between interference power and noise floor is between 0.5% and 2% for link transmission distances between 20 m and 60 m. The main insight garnered from the results presented in Fig. 4.6 is that INA adversely affects the success probability along links sharing a slot such that stringent reliability requirements are often violated, thus rendering the INA assumption invalid for multi-hop BBNs where reliability constraints are enforced. On the other hand, the proposed SRA offers an accurate and reliable method to perform slot re-use in applications which have reliability constraints.

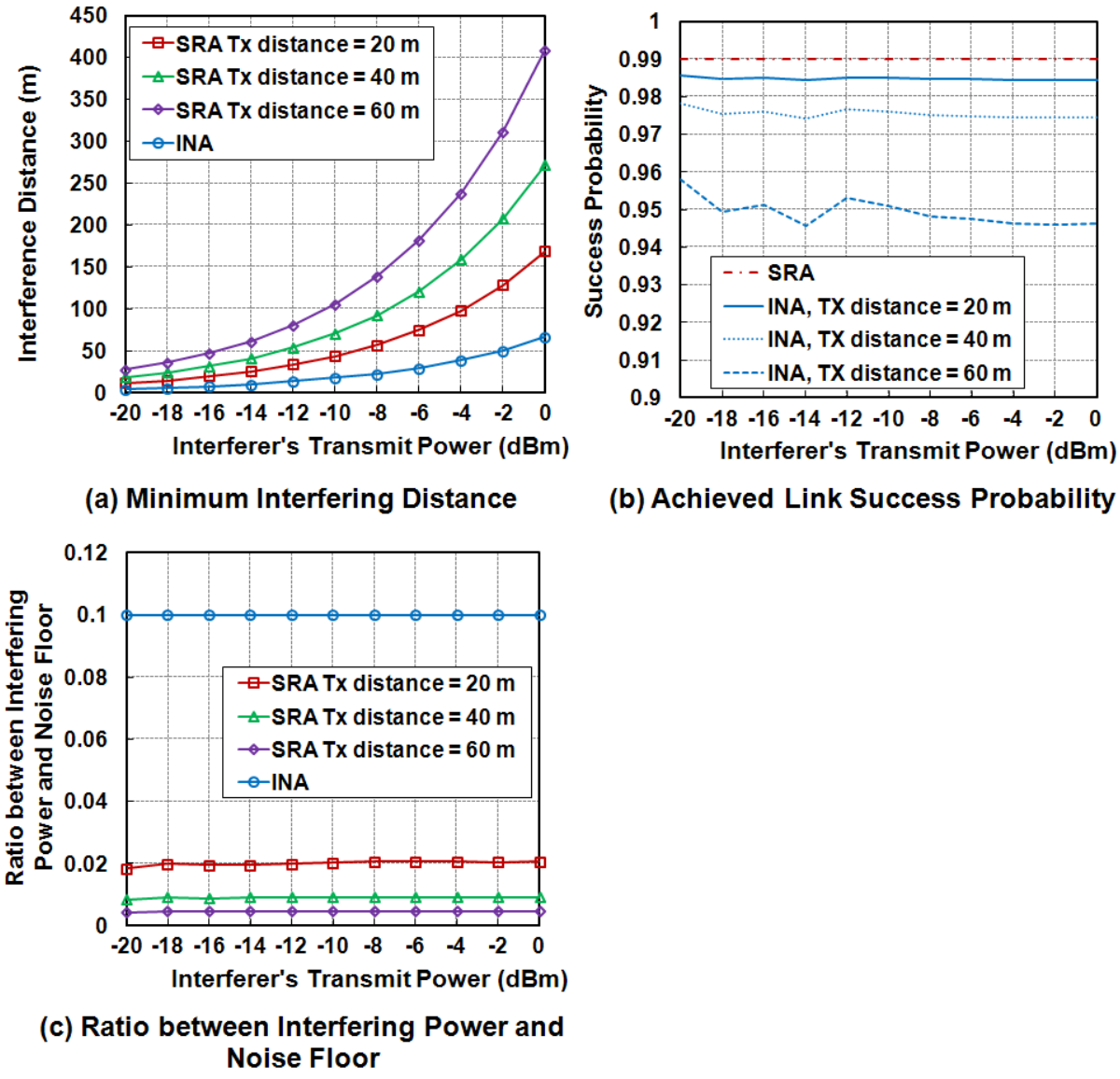

Fig. 4.6. The effect of the interference neglecting assumption (INA) and slot re-use with reliability awareness (SRA) on minimum interfering distance and success probability.

4.6.1.5 Evaluation of BSA Algorithm

The effectiveness of the BSA algorithm is demonstrated by determining the total number of slots required to transmit data from multiple source BANs to a BS, with and without slot re-use. The results in Fig. 4.7 are populated for a network topology where {16, 25, 36} source BANs and a single BS are randomly distributed in a 100 m by 100 m BBN area. The time slot

duration is set as $t_{slot} = 5$ ms. The following three steps are taken to obtain the results. First, the optimal routing path and transmission parameters for all the links along the routing paths are calculated for each source BAN by solving (4.1). Second, the number of slots required to deliver the data to the BS is calculated, without slot reuse. Third, the BSA algorithm is executed using Algorithm 4.4 to determine the minimum number of slots required for all links in the routing tree by exploiting slot reuse. Fig. 4.7 shows that as the number of source BANs increases from 16 to 36, the number of slots saved by using BSA as compared to no slot reuse increases from 0% to 12.4%, respectively. The main reason for the reduction in slots is the increased density of the network and increased opportunity for slot reuse. Furthermore, because there are more relay node possibilities in a network of 36 BANs than 16 BANs, the calculated routing paths populated from 36 BANs also consists of more hops with shorter link distances. The shorter link distances require lower transmit power and thus there is less inter-BAN interference, giving way to increased slot re-use.

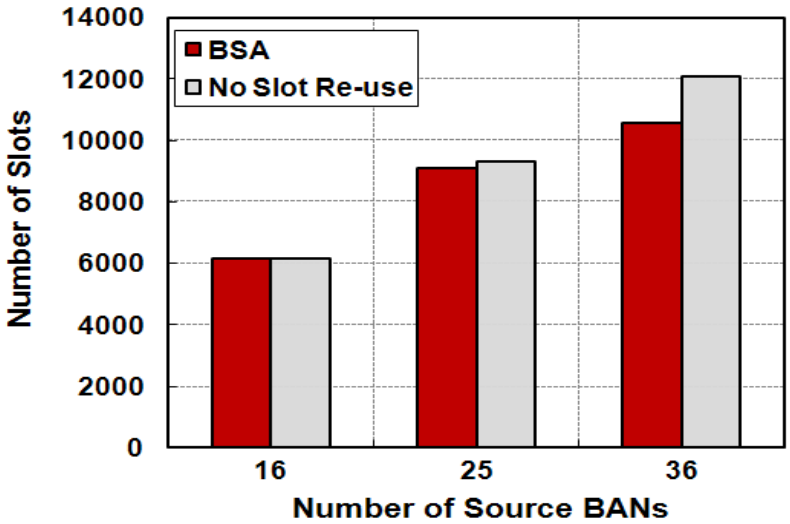

Fig. 4.7. Number of slots obtained as a function of the number of BANs in a network when slot reuse is applied using the BSA algorithm and when no slot reuse is applied.

4.6.1.6 Comparison of EQX Scheme against Optimal Solution Scheme

The numerical experiments described in Section 4.6.1.1 to Section 4.6.1.5 were designed to independently measure the performance of the sub-optimal routing, constrained power allocation, and scheduling algorithms of the EQX scheme against their optimal counterparts. In this experiment, we use the performance metric expressions derived in (4.14) to (4.23) to compare the performance of the full EQX scheme against the OPT scheme. The OPT scheme represents the final solution derived from solving (4.1). The network topology is configured according to Fig. 4.8 where 25 BANs and one BS are organized into a military platoon column formation [149] in a 100 m x 100 m network coverage area.

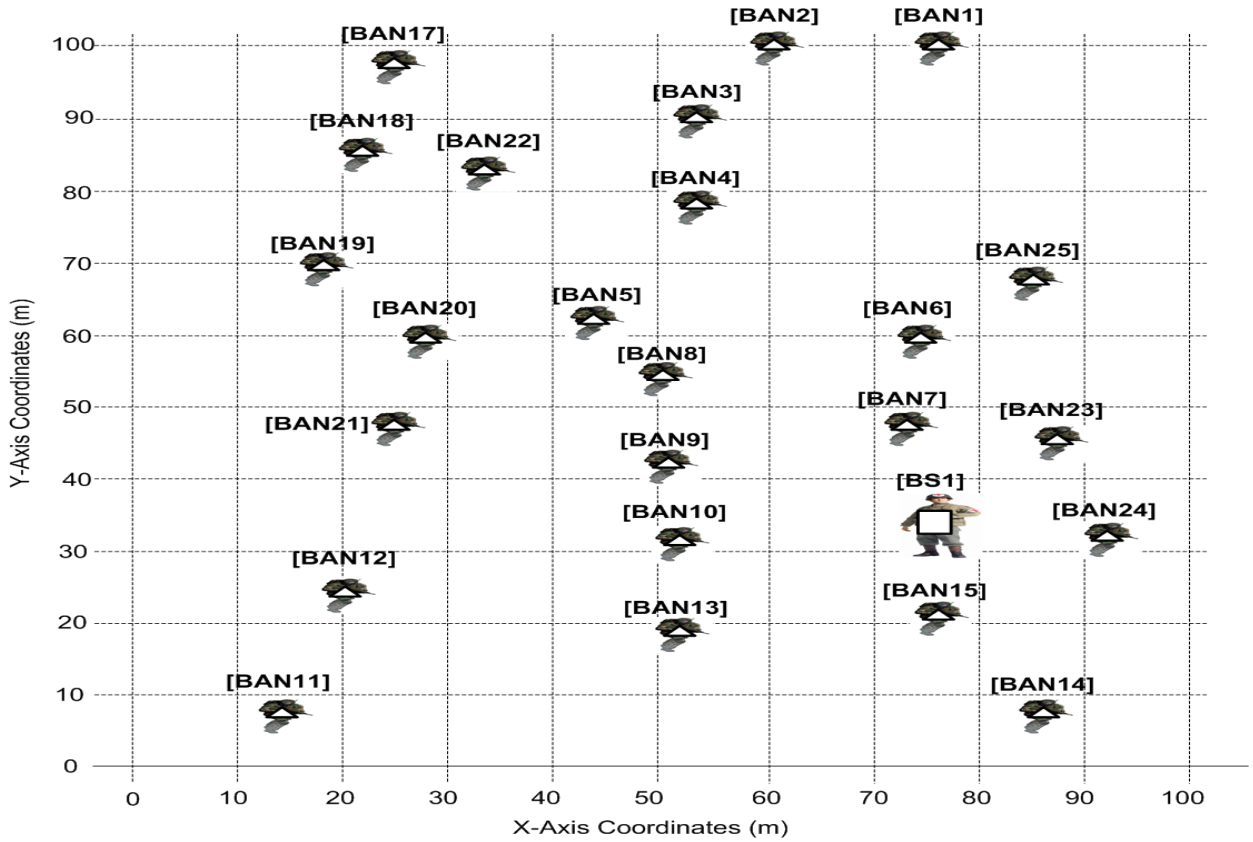

Fig. 4.8. Network topology depicting the location and alignment of soldiers and combat medic in a platoon column formation.

The route discovery process in EQX periodically forms routing paths between the 25 source BANs and the BS. The size of the route setup packet is $L_{rs} = 184$ bits, the route update frequency is $T_{rs} = 30$ seconds, the data update frequency is $T_{du} = 10$ seconds, and the desired neighbor size is $\mathbb{N}_{ndr} = 4$ based on the results obtained in Fig. 4.4, providing a neighbor discovery range of $d_{ndr} = 32$ m. The data update frequency is configured to the same value as the delay requirement in order to prevent the occurrence of network congestion and overflow. The route update is configured to be higher than the data update frequency to limit the energy expended for control traffic exchange. In this experiment, each SN, BNC, and BS is initially configured with its maximum battery capacity. At each increment of T_{du}, the SNs transmit their physiological data to the BS. Following the completion of the physiological data update process, the residual energy for each SN, BNC, and BS is updated according to the amount of energy that was consumed during the update. For example, let v represent the v^{th} round of physiological data updates and $v + 1$ the next round for physiological data updates. The energy remaining for a SN $i.k$'s next round of physiological data updates is updated as $E_{res,i.k}(v + 1) = E_{res,i.k}(v) - E_{i.k}(v)$, where $E_{i.k}(v)$ is the total energy consumed by SN $i.k$ at round v. The update process performed by the SNs is continued at each increment of T_{du} until the residual energy of either one of the SNs, BNCs, or BS is equal to or less than zero.

The results of the experiment are shown in Fig. 4.9. The total relative energy cost incurred in EQX is at most 15% higher than OPT when the number of updates performed is less than 1400. However, when the number of supported updates increases from 1400 to 1560, the relative energy cost difference increases from 15% to 25%. The sharp increase in relative energy cost is attributed to the fact that the residual energy for the BNCs serving as relay nodes along

frequently used minimum relative energy cost routes becomes very low. As a result, the source SNs and BNCs take higher relative energy cost routes that span several hops, thus increasing the total energy consumed in the network and subsequently increasing the total relative energy cost.

In Fig. 4.9b, it is expected for OPT to consistently achieve an average end-to-end delay lower than EQX because it maintains the minimum relative energy cost routes. However, the average end-to-end delay achieved in EQX is approximately 6% lower than OPT when the number of updates is less than 1000 because EQX exploits slot reuse opportunities and thus a reduced number of unique slots are employed for transmissions. The reduction in residual energy available in relay nodes forces the SNs and their BNCs to use longer routing paths, which explains the increase in delay experienced in EQX as the number of supported updates increase higher than 1000. Furthermore, to maintain the stringent end-to-end reliability objective over an increased number of hops, higher transmission power is used along each hop consequently limiting the opportunities for slot reuse because of increased interference power. Finally, it is seen that the EQX delay violates the delay constraint and exceeds the data update period specified by T_{du} when the number of updates exceeds 1300. The thesis does not consider the effect of buffer overrun or network congestion since we assume a TDMA MAC layer scheme. However, buffer overrun and network congestion resulting from the violation delay requirements could lead to packet loss and the inability for a combat medic to make timely decisions regarding a drastic change in a soldier's physiological status.

The average end-to-end success probability in Fig. 4.9c is seen to be consistently higher in EQX than OPT because the average end-to-end success probability produced by the BPA algorithm in EQX does not converge to the exact end-to-end reliability objective. Achieving an end-to-end success probability higher than the reliability requirement typically results in

additional incurred relative energy cost because success probability is directly proportional to relative energy cost. However, the increase in relative energy cost experienced in EQX is unavoidable due to the complexity required to concurrently iterate multiple variables (transmit power, retransmission limit, and payload size) for a large number of links until the end-to-end reliability constraint is satisfied. The energy and time required to set up routing paths is shown in Fig. 4.9d and Fig. 4.9e, respectively. The route setup energy and route setup time are predominantly lower in EQX than OPT because the designated neighbor discovery range in EQX reduces the number of route setup packets that are broadcast and exchanged with neighbors.

From the results provided in Fig. 4.9, we can conclude that the EQX scheme dependably supports the reliability and delay objectives for 1200 rounds of physiological data updates while only incurring 15% higher relative energy cost than the OPT scheme and requiring 54% less time to setup routing paths. Although the OPT scheme is shown to reliably support 2000 updates, the exorbitant solution complexity required to do so is not conducive to the physiological status monitoring of soldiers on the battlefield.

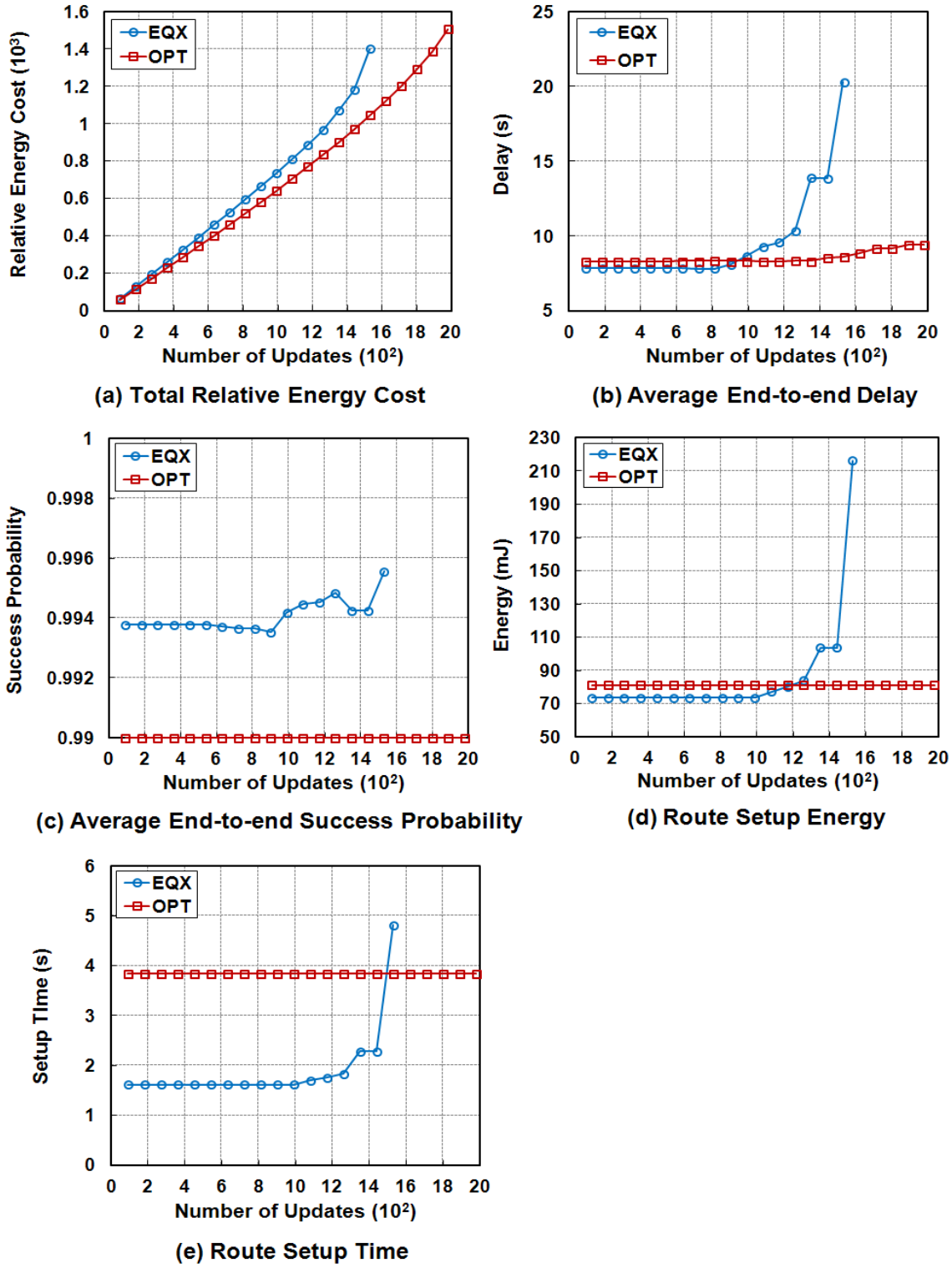

Fig. 4.9. Performance comparison between EQX scheme and OPT scheme for increasing number of physiological data update rounds.

4.6.2 Simulation Experiments

In this section, we evaluate the performance of EQX through simulations.

4.6.2.1 Simulation Settings

A simulator designed to model the operation and evaluate the performance of the EQX scheme in a multi-hop BBN drives the simulation experiments performed in this section. The simulator implements the proposed BRA, BPA, and BSA algorithms into EQX. Unless otherwise specified, each simulation experiment follows the network topology given in Fig. 4.8 where 25 soldiers, each equipped with a BAN and serving as a source for physiological data, and a single combat medic, equipped with a BS device and serving as the network sink, are organized in a 100 m x 100 m platoon column formation for the purpose of defending a civilian area from enemy attack. The end-to-end reliability and end-to-end delay objectives for the transmission of physiological data from the SNs to the BS are set at $\mathcal{P}_{req} = 99\%$ and $\mathcal{D}_{req} = 10$ seconds, respectively. The delay objective is set at $\mathcal{D}_{req} = 10$ seconds as opposed to the $\mathcal{D}_{req} = 1$ second in Section 3.5.1 because of the presence of multiple BANs. Nevertheless, the delay objective falls within the delay bound used in [126] for delivering medical information in an e-Health setting. The complete set of simulation settings is summarized in Table 4.2.

TABLE 4.2 SELECTED SIMULATION PARAMETERS

Description	**Parameters and Values**
Network coverage area	100 m x 100 m
Number of soldiers in platoon	$N_b = 25$
Route update period	$T_{ru} = 30$ seconds
Physiological data update frequency	$T_{du} = 10$ seconds
Route setup packet size	$L_{rs} = 184$ bits
Neighbor discovery range	$d_{ndr} = 32$ m
Shadowing	$\sigma_{i.k.i} = 6$ dB (On-body), $\sigma_i = 9$ dB (body-to-body)
QoS Objectives	$\mathcal{P}_{req} = 99\%$ and $\mathcal{D}_{req} = 10$ seconds

4.6.2.2 Simulation Results

4.6.2.2.1 Comparison of Analytical and Simulation Results

In this simulation experiment, we measure the following three performance metrics for each round of physiological data updates: *total relative energy cost*, *average end-to-end packet delivery ratio (PDR)*, and *average end-to-end delay*, where the average PDR metric is defined as the ratio of number of packets delivered to the number of packets sent. The simulation experiment is complete when one of the SNs does not have any residual energy or physiological data cannot be delivered from a SN to the BS because either a BNC or the BS does not have any remaining energy.

The total relative energy cost obtained with analytical and simulation techniques are shown in Fig. 4.10a as a function of increasing physiological data updates. The analytical results consistently fall within the confidence interval of the simulation results and well approximate the number of physiological data updates that can be supported when QoS objectives are considered. It is observed that the simulation relative energy cost results increase linearly as the number of updates reach 1300. However, an exponential like increase in relative energy cost is observed

when the updates increase from 1300 to 1500, which can be explained as follows. The residual energy for the relay BNCs providing the minimum relative energy cost routes become significantly depleted over time because they are frequently used by other BNCs and SNs in the network. As a result, instead of using their energy depleted BNC to forward data outside the BAN, source SNs transmit directly to the next hop BNC or BS with higher residual energy. However, the SN transmissions over the body-to-body channel endure Rayleigh fading conditions and thus require high relative energy cost to overcome fading induced errors and to satisfy the reliability objective. In Fig. 4.10b, the analytical results for average end-to-end delay is shown to match well with the simulation results. The simulation delay is shown to increase two fold when the number of updates is increased from 1200 to 1400 due to the high hop length of the routing paths and the number of retransmissions performed by the SNs to transmit directly to their neighboring BNCs or BS. In Fig. 4.10c, the average end-to-end PDR produced by the analytical results reside within the confidence interval of the simulation results when the number of updates is less than 1200 but fall outside the confidence interval when the number of updates is greater than 1200. The average end-to-end PDR for the simulation is shown to fall below the reliability objective when the number of updates is greater than 1200, providing an indication that configuring the retransmission limit in real-time does not guarantee the reliability objective can be consistently satisfied when the routing paths maintain a high hop length. This shortfall is an artifact of the fixed TDMA schedule that is composed based on the computed retransmission limit.

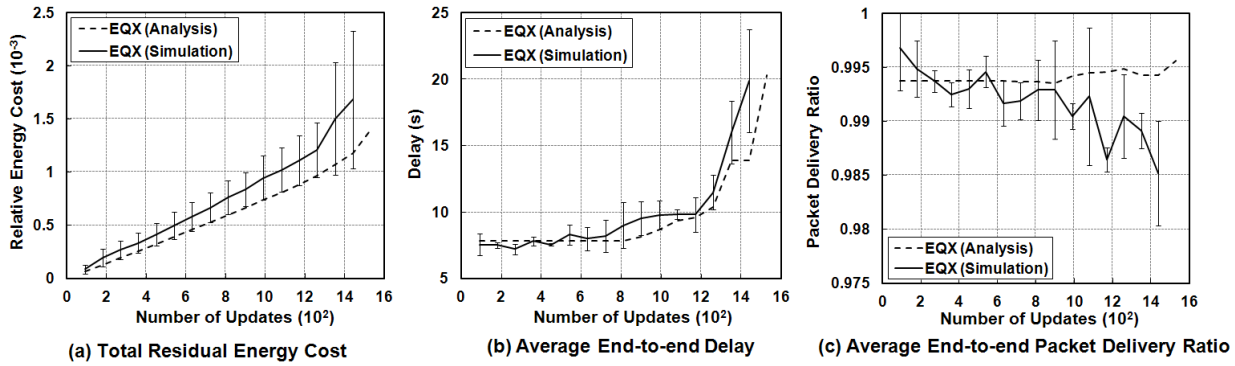

Fig. 4.10. Comparison of analysis and simulation performance of EQX.

4.6.2.2.2 EQX Performance Comparison against Other Schemes

We implement two other schemes to compare against EQX. The first scheme operates the same as EQX except the data transmitted from the SNs to the BNC is not overheard by neighboring BNCs or a BS (modified path 2 functionality), there is no communication between SNs and neighboring BNCs or BS (no path 1 transmission), and there is no slot reuse. This variant scheme of EQX is referred to EQV1. The second scheme is the same as EQV1 except it assumes a constant payload size of $L_p = 128$ bits large enough to hold at least 4 samples from any of the SNs. This scheme is referred to as EQX with JPR (joint transmit power and retransmission limit optimization) and without path 1 and slot reuse or *EQV2* for short.

The simulation performed in this experiment lasts until the energy of any one of the SNs in the network is depleted or until an energy feasible routing path between a SN and the BS ceases to exist due to insufficient energy resources for any potential relay BNC. We measure the following four performance metrics for the simulation: *total number of supported rounds*, *number of supported rounds where the reliability objective has been satisfied*, *number of supported rounds where the delay objective has been satisfied*, and *number of supported rounds where both QoS objectives have been satisfied*. The performance metrics are shown for the three

schemes in Fig. 4.11. The EQV1 scheme is shown to achieve the highest number of rounds, independent of the QoS objectives. However, when the PDR is higher than the reliability objective, the number of rounds supported in EQX is 1.8 times higher than EQV1 because EQX exploits the ability to overhear transmissions between the SN and neighboring BNC. As a result, the probability for successful data delivery is higher, as further evidenced by EQX's average PDR of 99% whereas the average PDR in EQV1 is only 97%. The advantage of jointly optimizing the transmit power, retransmission limit, and packet size is evident because the number of rounds supported by EQX and EQV1 is 4.1 and 2.3 times higher than EQV2, respectively. In EQX and EQV1, the packet size is adaptively modified depending on the channel condition. When the channel condition is poor (severe path loss and fading) the packet size is reduced to avoid packet errors and when the channel condition is good (low path loss and fading) the packet size is increased to reduce the number of required transmissions. On the other hand, EQV2 maintains a constant packet size that requires a higher transmit power and increased number of retransmissions to overcome high path loss and severe fading conditions. In a TDMA network where the retransmission limit is set, the number of retransmissions required to successfully deliver the data packet in EQV2 may be insufficient, thus leading to packet loss. EQV2 is shown to achieve an average end-to-end delay of 15.95 seconds, resulting in zero supported rounds. Similarly, the average end-to-end delay in EQV1 is on average 2.57 seconds higher than the delay objective, resulting in only 67 supported rounds out of a possible 1800 rounds. The presence of shadowing reduces the impact of interference on other transmitting links. Thus, an increased number of slot reuse opportunities are exploited in EQX resulting in an average end-to-end delay less than the delay objective. The metric most vital to physiological status monitoring is the number of update rounds supported when both QoS objectives are

supported. It can then be seen that EQX significantly outperforms EQV1 and EQV2 because it supports 8 times more updates than EQV1 whereas EQV2 does not support any updates.

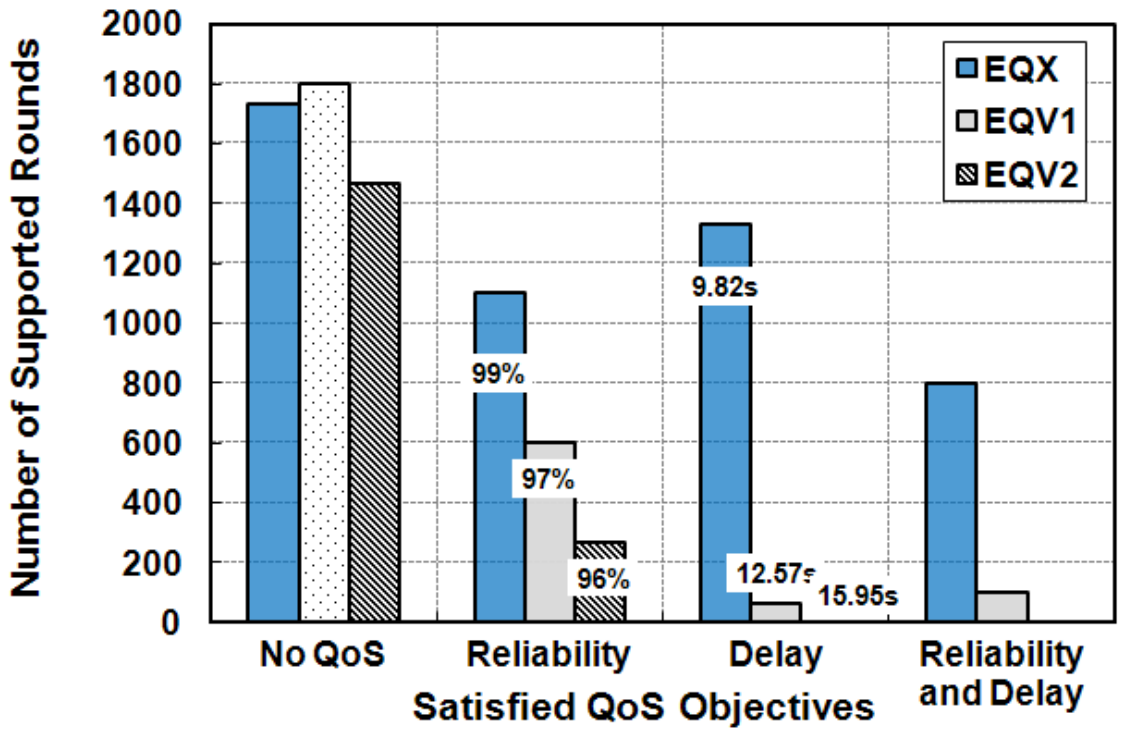

Fig. 4.11. Number of supported update rounds in terms of satisfied QoS objectives.

4.7 Summary

The problem of obtaining reliability and delay constrained minimum relative energy cost routes for the transmission of physiological data from SNs to BS in a multi-hop BBN is solved using optimal and sub-optimal solutions. Due to the exponential complexity required to obtain the optimal solution, a number of heuristic energy and QoS-aware algorithms exchanging information between the network, MAC, and physical layers are proposed to reduce complexity while obtaining close to optimal performance. The complexity of each proposed algorithm is in the polynomial class, rendering them suitable for implementation and execution in BNC and BS devices deployed in a multi-hop BBN. Numerical results show that the heuristic BRA algorithm

derives routing paths which provide an 11% higher relative energy cost than the routing paths obtained using an optimal routing algorithm, when the average routing path distance spans as long as 100 m. Furthermore, the proposed heuristic BPA algorithm is able to iteratively allocate transmit power, retransmission limit, and payload size to all links along a set of routing paths such that the resulting relative energy cost is approximately 15% higher than an optimal BBN multi-constrained power allocation algorithm employing the JPRS strategy. We have also demonstrated the importance of considering the effect of interference on success probability performance when slot reuse is employed - the assumption asserted in [106] stating interference can be neglected when the total interference power received at a receiver node is 10% of the noise floor leads to a decrease in success probability that can violate a stringent end-to-end reliability objective of 99%. The performance of the EQX scheme was compared against the optimal scheme for a network configuration representative of a platoon of soldiers deployed on a battlefield and shown to achieve no more than 15% higher relative energy cost while requiring less than half the time and consuming approximately 10% less energy to set up routes. The performance of EQX was also evaluated through simulation techniques and the results show the superior performance of the EQX scheme to EQV1 and EQV2 in terms of the number of physiological data update rounds that can be supported while concurrently supporting reliability and delay objectives. It is concluded, through analytical and simulation techniques, that the EQX scheme is suitable for supporting continuous physiological status monitoring of soldiers during tactical missions.

CHAPTER 5 ENERGY AND QOS AWARE DISTRIBUTED COMMUNICATION SCHEME FOR MULTI-HOP BODY-TO-BODY NETWORK

5.1 Introduction

The EQX communication scheme proposed in Chapter 4 is centralized in nature and requires network-wide information to minimize the relative energy cost required to transmit physiological data from SNs to a BS over the multi-hop BBN while achieving minimum delay and satisfying a stringent reliability objective. In this chapter, we focus on the design of an energy and QoS aware distributed (EQD) communication scheme to achieve minimum relative energy cost routes between the SNs and BS in a fully distributed manner. In order to overcome the large memory requirements, high maintenance costs, and long route setup times inherent of energy aware distributed routing protocols [116], [117], [119]-[121], we propose three innovative features that collectively reduce the memory footprint, minimize relative energy cost, and decrease delay.

The first innovative feature is the integration of an analog network coded cooperative communication (ANC-CC) relay scheme into the SNs and BNC in each BAN, which, to the best of the author's knowledge, has not been performed in the literature. Deep insight into ANC-CC reveals that the presence of *noise* caused by analog network coding is detrimental to the performance of ANC-CC. A solution is thus necessary to avoid performance degradation. The second innovative feature is the multi-receive policy (MRP) that exploits circumstances where data transmitted in the first hop of a two-hop relay scenario can also be received at the receiver of the second hop without the complexity of a diversity combiner technique. The third innovative feature facilitates the distributed routing operation of the EQD communication scheme. To obtain reliability and delay constrained minimum relative energy cost routing paths in a

distributed manner, the distributed Bellman-Ford algorithm is typically employed where each node has to use its memory to maintain all the paths satisfying the end-to-end reliability and delay objectives (as opposed to only maintaining the shortest path routes). Theoretically, this leads to a routing table size that increases exponentially as the number of hops to the sink increases and quickly consumes available memory. Given the practical assumption of finite memory and storage capacity in a BNC, a route storing strategy based on storing routes for a range of success probability values greater than or equal to the end-to-end reliability objective is proposed to significantly reduce the routing table size while also maintaining the minimum relative energy cost route.

The remainder of this chapter is organized as follows. Section 5.2 describes the integration of the ANC-CC relay scheme and multi-receive policy into the multi-hop BBN model. The EQD communication scheme is described in detail in Section 5.3 in terms of its operation and its three innovative features. The performance metrics used to evaluate EQD are provided in Section 5.4. In Section 5.5, the performance of EQD is evaluated using numerical results. A summary of the chapter is provided in Section 5.6.

5.2 System Model

5.2.1 Multi-hop BBN Network Model

The multi-hop BBN model considered in this chapter and shown in Fig. 5.1 is an extension to the multi-hop BBN model described in Section 4.2.1.

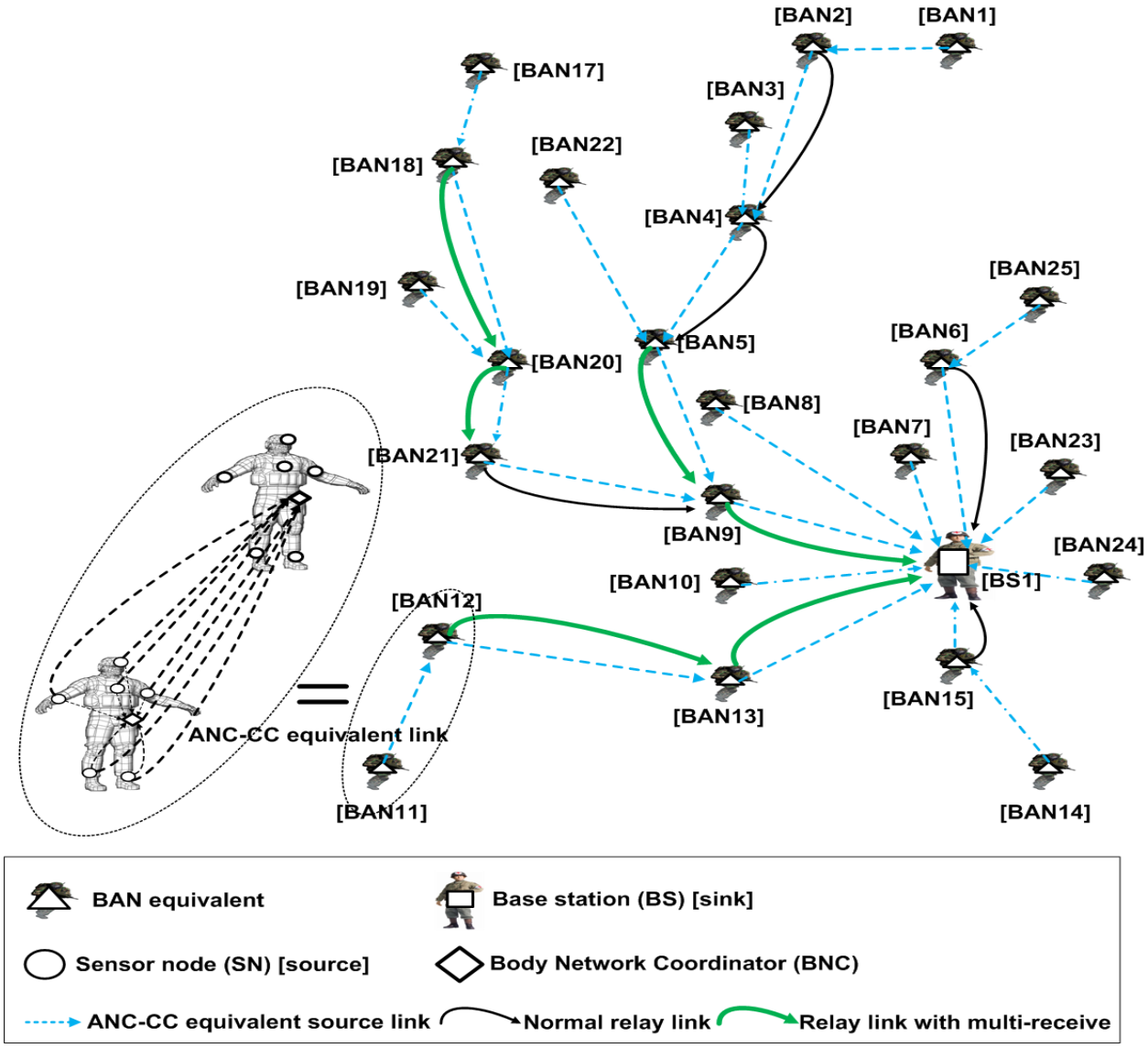

Fig. 5.1. Multi-hop BBN network model for EQD communication scheme.

Different from Section 4.2.1, the synergistic BAN model used to model the first hop transmission between SNs and the neighboring BNC or BS is replaced by the ANC-CC relay

scheme. Consider the ANC-CC equivalent link between BAN11 and BAN12 in Fig. 5.1 fully represented in Fig. 5.2a. The SNs in BAN11 are denoted by $i.k$ ($k \in [1, N_s]$), BNC i (i is assigned as ID #11) is the relay node where analog network coding is performed, and BNC j (j is assigned as ID #12) is the receiver where decoding takes place. A maximal ratio combiner is assumed at BNC j to handle multiple incoming signals from the SNs and BNC i.

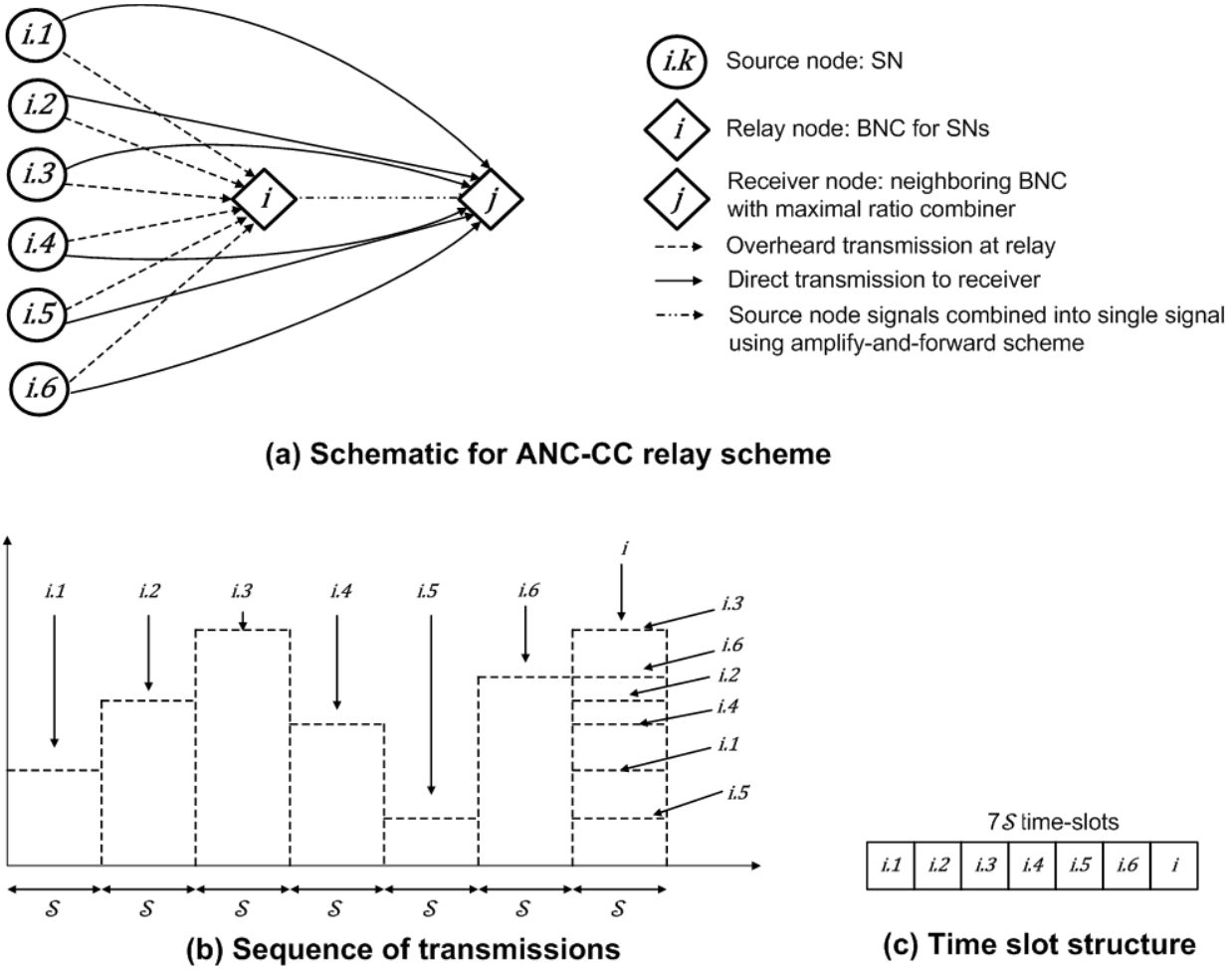

Fig. 5.2. Illustration of ANC-CC relay scheme with N_s SNs, one relay node BNC i, and one receiver node BNC.

Packets from SNs $i.1$, $i.2$, $i.3$, $i.4$, $i.5$, and $i.6$ are broadcast to both BNC i and BNC j. If the packets are correctly received by BNC i, their signals are combined into a single signal

using the analog network coding process illustrated in Fig 5.2b. The combined signal is then relayed to BNC *j*. The copies of the packets received by BNC *j* from the SNs are processed and used to decode and extract the individual signals from the incoming packet from BNC *i*. In ANC-CC, BNC *j* only requires a few error and interference free data bits from a SN to decode and extract the signals transmitted from BNC *i* because it uses the error and interference free bits to estimate the wireless channels from the SNs [125]. Therefore, data packets sent from the SNs with a low success probability greater than zero is sufficient for BNC *j* to reliably decode and extract the original data from BNC *i*, given the end-to-end success probability from the SNs to BNC *j* through BNC *i* meets the end-to-end reliability objective. From Fig. 5.2c, it can also be seen that the total number of time slots required to perform the transmissions is only $7\mathcal{S}$ because BNC *i* performs a linear combination of 6 incoming signals and outputs the combined signal in a single time slot. Comparatively, ANC-CC utilizes substantially fewer time slots than the conventional relay (CR) and cooperative communication (CC) two hop schemes where each signal transmitted by the 6 SNs to the BNC *i* is immediately relayed out in another time slot, thus requiring a total of $12\mathcal{S}$ time slots. As a result, we see that ANC-CC offers significant benefits in terms of reducing the number of required transmissions, thus reducing delay and relative energy cost.

After ANC-CC is applied to the SNs and BNCs comprising the first hop of a routing path, the MRP is applied to successive BNC relays comprising the remaining hops of the routing path to further reduce relative energy cost, increase end-to-end success probability, and decrease end-to-end delay. Consider the routing path in Fig. 5.1 connecting BAN11 to sink BS1. The BNC belonging to BAN11 does not forward data from any other BNCs and thus the BNC-to-BNC link between BAN11 and BAN12 is not eligible for MRP. On the other hand, the links

between BAN12 and BAN13 and BAN13 and BS1 are eligible for MRP because the BNC in BAN12 forwards data from the BNC in BAN11 and the BNC in BAN 13 forwards data from BAN12. Let BNC j (j is assigned as ID #12) and BNC k (k is assigned as ID #13) represent the two successive BNCs in the routing path and BS l (l is assigned as ID #1) the destination. The success probability over $link(j,k)$ and $link(k,l)$ is $\mathcal{P}_{jk}$ and $\mathcal{P}_{kl}$, respectively. An end-to-end reliability objective of $\mathcal{P}_{req}$ must be satisfied to successfully transmit data to BS l through the remaining hops comprising BNC j and BNC k. Assuming $\mathcal{P}_{jl} \ll \mathcal{P}_{req}$ due to the compounded path loss and fading conditions experienced over both $link(j,k)$ and $link(k,l)$, the CR scheme should be invoked because the success probability over $link(j,k)$ and $link(k,l)$ are high enough to support $\mathcal{P}_{req}$ (i.e., $\mathcal{P}_{jk}\mathcal{P}_{kl} \geq \mathcal{P}_{req}$), as shown in Fig. 5.3a.

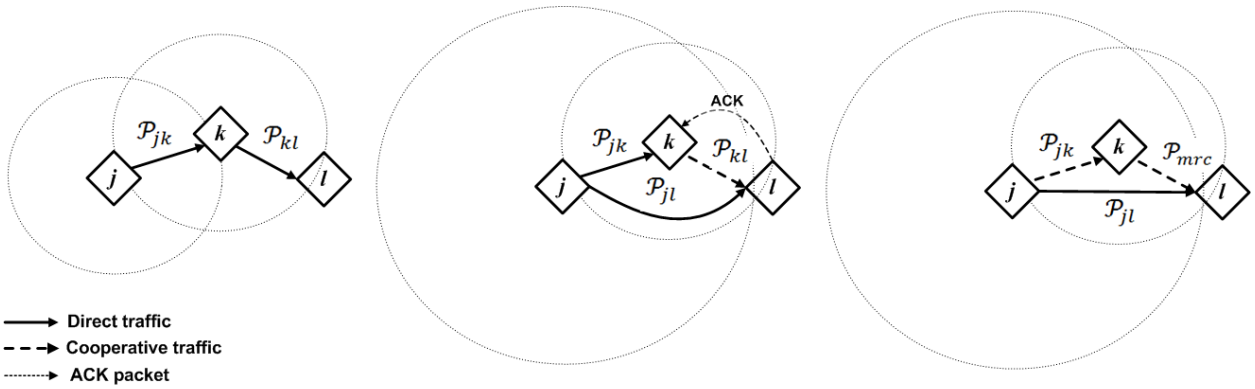

Fig. 5.3. Relay strategies for multi-hop BBN.

Although $\mathcal{P}_{jl} \ll \mathcal{P}_{req}$, there still exists a probability for BS l to receive the data packets directly from BNC j since $\mathcal{P}_{jl}$ can be greater than zero. Therefore, we consider the alternative data delivery approach illustrated in Fig. 5.3b where we allow both BNC k and BS l to receive the data packet broadcast by BNC j (i.e., multi-receive) instead of just BNC k. If BS l

successfully receives the data packet, an ACK message is generated by BS l to inform BNC k that there is no need to relay the data packet. Otherwise, if BS l does not receive the data packet, the communication operates in the same manner as the conventional two-hop relay approach (Fig. 5.3a). The proposed MRP is a form of CC but differs from the conventional energy efficient CC schemes described in the literature [25], [123], [100], [155]. In the conventional CC illustrated in Fig. 5.3c, a packet transmitted by BNC j is broadcast to both BNC k and BS l. If the packet is correctly decoded by BNC k, it is relayed to BS l thereafter, and the same copy of the packet originating from BNC j and BNC l are then processed at BS l to decode the received packet. If BNC k fails to decode the packet correctly, the packet is lost at BNC k, and thus BS l decodes the packet with only the copy received from BNC j. The success of CC mainly depends on the decoding process, the diversity combining technique (we assume a maximal ratio combiner (MRC) due to its noted proficiency in fading environments [156]) used at BS l, and the success probability for the transmission performed over $link(k,l)$.

5.2.2 Wireless Channel and Protocol Layers

The descriptions for the wireless channel, physical layer, and network layer are the same as those provided in Section 3.2.2 and Section 4.2.2. In order to align with the fully distributed nature of the EQD communication scheme, the scheduling of time slots is performed in a distributed manner as opposed to the centralized coordination employed in Chapter 4. Several works in the literature have focussed on distributed slot based TDMA protocols for the MAC layer [157]-[159]. Instead of adding a new one to the literature, we adopt the MeshMAC distributed beacon scheduling based MAC protocol [159] that extends the beacon mode of the IEEE 802.15.4 standard.

5.3 EQD Communication Scheme for Multi-hop BBN

5.3.1 Overview

In this section, we first describe the operational cycle and functional elements of the EQD communication scheme. We then introduce a route storing strategy to achieve the minimum routing table size required to facilitate energy and QoS-aware distributed routing in the multi-hop BBN. A detailed performance analysis is provided for the ANC-CC relay scheme and the MRP. Finally, the operational details for the EQD communication scheme are provided to describe the routing table structure used to store each route, the policies for adding and removing new and old routing entries to and from the routing table, and the distributed routing algorithm.

5.3.2 Description of EQD Communication Scheme

The operation of EQD consists of four main phases and is described using the flow diagram presented in Fig. 5.4. The initial phase marks the initial deployment of the SNs, BNCs, and BS, followed by the launch of the EQD communication scheme. In the first phase, each BNC exchanges the contents of its routing table, channel state information, and residual energy information with neighboring BNCs. The SNs also acquire channel state information for each BNC and/or BS in its neighbor discovery range by performing a channel probing process based on the work in [160]. In the second phase, the minimum relative energy cost to each neighboring BNC is calculated as part of the neighbor discovery process. The policies for adding new minimum relative energy cost route entries to the BNC's routing table are then enacted. In the third phase, the BNC executes the distributed routing algorithm to determine the routing entry that provides the minimum end-to-end relative energy cost. The MRP is applied to the routing entry if it consists of at least two successive BNCs serving as relay nodes. The routing information pertinent to the minimum end-to-end relative energy cost routing path selected by

the BNC is sent to each of its SNs so that the SNs have knowledge of the next hop node(s) to transmit to with a specific transmit power, retransmission limit, and packet size. In the fourth phase, the SNs route their data packets to the designated next hop BNC nodes using the ANC-CC relay scheme. Subsequent relay of the data packets is performed either using a CR scheme or a relay scheme operating under MRP. The four aforementioned phases are operated cyclically until a SN runs out of energy or the BNC needed to relay the data runs out of energy. If a SN has run out of energy or is unable to successfully deliver its data to the BS, EQD terminates. Otherwise, phase one is re-enacted.

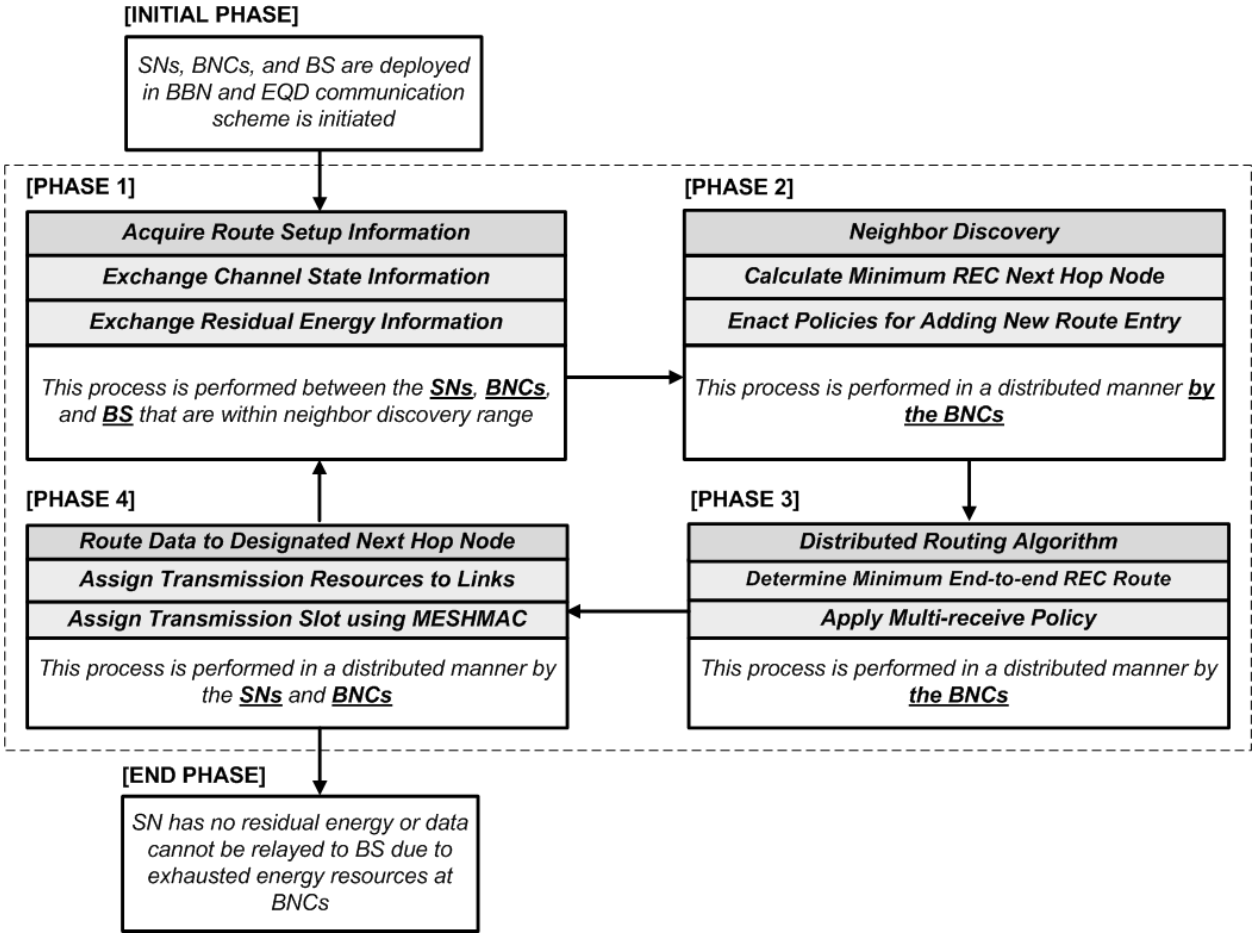

Fig. 5.4. Operational cycle and functional elements of EQD communication scheme.

5.3.3 Route Storing Strategy for Minimum BNC Routing Table Size

In this section, we first derive analytical expressions to determine the maximum number of routing table entries required at each BNC to support reliability and delay constrained minimum relative energy cost distributed routing in a multi-hop BBN. Next, we describe a route storing strategy to minimize the number of routing table entries maintained by a BNC while still retaining the minimum relative energy cost route.

To perform distributed routing, each BNC periodically broadcasts its routing table to the neighboring BNCs or BS within its neighbor discovery range (calculated from Algorithm 4.1). Each BNC updates its own routing table based on the routing entries possessed by its neighbors. For example, let $\mathcal{E}_{ete,j1}$ denote the relative energy cost along the routing path connecting BNC *j* to the BS and $\mathcal{E}_{ij}$ the relative energy cost between BNC *i* and BNC *j*. When BNC *i* receives a routing table update from BNC *j*, it creates a new routing path to the BS with the new relative energy cost $\mathcal{E}_{ete,i1} = \mathcal{E}_{ij} + \mathcal{E}_{ete,j1}$, which is then compared against the existing routing entries in BNC *i*'s routing table. The routing entry with the minimum relative energy cost to the BS will then be recorded in BNC *i*'s routing table.

To guarantee the routing path with the minimum relative energy cost is calculated at each BNC, each BNC must store all routing paths that satisfy the QoS requirements since only recording the path with the least relative energy cost (as is done in the distributed Bellman-Ford algorithm) is not sufficient for finding the minimum relative energy cost path. Continuing from the previous example, suppose the minimum relative energy cost path at BNC *j* satisfies the end-to-end reliability and delay objectives, such that $\mathcal{P}_{ete,j1} \geq \mathcal{P}_{req}$ and $\mathcal{D}_{ete,j1} \leq \mathcal{D}_{req}$, respectively. Given $\mathcal{P}_{ij}$, the success probability between BNC *i* and BNC *j*, and $\mathcal{P}_{ete,j1}$ are

greater than or equal to $\mathcal{P}_{req}$, respectively, a scenario is presented where $\mathcal{P}_{ete,i1} = \mathcal{P}_{ij}\mathcal{P}_{ete,j1} < \mathcal{P}_{req}$ if $\mathcal{P}_{ij} < 1$, thus leaving BNC *i* unable to find a routing path which satisfies the end-to-end reliability constraint to the BS via BNC *j*. For this reason, BNC *j* also has to maintain the routing paths with higher relative energy cost but higher end-to-end success probability to the BS. We thus propose the following approach to calculate the maximum number of routing paths required to maintain a reliability-constrained minimum relative energy cost route.

Let ρ represent an array of *Y* defined end-to-end success probability target values (PTV) in the range $[\mathcal{P}_{req}, 1]$. The values in the array are stored as $\rho(y) = \mathcal{P}_{req} + (y-1)\mathcal{P}_{step}, y \in [1, Y]$ with *Y* calculated as $Y = \lceil (1 - \mathcal{P}_{req})/\mathcal{P}_{step} \rceil + 1$. The PTVs are assigned to be equally spaced by a defined step increment of $\mathcal{P}_{step}$ to drive the analysis for calculating the maximum routing table size maintained by a BNC operating a distributed routing protocol. For example, if $\mathcal{P}_{req}$ is 99% and $\mathcal{P}_{step}$ is 0.1%, the PTVs in BNC *i*'s routing table would be 99%, 99.1%, 99.2%, 99.3%, ...,99.9%, and 100%. The value of $\mathcal{P}_{step}$ directly affects solution accuracy. The higher the value of $\mathcal{P}_{step}$, the lower the probability for discovering the minimum relative energy cost routing path since fewer routing paths are stored and vice versa. The routing table of a BNC *i* located a single hop from the BS contains one routing table entry for each PTV in ρ such that $\Omega_i(1, \rho(y)) = 1, y \in [1, Y]$, where $\Omega_i(H, \rho(y))$ is the number of stored routing table entries for a BNC *i* located H hops from the BS with a PTV of $\rho(y)$. Therefore, the maximum number of stored routing table entries for a BNC *i* located one hop from the BS is $\Omega_i(1, \rho) = Y$ since there are *Y* values in ρ each producing one routing table entry. For a BNC *i* located *H* hops from the BS ($H > 1$), the maximum number of stored routing table entries is calculated by:

$$\Omega_i(H,\rho) = \sum_{h=2}^{H}\sum_{y=1}^{Y}\Omega_i(h,\rho(y)) \tag{5.1}$$

From (5.1), the number of routing table entries at each hop h $(h \leq H)$ for a PTV of $\rho(y)$ is calculated as:

$$\Omega_i(h,\rho(y)) = (\mathbb{N}_i(h)+1)(\Omega_i(h-1,\rho(y)) + \Omega_i(h,\rho(y)-\mathcal{P}_{step}) + \frac{1}{\mathcal{P}_{step}}\mathrm{mod}(\rho(y),\mathcal{P}_{req})) \tag{5.2}$$

where $\mathbb{N}_i(h)$ denotes the number of neighboring BNCs for BNC *i* at hop h. The value for $\Omega_i(h,\rho(y))$ is calculated as a sum of three components: *i*) total number of routing table entries required at the PTV of $p(y)$ for the previous hop (i.e., $\Omega_i(h-1,\rho(y))$), *ii*) total number of routing table entries required at the PTV of $\rho(y)-\mathcal{P}_{step}$ for the current hop (i.e.,$\Omega_i(h,\rho(y)-p_{step})$), and *iii*) the total number of routing table entries required at the current PTV $\rho(y)$ and current hop *h*. Since each pair of evaluated PTVs in ρ is spaced by $\mathcal{P}_{step}$, the number of routes resulting from comparing $\rho(y)$ against the application end-to-end reliability objective $\mathcal{P}_{req}$ using the modulo operator is scaled by $\frac{1}{\mathcal{P}_{step}}$. Also, given that a BNC *i* must rely on the routing table entries of its single hop neighboring BNCs and also rely on the relay BNCs located between BNC *i* and the BS, the three aforementioned summed components must be multiplied by $\mathbb{N}_i(h)+1$, where '1' is added to account for BNC *i*. The numerical evaluation of (5.2) presented in Section 5.5 shows that the maximum number of routing table entries for a BNC grows exponentially as the number of hops to the BS increases.

Each BNC is configured to store a minimum relative energy cost route for each of the *Y* defined PTVs. This design feature limits the number of routing table entries to *Y*. Storing a

routing table entry for each of these PTVs, a BNC *i* located multiple hops from the BS discovers a minimum relative energy cost route to the BS by finding a PTV combination from its routing table and its neighbor BNC *j*'s routing table which meets the end-to-end reliability objective. For example, if both BNC *i* and BNC *j* are neighbors and maintain an array of PTVs in the range $[\mathcal{P}_{req}, 1]$ where $\mathcal{P}_{req} = 99\%$ and $\mathcal{P}_{step} = 0.1\%$, a PTV combination of 99.9% from BNC *i* and 100% from BNC *j* would satisfy $\mathcal{P}_{req}$ because $0.99 \times 1 \geq \mathcal{P}_{req}$. The feasibility of the route storing strategy is based on three realities: *i*) The end-to-end success probability for any route stored in a BNC's routing table must be greater than or equal to the end-to-end reliability objective, *ii*) any minimum relative energy cost route between BNC *i* and BNC *j* is calculated by solving (3.15) and setting the given PTV at $\mathcal{P}_{req}$, *iii*) any BNC *i* with PTVs in the range $[\mathcal{P}_{req}, 1]$ obtains a minimum relative energy cost route to the sink if it has a neighboring BNC *j* with PTVs in the range $[\mathcal{P}_{req}, 1]$.

5.3.4 Performance Analysis of ANC-CC Relay Scheme

An undesirable side effect of ANC-CC is ANC noise. ANC noise is introduced when multiple incoming signals from source nodes are combined using analog network coding at the relay node followed by signal extraction at the receiver node, producing a non-negligible noise term at the receiver node. Due to the presence of this ANC noise, the data extracted and decoded at the receiver node is not as reliable as the end-to-end reliability objective would require because the data is corrupted by ANC noise. As a result, it is of utmost importance to adequately account for and overcome ANC noise so the measured end-to-end success probability at the receiver node is the same as the intended end-to-end success probability (including ANC noise).

In this section, analytical expressions are derived to determine the relative energy cost, success probability, and delay achieved for the ANC-CC relay scheme when ANC noise is ignored and when ANC noise is considered.

Consider the network scenario in Fig 5.2 defined by $\mathcal{A}(\{i.k\}, i, j)$ where a set of N_s SNs each has an ID in the range $k \in [1, N_s]$, a single relay BNC is identified by ID *i*, and a single receiver BNC is identified by ID *j*. Let $\mathcal{P}_{i.k,i}$, $\mathcal{P}_{mrc}$, and $\mathcal{P}_{i.k,j}$ represent the success probability at BNC *i* for receiving data from SN *i.k*, success probability for MRC at BNC *j*, and the success probability for direct communication from SN *i.k* to BNC *j*, respectively. The success probability at BNC *j* after decoding and extracting data from SN *i.k* which has been processed with ANC-CC at BNC *i*, is:

$$\mathcal{P}_{i.k,i,j}^{anc} = 1 - \mathcal{P}_{i.k,i}(1 - \mathcal{P}_{mrc}) - \left(1 - \mathcal{P}_{i.k,i}\right)\left(1 - \mathcal{P}_{i.k,j}\right) \tag{5.3}$$

where the second component on the right is the probability a packet error occurs at BNC *j* when BNC *i* succeeds in relaying a copy of the packet and the third component is when BNC *i* fails in the relay. The expression for the BER of MRC over a Nakagami-*m* fading channel with OQPSK modulated data is derived in [156] based on the work in [161], as:

$$p_{b,mrc} = \left(\frac{1 - K_2}{2}\right)^{m\mathcal{B}} \sum_{b=1}^{2m\mathcal{B}-1} \binom{2m\mathcal{B} - 1 + b}{b} \left(\frac{1 + K_2}{2}\right)^{b} \tag{5.4}$$

where $K_2 = \sqrt{(\gamma_{mrc}/m)/(1 + \gamma_{mrc}/m)}$, $\mathcal{B} = 2$ for dual branch diversity, and γ_{mrc} is the total SNR[3] at the output of the MRC. The total SNR at the output of the maximal ratio combiner, without considering ANC noise, is calculated as [128]:

[3] In this chapter SNR is used instead of SINR because we assume a non-interfering distributed TDMA scheme (i.e., MeshMAC)

$$\gamma_{mrc1} = \gamma_{i.k,j} + \frac{\gamma_{i.k,i}\gamma_{ij}}{\gamma_{ij} + \sum_{k'=1,k'\neq k}^{N_s} \gamma_{i.k',j}} \tag{5.5}$$

The derivation for the SNR in (5.5) follows from the literature where the wireless channel in the ANC-CC scheme is modeled using the single-input dual-output Gaussian vector channel [162] to combine the direct path between SN *i.k* and BNC *j* (left component on right hand side of (5.5)) and the relay path from SN *i.k* to BNC *i* to BNC *j* (right component on right hand side of (5.5)).

When ANC noise is accounted for in the ANC-CC relay scheme, the total SNR obtained at BNC *j* as a result of the maximal ratio combiner becomes:

$$\gamma_{mrc2} = \gamma_{i.k,j} + \frac{\gamma_{i.k,i}\gamma_{ij}}{N_s \frac{\sigma_{anc}^2}{{\sigma_j}^2} + \gamma_{ij} + \frac{\sigma_{anc}^2}{{\sigma_j}^2} \sum_{k'=1,k'\neq k}^{N_s} \gamma_{i.k',i}} \tag{5.6}$$

where ${\sigma_j}^2$ is the variance for background additive white Gaussian noise with zero mean at BNC *j* and σ_{anc}^2 is the variance of the zero mean ANC noise. The variance of the ANC noise is calculated as [128]:

$$\sigma_{anc}^2 = \sigma_j^2 + \sum_{k'=1,k'\neq k}^{N_s} \xi_i \sigma_i^2 + \xi_i \sigma_j^2 \sum_{k'=1,k'\neq k}^{N_s} \frac{g_{i.k',i}}{g_{i.k',j}} \tag{5.7}$$

where ξ_i is the amplification factor for the amplify-and-forward operation at relay BNC *i* and is given as [162]:

$$\xi_i = \frac{P_{tx.ij} g_{ij}}{N_s {\sigma_i}^2 + \sum_{k=1}^{N_s} P_{tx.i.k,i} g_{i.k,i}} \tag{5.8}$$

In (5.7), the additional terms to the right of σ_j^2 represent the variance of the ANC noise. Specifically, the first term to the right of σ_j^2 is the noise resulting from performing analog network coding at BNC *i* and the second term to the right of σ_j^2 is the noise resulting from

extracting the desired signal from the combined signals. The expression in (5.7) can be simplified using the following three assumptions. First, the noise variance σ_i^2 in a BAN is determined to be approximately -95 dBm [25] which is approximately the same as the noise variance of -100 dBm for communication outside the BAN [163]. Therefore, we can make the following approximation: $\sigma_i^2 \approx \sigma_j^2$. Second, given $N_s = 6$, $P_{tx.i.k,i} \in [P_{min}, P_{max}]$, $g_{i.k,i} = 10^{-PL(d_0)_{dB} - 10\alpha \log_{10}(d_{i.k,i}/d_0)/10}$ using the on-body path loss parameters in Table 3.2, we assume $\sum_{k=1}^{N_s} P_{tx.i.k,i} g_{i.k,i} \gg N_s {\sigma_i}^2$. Third, the channel gain between a SN and neighboring BNC is approximately the same as the channel gain between a BNC and neighboring BNC because we assume the same body-to-body path loss parameters for both channels (from Table 3.2) and the distances (i.e., $d_{ij} \approx d_{i.k,j}$) are approximately the same. We can assume $d_{ij} \approx d_{i.k,j}$ because $d_{ij}, d_{i.k,j} \gg d_{i.k,i}$. Therefore, $g_{i.k,j} \approx g_{ij}$ $\forall k \in [1, N_s]$. After incorporating the three assumptions into (5.7), it can be rewritten as:

$$\sigma_{anc}^2 = \sigma_i^2 \left(1 + \frac{P_{tx.ij}}{\sum_{k=1}^{N_s} P_{tx.i.k,i} g_{i.k,i}} \left(\frac{\sum_{k'=1, k' \neq k}^{N_s} g_{i.k',i}}{(N_s - 1)} + (N_s - 1) g_{ij} \right) \right) \tag{5.9}$$

From (5.9), it is clear that that increasing or decreasing $P_{tx.ij} / \sum_{k=1}^{N_s} P_{tx.i.k,i}\, g_{i.k,i}$ increases and decreases σ_{anc}^2, respectively. It is also clear that σ_{anc}^2 decreases as the distance between BNC i and BNC j increases (decreasing g_{ij}) when $P_{tx.ij}$ and $P_{tx.i.k,i}$ have attained a transmit power level of P_{max}. It is typical for $P_{tx.ij}$ and $P_{tx.i.k,i}$ to approach P_{max} as d_{ij} increases in order to maintain a success probability above $\mathcal{P}_{req}$. Therefore, we can deduce that the variance in ANC noise is most detrimental at closer inter-BAN distances. This particular distance is determined in our numerical results.

When ANC noise is ignored, the SNR γ_{mrc1} serves as an input to (5.5) and thus the success probability for the MRC at BNC *j* is calculated as:

$$\mathcal{P}_{mrc1} = \mathcal{P}_s\left(\gamma_{mrc1}, m_{i.k,i}, L_{i.k,i}, X_{i.k,i}\right) \times \mathcal{P}_s\left(\gamma_{mrc1}, m_{i.k,j}, L_{i.k,j}, X_{i.k,j}\right) \times \mathcal{P}_s\left(\gamma_{mrc1}, m_{ij}, L_{ij}, X_{ij}\right) \tag{5.10}$$

When ANC noise is accounted for, the SNR γ_{mrc2} serves as an input to (5.5) and thus the success probability for the MRC at BNC *j* is calculated as:

$$\mathcal{P}_{mrc2} = \mathcal{P}_s\left(\gamma_{mrc2}, m_{i.k,i}, L_{i.k,i}, X_{i.k,i}\right) \times \mathcal{P}_s\left(\gamma_{mrc2}, m_{i.k,j}, L_{i.k,j}, X_{i.k,j}\right) \times \mathcal{P}_s\left(\gamma_{mrc2}, m_{ij}, L_{ij}, X_{ij}\right) \tag{5.11}$$

The presence of ANC noise reduces γ_{mrc2} and subsequently produces a lower value for $\mathcal{P}_{mrc2}$. We design an algorithm to determine the minimum relative energy cost required to satisfy the specified reliability and delay constraints for the ANC-CC relay scheme, with and without ANC noise. By exploiting the ability to adaptively modify transmit power, retransmission limit, and packet size, we can overcome ANC noise while obtaining minimum relative energy cost. Before the algorithm is described, we first provide calculations for the total relative energy cost and delay in an ANC-CC relay scheme.

The total relative energy cost required to transmit data in $\mathcal{A}(\{i.k\}, i, j)$ for ANC-CC consists of three components. The first component of the relative energy cost is incurred at the SNs and is given by:

$$\mathcal{E}_{i.k}^{anc} = n_{i.k} L_{i.k} \phi\left(\bar{\gamma}_{i.k,j}, m_{i.k,j}, L_{i.k}, X_{i.k}\right) \frac{E_b(P_{tx.i.k})}{E_{res,i.k}}, \forall k \in [1, N_s] \tag{5.12}$$

The second component of the relative energy cost, incurred at the relay BNC *i*, includes the energy for receiving data from the SNs and sending the correctly received data to BNC *j* after it has been combined into a single signal and amplified:

$$\mathcal{E}_i^{anc} = \sum_{k=1}^{N_s} n_{i.k,j} L_{i.k,j} \phi\left(\bar{\gamma}_{i.k,j}, m_{i.k,i}, L_{i.k,j}, X_{i.k,j}\right) \frac{E_b(P_{rx})}{E_{res,i}} + \cdots$$

$$\cdots + \left(1 - p_{e,ij}\right) n_{ij} L_{ij} \phi\left(\bar{\gamma}_{ij}, m_{ij}, L_{ij}, X_{ij}\right) \frac{E_b\left(P_{tx.ij}\right)}{E_{res,i}} \tag{5.13}$$

The analog network coding process at BNC *i* uses a linear combination of incoming data packets as opposed to the aggregation of incoming data packets. Therefore, the payload size for $link(i,j)$ is $L_{p,ij} = \max\left(L_{p,i.k,i}\right), \forall k \in [1, N_s]$ and the total data traffic along $link(i,j)$ is $n_{ij} L_{p,ij} = \max\left(n_{i.k,i} L_{p,i.k,i}\right), \forall k \in [1, N_s]$.

The third component of the relative energy cost is incurred at the receiver BNC *j* and consists of the energy required to receive packets from all SNs and BNC *i*. It is derived as:

$$\mathcal{E}_j^{anc} = \sum_{k=1}^{N_s} n_{i.k} L_{i.k} \phi\left(\bar{\gamma}_{i.k,j}, m_{i.k,j}, L_{i.k}, X_{i.k}\right) \frac{E_b(P_{rx})}{E_{res,j}} + \cdots$$

$$\cdots + \left(1 - p_{e,ij}\right) n_{ij} L_{ij} \phi\left(\bar{\gamma}_{ij}, m_{ij}, L_{ij}, X_{ij}\right) \frac{E_b(P_{rx})}{E_{res,j}} \tag{5.14}$$

Hence, the total relative energy cost for transmitting data in $\mathcal{A}(\{i.k\}, i, j)$ for ANC-CC is:

$$\mathcal{E}_{i.k,i,j}^{anc} = \sum_{k=1}^{N_s} \mathcal{E}_{i.k}^{anc} + \mathcal{E}_i^{anc} + \mathcal{E}_j^{anc} \tag{5.15}$$

The total delay for transmitting data in $\mathcal{A}(\{i.k\}, i, j)$ for ANC-CC is:

$$\mathcal{D}_{i.k,i,j}^{anc} = t_{slot} \left(\sum_{k=1}^{N_s} \max\left(\mathcal{S}_{i.k,i}, \mathcal{S}_{i.k,j}\right) + \bar{\mathcal{P}}_{i.k,i} \mathcal{S}_{ij} \right) \tag{5.16}$$

where $\bar{\mathcal{P}}_{i.k,i}$ is the average success probability for all SN transmissions to BNC *i*, $\max(\mathcal{S}_{i.k,i}, \mathcal{S}_{i.k,j})$ selects the highest number of transmission slots between $link(i.k, i)$ and

$link(i.k,j)$, and $\mathcal{S}_{ij}$ is the number of slots from BNC i to BNC j calculated as $\mathcal{S}_{ij} = \max\left(\max\left(\mathcal{S}_{i.k,i}, \mathcal{S}_{i.k,j}\right)\right), \forall k \in [1, N_s]$.

Algorithm 5.1 is designed to provide the minimum delay and relative energy cost for the ANC-CC relay scheme under delay constraint $\mathcal{D}_{req}$ and reliability constraint $\mathcal{P}_{req}$, with the nodes in $\mathcal{A}(\{i.k\}, i, j)$ serving as the source nodes, relay node, and receiver node, respectively. The Boolean input ℵ determines whether the relative energy cost, success probability, and delay is calculated using ANC noise (i.e., $\aleph = 1$) or not calculated using ANC noise ($\aleph = 0$). Different from Algorithm 3.2 where the minimum delay and relative energy cost for intra and inter BAN links is determined using two successive while loops, Algorithm 5.1 only employs a single while loop to concurrently account for the relative energy cost contribution of $link(i.k,i), link(i.k,j)$, and $link(i,j)$. This modification is necessary because the calculation of the relative energy cost, success probability, and delay is dependent on the joint inputs from the three aforementioned links. In line 3 of Algorithm 5.1, we then initialize the transmit power, retransmission limit, and packet size for all nodes in $\mathcal{A}$ to the maximum power, maximum retransmission limit, and maximum packet size to increase the probability of obtaining a feasible default solution. Three minimum joint delay and relative energy cost values $\mathcal{E}'_{min}$, $\mathcal{E}''_{min}$, and $\mathcal{E}'''_{min}$ are provided. $\mathcal{E}'_{min}$ is the minimum joint delay and relative energy cost achieved for a SN or BNC denoted by a node a for $\{P_{tx.a}(z), \varphi_a, X_a\}$, $\mathcal{E}''_{min}$ is the minimum joint delay and relative energy cost achieved for node a for $\{P_{tx.a}(z'), \varphi'_a, X'_a\}$ where $P_{tx.a}(z') \leq P_{max}, \varphi'_a \geq 1, X'_a \leq X_{max}$, and $\mathcal{E}'''_{min}$ is the minimum joint delay and relative energy cost after the transmit power, retransmission limit, and packet size for all nodes in $\mathcal{A}$ have been optimized. Algorithm 5.1 operates similarly to previously described search algorithms in the thesis (e.g., Algorithm 3.2). However, since each

node is initialized to use the maximum retransmission limit and we evaluate the total ANC-CC relay delay at each iteration of the while loop between lines 9 and 22, it is possible to satisfy the reliability constraint and never satisfy the delay constraint, thus preventing the transmit power, retransmission limit, and packet size of node a in line 12 from being updated. As a result, Algorithm 5.1 could enter an infinite loop where the delay constraint is never satisfied. To avoid this scenario, a condition is added in lines 15 to 17 to update the transmit power, retransmission limit, and packet size of node a when no feasible solution has been obtained (i.e., $\mathcal{E}'_{min} = \infty$), the reliability constraint is satisfied, and the achieved total delay $\mathcal{D}^{anc}$ is less than the previous minimum total delay $\mathcal{D}_{min}$. Algorithm 5.1 terminates when the joint delay and relative energy cost $\mathcal{E}''_{min}$ obtained by iterating through all nodes in $\mathcal{A}$ does not improve upon the previous minimum joint relative energy cost $\mathcal{E}'''_{min}$.

After Algorithm 5.1 is executed, the computed transmit powers, retransmission limits, and packet sizes are assigned to the nodes in $\mathcal{A}(\{i.k\}, i, j)$ prior to the source nodes performing data transmission. If node j is a BS, the extracted incoming signals are stored as physiological data and later interpreted by the combat medic holding the BS. If node j is a BNC, the extracted incoming signals from SNs $i.k$ and BNC i are organized as individual physiological data and subsequently aggregated into minimum relative energy cost data packets to transmit to the next hop node.

Algorithm 5.1 Minimum Joint Delay and Relative Energy Cost for ANC-CC Relay Scheme

Input: $\boldsymbol{PL(d_0)}, \boldsymbol{\alpha}, \boldsymbol{d_0}, \boldsymbol{d}, \boldsymbol{m}, P_{min}, P_{max}, X_{max}, \boldsymbol{L_s}, \varphi_{max}, \boldsymbol{r}, \mathcal{P}_{req}, \mathcal{D}_{req}, \mathcal{A}, \aleph$;
Output: $\boldsymbol{FS}$;
Initialize: $P_{tx.a}(z) = P_{max}, \varphi_a = \varphi_{max}, X_a = X_{max}, \forall a \in \mathcal{A}; \mathcal{E}''_{min} = \infty; \mathcal{E}'''_{min} = \infty; \mathcal{D}_{min} = \infty$;
while $(\mathcal{E}''_{min} < \mathcal{E}'''_{min})$ **do**
  for each SN and BNC in $\mathcal{A}(\{i.k\}, i, j)$ **do** //each SN and BNC is denoted by *a;*
    $P_{tx}(z) = P_{max}; \mathcal{E}'_{min} = \infty$;
    while $(P_{tx}(z) \geq P_{min})$ **do**
      $\varphi = \varphi_{max}; X = X_{max}$;
      while $(\varphi \geq 1)$ and $(X \geq 1)$ **do**
        Calculate $\mathcal{P}^{anc}, \mathcal{E}^{anc}$, and $\mathcal{D}^{anc}$ using (5.3), (5.15), and(5.16), respectively, for all SNs and BNCs in $\mathcal{V}$ with $\{P_{tx.a}(z), \varphi_a, X_y\}, \forall a \in \mathcal{A}(\{i.k\}, i, j)$ as inputs, with $(\aleph = 1)$ or without ANC Noise $(\aleph = 0)$;
        if $(\mathcal{E}^{anc}\mathcal{D}^{anc} < \mathcal{E}'_{min})$ and $(\mathcal{P}^{anc} \geq \mathcal{P}_{req})$ and $(\mathcal{D}^{anc} \leq \mathcal{D}_{req})$ **then**
          $\mathcal{E}'_{min} = \mathcal{E}^{anc}\mathcal{D}^{anc}; P_{tx.a}(z) = P_{tx}(z); \varphi_a = \varphi; X_a = X; \mathcal{D}_{min} = \mathcal{D}^{anc}$;
          $X = X - 1$; //decrement retransmission limit
        else if $(\mathcal{P}^{anc} \geq \mathcal{P}_{req})$ and $(\mathcal{E}'_{min} == \infty)$ **then**
          if $(\mathcal{D}^{anc} < \mathcal{D}_{min})$ **then**
            $\mathcal{D}_{min} = \mathcal{D}^{anc}; P_{tx.a}(z) = P_{tx}(z); \varphi_a = \varphi; X_a = X$;
          end if
          $X = X - 1$; //decrement retransmission limit
        else
          $\varphi = \varphi - 1$; // decrement number of samples per packet
        end if
      end while
      if $(\mathcal{E}'_{min} \geq \mathcal{E}''_{min})$ && $(\mathcal{E}'_{min} \neq \infty)$ **then**
        terminate while loop
      else
        $z = z - 1$; //decrement power level
      end for
      $\mathcal{E}''_{min} = \mathcal{E}'_{min}$; //store the lowest joint delay and REC obtained at $P_{tx}(z)$
    end while
  end for
  $\mathcal{E}'''_{min} = \mathcal{E}''_{min}$;
end while
return FS$(\mathcal{E}'''_{min}, P_{tx.y}(z), \varphi_y, X_a)$;

5.3.5 Performance Analysis of Relay Scheme under Multi-Receive Policy

The MRP is invoked to further reduce relative energy cost, increase end-to-end success probability, and decrease end-to-end delay for successive BNC relays that comprise the hops beyond the first hop from the source BAN. Let $\mathcal{A}(j,k,l)$ represent the successive nodes network scenario illustrated in Fig. 5.3b. The total relative energy cost resulting from enacting the MRP is calculated as:

$$\mathcal{E}_{jkl}^{mrp} = n_{jk}L_{jk}\phi\left(\bar{\gamma}_{jk}, m_{jk}, L_{jk}, X_{jk}\right)\left(\frac{E_b(P_{tx.jk})}{E_{res,j}} + \frac{E_b(P_{rx})}{E_{res,k}} + \frac{E_b(P_{rx})}{E_{res,l}}\right) + \ldots$$

$$\ldots + p_{e,jl}\left(1 - p_{e,jk}\right)n_{kl}L_{kl}\phi(\bar{\gamma}_{kl}, m_{kl}, L_{kl}, X_{kl})\left(\frac{E_b(P_{tx.kl})}{E_{res,k}} + \frac{E_b(P_{rx})}{E_{res,l}}\right) \quad (5.17)$$

where $p_{e,jl}$ and $p_{e,jk}$ are the PERs for direct communication over the specified link. In MRP, we can assume the length of the ACK messages are far less than the data packet length and they can be transmitted multiple times in a short period to assure they can be received by the *BNC k*. Our previous work [155] has shown the required energy cost for the transmission of ACK messages can be neglected because the ACK message size is less than 5% of a data packet and thus the energy contribution of the ACK messages are not accounted for in (5.17). The end-to-end success probability for MRP in $\mathcal{A}(j,k,l)$ is derived as:

$$\mathcal{P}_{jkl}^{mrp} = \mathcal{P}_{jl} + \left(1 - \mathcal{P}_{jl}\right)\mathcal{P}_{jk}\mathcal{P}_{kl} \quad (5.18)$$

The end-to-end delay is derived as the product of number of time slots and slot duration, given by:

$$\mathcal{D}_{ij\ell}^{mrp} = t_{slot}\left(\mathcal{S}_{jk} + \mathcal{P}_{jk}(1 - \mathcal{P}_{jl})\mathcal{S}_{kl}\right) \quad (5.19)$$

where the total number of required slots is represented by the aggregate terms within the parenthesis. The relative energy cost in (5.17), success probability in (5.18), and delay in (5.19)

are compared against the relative energy cost, success probability, and delay of the CR scheme to determine whether or not the multi-receive strategy should be applied. Let $\mathcal{E}_{jkl}^{cr}, \mathcal{P}_{jkl}^{cr}$, and $\mathcal{D}_{jkl}^{cr}$ be the relative energy cost, success probability, and delay for the successive nodes in $\mathcal{A}(j,k,l)$ utilizing just the CR scheme. The relative energy cost is calculated as:

$$\mathcal{E}_{jkl}^{cr} = n_{jk}L_{jk}\phi\left(\bar{\gamma}_{jk}, m_{jk}, L_{jk}, X_{jk}\right)\left(\frac{E_b(P_{tx.jk})}{E_{res,j}} + \frac{E_b(P_{rx})}{E_{res,k}}\right) + \ldots$$

$$\ldots + \left(1 - p_{e,jk}\right)n_{kl}L_{kl}\phi(\bar{\gamma}_{kl}, m_{kl}, L_{kl}, X_{kl})\left(\frac{E_b(P_{tx.kl})}{E_{res,k}} + \frac{E_b(P_{rx})}{E_{res,l}}\right) \quad (5.20)$$

The end-to-end success probability is derived as the product of the success probability along the two links:

$$\mathcal{P}_{jkl}^{cr} = \mathcal{P}_{jk}\mathcal{P}_{kl} \quad (5.21)$$

The end-to-end delay is derived as the sum of the time slot duration along the two links and is given by:

$$\mathcal{D}_{jkl}^{cr} = t_{slot}\left(\mathcal{S}_{jk} + \mathcal{P}_{jk}\mathcal{S}_{kl}\right) \quad (5.22)$$

For each routing entry in BNC j's routing table consisting of two next hop nodes BNC k and BS l, BNC j invokes the multi-receive strategy if $\mathcal{E}_{jkl}^{mrp} < \mathcal{E}_{jkl}^{cr}, \mathcal{P}_{jkl}^{mrp} \geq \mathcal{P}_{jkl}^{cr}$, and $\mathcal{D}_{jkl}^{mrp} \leq \mathcal{D}_{jkl}^{cr}$. To demonstrate the usefulness of MRP, we compare its performance against the relative energy cost, success probability, and delay achieved with a conventional CC scheme that is commonly adopted in the literature to support energy efficient relay. The success probability for CC is calculated as:

$$\mathcal{P}_{jkl}^{cc} = \mathcal{P}_{jk}(1 - \mathcal{P}_{mrc}^{cc}) + \left(1 - \mathcal{P}_{jk}\right)\left(1 - \mathcal{P}_{jl}\right) \quad (5.23)$$

where $\mathcal{P}_{mrc}^{cc}$ is the success probability for using the MRC to combine incoming signals from $link(j,l)$ and $link(k,l)$ in a CC relay scheme, the first component on the right of (5.23) is the

probability of unsuccessful delivery at BS l when BNC k succeeds in relaying a copy of the packet, and the second component is when BNC k fails in the relay. To calculate $\mathcal{P}_{mrc}^{cc}$, we first calculate the total SNR as $\gamma_{mrc}^{cc} = \gamma_{jl} + \gamma_{jk}\gamma_{kl}/(1 + \gamma_{kl} + \gamma_{jk})$ and substitute its result into (5.4) for the MRC BER. The MRC BER is then used to calculate $\mathcal{P}_{mrc}^{cc}$ as:

$$\mathcal{P}_{i.k,i,j}^{mrc} = \mathcal{P}_s(\gamma_{mrc}^{cc}, m_{jk}, L_{jk}, X_{jk}) \times \mathcal{P}_s(\gamma_{mrc}^{cc}, m_{jl}, L_{jl}, X_{jl}) \times \mathcal{P}_s(\gamma_{mrc}^{cc}, m_{kl}, L_{kl}, X_{kl}) \quad (5.24)$$

The relative energy cost for CC in $\mathcal{A}(j,k,l)$ is calculated as:

$$\mathcal{E}_{jkl}^{cc} = n_{jk}L_{jk}\phi(\bar{\gamma}_{jk}, m_{jk}, L_{jk}, X_{jk})\left(\frac{E_b(P_{tx.jk})}{E_{res,j}} + \frac{E_b(P_{rx})}{E_{res,k}} + \frac{E_b(P_{rx})}{E_{res,l}}\right) + \ldots$$

$$\ldots + (1 - p_{e,ij})n_{kl}L_{kl}\phi(\bar{\gamma}_{kl}, m_{kl}, L_{kl}, X_{kl})\left(\frac{E_b(P_{tx.jk})}{E_{res,k}} + \frac{E_b(P_{rx})}{E_{res,l}}\right) \quad (5.25)$$

The end-to-end delay is:

$$\mathcal{D}_{jkl}^{cc} = t_{slot}(\mathcal{S}_{jk} + \mathcal{P}_{jk}\mathcal{S}_{kl}) \quad (5.26)$$

5.3.6 EQD Operation

The operation of the EQD scheme is described in terms of the calculation for the minimum relative energy cost to a next hop node, the routing entry structure, the policies for adding the calculated minimum relative energy cost routes to the routing table, and the distributed routing algorithm.

5.3.6.1 Minimum Relative Energy Cost to Next Hop Node

The minimum relative energy cost to a next hop node is calculated for two scenarios. In the first scenario, BNC *i* is the relay for data from SNs *i.k*. In order to build minimum relative energy cost routing table entries between the SNs and BNC *i* and a next hop node *j* (e.g., BNC or BS), Algorithm (3.1) and Algorithm (3.2) are executed for each success probability target value $\rho(y)$, where $\rho(y)$ serves as the algorithm's input for the reliability objective (i.e., $\mathcal{P}_{req} = \rho(y)$).

In the second scenario, BNC *i* serves as the relay node for another BNC or set of SNs. In order to build minimum relative energy cost routing table entries between BNC *i* and a next hop node *j*, Algorithm (4.2) is executed for each $\rho(y) \in \rho$.

Lemma 4.1: Each set of links involved in the described scenarios must use the minimum relative energy cost $\mathcal{E}_{ij,min}$ to achieve the minimum relative energy cost to the BS along a routing path comprising BNC *i* and a next hop BNC *j* or BS.

Proof: Assume the minimum relative energy cost along a path from BNC *i* to the BS is $\mathcal{E}_{ete,i1,min} = \mathcal{E}_{other,min} + \mathcal{E}_{cur,ij}$, where $\mathcal{E}_{cur,ij}$ is the current relative energy cost on $link(i,j)$ and $\mathcal{E}_{other,min}$ is the minimum relative energy cost for all the other links along the path from BNC *i* to the BS. Suppose the transmission parameters for $link(i,j)$ are not equal to the optimal transmission parameters, we then have $\mathcal{E}_{ij,cur} > \mathcal{E}_{ij,min}$ since the optimal transmission parameters are required to achieve the minimum relative energy cost as previously shown in (3.15). This finally leads to $(\mathcal{E}_{ete,i1,min} = \mathcal{E}_{other,min} + \mathcal{E}_{cur,ij}) > (\mathcal{E}'_{ete,i1,min} = \mathcal{E}_{other,min} + \mathcal{E}_{cur,ij})$, which contradicts with the statement that $\mathcal{E}_{ete,i1,min}$ provides the minimum relative energy cost along the routing path from BNC *i* to the BS. ■

5.3.6.2 Structure for Route Entry

The contents of the minimum relative energy cost routing entry are stored in the format shown in Fig. 5.5.

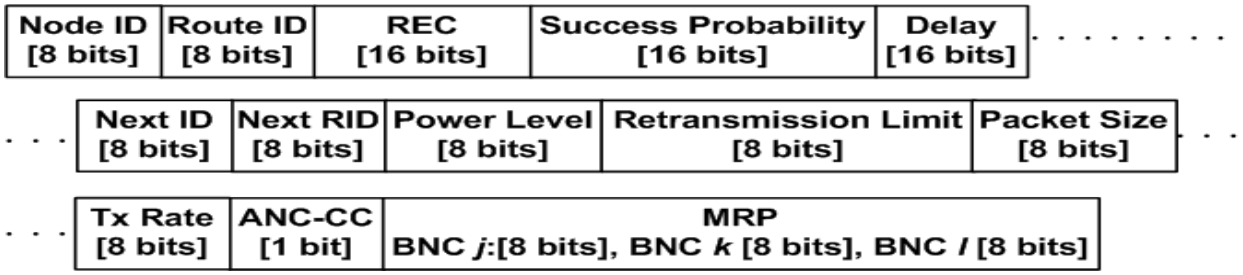

Fig. 5.5. Routing table structure.

The considered fields are explained as follows:

- *Node ID*: ID of the current node.
- *Route ID*: This ID identifies a unique route from the current node to the BS.
- *Relative Energy Cost*: The relative energy cost field indicates the relative energy cost required to use the current path destined to the BS.
- *Success Probability*: The end-to-end success probability from the current BNC to the BS that is stored as a PTV using the following rounding function: $\rho(y) = p_{step} \left\lfloor \frac{\mathcal{P}_{ete,i1}}{p_{step}} \right\rfloor, y \in [1, Y]$, where $\mathcal{P}_{ete,i1}$ is the end-to-end success probability before the rounding function.
- *Delay*: The end-to-end delay from the current BNC to the BS.
- *Next ID*: The next hop node along the path.
- *Next RID*: Since multiple routes to the BS can exist in a routing table, this field combined with the "Next" field indicates the exact route that should be selected in the next node's routing table to reach the sink.
- *Power Level*: The transmit power for the current link.

- *RTX*: The retransmission limit for the current link.
- *Packet Size*: Packet size, in bits.
- *Tx Rate*: Rate at which data packets are transmitted per second (specified by n).
- *ANC-CC*: Indicates whether the node is configured to use ANC-CC strategy (i.e., $0 = no, 1 = yes$)
- *MRP*: An array with the Node IDs of the BNCs that employ MRP.

The default destination is always the BS, thus there is no need to record the destination in the routing table. The SNs maintain a routing table with only a single routing entry. The routing entry contains fields for node ID, next ID1, next ID2, power level, retransmission limit, packet size, and tx rate. The fields next ID1 and next ID2 determine the two BNCs that receive the SN data as part of the ANC-CC relay scheme. Naturally, next ID1 is the BNC directly connected to the SN whereas next ID2 is a neighboring BNC or BS.

5.3.6.3 Policies for Adding New Route Entries

Let $\mathcal{E}_{ete,new,i1}$, $\mathcal{P}_{ete,new,i1}$, and $\mathcal{D}_{ete,new,i1}$ be the total relative energy cost required along a path to the BS, end-to-end success probability, and end-to-end delay of a new route entry for BNC i, respectively, and $\mathcal{E}_{ete,\rho(y),i1}$, $\mathcal{P}_{ete,\rho(y),i1}$, and $\mathcal{D}_{ete,\rho(y),i1}$, be the total relative energy cost required along a path to the BS, end-to-end success probability, and end-to-end delay, respectively, for the minimum relative energy cost route stored as $\rho(y)$ in BNC i's routing table. The following policies are applied to process the new route entry:

Policy 1: If $\mathcal{P}_{ete,new,i1} < \mathcal{P}_{req}$ or $\mathcal{D}_{ete,new,i1} > \mathcal{D}_{req}$ the new route entry is discarded.

Given the condition where $\mathcal{P}_{ete,\rho(y),i1} \approx \rho(y) = p_{step} \left\lfloor \frac{\mathcal{P}_{ete,new,i1}}{p_{step}} \right\rfloor, y \in [1, Y]$, the following two policies are enacted:

Policy 2: If $\mathcal{E}_{ete,new,i1} > \mathcal{E}_{ete,\rho(y),i1}$ or $\mathcal{E}_{ete,new,i1} = \mathcal{E}_{ete,\rho(y),i1}$ and $\mathcal{D}_{ete,new,i1} > \mathcal{D}_{ete,\rho(y),i1}$, the new route entry is discarded.

Policy 3: If $\mathcal{E}_{ete,new,i1} < \mathcal{E}_{ete,\rho(y),i1}$ or $\mathcal{E}_{ete,new,i1} = \mathcal{E}_{ete,\rho(y),i1}$ and $\mathcal{D}_{ete,new,i1} < \mathcal{D}_{ete,\rho(y),i1}$, the new route is inserted into the routing table.

5.3.6.4 Distributed Routing Algorithm

The distributed routing algorithm performed by each BNC in the multi-hop BBN is responsible for populating routing entries in a BNC's routing table. It is detailed in Algorithm 5.2.

Algorithm 5.2 EQD Distributed Routing Algorithm

1: **Input:** $i, j, \rho, Y, \mathcal{P}_{req}$;
2: **Output:** Minimum relative energy cost routing table
3: **Initialization:** Set y_i and y_j to 1 // index to ρ for BNCs *i* and *j*
4: **while** $(y_i \leq Y)$ **do**
5: **if** $\left(\rho(y_i)\rho(y_j) \geq \mathcal{P}_{req}\right)$ **then**
6: Store BNC *j*'s entries for total REC, end-to-end success probability, and end-to-end delay as $\mathcal{E}_{ete,\rho(y_i),j1}$, $\mathcal{P}_{ete,\rho(y_i),j1}$, and $\mathcal{D}_{ete,\rho(y_i),j1}$, respectively.
7: Calculate link REC $\mathcal{E}_{ij}$, link success probability $\mathcal{P}_{ij}$, and link delay $\mathcal{D}_{ij}$ for $link(i,j)$ using Algorithm 5.1 if BNC *i* is a relay for its SNs or Algorithm 4.2 if BNC *i* a relay for another BNC, with $\rho(y_i)$ as the input for the reliability objective.
8: Calculate total REC, end-to-end success probability and total delay for new path from BNC *i* to the BS: $\mathcal{E}_{ete,new,i1} = \mathcal{E}_{ij} + \mathcal{E}_{ete,\rho(y_j),j1}$, $\mathcal{P}_{ete,new,i1} = \mathcal{P}_{ij}\mathcal{P}_{ete,\rho(y_j)j1}$, and $\mathcal{D}_{ete,new,i1} = \mathcal{D}_{ij} + \mathcal{D}_{ete,\rho(y_j)j1}$.
9: Apply Policy 1. If route is discarded, increment PTV index of *j*: $y_j = y_j + 1$; Go to 5.
10: Apply Policies 2 and 3. If $y_j = Y$, increment PTV index of *i*: $y_i = y_i + 1$; Go to 5.
11: Set the ANC-CC field to 1 if BNC *i* relays source data from its SNs, else set it to 0.
12: Assign current, next hop, and next next hop nodes for MRP if MRP condition is satisfied, else set it to NULL.
13: **end if**
14: **end while**

In Algorithm 5.2 each BNC broadcasts its entire routing table every T_{ru} so that its neighbors can update their own routing tables. However, a routing table is not broadcast if no changes have been made to it since its last broadcast, inevitably leading to reduced communication and computation overhead.

5.4 Network Performance Analysis of EQD

In this section, we derive analytical expressions to determine the network performance of EQD in terms of the network relative energy cost, energy consumption for route setup, route setup time, average end-to-end success probability, and maximum end-to-end packet delay.

5.4.1 Network Relative Energy Cost

The network relative energy cost for EQD is the sum of the minimum relative energy cost routing paths in each of the routing tables of the source SNs and their BNCs. Each minimum relative energy cost route consists of the relative energy cost for the ANC-CC relay scheme (accounting for ANC noise) calculated using (5.15) and the relative energy cost for relaying between BNCs and the BS calculated either using MRP (5.17), conventional routing (5.20), or single hop BNC to BNC or BS transmission (Algorithm 4.2). Let $\mathcal{E}_{i.k,i,j}^{anc}$ denote the total relative energy cost for ANC-CC and $\mathcal{E}_{ete,j1}$ denote the end-to-end relative energy cost from the relay BNC j to the BS ($\mathcal{E}_{ete,j1}$ is zero if the BS is j). The total network relative energy cost for the N_b BANs in the network is:

$$\mathcal{E}_{EQD} = \sum_{i=2}^{N} \mathcal{E}_{i.k,i,j}^{anc} + \mathcal{E}_{ete,j1} \tag{5.27}$$

5.4.2 Energy Consumption for Route Setup

Each BNC periodically exchanges the contents of its routing table with its neighbors. Each routing table entry has size L_{rt} bits and is transmitted with the minimum power and

minimum retransmission limit required to successfully deliver the routing table entry while also minimizing energy consumption. The minimum energy required for exchanging a single routing table entry can be determined using Algorithm 4.2 with $L_{rt} = r$ by simply multiplying the obtained minimum relative energy cost by residual energy, which then results in total energy consumption E_{rt} for transmitting and receiving the routing table entry. Assuming the average number of neighbors for each BNC is $\mathbb{N}_{ndr}$ and the average number of exchanged routing table entries is Y due to the PTV based route storing strategy, the total energy consumed for route setup in EQD is calculated as:

$$E_{EQD,rs} = N_b \mathbb{N}_{ndr} E_{rt} \tag{5.28}$$

5.4.3 Route Setup Time

The route setup time is calculated by determining the total amount of time required to build routing paths for all the SNs and BNCs. The calculation follows the same methodology as that of the energy consumption for route setup in (5.28) and is derived as:

$$\mathcal{D}_{EQD,rs} = \frac{N_b \mathbb{N}_{ndr} L_{rt}}{\mathcal{R}} \tag{5.29}$$

5.4.4 Average End-to-end Success Probability

Since success probability and relative energy cost are directly related (i.e., the higher the success probability, the higher the relative energy cost) and the minimum relative energy cost route is selected at each BNC, the average end-to-end success probability is equal to the lowest PTV value stored in the array ρ. As a result, the average end-to-end success probability is calculated as:

$$\mathcal{P}_{EQD} = \rho(1) = \mathcal{P}_{req} \tag{5.30}$$

5.4.5 Total Packet Delay

The total packet delay is calculated as the sum of the end-to-end delay at each of the N_b BNCs and is calculated as:

$$\mathcal{D}_{EQD} = \sum_{i=2}^{N} \mathcal{D}_{ete,i1} \tag{5.31}$$

5.5 Performance Evaluation

In this section we conduct numerical studies to achieve the following four objectives. The first and second objectives are to evaluate the performance of the ANC-CC relay scheme and the multi-receive policy. Our third objective is to use our PTV based model to approximate the maximum routing table size necessary for a node operating a conventional distributed routing protocol to maintain the minimum relative energy cost route when reliability and delay constraints are concerned. The fourth objective is to compare the performance of the comprehensive EQD scheme against the EQX scheme proposed in Chapter 4. Unless otherwise specified, the SNs and BNCs are configured according to the parameters in Table 3.1 and the assumed path loss and fading parameters for the on-body and body-to-body channels are given in Table 3.2.

5.5.1 Numerical Studies

5.5.1.1 Evaluation of ANC-CC Relay Scheme

The performance of the ANC-CC relay scheme is evaluated for the network scenario depicted in Fig. 5.2 where N_s SNs *i.k* transmit data through an on-body channel to their BNC *i* over a distance of $d_{i.k,i}$ and through a body-to-body channel to a neighboring BNC *j* over a distance of $d_{i.k,j}$. The BNC *i* transmits the combined incoming data through a body-to-body channel to a neighboring BNC *j* over a distance of d_{ij}. The path loss and fading parameters for

the on-body and body-to-body channels are configured with the parameters in Table 3.2. The body-to-body distance is varied in the range $d_{ij} = d_{i.k,j} = [5,30]$ m. The noise variance at BNC i and BNC j is approximated as $\sigma_i^2 = \sigma_j^2 = -100$ dBm, same as [25] and [163]. The reliability and delay objectives are $\mathcal{P}_{req} = 99\%$ and $\mathcal{D}_{req} = 1$ second, respectively. Algorithm 5.1 is executed to determine the relative energy cost, average success probability, delay, and ANC noise for ANC-CC mitigating ANC noise (AMA) and ANC-CC ignoring ANC noise (AIA). The performance of ANC-CC is compared against the EQS communication scheme described in Chapter 3 where the synergistic BAN model and dual-BAN aggregation concept are implemented to support the energy efficient transmission of SN data over a single hop.

Fig. 5.6a shows the relative energy cost achieved in AMA is substantially higher than EQS when $d_{ij} < 15$ m. The difference in relative energy cost is attributed to the fact that the energy consumed for receiving, amplifying, and transmitting data at relay BNC i exceeds the energy required to transmit directly from the SNs to BNC j (EQS via path 1). The relative energy cost benefit of AMA over EQS is realized when $d_{ij} \geq 15$ m. Although the transmission scheme in EQS reverts from path 1 to path 2 (where data packets from the SNs are transmitted using a combination of the SNs to BNC j and SNs to BNC i to BNC j routing paths) to obtain low relative energy cost, AMA achieves 2% to 36% lower relative energy cost than EQS as d_{ij} is increased from 15 m to 30 m because the analog network coding operation performed at BNC i reduces the total outgoing traffic at BNC i by a factor of approximately $1/N_s$ due to the linear combining process. Furthermore, the maximal ratio combiner at BNC j reduces the total relative energy cost required to maintain the success probability above the reliability objective and overcome fading and path loss induced errors. Fig. 5.6b shows the delay for EQS increases

almost exponentially when $d_{ij} \geq 15$ m whereas the delay in AMA only increases by 20% as d_{ij} is doubled from 15 m to 30 m. The gradual increase in delay experienced in AMA is due to the reduced number of time slots required for the data transmission between BNC *i* and BNC *j*.

The effect of ANC noise on the performance of the ANC-CC relay scheme is also demonstrated through the results shown in Fig. 5.6. In Fig. 5.6d, it is seen that the ANC noise steadily decreases as d_{ij} increases, for the following reason. When the transmit power $P_{tx.ij}$ reaches P_{max}, all terms in (5.9) except $(N_s - 1)g_{ij}$ become constant. As a result, g_{ij} decreases as d_{ij} increases thus resulting in decreased ANC noise. Ignoring the presence of ANC noise has an adverse effect on average success probability, as shown in Fig. 5.6c where the success probability in AIA consistently violates the reliability objective. This result clearly illustrates the importance of accounting for ANC noise. Mitigating ANC noise such that the success probability in ANC-CC is maintained above the reliability objective only requires a relative energy cost increase between 1% and 8% higher than AIA, as shown in Fig. 5.6a. The required increase in relative energy cost steadily declines from 8% to 1% as d_{ij} increases from 5 m to 30 m because the ANC noise figure declines from 6.5 dB to 2 dB. In Fig. 5.6b, the 26% higher delay for AMA as compared to AIA when $d_{ij} = 5$ m indicates that the ability to increase the retransmission limit and decrease packet size are vital to overcoming ANC noise in an energy and QoS aware BAN communication scheme. Similar to the trend exhibited in Fig. 5.6a, it is seen that the effect of overcoming ANC noise on delay decreases as d_{ij} increases and the ANC noise subsequently decreases.

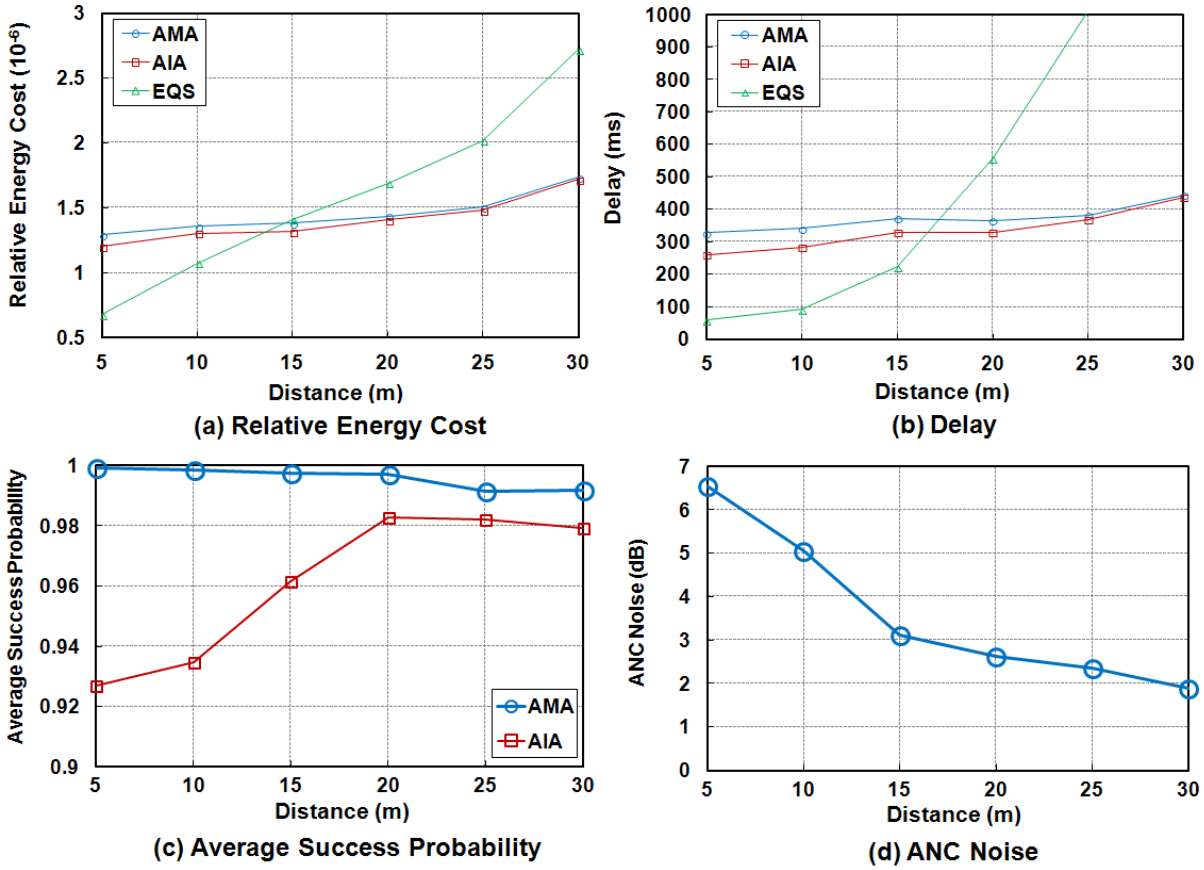

Fig. 5.6. Performance of ANC-CC relay scheme.

5.5.1.2 Effect of Multi-Receive Policy on Performance

In this numerical study we compare the performance of the multi-receive policy (MRP) against CC for transmission along the three successive nodes given in Fig. 5.3. The hop distance between each pair of nodes is randomly varied in the range $[d_{min}, d_{max}]$ where $d_{min} = 5$ m is the minimum distance of a hop and d_{max} in the maximum distance. We populate 50 different routes and average the results. The reliability and delay objectives between BNC i and BS l is $\mathcal{P}_{req} = 99\%$ and $\mathcal{D}_{req} = 1$ second (since only a single routing path is considered), respectively. We assume the BNCs and BS have their maximum battery capacity. In Fig. 5.7a, MRP increasingly saves more relative energy cost than CC as the maximum hop distance decreases

from 25 m. For example, when $d_{max} = 25$ m, MRP requires 14% less relative energy cost than CC and when $d_{max} = 10$ m, MRP requires 18% less relative energy cost. The superior performance exhibited by MRP is directly attributable to the success probability $\mathcal{P}_{jl}$ between BNC j and BS l. As $\mathcal{P}_{jl}$ decreases, the probability of BS l requiring relayed data from BNC k also decreases which minimizes the relative energy cost consumed at BS l due to fewer data packet receptions. On the other hand, it can be seen that the relative energy cost of CC slowly converges to that of MRP as the maximum hop distance approaches 40 m. At a distance of 40 m, the value for $\mathcal{P}_{jl}$ is close to zero and thus BS l relies on also receiving data from BNC k, which leads to higher relative energy cost. In Fig. 5.7b, the success probability for MRP is consistently higher than CC, again due to the non-negligible success probability contributed from $\mathcal{P}_{jl}$. It can also be observed that the success probability for MRP steadily decreases as the maximum hop distance increases and eventually converges to the same success probability as CC because $\mathcal{P}_{jl}$ becomes zero. The same trend demonstrated in Fig. 5.7a and Fig. 5.7b is also captured in Fig. 5.7c where the delay for MRP is consistently lower than CC but the difference in delay decreases as the maximum hop distance increases. The results in Fig. 5.7 demonstrate the effectiveness of employing MRP along routes consisting of two hops and thus it is well suited as a relative energy cost saving mechanism for the EQD communication scheme.

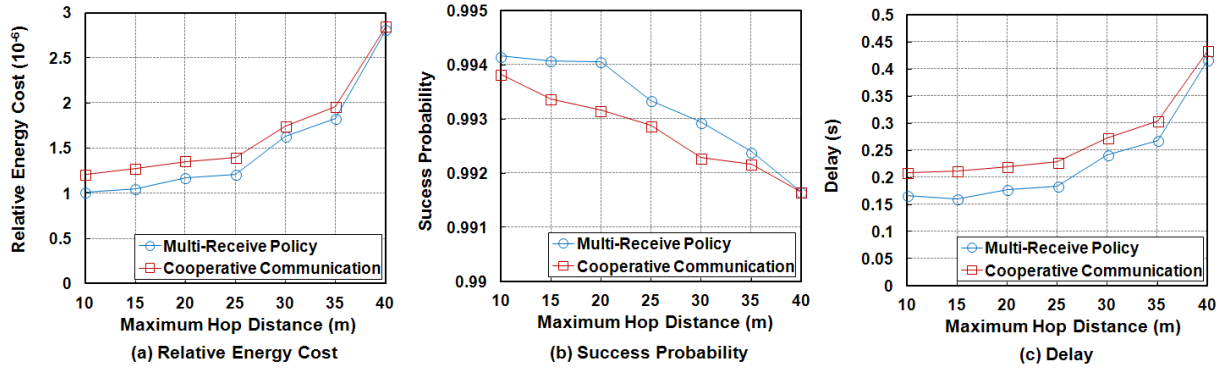

Fig. 5.7. Performance evaluation of MRP and CC under a three node configuration.

5.5.1.3 Effect of Routing Table Size on Protocol Performance

In this study, we perform two tasks. For the first task, we determine the average routing table size maintained by BNCs in a multi-hop BBN that uses a conventional distributed routing protocol (DRP) to obtain the minimum relative energy cost route to the BS. The DRP combines the restricted shortest path and distributed Bellman-Ford algorithm and maintains all routing paths satisfying the end-to-end reliability and delay objectives. To determine the *average* routing table size, we configure a network scenario where 25 BANs are uniformly distributed in a 100 m x 100 m area with a BS set at (0,0) m. Each BNC runs DRP and builds routing paths to the BS by exchanging routing table entries with its neighbors that reside within the neighbor discovery range calculated in Section 4.6.1.1 as $d_{nbr} = 32$ m, providing an average number of neighbors of $\mathbb{N}_{nbr} = 4$. When each BNC has performed at least five rounds of routing table updates with their neighbors (providing convergence to a steady state for the routing table) and is in possession of a feasible routing path to the BS, the average routing table size for each BNC, as a function of the number of hops to the BS, is recorded. We assume the SNs and BNC in each BAN has its maximum battery capacity and the QoS requirements are set at $\mathcal{P}_{req} = 99\%$ and $\mathcal{D}_{req} = 10$ seconds (since several routing paths are considered). We also assume there is no limit

on the number of routing table entries a BNC can maintain. This assumption is generally implied in the literature because special consideration is not afforded for the limited memory capacity of MICAz based motes (e.g., [119]). For the second task, we use the analytical expressions provided in (5.1) and (5.2) to calculate the *maximum* routing table size maintained by the BNCs operating DRP. Based on the network configuration used for the first task, the inputs for (5.1) and (5.2) are set as: $\mathbb{N} = 4, H = 5$, and $\mathcal{P}_{step} = 1\%$. The results obtained for the first and second tasks are compared against the maximum routing table size permitted in the memory of microprocessors typically used for the MICAz mote. Given the maximum routing entry size of $L_{rt} = 139$ bits and the memory size for the Atmega 128L as 4Kbytes [164] and 10 Kbytes for the MSP430 [165], the maximum routing table size is calculated as 230 and 575 entries, respectively.

In Fig. 5.8a, the routing table size for DRP is shown to increase exponentially as the number of hops to the BS increases, which is in line with our hypothesis. Our PTV based analytical model also demonstrates the exponential increase and matches well with the network configuration driven results obtained for DRP. It can also be seen that the routing table size for a BNC configured with either the Atmega 128L or MSP430 microprocessor exceeds the maximum possible routing table size when the number of hops reaches 5. As a result, there is no guarantee that BNCs with routing paths consisting of up to 5 hops perform routing using the optimal minimum relative energy cost route. To validate this statement, we perform another study where we set the maximum routing table size of BNCs using DRP to that of the Atmega 128L (i.e., 230 routes). In the route storing process for DRP, all new routing entries are added into the routing table until the maximum routing table size has been reached. When a new routing entry with the lowest relative energy cost is obtained and the routing table size has reached its maximum

capacity, the new route entry is inserted and the entry in the routing table with the highest relative energy cost is discarded. We compare the minimum relative energy cost routes obtained using DRP against a DRP implementation that stores routing entries based on PTVs configured with $\mathcal{P}_{req} = 99\%$, $\mathcal{P}_{step} = 0.01\%$, and $Y = 100$ using the route storing policies described in Section 5.3.6.3. We refer to this implementation as DRP-PTV. By setting $\mathcal{P}_{step} = 0.01\%$, we provide high enough success probability resolution to maintain the optimal minimum relative energy cost route at each BNC. In Fig. 5.8b, the relative energy cost for the routes obtained with DRP is the same as DRP-PTV when the number of hops to the BS is equal to or less than 3. However, when the number of hops to the BS increases past 4, it is seen that the relative energy cost for DRP becomes higher than DRP-PTV due to the fact that the routing entries needed to provide minimum relative energy cost routes for other BNCs are discarded because of memory constraints. On the other hand, the BNCs in DRP-PTV always maintain a routing table size of 101 that is far less than the maximum allowed number of routes.

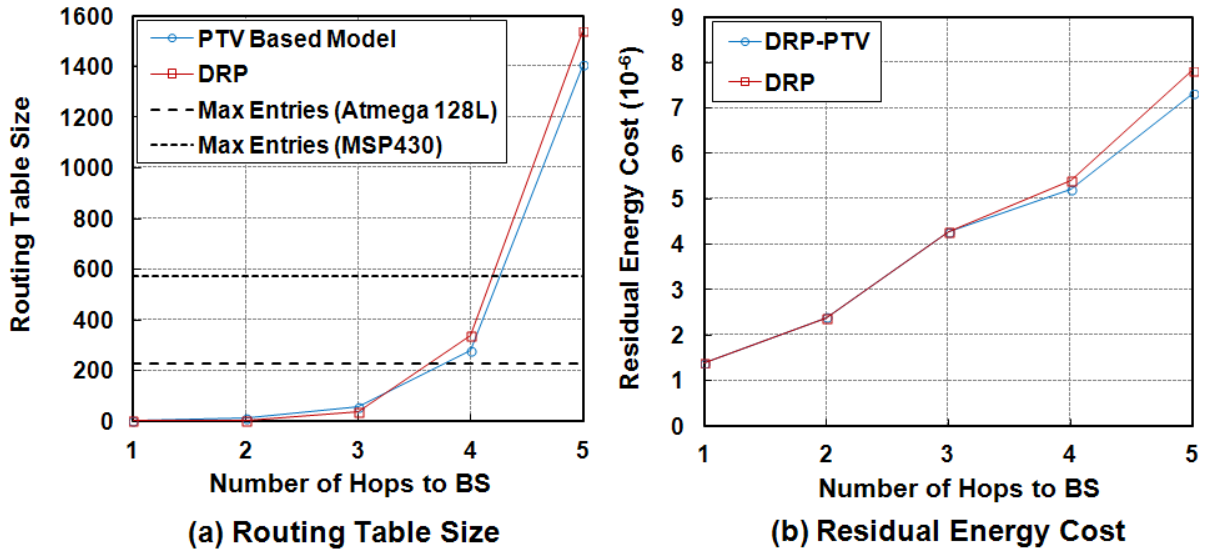

Fig. 5.8. Routing table size and relative energy cost for Restricted Shortest Path Distributed Bellman Ford routing protocol (DRP) and the PTV based model as a function of hops to the BS.

5.5.1.4 Comparison of EQD Scheme against EQX Scheme

The EQX communication scheme designed in Chapter 4 is centralized in nature and thus has the benefit of possessing network-wide knowledge in order to make minimum relative energy cost decisions while satisfying reliability constraints and reducing total delay. We compare the performance of the fully distributed EQD communication scheme against the EQX communication scheme for the same network configuration described in Section 4.6.1.6, to further exhibit the value of integrating the ANC-CC relay scheme, multi-receive policy, and route storing strategy into EQD. For the route discovery process used in EQD, individual routing table entries, each with L_{rt} bits are exchanged between neighbors instead of exchanging route setup packets as is done in EQX. The distributed routing algorithm provided in Algorithm 5.2 is performed at the route update frequency of $T_{rs} = 30$ seconds, the data update frequency is $T_{du} = 10$ seconds, and the desired neighbor size is $\mathbb{N}_{ndr} = 4$ providing a neighbor discovery range of $d_{ndr} = 32$ m. The SNs and BNCs employ the Atmega 128L microprocessor and thus the maximum routing table size is 230. Each BNC is configured to store $Y = 11$ routes by setting $\mathcal{P}_{step} = 0.1\%$. We select a routing table size of 11 to reduce the energy and delay incurred by the route setup process. Each SN, BNC, and BS is initially configured with its maximum battery capacity. The data update process is continuously performed at each increment of T_{du} until the residual energy of either one of the SNs, BNCs, or BS is equal to or less than zero. The analytical expressions provided in Section 5.4 are used to determine the performance of EQD.

In Fig. 5.9a, it is clearly shown that EQD consistently maintains a lower relative energy cost than EQX and also performs a higher number of physiological data updates. The lower relative energy cost is directly attributable to the ANC-CC relay scheme which provides relative

energy cost savings for the first hop transmissions for the SNs, the multi-receive policy which provides relative energy cost reductions along routing paths with more than two hops, and the PTV based route storing policy that allows low relative energy cost routes (with success probability greater than the reliability objective) to be maintained at each BNC. In Fig. 5.9b, the delay incurred for EQD is shown to be higher than EQX when the number of updates is less than 1000, indicating that the slot re-use scheme employed in EQX is more effective in reducing delay than the combination of ANC-CC and MRP. The delay for EQD remains relatively steady when the number of performed updates is greater than 1000 because the optimal minimum relative energy cost routes to the BS are still available since the intermediate BNCs serving as relays have not experienced a significant reduction in residual energy, as is the case with EQX. Fig. 5.9c provides a validation that EQD performs its routing using the minimum available relative energy cost routes because the achieved average success probability is the lowest required to meet the reliability constraint. In Fig. 5.9d and Fig. 5.9e, the energy and time required for route setup is shown to be approximately two times higher in EQD than EQX due to the routing table exchange process between neighboring BNCs. To reduce the route setup energy and time, the number of routes stored in each routing table can be reduced. However, by reducing the number of routing table entries, the probability of obtaining the minimum relative energy cost route decreases, thus increasing the total relative energy cost in the network.

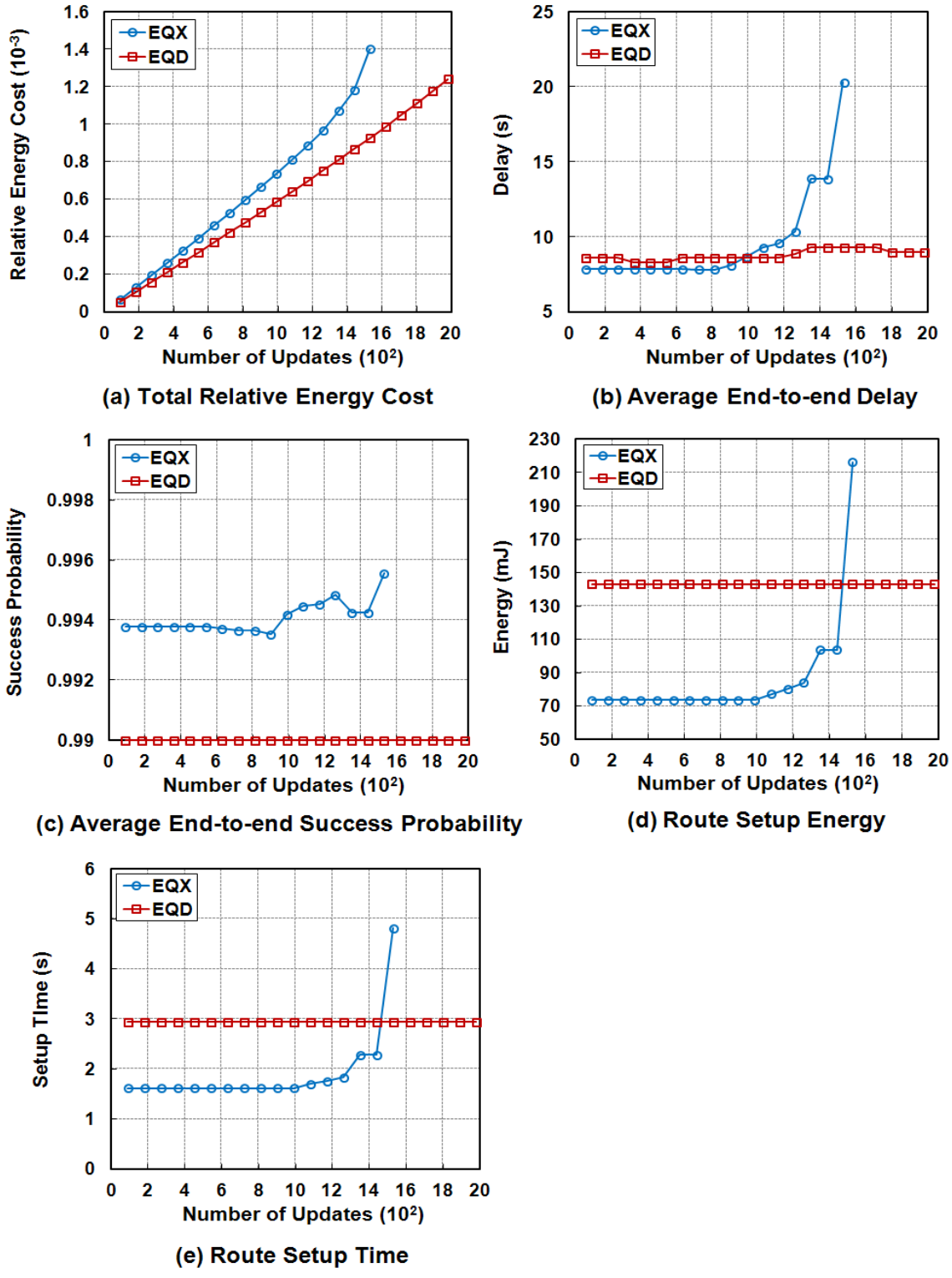

Fig. 5.9. Performance comparison between EQD scheme and EQX scheme for increasing number of physiological data update rounds.

5.6 Summary

In this chapter, the problem of obtaining reliability and delay constrained minimum relative energy cost routes in a fully distributed manner for the transmission of physiological data from SNs to BS in a multi-hop BBN is solved through the design of the EQD communication scheme. The EQD communication scheme is comprised of three key features that facilitate its distributed operation and enhance its overall performance. The first feature is an ANC-CC relay scheme employed for the first hop inter-BAN transmission between SNs and a neighboring BNC or BS. In spite of the presence of ANC noise, our numerical results show that the ANC-CC relay scheme provides significant benefits for BANs in terms of relative energy cost, success probability, and delay when stringent reliability and delay constraints are concerned and the distance between the BAN and neighboring destination (e.g., BNC or BS) is greater than or equal to 15 m. The results also suggest that it would be highly advantageous to adaptively disable the relay BNC in the ANC-CC relay scheme when the distance between the BAN and neighboring destination is less than 15 m in order to obtain significant reduction in relative energy cost and delay. The second feature is the multi-receive policy that is applied to the relaying BNCs along routing paths consisting of more than two hops. When compared against the conventional cooperative communication relay scheme adopted in the literature, our numerical results show that the multi-receive policy achieves lower relative energy cost, higher success probability, and lower delay without the extra processing required of a diversity combiner. The third feature is the integration of a route storing strategy into the proposed distributed routing algorithm, designed to maintain a routing table size within the memory constraints of a BNC while also maintaining the minimum relative energy cost routes necessary to provide the optimal minimum relative energy cost end-to-end routing paths between all BNCs and the BS. Evaluating the performance of the

EQD communication scheme with the aforementioned features against the EQX communication scheme described in Chapter 4 shows that EQD offers significant performance improvements in terms of relative energy cost and the number of physiological data update rounds that can be supported, albeit at the cost of longer route setup times and higher energy consumption for route setup than EQX.

CHAPTER 6 CONCLUSIONS AND FUTURE WORK

6.1 Thesis Conclusions

In this thesis, the EQS, EQX, and EQD communication schemes were designed to solve the problem of minimizing the relative energy cost required to remotely monitor the physiological status of soldiers in a single-hop and multi-hop BBN. The reliable and timely delivery of the physiological status updates is guaranteed through the enforcement of QoS requirements such as high end-to-end success probability and low end-to-end delay for the delivery of data. The presence of multiple data delivery paths available through on-body and body-to-body wireless channels, the synergistic cooperation between SNs and BNCs, and the ability to combine specific features from the network, MAC, and physical layers are all exploited to facilitate QoS constrained minimum relative energy cost transmissions between the SNs and BS in a military operating environment plagued by fading conditions. The research performed for the design of the aforementioned energy and QoS aware communication schemes leads to the following six major conclusions:

1. The number of physiological data updates supported in the communication schemes are increased when the SNs are afforded the ability to transmit to a neighboring destination (i.e., BNC or BS) using direct single-hop transmission from the SNs to the neighboring destination over the body-to-body wireless channel or using indirect transmission from the SNs to the neighboring destination via their BNC that requires multi-hop transmission over the on-body and body-to-body wireless channels.
2. Synergistic cooperative communication between SNs and their BNC is a vital factor for the improvement in relative energy cost, success probability, and delay for single hop transmissions between source (i.e., SNs) and destination (neighboring BNC or BS). This

thesis has demonstrated that the synergistic cooperation provided by the dual aggregation concept described in Chapter 3 and the ANC-CC relay scheme described in Chapter 5 reduce relative energy cost by taking advantage of data packet reception over multiple paths and the efficacy of analog network coding and diversity combining, respectively.

3. The joint optimization of transmit power, retransmission limit, and packet size through the JPRS strategy provides significant performance enhancement for data transmissions performed within the BAN and along single and multiple hop BBNs. Reducing packet size while slowly increasing transmit power and retransmissions extends the BNC's transmission range where the reliability requirement is supported while only incurring a small increase in relative energy cost for inter-BAN transmissions between 5 m and 30 m, particularly under Rayleigh fading conditions.
4. When relative energy cost, success probability, and delay constraints are incorporated into the conventional distributed Shortest-Path-First Bellman-Ford algorithm, an increased level of relative energy cost is incurred for SNs located several hops away from the BS because intermediate relay nodes are unable to maintain the necessary routing table entries that provide minimum relative energy cost routing paths. Therefore, route storing strategies taking memory constraints into account while also maintaining the routing paths necessary to obtain minimum relative energy cost routes should be given special consideration. An example of such a routing strategy is provided in Chapter 5 where we show that minimum relative energy cost routes are obtainable using significantly fewer routes than the conventional distributed Bellman-Ford algorithm.
5. In spite of the negative effect of ANC noise, an ANC-CC relay scheme is desirable for integration into the SNs and BNC in a BAN along with the next hop node to the BAN

because it achieves considerable relative energy cost savings and delay reduction for next hop nodes with a distance of at least 15 m from the source BAN. This is because multiple signals emanating from the SNs can be combined into a single signal at their BNC and successfully decoded at the next hop node that acts as receiver, with only few error free bits received from the SNs.

6. Slot reuse for minimum delay transmission schedules in reliability-constrained wireless networks is attainable by reducing SINR through transmit power reduction but increasing the retransmission limit and decreasing packet size. The increase in retransmission limit and decrease in packet size require an overall increase in relative energy cost, but the increase in relative energy cost provides a higher decrease in delay.

6.2 Engineering Significance of Thesis Findings

The growing need for energy efficient and QoS supporting communication schemes is becoming increasingly evident as the future soldier seeks smaller and less invasive SNs. The proposed EQS, EQX, and EQD communication schemes in this thesis are designed to satisfy those needs by providing on-body and body-to-body communication capabilities to the SNs in order to enhance SN and BNC performance in military operating environments. By jointly optimizing the performance of the schemes at the BAN and BBN levels, the transmission paths yielding the highest number of physiological data updates is obtained. As opposed to most of the work in the literature, the analysis performed in this thesis considers the on-body and body-to-body fading in the BAN and BBN, respectively, which significantly impacts the relative energy cost incurred by the SNs and BNCs especially when reliability and delay are considered.

In Chapter 3, we show that the combination of the synergistic BAN model and the dual aggregation concept is an effective technique to overcome the deleterious effects of body-to-

body fading and path loss while maintaining minimum relative energy cost and sustaining high success probability and low delay. As a result, it is recommended that future designs of SNs are not limited to only supporting intra-BAN transmissions. Rather, SNs should also be designed to support inter-BAN transmissions to take advantage of the synergistic cooperation that is possible with its BNC. The strategy to jointly optimize transmit power, retransmission limit, and packet size requires higher operational complexity at the SNs and BNCs than a strategy that only optimizes transmit power and retransmission limit but achieves significant improvements in terms of relative energy cost, success probability and delay. These improvements can be sustainable in future implementations of SNs and BNCs because the complexity required to perform the optimization of the three parameters can be minimized through the use of the efficient multi search direction algorithms proposed throughout this thesis.

In Chapter 4, we show that obtaining the optimal minimum relative energy cost routes in a multi-hop BBN via a centralized BS is not practical in military operating environments because the optimal solution requires substantial complexity. It is recommended that the inherent interaction between the network, MAC, and physical layers is exploited to employ lower complexity modularized energy and QoS aware routing, constrained power allocation, and slot scheduling algorithms that can be easily implemented in the BNC and BS devices carried by soldiers and the combat medic, respectively. We also reveal that the ability to perform slot reuse is not only controllable through the adjustment of transmit power and the reduction of SINR. While reducing transmit power has the positive effect of reducing interference, it also reduces the link success probability. However, by employing the JPRS strategy, the retransmission limit and packet size can be adjusted to sustain the required link success probability while providing

increased opportunities for slot re-use. This finding further demonstrates the significance of adopting the JPRS strategy for future BBN communication schemes.

In Chapter 5, the combination of the ANC-CC relay scheme, multi-receive policy, and route storing strategy in the EQD communication scheme facilitates the ability to perform minimum relative energy cost and QoS constrained fully distributed routing in a multi-hop BBN. Research towards the ANC-CC relay scheme mainly considers the impact of increased number of source nodes on performance due to the occurrence of ANC noise. However, in BANs, the number of source nodes (i.e., SNs) employing the ANC-CC relay schemes remain constant. We have then identified that ANC noise is largely dependent on the distance between the BAN housing the SNs and BNC and the neighboring next hop node (i.e., BNC or BS). That is, as the distance between the BAN and next hop node increases the ANC noise decreases. As a result, less relative energy cost is incurred to overcome ANC noise. This finding suggests that the ANC-CC relay scheme is most suitable for longer distances between BAN and next hop node. This finding is significant because the relative energy cost obtained when SNs and the BNC adopt the ANC-CC relay scheme for transmissions to next hop nodes at longer distances is lower than when SNs and the BNC adopt a non ANC-CC relay scheme at shorter distances, which then means that the ANC-CC relay scheme supports routing paths with lower number of hops and delay. Finally, as we have shown in the numerical results in Section 5.5, the consideration of the limited memory footprint in BNCs is vital to supporting minimum relative energy cost and QoS constrained distributed routing because failing to do so results in the removal of non-minimum relative energy cost routing entries at intermediate BNCs (due to exceeding the BNC's memory limit), thus preventing source BNCs from acquiring minimum relative energy cost routing entries. As a result, future research towards distributed routing protocols in multi-hop BBNs

must account for the limited routing table size of BNCs because it has a strong impact on the ability for BNCs to acquire the minimum relative energy cost route.

6.3 Suggestions for Future Work

Four logical extensions to the work performed in this thesis have been identified as future work.

1. Modeling of Carrier Sense Medium Access (CSMA)-based Medium Access

   In this thesis, a TDMA scheme is employed at the MAC layer because of its ability to provide for tractable analysis and performance benefits through slot re-use. The integration of CSMA into our cross-layer based optimization models is a highly complex endeavor due to the ensuing analysis for relative energy cost and QoS. Nevertheless, while TDMA is suitable for intra-BAN transmissions, CSMA may be more desirable for BBN transmissions over multi-hops due to its lack of dependence on a centralized scheduling entity and synchronization amongst neighboring transmitters. Therefore, future work in this area is a necessity.

2. Probabilistic Modeling of Mobility

   Mobility is an important aspect of BANs that can be captured through stochastic geometry techniques and probabilistic modelling. Several models exist in the literature to model the movement of soldiers in tactical scenarios such as the random way point model and reference group mobility model employed in [166]. They have been evaluated both analytically and through simulation. However, the impact of mobility on energy consumption and QoS for BANs in multi-hop BBNs requires further analytical research.

3. Magnetic Induction for Communications in a BAN

The security and protection of a soldier's physiological information from the enemy is vital in military-based monitoring applications. While this thesis considers interference mitigation, it does so for the primary purpose of minimizing delay and secondary purpose of minimizing relative energy cost. Several security protocols offering encryption for sensitive transmissions are available in the literature [86], [90] but still have vulnerabilities when applied to transmissions occurring over the ISM frequency band at 2.4 GHz. In addition, the support of encryption carries a burden on energy consumption since the total traffic load (e.g., control, data, and encryption, packets) will be increased. Therefore, the investigation of magnetic induction for communications at the BAN level is intriguing because not only is it immune to multipath and fading effects, communications through magnetic coupling occur at low frequencies that are difficult to intercept and thus offers a light-weight alternative to add-on encryption schemes. Research must focus on the required energy consumption for the magnetic induction enabled communication devices transmitting under stringent QoS requirements. The key concern with magnetic induction communication is its practical feasibility in mobile scenarios and further research must also be conducted to ascertain the reliability of device to device transmissions over a long period of time.

4. Prototype Design for BAN and Energy and QoS Aware Communication Scheme for Multi-hop BBNs

   While the analyses and simulations performed in this thesis provide approximate performance for the EQS, EQX, and EQD communication scheme, the prototype design of the aforementioned communication schemes provide performance under real-life conditions and actual military tactical scenarios. The tasks towards the design of the BAN

prototype first require the validation of the SN and BNC transmission behavior along the on-body and body-to-body wireless channels to further substantiate the synergistic BAN model and dual aggregation concept. Secondly, the efficacy of the JPRS strategy must be evaluated. After performing the first two tasks, the remaining tasks require the full implementation and evaluation of the EQS, EQX and EQD communication schemes under a number of different scenarios.

REFERENCES

[1] S. McGrath, E. Grigg, S. Wendelken, G. Blike, M. De Rosa, A. Fiske*, et al.*, "Artemis: A vision for remote triage and emergency management information integration," *Dartmouth University,* pp. 1-9, 2003.

[2] K. Friedl, "Physiological Monitoring of the Warfighter," *Journal of Diabetes Science and Technology,* vol. 1, no. 1, pp. 116-116, 2007.

[3] N. Watthanawisuth, T. Lomas, A. Wisitsoraat, and A. Tuantranont, "Wireless wearable pulse oximeter for health monitoring using ZigBee wireless sensor network," in *Proc. International Conference on Electrical Engineering/Electronics Computer Telecommunications and Information Technology,* 2010, pp. 575-579.

[4] C. Chan, C. Poon, R. C. Wong, and Y. Zhang, "A hybrid body sensor network for continuous and long-term measurement of arterial blood pressure," in *Proc. 4th IEEE/EMBS International Summer School and Symposium on Medical Devices and Biosensors,* 2007, pp. 121-123.

[5] Z. Zhang, H. Wang, A. V. Vasilakos, and H. Fang, "ECG-cryptography and authentication in body area networks," *IEEE Transactions on Information Technology in Biomedicine,* vol. 16, no. 6, pp. 1070-1078, 2012.

[6] A. Salman, E. G. Allstot, A. Y. Chen, A. M. Dixon, D. Gangopadhyay, and D. J. Allstot, "Compressive sampling of EMG bio-signals," in *Proc. IEEE International Symposium on Circuits and Systems (ISCAS),* 2011, pp. 2095-2098.

[7] Z. Zhang, T.-P. Jung, S. Makeig, and B. D. Rao, "Compressed sensing of EEG for wireless telemonitoring with low energy consumption and inexpensive hardware," *IEEE Transactions on Biomedical Engineering,* vol. 60, no. 1, pp. 221-224, 2013.

[8] S. L. Cotton and W. G. Scanlon, "An experimental investigation into the influence of user state and environment on fading characteristics in wireless body area networks at 2.45 GHz," *IEEE Transactions on Wireless Communications,* vol. 8, no. 1, pp. 6-12, 2009.

[9] S. L. Cotton and W. G. Scanlon, "Characterization of the on-body channel in an outdoor environment at 2.45 GHz," in *Proc. European Conference on Antennas and Propagation,* 2009, pp. 722-725.

[10] W. G. Scanlon and S. L. Cotton, "Understanding on-body fading channels at 2.45 GHz using measurements based on user state and environment," in *Proc. Loughborough Antennas and Propagation Conference,* 2008, pp. 10-13.

[11] S. L. Cotton, A. McKernan, and W. G. Scanlon, "Received signal characteristics of outdoor body-to-body communications channels at 2.45 ghz," in *Proc. Loughborough Antennas and Propagation Conference*, 2011, pp. 1-4.

[12] S. Cotton, A. McKernan, A. Ali, and W. Scanlon, "An experimental study on the impact of human body shadowing in off-body communications channels at 2.45 GHz," in *Proc. 5th European Conference on Antennas and Propagation*, 2011, pp. 3133-3137.

[13] D. Smith, L. Hanlen, J. Zhang, D. Miniutti, D. Rodda, and B. Gilbert, "Characterization of the dynamic narrowband on-body to off-body area channel," in *Proc. IEEE International Conference on Communications (ICC),* 2009, pp. 1-6.

[14] R. Rosini, R. D'Errico, and R. Verdone, "Body-to-body communications: a measurement-based channel model at 2.45 ghz," in *Proc. IEEE 23rd International Symposium on Personal Indoor and Mobile Radio Communications (PIMRC),* 2012, pp. 1763-1768.

[15] Y. Nechayev, Z. H. Hu, and P. Hall, "Fading of the transmission channel between two wireless body area networks in an office at 2.45 GHz and 5.8 GHz," in *Proc. Loughborough Antennas and Propagation Conference,* 2010, pp. 489-492.

[16] H. Ghasemzadeh and R. Jafari, "Data aggregation in body sensor networks: A power optimization technique for collaborative signal processing," in *Proc. 7th Annual IEEE Communications Society Conference on Sensor Mesh and Ad Hoc Communications and Networks (SECON),* 2010, pp. 1-9.

[17] C. Guo, R. Venkatesha Prasad, and M. Jacobsson, "Packet forwarding with minimum energy consumption in body area sensor networks," in *Proc. 7th IEEE Consumer Communications and Networking Conference (CCNC),* 2010, pp. 1-6.

[18] H. Moungla, N. Touati, and A. Mehaoua, "A reliable, efficient routing protocol for dynamic topology in Wireless Body Area Networks using min-max multi-commodity flow model," in *Proc. IEEE 14th International Conference on e-Health Networking, Applications and Services*, 2012, pp. 470-473.

[19] S.-H. Seo, S. Gopalan, S.-M. Chun, K.-J. Seok, J.-W. Nah, and J.-T. Park, "An energy efficient configuration management for multi-hop wireless body area networks," in *Proc. 3rd IEEE International Conference on Broadband Network and Multimedia Technology*, 2010, pp. 1235-1239.

[20] X. Shi, M. Médard, and D. E. Lucani, "When both transmitting and receiving energies matter: an application of network coding in wireless body area networks," in *Workshops NETWORKING*, 2011, pp. 119-128.

[21] Q. Shen and W. Zhuang, "Energy efficient scheduling for delay constrained communication in wireless body area networks," in *Proc. IEEE Global Communications Conference (GLOBECOM)*, 2012, pp. 262-267.

[22] S. J. Marinkovic, E. M. Popovici, C. Spagnol, S. Faul, and W. P. Marnane, "Energy-efficient low duty cycle MAC protocol for wireless body area networks," *IEEE Transactions on Information Technology in Biomedicine,* vol. 13, no. 6, pp. 915-925, 2009.

[23] G. Fang and E. Dutkiewicz, "BodyMAC: Energy efficient TDMA-based MAC protocol for wireless body area networks," in *Proc. 9th International Symposium on Communications and Information Technology*, 2009, pp. 1455-1459.

[24] O. Omeni, A. C. W. Wong, A. J. Burdett, and C. Toumazou, "Energy efficient medium access protocol for wireless medical body area sensor networks," *IEEE Transactions on Biomedical Circuits and Systems,* vol. 2, no. 4, pp. 251-259, 2008.

[25] J. Dong and D. Smith, "Cooperative body-area-communications: Enhancing coexistence without coordination between networks," in *Proc. IEEE 23rd International Symposium on Personal Indoor and Mobile Radio Communications (PIMRC)*, 2012, pp. 2269-2274.

[26] X. Wang and L. Cai, "Interference analysis of co-existing wireless body area networks," in *Proc. IEEE Global Telecommunications Conference (GLOBECOM)*, 2011, pp. 1-5.

[27] R. Kazemi, R. Vesilo, E. Dutkiewicz, and R. Liu, "Dynamic power control in Wireless Body Area Networks using reinforcement learning with approximation," in *Proc. IEEE 22nd International Symposium on Personal Indoor and Mobile Radio Communications (PIMRC)*, 2011, pp. 2203-2208.

[28] G. Fang, E. Dutkiewicz, K. Yu, R. Vesilo, and Y. Yu, "Distributed inter-network interference coordination for wireless body area networks," in *Proc. IEEE Global Telecommunications Conference (GLOBECOM)*, 2010, pp. 1-5.

[29] A. Zhang, L. W. Hanlen, D. Miniutti, D. Rodda, and B. Gilbert, "Interference in body area networks: Are signal-links and interference-links independent?," in *Proc. IEEE 20th International Symposium on Personal, Indoor and Mobile Radio Communications (PIMRC)*, 2009, pp. 456-460.

[30] S. Xiao, A. Dhamdhere, V. Sivaraman, and A. Burdett, "Transmission power control in body area sensor networks for healthcare monitoring," *IEEE Journal on Selected Areas in Communications,* vol. 27, no. 1, pp. 37-48, 2009.

[31] N. Ababneh, N. Timmons, and J. Morrison, "Cross-layer optimization protocol for guaranteed data streaming over Wireless Body Area Networks," in *Proc. 8th International Wireless Communications and Mobile Computing Conference*, 2012, pp. 118-123.

[32] L. Hughes, X. Wang, and T. Chen, "A Review of Protocol Implementations and Energy Efficient Cross-Layer Design for Wireless Body Area Networks," *Sensors,* vol. 12, no. 11, pp. 14730-14773, 2012.

[33] H. Su and X. Zhang, "Battery-dynamics driven TDMA MAC protocols for wireless body-area monitoring networks in healthcare applications," *IEEE Journal on Selected Areas in Communications,* vol. 27, no. 4, pp. 424-434, 2009.

[34] E. Reusens, W. Joseph, B. Latré, B. Braem, G. Vermeeren, E. Tanghe*, et al.*, "Characterization of on-body communication channel and energy efficient topology design for wireless body area networks," *IEEE Transactions on Information Technology in Biomedicine,* vol. 13, no. 6, pp. 933-945, 2009.

[35] E. E. Egbogah and A. O. Fapojuwo, "A survey of system architecture requirements for health care-based wireless sensor networks", *Sensors*, vol. 11, no. 5, pp. 4875-4898, 2011.

[36] V. Shnayder, B.-r. Chen, K. Lorincz, T. R. F. Jones, and M. Welsh, "Sensor networks for medical care," in *SenSys*, 2005, pp. 314-314.

[37] J. Ko, J. H. Lim, Y. Chen, R. Musvaloiu-E, A. Terzis, G. M. Masson*, et al.*, "MEDiSN: medical emergency detection in sensor networks," *ACM Transactions on Embedded Computing Systems,* vol. 10, no. 1, p. 11-1-11-23, 2010.

[38] T. Gao, T. Massey, L. Selavo, D. Crawford, B.-r. Chen, K. Lorincz*, et al.*, "The advanced health and disaster aid network: A light-weight wireless medical system for triage," *IEEE Transactions on Biomedical Circuits and Systems,* vol. 1, no. 3, pp. 203-216, 2007.

[39] H. B. Lim, D. Ma, B. Wang, Z. Kalbarczyk, R. K. Iyer, and K. L. Watkin, "A soldier health monitoring system for military applications," in *Proc. International Conference on Body Sensor Networks*, 2010, pp. 246-249.

[40] A. Milenković, C. Otto, and E. Jovanov, "Wireless sensor networks for personal health monitoring: Issues and an implementation," *Computer communications,* vol. 29, no. 13, pp. 2521-2533, 2006.

[41] J. Y. Khan, M. R. Yuce, and F. Karami, "Performance evaluation of a wireless body area sensor network for remote patient monitoring," in *Proc. 30th Annual International Conference of the IEEE Engineering in Medicine and Biology Society,* 2008, pp. 1266-1269.

[42] A. D. Jurik and A. C. Weaver, "Remote medical monitoring," *Computer,* vol. 41, no. 4, pp. 96-99, 2008.
[43] S. B. Eisenman, E. Miluzzo, N. D. Lane, R. A. Peterson, G.-S. Ahn, and A. T. Campbell, "BikeNet: A mobile sensing system for cyclist experience mapping," *ACM Transactions on Sensor Networks,* vol. 6, no. 1, pp. 1-39, 2009.
[44] F. Hu, Y. Xiao, and Q. Hao, "Congestion-aware, loss-resilient bio-monitoring sensor networking for mobile health applications," *IEEE Journal on Selected Areas in Communications,* vol. 27, no. 4, pp. 450-465, 2009.
[45] D. Niyato, E. Hossain, and S. Camorlinga, "Remote patient monitoring service using heterogeneous wireless access networks: architecture and optimization," *IEEE Journal on Selected Areas in Communications,* vol. 27, no. 4, pp. 412-423, 2009.
[46] Y. He, W. Zhu, and L. Guan, "Optimal resource allocation for pervasive health monitoring systems with body sensor networks," *IEEE Transactions on Mobile Computing,* vol. 10, no. 11, pp. 1558-1575, 2011.
[47] C. A. Boano, M. Lasagni, K. Romer, and T. Lange, "Accurate temperature measurements for medical research using body sensor networks," in *Proc. 14th IEEE International Symposium on Object/Component/Service-Oriented Real-Time Distributed Computing Workshops,* 2011, pp. 189-198.
[48] Z. Ji, X. Zhang, I. Ganchev, and M. O'Droma, "A personalized middleware for ubiquitous mHealth services," in *Proc. IEEE 14th International Conference on e-Health Networking, Applications and Services*, 2012, pp. 474-476.
[49] Y. Zatout, E. Campo, and J.-F. Llibre, "WSN-HM: Energy-efficient Wireless Sensor Network for home monitoring," in *Proc. 5th International Conference on Intelligent Sensors, Sensor Networks and Information Processing*, 2009, pp. 367-372.
[50] J. B. Sliman, Y.-Q. Song, A. Koubâa, and M. Frikha, "Three-Tiered Architecture for Large-Scale Wireless Hospital Sensor Networks," in *Proc. International Joint Conference on Biomedical Engineering Systems,* 2009, pp. 1-12.
[51] D. Singh, H.-J. Lee, and W.-Y. Chung, "An energy consumption technique for global healthcare monitoring applications," in *Proc. 2nd International Conference on Interaction Sciences: Information Technology, Culture and Human*, 2009, pp. 539-542.
[52] J. Jung, K. Ha, J. Lee, Y. Kim, and D. Kim, "Wireless body area network in a ubiquitous healthcare system for physiological signal monitoring and health consulting," *International Journal of Signal Processing, Image Processing and Pattern Recognition,* vol. 1, pp. 47-54, 2008.
[53] M. Nabi, T. Basten, M. Geilen, M. Blagojevic, and T. Hendriks, "A robust protocol stack for multi-hop wireless body area networks with transmit power adaptation," in *Proc. Fifth International Conference on Body Area Networks*, 2010, pp. 77-83.
[54] M. C. Domingo, "Packet Size Optimization for Improving the Energy Efficiency in Body Sensor Networks," *ETRI Journal,* vol. 33, no. 3, pp. 209-309, 2011.
[55] B. Braem, B. Latré, C. Blondia, I. Moerman, and P. Demeester, "Improving reliability in multi-hop body sensor networks," in *Proc. Second International Conference on Sensor Technologies and Applications,* 2008, pp. 342-347.
[56] R. W. Hoyt, M. Buller, M. S. Redin, R. D. Poor, and S. R. Oliver, "Soldier Physiological Monitoring-Results of Dismounted Battlespace Battle Lab Concept Experimentation Program Field Study," DTIC Document, 1997.

[57] D. Schmorrow and A. A. Kruse, "DARPA's Augmented Cognition Program-tomorrow's human computer interaction from vision to reality: building cognitively aware computational systems," in *Proc. IEEE 7th Conference on Human Factors and Power Plants,* 2002, pp. 7-1-7-4.

[58] M. Buller, R. W. Hoyt, J. Ames, W. Latzka, and B. Freund, "Enhancing warfighter readiness through physiologic situational awareness-The Warfighter Physiological Status Monitoring-Initial capability," in *Proc. 1st International Conference on Augmented Cognition,* 2005, pp. 335-341.

[59] R. Matthews, N. J. McDonald, P. Hervieux, P. J. Turner, and M. A. Steindorf, "A wearable physiological sensor suite for unobtrusive monitoring of physiological and cognitive state," in *Proc. 29th Annual International Conference of the IEEE Engineering in Medicine and Biology Society,* 2007, pp. 5276-5281.

[60] D. Minnen, T. Westeyn, D. Ashbrook, P. Presti, and T. Starner, "Recognizing soldier activities in the field," in *Proc. 4th International Workshop on Wearable and Implantable Body Sensor Networks*, 2007, pp. 236-241.

[61] J. Salinas, R. Nguyen, M. I. Darrah, G. A. Kramer, M. L. Serio-Melvin, E. A. Mann*, et al.*, "Advanced monitoring and decision support for battlefield critical care environment," *US Army Medical Department journal,* pp. 73-81, 2011.

[62] D.-K. Cho, A. Chang, M.-H. Tsai, and M. Gerla, "Networked medical monitoring in the battlefield," in *Proc. IEEE Military Communications Conference (MILCOM),* 2008, pp. 1-7.

[63] A. A. Gohari, R. Pakbaz, P. M. Melliar-Smith, L. E. Moser, and V. Rodoplu, "RMR: Reliability map routing for tactical mobile ad hoc networks," *IEEE Journal on Selected Areas in Communications,* vol. 29, no. 10, pp. 1935-1947, 2011.

[64] S. H. Lee, S. Lee, H. Song, and H. S. Lee, "Wireless sensor network design for tactical military applications: remote large-scale environments," in *Proc. IEEE Military Communications Conference (MILCOM),* 2009, pp. 1-7.

[65] S. L. Cotton, W. G. Scanlon, and B. K. Madahar, "Millimeter-wave soldier-to-soldier communications for covert battlefield operations," *IEEE Communications Magazine,* vol. 47, no. 10, pp. 72-81, 2009.

[66] D.-K. Cho, S.-H. Lee, A. Chang, T. Massey, C.-W. Chang, M.-H. Tsai*, et al.*, "Opportunistic medical monitoring using bluetooth P2P networks," in *Proc. International Symposium on a World of Wireless, Mobile and Multimedia Networks*, 2008, pp. 1-6.

[67] F. Hu, M. Jiang, L. Celentano, and Y. Xiao, "Robust medical ad hoc sensor networks (MASN) with wavelet-based ECG data mining," *Ad Hoc Networks,* vol. 6, no. 7, pp. 986-1012, 2008.

[68] R. W. Hoyt, M. J. Buller, H.-C. Gunga, A. Werner, F. Sattler, J. Koch*, et al.*, "Real-time physiological and psycho-physiological status monitoring," NATO RTO publication RTO-TR-HFM-132, NATO Research and Technology Organization, 2010.

[69] S.-I. Yang and S.-B. Cho, "Recognizing human activities from accelerometer and physiological sensors," in *Proc. IEEE International Conference on Multisensor Fusion and Integration for Intelligent Systems,* 2008, pp. 100-105.

[70] E. I. Shih, A. H. Shoeb, and J. V. Guttag, "Sensor selection for energy efficient ambulatory medical monitoring," in *Proc. 7th international conference on Mobile systems, applications, and services*, 2009, pp. 347-358.

[71] J. Misic and V. B. Misic, "Bridge performance in a multitier wireless network for healthcare monitoring," *IEEE Wireless Communications,* vol. 17, no. 1, pp. 90-95, 2010.
[72] J.-L. Lin, H.-C. Liu, Y.-T. Tai, H.-H. Wu, S.-J. Hsu, F.-S. Jaw*, et al.*, "The development of wireless sensor network for ECG monitoring," in *Proc. 28th Annual International Conference of the IEEE Engineering in Medicine and Biology Society,* 2006, pp. 3513-3516.
[73] X. Liang and I. Balasingham, "Performance analysis of the IEEE 802.15. 4 based ECG monitoring network," in *Proc. 7th IASTED International Conferences on Wireless and Optical Communications*, 2007, pp. 99-104.
[74] A. Alesanco and J. Garcia, "Clinical assessment of wireless ECG transmission in real-time cardiac telemonitoring," *IEEE Transactions on Information Technology in Biomedicine,* vol. 14, no. 5, pp. 1144-1152, 2010.
[75] D. Spulak, R. Cmejla, and V. Fabián, "Parameters for mean blood pressure estimation based on electrocardiography and photoplethysmography," in *Proc. International Conference on Applied Electronics*, 2011, pp. 1-4.
[76] Y. Chen, C. Wen, G. Tao, and M. Bi, "Continuous and noninvasive measurement of systolic and diastolic blood pressure by one mathematical model with the same model parameters and two separate pulse wave velocities," *Annals of biomedical engineering,* vol. 40, no. 4, pp. 871-882, 2012.
[77] F. E. Tay, D. G. Guo, L. Xu, M. N. Nyan, and K. L. Yap, "MEMSWear-biomonitoring system for remote vital signs monitoring," *Journal of the Franklin Institute,* vol. 346, no. 6, pp. 531-542, 2009.
[78] A. Burns, B. R. Greene, M. J. McGrath, T. J. O'Shea, B. Kuris, S. M. Ayer*, et al.*, "SHIMMER™–A wireless sensor platform for noninvasive biomedical research," *IEEE Sensors Journal,* vol. 10, no. 9, pp. 1527-1534, 2010.
[79] B. Shrestha, E. Hossain, and S. Camorlinga, "IEEE 802.15. 4 MAC with GTS transmission for heterogeneous devices with application to wheelchair body-area sensor networks," *IEEE Transactions on Information Technology in Biomedicine,* vol. 15, no. 5, pp. 767-777, 2011.
[80] C. Li, H.-B. Li, and R. Kohno, "Performance evaluation of IEEE 802.15. 4 for wireless body area network (WBAN)," in *Proc. IEEE International Conference on Communications (ICC) Workshops,* 2009, pp. 1-5.
[81] L. M. S. Committee, "Part 15.4: wireless medium access control (MAC) and physical layer (PHY) specifications for low-rate wireless personal area networks (LR-WPANs)," *IEEE Computer Society,* 2003.
[82] Y. Zhang and H. Xiao, "Bluetooth-based sensor networks for remotely monitoring the physiological signals of a patient," *IEEE Transactions on Information Technology in Biomedicine,* vol. 13, no. 6, pp. 1040-1048, 2009.
[83] A. Chipcon, "CC2420 2.4 GHz IEEE 802.15. 4/ZigBee-ready RF Transceiver Data Sheet (rev. 1.3) http://www.chipcon.com/files," *CC2420 Data Sheet,* vol. 1.
[84] C. S. Radio, "BlueCore2-External Product Data Sheet," *CSR Support,* p. 32, 2006.
[85] J.-S. Lee, Y.-W. Su, and C.-C. Shen, "A comparative study of wireless protocols: Bluetooth, UWB, ZigBee, and Wi-Fi," in *Proc. 33rd Annual Conference of the IEEE Industrial Electronics Society,* 2007, pp. 46-51.

[86] L. M. R. Tarouco, L. M. Bertholdo, L. Z. Granville, L. M. R. Arbiza, F. Carbone, M. Marotta*, et al.*, "Internet of Things in healthcare: Interoperatibility and security issues," in *Proc. IEEE International Conference on Communications*, 2012, pp. 6121-6125.

[87] A. Natarajan, B. de Silva, K.-K. Yap, and M. Motani, "Link layer behavior of body area networks at 2.4 ghz," in *Proc. 15th Annual International Conference on Mobile Computing and Networking*, 2009, pp. 241-252.

[88] G. Wu, J. Ren, F. Xia, and Z. Xu, "An adaptive fault-tolerant communication scheme for body sensor networks," *Sensors,* vol. 10, no. 11, pp. 9590-9608, 2010.

[89] M. A. Razzaque, C. S. Hong, and S. Lee, "Data-centric multiobjective QoS-aware routing protocol for body sensor networks," *Sensors,* vol. 11, no.1, pp. 917-937, 2011.

[90] X. Liang, X. Li, Q. Shen, R. Lu, X. Lin, X. Shen*, et al.*, "Exploiting prediction to enable secure and reliable routing in wireless body area networks," in *Proc. IEEE Conference on Computer Communications (ICC)*, 2012, pp. 388-396.

[91] G. Zhou, J. Lu, C.-Y. Wan, M. D. Yarvis, and J. A. Stankovic, "Bodyqos: Adaptive and radio-agnostic qos for body sensor networks," in *Proc. IEEE Conference on Computer Communications (ICC),* 2008, pp. 1238-1246.

[92] J. S. Yoon, G.-S. Ahn, S.-S. Joo, and M. J. Lee, "PNP-MAC: preemptive slot allocation and non-preemptive transmission for providing QoS in body area networks," in *Proc. IEEE Consumer Communications and Networking Conference (CCNC),* 2010, pp. 1-5.

[93] I. Demirkol, C. Ersoy, and F. Alagoz, "MAC protocols for wireless sensor networks: a survey," *IEEE Communications Magazine,* vol. 44, no. 4, pp. 115-121, 2006.

[94] A. Natarajan, M. Motani, B. de Silva, K.-K. Yap, and K. C. Chua, "Investigating network architectures for body sensor networks," in *Proc. 1st ACM SIGMOBILE international workshop on Systems and networking support for healthcare and assisted living environments*, 2007, pp. 19-24.

[95] A. Natarajan, B. De Silva, K.-K. Yap, and M. Motani, "To hop or not to hop: Network architecture for body sensor networks," in *Proc. IEEE Communications Society Conference on Sensor, Mesh and Ad Hoc Communications and Networks (SECON),* 2009, pp. 1-9.

[96] A. Seyedi and B. Sikdar, "Energy efficient transmission strategies for body sensor networks with energy harvesting," *IEEE Transactions on Communications,* vol. 58, no. 7, pp. 2116-2126, 2010.

[97] N. Ababneh, N. Timmons, J. Morrison, and D. Tracey, "Energy-balanced rate assignment and routing protocol for body area networks," in *Proc. International Conference on Advanced Information Networking and Applications Workshops*, 2012, pp. 466-471.

[98] N. Javaid, Z. Abbas, M. Fareed, Z. Khan, and N. Alrajeh, "M-ATTEMPT: A new energy efficient routing protocol for wireless body area sensor networks," *Procedia Computer Science,* vol. 19, pp. 224-231, 2013.

[99] Y. Zatout, "Energy aware mechanisms for health-care monitoring at home," in *Proc. IEEE 23rd International Symposium on Personal Indoor and Mobile Radio Communications (PIMRC)*, 2012, pp. 2530-2534.

[100] X. Huang, H. Shan, and X. Shen, "On energy efficiency of cooperative communications in wireless body area network," in *IEEE Wireless Communications and Networking Conference,* 2011, pp. 1097-1101.

[101] J. Ben-Othman and B. Yahya, "Energy efficient and QoS based routing protocol for wireless sensor networks," *Journal of Parallel and Distributed Computing,* vol. 70, no. 8, pp. 849-857, 2010.
[102] G. H. EkbataniFard, R. Monsefi, M.-R. Akbarzadeh-T, and M. Yaghmaee, "A multi-objective genetic algorithm based approach for energy efficient QoS-routing in two-tiered wireless sensor networks," in *Proc. IEEE International Symposium on Wireless Pervasive Computing*, 2010, pp. 80-85.
[103] H. Cao, S. González-Valenzuela, and V. C. Leung, "Employing IEEE 802.15. 4 for quality of service provisioning in wireless body area sensor networks," in *Proc. IEEE International Conference on Advanced Information Networking and Applications*, 2010, pp. 902-909.
[104] C. Otto, A. Milenkovic, C. Sanders, and E. Jovanov, "System architecture of a wireless body area sensor network for ubiquitous health monitoring," *Journal of Mobile Multimedia,* vol. 1, no. 4, pp. 307-326, 2006.
[105] H. Kwon, T. H. Kim, S. Choi, and B. G. Lee, "A cross-layer strategy for energy efficient reliable delivery in wireless sensor networks," *IEEE Transactions on Wireless Communications,* vol. 5, no. 12, pp. 3689-3699, 2006.
[106] L. Shi and A. Fapojuwo, "TDMA scheduling with optimized energy efficiency and minimum delay in clustered wireless sensor networks," *IEEE Transactions on Mobile Computing,* vol. 9, no. 7, pp. 927-940, 2010.
[107] L. Shi and A. O. Fapojuwo, "Minimizing Power Cost in QoS Constrained Wireless Sensor Networks," *International journal of wireless information networks,* vol. 20, no. 1, pp. 13-26, 2013.
[108] H.-W. Tseng and Y.-R. Chuang, "A Cross-Layer Judgment Scheme for Solving Retransmission Problem in IEEE 802.15. 4-Based Wireless Body Sensor Networks," *IEEE Sensors Journal,* vol. 13, no. 8, pp. 3124-3135, 2013.
[109] J. Ammer and J. Rabaey, "The energy-per-useful-bit metric for evaluating and optimizing sensor network physical layers," in *Proc. IEEE Communications Society on Sensor and Ad Hoc Communications and Networks (SECON)*, 2006, pp. 695-700.
[110] A. Ehyaie, M. Hashemi, and P. Khadivi, "Using relay network to increase life time in wireless body area sensor networks," in *Proc. IEEE International Symposium on a World of Wireless, Mobile and Multimedia Networks & Workshops*, 2009, pp. 1-6.
[111] J. Elias and A. Mehaoua, "Energy-aware topology design for wireless body area networks," in *Proc. IEEE International Conference on Communications (ICC)*, 2012, pp. 3409-3410.
[112] L. Galluccio, G. Morabito, and S. Palazzo, "Analytical evaluation of a tradeoff between energy efficiency and responsiveness of neighbor discovery in self-organizing ad hoc networks," *IEEE Journal on Selected Areas in Communications,* vol. 22, no. 7, pp. 1167-1182, 2004.
[113] A. Willig, N. Karowski, and J.-H. Hauer, "Passive discovery of IEEE 802.15. 4-based body sensor networks," *Ad Hoc Networks,* vol. 8, no. 7, pp. 742-754, 2010.
[114] H. Liu, D. Li, and X. Jia, "QoS topology control with minimal total energy cost in Ad hoc wireless networks," in *Mobile Ad-hoc and Sensor Networks*, 2006, pp. 622-637.

[115] L. Yang, H.-C. Yang, and K. Wu, "Minimum-energy route configuration for wireless ad hoc networks," in *Proc. IEEE International Performance, Computing, and Communications Conference,* 2006, pp. 6-14.
[116] W. L. Huang and K. B. Letaief, "Cross-layer scheduling and power control combined with adaptive modulation for wireless ad hoc networks," *IEEE Transactions on Communications,* vol. 55, no. 4, pp. 728-739, 2007.
[117] M. Yu, A. Malvankar, W. Su, and S. Y. Foo, "A link availability-based QoS-aware routing protocol for mobile ad hoc sensor networks," *Computer Communications,* vol. 30, no. 18, pp. 3823-3831, 2007.
[118] D. S. De Couto, D. Aguayo, J. Bicket, and R. Morris, "A high-throughput path metric for multi-hop wireless routing," *Wireless Networks,* vol. 11, no. 4, pp. 419-434, 2005.
[119] F. De Rango, F. Guerriero, and P. Fazio, "Link-stability and energy aware routing protocol in distributed wireless networks," *IEEE Transactions on Parallel and Distributed Systems,* vol. 23, no. 4, pp. 713-726, 2012.
[120] J. Zhu and X. Wang, "Model and protocol for energy efficient routing over mobile ad hoc networks," *IEEE Transactions on Mobile Computing,* vol. 10, no. 11, pp. 1546-1557, 2011.
[121] W. Liu, C. Zhang, G. Yao, and Y. Fang, "DELAR: a device-energy-load aware relaying framework for heterogeneous mobile ad hoc networks," *IEEE Journal on Selected Areas in Communications,* vol. 29, no. 8, pp. 1572-1584, 2011.
[122] J. Vazifehdan, R. Prasad, and I. Niemegeers, "Energy-efficient reliable routing considering residual energy in wireless ad hoc networks," *IEEE Transactions on Mobile Computing,* vol. 13, no. 2, pp. 443-447, 2013.
[123] L. Shi and A. O. Fapojuwo, "Cross-layer optimization with cooperative communication for minimum power cost in packet error rate constrained wireless sensor networks," *Ad Hoc Networks,* vol. 10, no. 7, pp. 1457-1468, 2012.
[124] W. Sun, Y. Ge, and W.-C. Wong, "Inter-user interference in Body Sensor Networks: A case study in moderate-scale deployment in hospital environment," in *Proc. IEEE 14th International Conference on e-Health Networking, Applications and Services,* 2012, pp. 447-450.
[125] S. Katti, S. Gollakota, and D. Katabi, "Embracing wireless interference: analog network coding," in *ACM SIGCOMM Computer Communication Review*, 2007, pp. 397-408.
[126] Z. Yi, M. Ju, and I.-M. Kim, "Outage probability and optimum power allocation for analog network coding," *IEEE Transactions on Wireless Communications,* vol. 10, no. 2, pp. 407-412, 2011.
[127] C. Zhang, J. Ge, J. Li, and Y. Hu, "Energy-aware power allocation for asymmetric analog network coding with statistical CSI," in *IEEE Wireless Communications and Networking Conference*, 2013, pp. 2565-2569.
[128] S. Sharma, Y. Shi, J. Liu, Y. T. Hou, and S. Kompella, "Is network coding always good for cooperative communications?," in *Proc. IEEE Conference on Computer Communications (ICC)*, 2010, pp. 1-9.
[129] S. Wang, Q. Song, X. Wang, and A. Jamalipour, "Rate and power adaptation for analog network coding," *IEEE Transactions on Vehicular Technology,* vol. 60, no. 5, pp. 2302-2313, 2011.

[130] Y. Li, X. Zhang, M. Peng, and W. Wang, "Power provisioning and relay positioning for two-way relay channel with analog network coding," *IEEE Signal Processing Letters,* vol. 18, no. 9, pp. 517-520, 2011.
[131] B. M. Williamson, J. J. LaViola, T. Roberts, and P. Garrity, "Multi-Kinect Tracking for Dismounted Soldier Training," in *The Interservice/Industry Training, Simulation & Education Conference*, 2012.
[132] Z. Zhou, Z. Peng, J.-H. Cui, and Z. Shi, "Efficient multipath communication for time-critical applications in underwater acoustic sensor networks," *IEEE/ACM Transactions on Networking,* vol. 19, no. 1, pp. 28-41, 2011.
[133] H. Dubois-Ferrière, D. Estrin, and M. Vetterli, "Packet combining in sensor networks," in *Proc. 3rd international conference on Embedded networked sensor systems*, 2005, pp. 102-115.
[134] A. Goldsmith, *Wireless communications*: Cambridge university press, 2005.
[135] B. B. Haile, "Co-channel interference in heterogeneous networks: Rician/Rayleigh scenario," M.S. thesis, Dept. Comnet, Aalto Univ., Helsinki, Finland, 2010.
[136] P. Mary, M. Dohler, J.-M. Gorce, G. Villemaud, and M. Arndt, "BPSK bit error outage over Nakagami-m fading channels in lognormal shadowing environments," *IEEE Communications Letters,* vol. 11, no. 7, pp. 565-567, 2007.
[137] R. W. Butler and A. T. Wood, "Laplace approximations for hypergeometric functions with matrix argument," *Annals of Statistics,* pp. 1155-1177, 2002.
[138] A. Koubâa, M. Alves, and E. Tovar, "GTS allocation analysis in IEEE 802.15. 4 for real-time wireless sensor networks," in *Proc. International Parallel and Distributed Processing Symposium*, 2006, pp.1-8.
[139] Q. Dong and W. Dargie, "A survey on mobility and mobility-aware MAC protocols in wireless sensor networks," *IEEE Communications Surveys & Tutorials,* vol. 15, no. 1, pp. 88-100, 2013.
[140] A. Bartoli, J. Hernández-Serrano, M. Soriano, M. Dohler, A. Kountouris, and D. Barthel, "Secure lossless aggregation over fading and shadowing channels for smart grid M2M networks," *IEEE Transactions on Smart Grid,* vol. 2, no. 4, pp. 844-864, 2011.
[141] MicaZ Datasheet, "Crossbow Corp," ed.
[142] Q. Wang, M. Hempstead, and W. Yang, "A realistic power consumption model for wireless sensor network devices," in *Proc. IEEE Communications Society on Sensor and Ad Hoc Communications and Networks (SECON),* 2006, pp. 286-295.
[143] E. E. Egbogah and A. O. Fapojuwo, "Achieving Energy Efficient Transmission in Wireless Body Area Networks for the Physiological Monitoring of Military Soldiers," in *Proc. IEEE Military Communications Conference (MILCOM),* 2013, pp. 1371-1376.
[144] E. E. Egbogah, A. O. Fapojuwo, and L. Shi, "Energy and Quality of Service Aware Communication in Body-to-body Networks under Quality of Service Constraints," *Ad Hoc Networks,* submitted, 2014.
[145] Q. Wang, T. Tayamachi, I. Kimura, and J. Wang, "An on-body channel model for UWB body area communications for various postures," *IEEE Transactions on Antennas and Propagation,* vol. 57, no. 4, pp. 991-998, 2009.
[146] M. R. Yuce, P. C. Ng, and J. Y. Khan, "Monitoring of physiological parameters from multiple patients using wireless sensor network," *Journal of medical systems,* vol. 32, no. 8, pp. 433-441, 2008.

[147] N. Seitz, "ITU-T QoS standards for IP-based networks," *IEEE Communications Magazine,* vol. 41, no. 6, pp. 82-89, 2003.
[148] W. Mandak, T. Krout, S. Durbano, and R. Shearer, "Network-Centric Applications and Tactical Networks "," in *Proc. Of the Eighth International Command and Control Research and Technology Symposium*, 2003.
[149] U.S. Army, "FM 3-21.8 The Infantry Rifle Platoon and Squad," Available online: www.us.army.mil, last accessed April 2014.
[150] K. Holmström, "The TOMLAB optimization environment in Matlab," 1999.
[151] Z. Ugray, L. Lasdon, J. Plummer, F. Glover, J. Kelly, and R. Martí, "Scatter search and local NLP solvers: A multistart framework for global optimization," *INFORMS Journal on Computing,* vol. 19, no. 3, pp. 328-340, 2007.
[152] W. Zhang, "Branch-and-Bound Search Algorithms and Their Computational Complexity," DTIC Document, 1996.
[153] E. E. Egbogah, A. O. Fapojuwo, and L. Shi, "An energy efficient transmission scheme for monitoring combat soldier physiological state using tactical wireless sensor networks," *Ad Hoc Networks,* under second round of review, 2013.
[154] E. E. Egbogah, A. O. Fapojuwo, and L. Shi, "An energy efficient transmission scheme for monitoring of combat soldier health in tactical mobile ad hoc networks," in *Proc. IEEE MILITARY COMMUNICATIONS CONFERENCE (MILCOM),* 2012, pp. 1-7.
[155] L. Shi, E. Egbogah, and A. Fapojuwo, "Combined cooperative communication and multicast for minimum power cost in coded wireless sensor networks," in *Proc. IEEE Wireless Communications and Networking Conference (WCNC),* 2011, pp. 755-760.
[156] Y. G. Kim and N. C. Beaulieu, "New results on maximal ratio combining in Nakagami-m fading channels," in *Proc. IEEE International Conference on Communications (ICC),* 2012, pp. 4761-4765.
[157] T. Herman and S. Tixeuil, "A distributed TDMA slot assignment algorithm for wireless sensor networks," in *Algorithmic Aspects of Wireless Sensor Networks*, 2004, pp. 45-58.
[158] S. Li, D. Qian, Y. Liu, and J. Tong, "Adaptive distributed randomized TDMA scheduling for clustered wireless sensor networks," in *Proc. International Conference on Wireless Communications, Networking and Mobile Computing (WiCom)*, 2007, pp. 2688-2691.
[159] P. Muthukumaran, R. de Paz, R. Spinar, and D. Pesch, "MeshMAC: Enabling Mesh Networking over IEEE 802.15. 4 through distributed beacon scheduling," in *Ad Hoc Networks*, 2010, pp. 561-575.
[160] T. Aurisch and J. Tölle, "Relay Placement for Ad-hoc Networks in Crisis and Emergency Scenarios," in *Proc. Information Systems and Technology Panel Symposium, Bucharest, Romania*, 2009.
[161] Q. Zhang, "Maximal-ratio combining over Nakagami fading channels with an arbitrary branch covariance matrix," *IEEE Transactions on Vehicular Technology,* vol. 48, no. 4, pp. 1141-1150, 1999.
[162] J. N. Laneman, D. N. Tse, and G. W. Wornell, "Cooperative diversity in wireless networks: Efficient protocols and outage behavior," *IEEE Transactions on Information Theory,* vol. 50, no. 12, pp. 3062-3080, 2004.
[163] K. Srinivasan, P. Dutta, A. Tavakoli, and P. Levis, "Understanding the causes of packet delivery success and failure in dense wireless sensor networks," in *Proc. 4th International Conference on Embedded networked sensor systems*, 2006, pp. 419-420.

[164] A. Atmega128, "128L microprocessor Datasheet," *Atmel Corporation*.
[165] T. Instruments, "MSP430 DataSheet," ed, 2001.
[166] E. E. Egbogah, A. Fapojuwo, and N. Chan, "Scalable team oriented reliable multicast routing protocol for tactical mobile ad hoc networks," in *Proc. IEEE Military Communications Conference (MILCOM)*, 2008, pp. 1-7.